AN EXPERIMENTAL INVESTIGATION ON THE STRENGTH EVOLUTION OF COLLOIDAL SILICA GROUT DURING CURING AND RE-HEALING, AND ON ITS MODIFICATION USING CLAYS AND POLYMERS

by

David William Thomas Morrison

A thesis submitted to the Department of Civil and Environmental Engineering of the University of Strathclyde in fulfilment of the requirements for the degree of

Doctor of Philosophy

July 2026

Glasgow, Scotland

SGRÙDADH DEUCHAINNEIL AIR ÈABHLAID NEART GRÙTA SILICE CHOLLOIDEACH RÈ CIÙRAIDH AGUS ATH-SLÀNACHAIDH, AGUS AIR ATHARRACHADH LE CRIADHAN AGUS POILIMEARAN

le

Daibhidh Uilleim Moireasdan

Teusas ga chur a-steach do Roinn na h-Innleadaireachd Togalaich is Àrainneachail de dh'Oilthigh Shrath Chluaidh ann an riarachadh de dh'fheumalachdan a' cheuma

Dotair ri Feallsanachd

An t-Iuchar 2026

Glaschu, Alba

Declaration

I hereby declare that the work presented in this thesis has not been submitted for any other degree or professional qualification, and that it is the result of my own independent work.

David William Thomas Morrison

09/07/2026

Date

Abstract

Colloidal silica (CS) is a novel, environmentally friendly grout with water-like viscosity and nano-scale particle size, which forms rigid gels with low hydraulic conductivity in precisely controllable durations. CS grout has great promise as an injectable barrier and soil stabiliser in a range of fields, but its large-scale application has so far been limited. This thesis presents an experimental investigation into the process by which CS grout increases in strength during curing, and the factors which affect it, and it is also the first work to study the re-healing ability of CS grout, and its combination with clays and polymers.

Shear vane and compression tests found the strength of CS grout and grouted soil to increase with curing time via power laws, with this attributed to continuous deposition and condensation of silicates at joining points between particles in the network. Samples of each were also found to re-heal after breaking before increasing in strength again, although at a slowed rate. After breaking, gel fragments are proposed to quickly re-connect due to the continued presence of the original gelation conditions, before gaining strength again through a similar mechanism to that in curing. Higher silica mass fraction, NaCl concentration, and smaller particle size each increased the strength of the grout, and adding NaCl could be used to offset loss in strength from small reductions in silica content. Higher ionic strength in water surrounding samples gave a linear increase in their strength, and those cured in fresh water were relatively weaker due to diffusion of ions out of the grout. Surrounding water at pH 9 also gave higher strength than pH 7; it is suggested that electrolyte and alkaline conditions reinforce the gel by promoting redistribution of silica to weak points in the network by increasing its solubility. Additional CS in surrounding water also strengthened samples, as the added silica could be presumably be redistributed onto the existing gel network. Secondary injection of alkaline salt solution, or additional CS, could therefore be used to increase grout strength after application, or to promote re-healing.

Adding kaolin and bentonite clays each increased CS's viscosity and accelerated its gelation, but bentonite had a stronger effect due to its swelling behaviour. Kaolin increased the strength of CS grout, although it had less effect than varying silica content;

it could therefore be used to partially replace mass of silica to lower costs, with a small reduction in strength.

Polyethylene glycol (PEG), polyacrylamide (PAM), and polyvinyl alcohol (PVA) were combined with CS to produce novel gels. CS/PEG variants were identified which deformed plastically and dried without cracking, with potential for use as impermeable barriers, as well as other variants which had improved water retention. PAM gels using the crosslinker polyethylenimine had high flexibility but were difficult to combine with CS due to agglomeration of silica. CS/PVA variants were produced which were soft and plastically-deformable, providing crack resistance, or that were condensed, likely with lower hydraulic conductivity and greater strength. Ultra-strong and flexible PVA and CS/PVA gels were also created via drying and freeze-thaw methods.

Geàrr-chunntas

'S e grùta ùr a th' ann silice cholloideach (SC) a tha math dhan àrainneachd, le tiughad mar uisge agus meud-mìrein nano-sgèileach, a chruthaicheas shiligean raga le treòrachd-hiodrolach ìosal ann an ùineachan mion-smachdach. Tha gealltanas mòr aig SC mar bhachadh in-steallach 's seasmhaiche-ùire ann an iomadach raon, ach tha a cleachdadh gu ruige seo cuingichte. Taisbeanaidh an teusas seo sgrùdadh probhail den phròiseas tron neartaich grùta SC rè a chiùraidh, 's na factaran a riaghaileas e, agus sgrùdaidh e airson na ciad uarach a chomas ath-slànachaidh 's a cho-mheasgachadh le criadhan is polimearan.

Lorg deuchainnean fiaraidh is co-bhrùthachaidh gun do dh'fhàs neart grùta SC 's ùir ghrùtaichte thairis air ùine a rèir laghan cumhachd, le seo air a chur às leth do thasgadh is cho-dhlùthachadh leantainneach de shiliceatan aig àitean ceanglaidh eadar mìreanan anns an lìonra. Shealladh gun do dh'ath-slànaich sampallan den dà sheòrsa às dèidh am bristidh, mus do neartaich iad a-rithist, ach aig reat na bu shlaodaiche. Thathar a' cur air adhart gun ath-cheangail bloighean lìonraidh gu luath às dèidh bristeadh ri linn làithreachd maireannach nan tomhnaidhean siligidh tùsail, mus neartaich an siligean a-rithist tro mheadhan coltach ri ciùradh. Dh'àrdaich uireadan de shilice 's NaCl na bu mhotha, agus meud-mìre na bu lugha neart a' ghrùta, agus ghabhadh NaCl a chleachdadh gus an call neirt bho lùghdachaidhean beaga ann am meud silice fhrith-chothromachadh. Dh'adhbharaich neart-idheonach na b' àirde ann an uisge timcheall air sampallan meudachadh loidhneach ann an neart, agus chaidh an fheadhainn a chiùradh ann am fìor-uisge a lagachadh ri linn lìonsgaradh de dh'idheonaichean às a' ghrùta. Thug uisge cuairteachaidh aig pH 9 neart na bu mhotha na pH 7; thathar a' moladh gun daingnich salainn agus tomhnaidhean alcaileach an siligean le bhith a' brosnachadh ath-sgaoileadh silice gu àitean laga anns an lìonra mar thoradh air a h-eadar-sgaoileachd àrdachadh. Neartaich cuideachd tuilleadh silice ann an uisge cuairteachaidh sampallan, o choinn 's gur mathaid gun deigheadh an t-silice a bharrachd ath-riarachadh air lìonraidhean nan siligean. Rachadh in-stealladh dàrnach de dh'eadar-sgaoileadh salainn alcaileach, no tuilleadh SC, a chleachdadh, mar sin, gus an grùta a neartachadh às dèidh a chur an gnìomh, air neo gus ath-slànachadh a bhrosnachadh.

Dh'àrdaich cur ris an dà chuid chriadhan caoilin 's beantonait tiughad SC, 's luathaich iad a siligeadh, ach bha buaidh na bu làidire aig beantonait air sgàth a feart bòcaidh. Mheudaich caoilin neart grùta SC, ach bha buaidh na bu lugha aige na bhith ag atharrachadh an uireid de shilice; rachadh a chleachdadh, mar sin, a leth-dhol an àite tomad silice gus cosgais ìsleachadh, le lughdachadh beag ann an neart.

Chaidh gliocol poili-eitilein (PEG), poili-acriolamaid (PAM), is alcol poili-bhinil (PVA) a cho-mheasgachadh le SC gus siligein ùra a chruthachadh. Dh'aithnicheadh eug-samhailean SC/PEG a mhì-dhelabhaich gu plastaigeach 's a thiormaich gun sgàineadh, le comas airson cleachdadh mar bhacaidhean neo-dhrùidhteach, agus feadhainn eile le glèidheadh uisge na b' fheàrr. Bha sùbailteachd àrd aig siligein PAM a chaidh a dhèanamh leis a' chrois-cheanglaiche poili-eitileinimean, ach bha iad doirbh co-mheasgachadh le SC air sgàth binndeachadh silice. Chaidh eug-samhailean SC/PVA a dhèanamh a bha bog 's mì-dhealbhaichte gu plastaigeach, a' solar comhaireachd do sgàineadh, air neo a bha cho-dhlùthaichte, le coltas gun robh treòrachd-hiodrolach na b' ìsle 's neart na bu mhotha aca. Chaidh siligein SC/PVA ro-làidir is sùbailte a chruthachadh a bharrachd, le modhan tiormachaidh is reòthadh-aiteamh.

Publications Associated with This Research

Morrison, D., Pedrotti, M., Lunn, R., Draper, E., & Graham, J. (2022, March 6-10). *Modifying Colloidal Silica Grout for Nuclear Decommissioning Applications* WM2022 Conference, Phoenix, AZ, USA.

Morrison, D. W. T., Pedrotti, M., Lunn, R. J., & Draper, E. R. (2026). *An Experimental Investigation on the Effect of Grout Composition and Curing Conditions on the Strength of Colloidal Silica Grout* [Unpublished manuscript]. University of Strathclyde.

Acknowledgements

I would like to first express my sincere gratitude to my academic supervisors Dr Matteo Pedrotti, Prof Rebecca J Lunn, and Prof Emily R Draper, whose advice and support was instrumental to my work.

I would also like to thank my industrial supervisor Dr James Graham, and everyone at the Nuclear Decommissioning Authority (NDA) and United Kingdom National Nuclear Laboratory (NNL) for all that I learned, and the connections I made through various fascinating conferences and site visits.

I also gratefully acknowledge the funding I received from the NDA, the Scottish Research Partnership in Engineering (SRPe), and the University of Strathclyde.

Furthermore, I would like to thank all of the technical staff, academics, and my fellow PhD students at the University of Strathclyde's Department of Civil and Environmental Engineering (and beyond) who assisted, guided, supported, and endured me over the years, including (but not limited to) Lucas, Maria-Giulia, Eve, Gea, Derek, Mara, Jim, and Gavin.

And finally, thank you to all of my friends in Scotland, Australia, and elsewhere, to my family, especially my Dad and my Nana, and above all to my partner Maria for bearing with me and keeping me going. Mo mhìle beannachd leibh uile.

Table of Contents

List of Figures

List of Tables

Glossary of Terms

Below is a glossary of technical terms used in this document. The symbol '*' refers to uses which are specific to this thesis.

Term	*Definition*
Accelerator*	Salt solution mixed with CS to initiate gelation.
Aggregation	Linking together of colloidal particles to form larger clusters.
Coagulation	Joining of colloidal particles into closely-packed clumps which then settle out as precipitate.
Colloid	A dispersion of insoluble particles of size 1–1 000 nm, such that the particles are too small to be affected by gravity.
Colloidal silica	Stable dispersion of amorphous silica particles in a liquid solvent.
Colloidal silica grout*	Gelling or gelled mixture of colloidal silica and accelerator.
Co-ion	An ion with like charge to a charged surface
Counter-ion	An ion with opposite charge to a charged surface
Curing*	The process of gelled CS grout increasing in strength over time.
Curing time*	Time from when CS and accelerator are mixed until the sample is mechanically tested or broken for the first time.
Curing water*	Solution in which a sample is immersed while curing.
Debye length	Distance over which an electrostatic potential decays in an electrolyte solution due to ionic screening. Representative of the 'thickness' of the electric double layer.
Diffuse layer	Loosely associated outer layer of ions around a colloidal particle, which decay exponentially in concentration with distance.
Electric double layer	Layer of counter-ions which surrounds a colloidal particle with surface charge: composed of the Stern and diffuse layers.
Flocculation	Linking of colloidal particles by 'bridges' of a flocculating agent which are long enough such that aggregated structures remain open and voluminous.
Gelation	Linking of colloidal particles or monomers into branched chains which eventually form a three-dimensional network spanning the full volume of the original mixture.
Gel time*	Time it takes for a sample to gel, defined by the protocols in 3.3.1 and 3.3.2.
Dispersion	Heterogeneous mixture in which particles of one substance are evenly distributed throughout another.
Healing time*	Time between a sample being broken and a final mechanical test.
Hydrogel	Substance with a coherent network of branched chains which, by capillary action, retains a liquid in its pore-spaces.
Isoelectric point	pH at which the zeta potential of a colloidal particle is zero.
Point of zero charge	pH at which the net surface charge density of a colloidal particle is zero.
Polymer	Long chain molecules which comprise of many repeating units, called monomers.

Radius of gyration	The root-mean-square distance of all of a dispersed polymer's segments from its centre of mass.
Sample age*	Total duration since CS and accelerator were mixed for a sample, encompassing curing and healing times.
Slipping plane	Boundary inside of which molecules of a dispersing liquid are bound to a colloidal particle, as opposed to flowing freely, as in the bulk.
Sol	Dispersion of solid colloidal particles in a liquid.
Solution	Homogeneous mixture in which one substance (the solute) is completely dissolved in another (the solvent) at the molecular or ionic level.
Specific surface area	Surface area per unit mass of a material.
Stern layer	Inner layer of immobile counter-ions tightly bound to a colloidal particle's surface,
Suspension	A dispersion of solid particles in a fluid, where the particles are large enough (> 1 μm) to eventually settle out due to gravity.
Xerogel	Desiccated hydrogel whose network has shrunk and collapsed.
Zeta potential	The difference in electric potential between the slipping plane and a point at an infinite distance from a colloidal particle.

List of Acronyms

Below is a list of acronyms used throughout this document.

Acronym	*Definition*
AGF	Artificial ground freezing
ccc	Critical coagulation concentration
CS	Colloidal silica
DI	Deionised (water)
DGR	Deep geological repository
EDL	Electric double layer
IEP	Isoelectric point
IIC	Ion-ion correlation
ITZ	Interfacial transition zone
MBAm	Methylene-bis-acrylamide
PAM	Polyacrylamide
PEG	Polyethylene glycol
PEI	Polyethylenimine
PMHS	Polydimethylsiloxane
PVA	Polyvinyl alcohol
pzc	Point of zero charge
P&A	Plug and abandonment
SANS	Small-angle neutron scattering
SAXS	Small-angle x-ray scattering
SEM	Scanning electron microscopy
SSA	Specific surface area
UCS	Unconfined compressive strength

Chapter 1: Introduction

1.1 Background

Grouts are fluid-like materials which harden after application to perform a desired function (Nonveiller, 1989). In civil engineering, grouts can be injected subterraneously to increase the strength and density of soils, fill fissures in rock or concrete, or to manage the flow of water or contaminants by acting as a barrier (Warner, 2004). Conventionally, cements have been used for grouting, but they are limited in a number of key ways; for example, the high viscosity and particular rheology (generally modelled as a Bingham fluid) of most cements means that they require high pressures to be injected, which can induce ground heave (Chai et al., 2005; Funehag & Gustafson, 2008a), and their large particle sizes give them comparatively poor penetration (Karol, 2003). Cements are also caustic, toxic, and carcinogenic; their high pH can affect local ecosystems; and the CO_2 given off during cement production makes it a major contributor to climate change (Miller et al., 2016). There is, therefore, significant interest in the development of novel grouting materials (Northcroft, 2006; Sögaard, Funehag, & Abbas, 2018; Spagnoli et al., 2025).

Since the 1990s, colloidal silica (CS) grout has been investigated, and more recently employed, as one such alternative material. CS is a novel chemical grout which begins as a low-viscosity liquid before transitioning to a rigid gel in situ, after application; it is environmentally friendly and non-toxic (Gallagher et al., 2013), with nano-scale particle size, and precisely controllable gelation time (Iler, 1979; Moridis et al., 1995; Pedrotti et al., 2017; Persoff et al., 1995; Yates, 1990). These properties allow it to be easily injected into soil at minimal pressure to fill free pore space without presenting any risk of ground heave: this type of grouting is called permeation grouting (Fraccica et al., 2022). The gel CS grout produces has very low hydraulic conductivity (Moridis et al., 1996; Pedrotti et al., 2020), which has led to its research and occasional application in a variety of fields, such as for preventing ingression of water in tunnelling and underground construction (Ashcroft et al., 2025; Bahadur et al., 2007; Butrón et al., 2010; Funehag & Fransson, 2006; Funehag & Gustafson, 2008b; Haugsand et al., 2025; Holter & Hognestad, 2012; Holter et al., 2025; Tsuji et al., 2014; Tsuji et al., 2017), for water shut-off and conformance control in oil reservoirs (Al-Moshin et al., 2022; Ali, Al Ramadan, & Aljawad, 2024; Ali, Al

Ramadan, Aljawad, et al., 2024; Ali, Alabdrabalnabi, et al., 2024; Almoshin et al., 2025; Ghaffari et al., 2022; Huang et al., 2017; Jurinak & Summers, 1991a), and as an injectable hydraulic barrier material at contaminated sites (Hakem et al., 1997; Lunn et al., 2018; Manchester et al., 2001; Moridis et al., 1996; Moridis et al., 1999; Moridis et al., 1997; Moridis et al., 1995; North-Abbott et al., 2001; Pedrotti et al., 2020; Persoff et al., 1999; Persoff et al., 1995; Wong, 2021). CS grout also provides mechanical improvement to loose and weak soils and has been investigated and employed for soil stabilisation and increasing resistance to liquefaction (Bakhshandeh et al., 2025; Birid & Varak, 2024; Ciardi et al., 2020; Conlee, 2010; Gallagher et al., 2007; Gallagher & Finsterle, 2004; Gallagher & Lin, 2009; Gallagher & Mitchell, 2002; Ghadr et al., 2020; Huang & Wang, 2016; Krishnan et al., 2021; Sharafutdinov et al., 2024; Spagnoli et al., 2024; Terui et al., 2025). Furthermore, CS grout's good sorption properties have led to research on its use as a chemical barrier for trapping contaminants via sorption (Bots et al., 2020; Hakem et al., 1997; Hölttä & Hakanen, 2008; Hölttä et al., 2009; Yossapol, 2002). Unlike other chemical grouts, CS grout is relatively affordable, does not exhibit syneresis or volume change, is environmentally inert, and contains no toxic components (Chang et al., 1994; Gallagher et al., 2013; Jurinak & Summers, 1991a; Northcroft, 2006).

In spite of its excellent properties and potential, however, wide-scale application of CS grout has thus far been limited. This is likely, in part, due to its lower strength in comparison to cements, it's higher material cost (calculated by Gallagher et al. (2013) as ~ 2.7× greater), and the lack of a comprehensive understanding of its gelling behaviour, transport, and long-term stability in soils, acquired through empirical evidence and accurate models (Pedrotti et al., 2026; Pedrotti et al., 2017).

1.2 Thesis overview

This work presents an experimental investigation into factors governing the strength evolution of CS grout over time, termed here its curing, and the physical mechanisms which drive the process. The factors in question relate to both the composition of the grout, for example, its electrolyte content and silica mass fraction, as well as the nature of its curing environment, such as the electrolyte content of surrounding groundwater. Where the composition of the grout was changed, the effect this had on the gelation also had to be understood.

Also presented here is the first study known to the author on the ability of gelled CS grout (and CS-grouted soil) to re-heal after suffering damage; this is a property not found in conventional grouting materials which may provide CS grout with previously unconsidered resilience in all applications.

The effect of adding clays to CS grout on its gelation, strength evolution, and re-healing, was also studied; clays such as bentonite have desirable properties, such as very low hydraulic conductivity and high sorption capacity, which could be beneficial to impart into CS grout (Sobti & Singh, 2017; Vinšová et al., 2008). Replacing mass of silica in the grout with clay may also allow for reduction in material cost while maintaining mechanical strength.

Finally, the possibility of combining CS grout with various polymers and polymer hydrogels was investigated. Polymer hydrogels are highly modifiable materials which can be made to be super-strong, flexible, and re-healable (Fan et al., 2020; Tanaka et al., 2005): they have been the object of intensive research in medical fields (Caliari & Burdick, 2016; Li & Mooney, 2016; Mantha et al., 2019), but have rarely been considered for large-scale engineering application. Incorporation of these favourable properties into CS grout could be of great benefit to its application.

In these investigations, the effect of the different factors and additives on CS grout were investigated through the following tests: viscometer measurements were employed to study viscosity evolution and gelation, and shear vane and unconfined compressive strength (UCS) tests were used to measure the strength evolution during curing and re-healing of gelled CS grout and grouted soil. Scanning electron microscopy (SEM) was also performed to examine the structure of certain samples. Furthermore, for investigating the interaction and gelation of polymers, solid-state tests were used, with rheometer tests undertaken on particular samples of interest to evaluate mechanical properties.

1.3 Research aims

The aims of this research were as follows:

- To develop the understanding of how grout properties and environmental conditions impact the gelation, curing, and re-healing of CS grout, and to propose conceptual models which describe the physical mechanisms behind these

processes: this will allow grout compositions to be tailored to specific requirements and applications.

- To study the impact of adding clays on the viscosity, gelation, strength evolution, and re-healing of CS grout; to assess the feasibility of the technique; and to determine if it can be used to increase strength and/or reduce cost.
- To identify candidate polymers and polymer gelation techniques which may be suitable for application in combination with CS grout; to investigate how the polymers interact with CS; to successfully produce polymer hydrogels; and to simultaneously gel CS grout and polymers to form double-network gels.

1.4 Thesis structure

This thesis has been arranged into the following chapters:

- **Chapter 2: Literature Review.** Background theory on CS grout is provided, along with a review of research relevant to the present investigation, and a brief history on the application of CS grout, identifying gaps in knowledge, and opportunities for improvement in applicability.
- **Chapter 3: Methodology.** The various materials employed in this investigation are outlined, as well as the methods employed for sample preparation, and the experimental procedures.
- **Chapter 4: Effect of Grout Composition & Curing Conditions on the Strength Evolution of CS Grout.** Viscometer tests investigate how grout properties affect the gelation of CS grout. Shear vane tests demonstrate how the same factors, as well as environmental conditions, impact the evolution in the grout's shear strength during curing. UCS tests on CS-grouted sand provide a point of comparison for the shear vane tests, and increase their relevance to grouting application. SEM imaging then examines the microstructure of grout samples.
- **Chapter 5: The Re-healing Ability of CS Grout.** Shear vane tests demonstrate the re-healing ability of CS grout and determine how various factors affect re-healing behaviour. UCS tests then investigate re-healing in CS-grouted sand.
- **Chapter 6: Adding Clay to CS Grout.** Viscometer and shear vane tests are carried out on CS grout with kaolin and bentonite clays added to determine their impacts

on gelation and mechanical properties. UCS tests are then undertaken on sand grouted with CS/kaolin mixtures.

- **Chapter 7: Combining CS grout with Polymers.** A literature review identifies three candidate polymers, plus associated gelation systems, for combination with CS grout. An experimental investigation then studies how the different polymers interact with CS, create polymer hydrogels, and produce various CS/polymer nanocomposite gels. Rheometer tests on different gels of interest are carried out, and UCS tests conducted on sand grouted with particular polymer gel mixes.
- **Chapter 8: Discussion.** The results of the investigations are discussed, with conceptual models proposed to explain the mechanisms behind CS grout curing and re-healing, how the factors and additives studied here impact the processes, and what the findings mean for the practical application of CS grout. The feasibility of adding clays and combining with polymers is also discussed in relation to the practical application of the grout.
- **Chapter 9: Conclusion.** The main findings of the investigation are summarised, with recommendations made for future work and practical deployment.

Chapter 2: Literature Review

2.1 Introduction

This chapter presents a review of literature on CS grout. A background on the theory of CS is first provided, along with summaries of recent research relevant to this investigation, and the history of CS grout's application. Gaps in knowledge and opportunities for further application are also identified. This chapter deals only with CS grout: a background on the clays used in this investigation is provided in section 6.2, and a literature review on polymers and polymer hydrogels can be found in section 7.2.

2.2 Colloidal silica

A colloid is a mixture in which insoluble particles of size on the order of 1–1 000 nm of one substance (the dispersed phase) are evenly distributed throughout another substance (the continuous phase). Sols are a variety of colloid in which solid particles are dispersed in a liquid phase. Colloidal silica, also known as silica sol, is a stable dispersion of amorphous silica (SiO_2) particles in a liquid solvent (Bergna & Roberts, 2006; Blute et al., 2007; Iler, 1979). CS is commercially available with a variety of particle sizes, pHs, and silica particle concentrations, in both aqueous and organic solvents, but it is most commonly found in the ranges of 15-50 wt% silica particles, of size 5-100 nm, in alkaline aqueous solution of pH 9-10.5. It takes the form of a low-viscosity liquid of colour ranging from transparent and colourless to opaque white, depending on the size and mass fraction of silica particles. CS used in grouting applications is conventionally gelled by mixing with a salt solution called the 'accelerator', usually NaCl; in this work, the gelling mixture of CS and accelerator is referred to as CS grout.

2.2.1 Chemistry and structure

The internal structure of CS particles, shown in Figure 2.1, comprises of an amorphous network of covalently bonded oxygen and silicon atoms with tetrahedral structure defined by the structural unit $[SiO_4]^{4-}$ (Iler, 1979). The surfaces of particles, however, are covered in large part by silanol (SiOH) groups. Silanol has a tendency to dissociate in aqueous solution, acquiring electric charge; the number of silanol groups which dissociate, the nature of their dissociation, and therefore the total surface charge of CS particles, depends on the pH of the surrounding solvent. The reactions which govern this effect are as follows:

$$SiOH \leftrightarrow SiO^- + H^+, \quad (2.1)$$

and

$$SiOH + H^+ \leftrightarrow SiOH_2^+, \quad (2.2)$$

where reaction 2.1 prevails within the range pH 2-12, and 2.2(2.2 at pH < 0, meaning that silanol is slightly acidic under most conditions (Duval et al., 2002; Leroy et al., 2013; Sonnefeld et al., 2001; Sverjensky, 2005). Commercial CS typically has pH high enough to generate sufficient mutual negative repulsion between particles, via deprotonation of silanol to SiO^-, to maintain the stability of the colloid towards aggregation. The pH at which the surface charge is zero is called the point of zero charge (pzc).

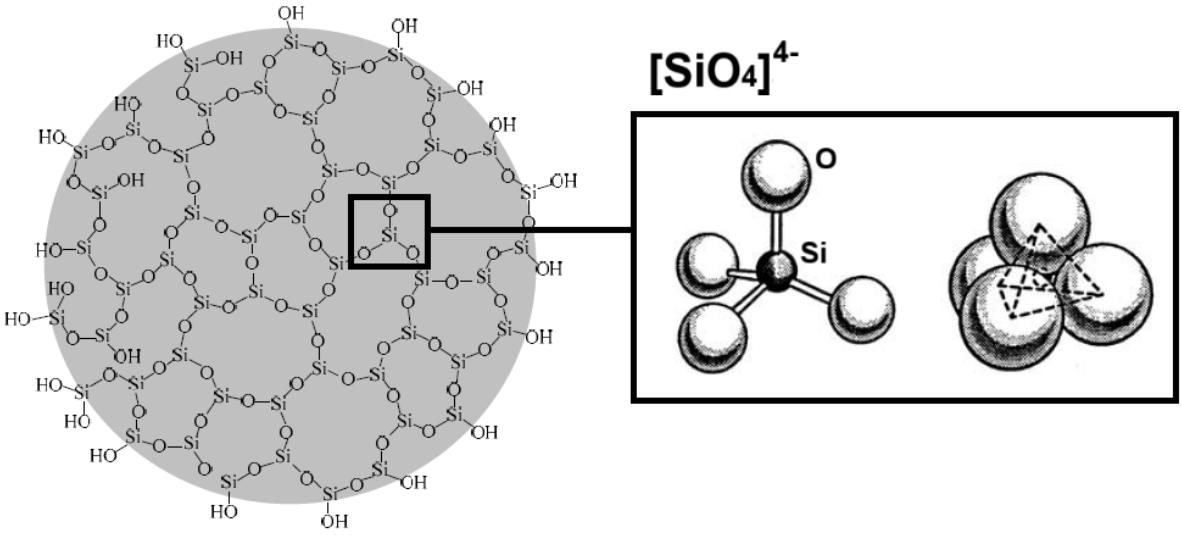

Figure 2.1. 2D representation of a CS particle, showing the amorphous silica interior, and surface silanol groups, from M. Zhao et al. (2019). Highlighted is a single tetrahedral structural unit, $[SiO_4]^{4-}$, adapted from Bergna and Roberts (2006).

Beyond the surface of each silica particle, there exists an electric double layer (EDL), consisting of the Stern layer of immobile counter-ions adsorbed to the particle surface, and the diffuse layer, a loosely bound cloud of ions around the particle which decay exponentially in concentration with distance (Bergna & Roberts, 2006; Iler, 1979). Within the diffuse layer, the 'slipping plane' defines the boundary inside of which molecules of the dispersing liquid are bound to the particle, as opposed to flowing freely, as in the bulk (Mahanty & Ninham, 1976). The zeta potential is the potential difference between the slipping plane and a point at an infinite distance from the particle, and it can be measured by electrophoresis. The counter-ions of the EDL partially screen the surface charge of the particle, causing its electric potential to decay exponentially with distance, rather than by

the inverse square law (Park & Seo, 2011). The Debye length represents the thickness of the EDL and depends on the temperature and electrolyte content of the solvent. A representation of the EDL is provided in Figure 2.2.

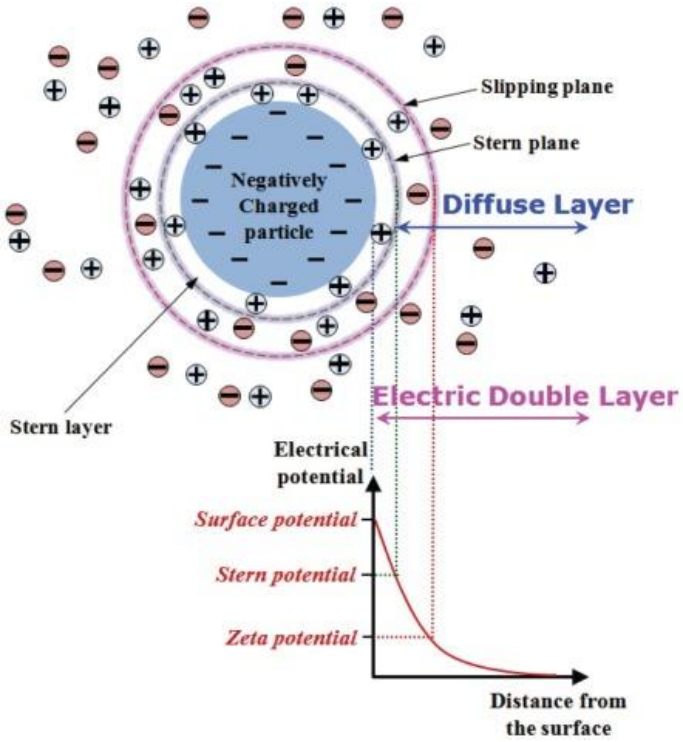

Figure 2.2. Representation of the EDL of a negatively charged colloidal particle, showing the inner Stern layer of adsorbed counter-ions, the outer diffuse layer of ions, and the slipping plane. The graph shows the exponential drop-off in the magnitude of electric potential from the particle surface. From Park and Seo (2011).

2.2.2 Stability and aggregation

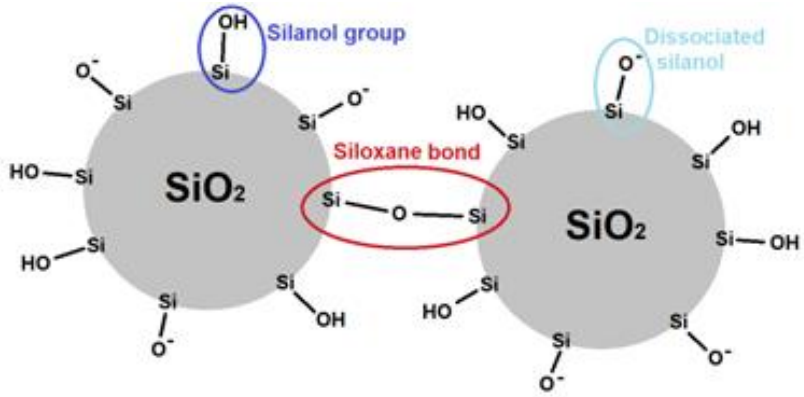

Figure 2.3. Formation of a siloxane bond (red) between two CS particles. Also highlighted is a surface silanol group (dark blue), and another which has become deprotonated/dissociated (light blue).

According to DLVO theory, the stability of a colloid depends on repulsive inter-particle forces overpowering attractive van der Waals forces (Derjaguin & Landau, 1941; Verwey,

1947). As CS conventionally relies on mutual electrostatic repulsion of particles, it can therefore become destabilised by changes in the electrostatic environment of the solvent which depress this force, such as by varying pH, or adding electrolyte (Baxter & Bryant, 1952). If mutual repulsion is reduced, particles may approach close enough to collide. Iler (1979) states that, upon contact, covalent siloxane bonds (Si-O-Si) can form between particles, as shown in Figure 2.3, causing them to adhere. The siloxane bonds are formed via the condensation of surface silanol groups,

$$\mathrm{SiOH} + \mathrm{SiOH} \rightarrow (\mathrm{Si} - \mathrm{O} - \mathrm{Si}) + \mathrm{H_2O}, \qquad (2.3)$$

with the reaction catalysed by the presence of hydroxide ions ($\mathrm{OH^-}$).

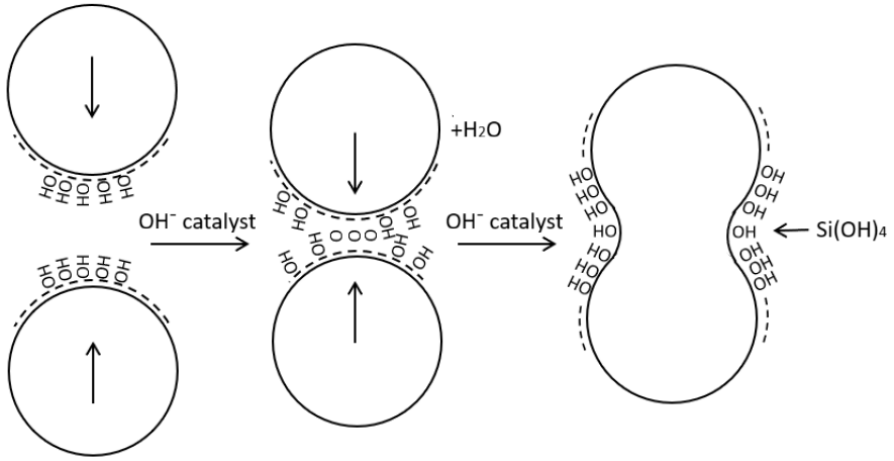

Figure 2.4. *Left to right:* Collision and siloxane bond formation between two CS particles via condensation of surface silanol groups, catalysed by dissolved hydroxide ions. Deposition of silicates then occurs at the contact point, creating a neck. Adapted from Iler (1979).

Further to this, however, at the point where the two spherical particles contact, there exists a negative radius of curvature, at which the solubility of silica is very low; this is a consequence of the Gibbs-Thomson effect for the chemical potential energy of curved surfaces (Hulett, 1926). Iler (1979) proposes that monomers of dissolved silicate are instantly deposited at this point, resulting in a 'neck' forming between the particles, as shown in Figure 2.4. From this point, particles may continue to link together into larger groups, called aggregates: these have reduced mobility compared to CS nanoparticles, thereby causing an increase in viscosity (Carroll et al., 2002). CS can aggregate in a few different ways, leading to different outcomes; the most relevant of these are described in the following subsections (2.2.2.1 and 2.2.2.2), with an illustrative diagram provided in Figure 2.5.

2.2.2.1 Coagulation & flocculation

Coagulation occurs when particles join together into closely-packed clumps, in which they are more concentrated than they were in the original sol. These 'coagula' then settle out as relatively dense precipitate (Bergna & Roberts, 2006; Iler, 1979). Flocculation, on the other hand, occurs when particles are linked by 'bridges' of some flocculating agent which are long enough such that aggregated structures remain open and voluminous. In concentrated CS, however, it is generally not possible to distinguish between coagulation and flocculation. Unlike a gel, precipitate from coagulation or flocculation encloses only part of the liquid in which it was formed.

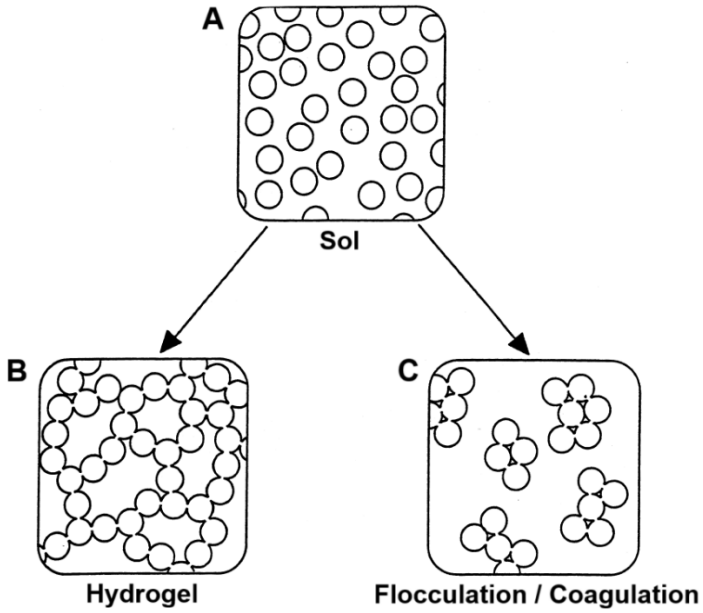

Figure 2.5. Schematics showing the structure of a CS sol (*A*), a hydrogel with its branched network (*B*), and precipitate from flocculation or coagulation, which forms dense clusters of particles. Adapted from Bergna and Roberts (2006).

2.2.2.2 Gelation

In the case of gelation, aggregates grow as branched chains which eventually form a three-dimensional network spanning the full volume of the original sol, as shown in the diagrams in Figure 2.6 (Abdelfatah, 2018; Dietler et al., 1986). On initiating gelation, CS remains at low viscosity for an extended duration, which Hunt et al. (2013) call the 'induction period'. Once the particle chains encompass ~ 0.5 of the total volume, however, the viscosity of the mixture rises rapidly, resulting in a sharp change in viscosity observed around the gel time, highlighted in the viscosity plot in Figure 2.6 (Audsley & Aveston, 1962; Iler, 1979). During gelation, the concentration of silica particles in any particular macroscopic region does not vary from that of the original; instead, the medium simply

increases in viscosity until it solidifies with a coherent network which, by capillary action, retains the liquid: the resulting substance is called a hydrogel (Iler, 1979).

A range of factors may influence the gelation rate of CS, including temperature, pH, electrolyte content, and the silica mass fraction. The effects of these factors are described in the following subsections (2.2.2.3-2.2.2.6). Control of these factors allows CS grout gel times to be precisely tailored within a range of minutes to days (Iler, 1979; Yates, 1990).

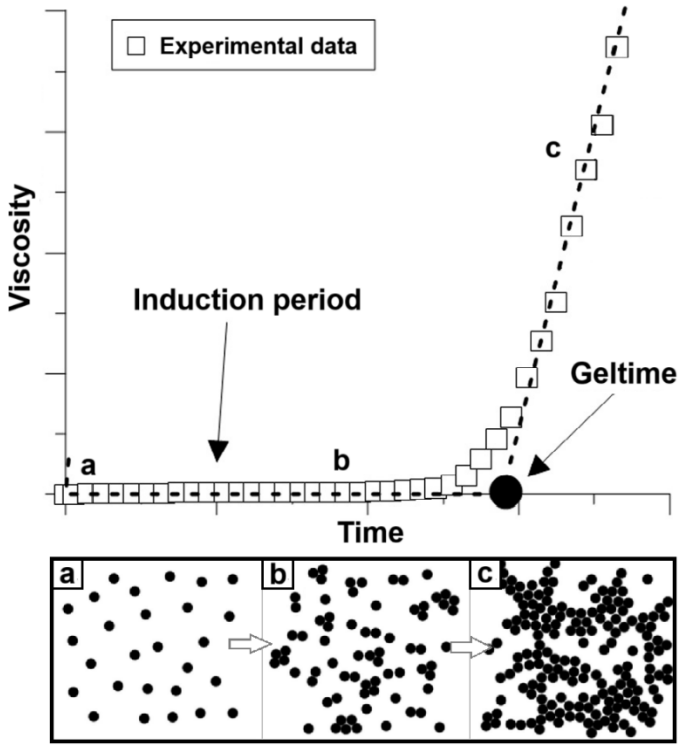

Figure 2.6. Example plot of the viscosity of CS during gelation. Below are diagrams illustrating the transition of CS from a dispersion of individual silica particles into one of larger aggregates, and finally to a fully-encompassing network. The diagrams are linked to points in time on the viscosity graph. Adapted from Pedrotti et al. (2017) and Sögaard, Funehag and Abbas (2018).

2.2.2.3 Effect of pH

A plot describing how pH affects the stability, and, by extension, the gel time of CS is provided in Figure 2.7B, based on DLVO theory. The rate of gelation of CS depends on both the frequency of collisions between particles, and the rate of siloxane bond formation, both of which vary with pH (Iler, 1979). From the figure, it can be seen that gel time is at a minimum around pH 6, and that raising pH beyond this gives continually increasing gel time until stability is eventually achieved in the region of pH 8-11 (in the absence of dissolved electrolyte). This effect is caused by rising negative surface charge of CS particles generating increasing mutual repulsion, which raises the potential barrier

that approaching particles must overcome in order to contact, thereby decreasing the frequency of successful collisions (Iler, 1979). Figure 2.7A shows the zeta potential of CS with pH, which becomes increasingly negative as pH approaches 11 (Xu et al., 2006). At ≳ pH 11, the silica particles start to dissolve due to growing solubility of silica: this eventually destroys the sol (Iler, 1979).

As pH decreases, however, the concentration of hydroxide ions decreases; as mentioned in 2.2.2, hydroxide acts as a catalyst for siloxane bond formation (Iler, 1979). Below the pH 6 stability time minimum, the decreasing concentration of hydroxide ions inhibiting the polymerisation of silica particles becomes the dominant factor, causing an increase in gel time, proportional in the range pH 3-5 (Jurinak & Summers, 1991a), up to a metastable region around pH 2: this corresponds to the isoelectric point (IEP) of CS (see Figure 2.7A), at which zeta potential is zero, and it lies in the range pH 2-4, depending on the variety of CS (Bolt, 1957; Jurinak & Summers, 1991a; Trompette & Clifton, 2004; Xu et al., 2006). Below this pH, gel time again decreases. Gallagher (2000) found the gel time minimum of CS to lie in the range pH 5-7.

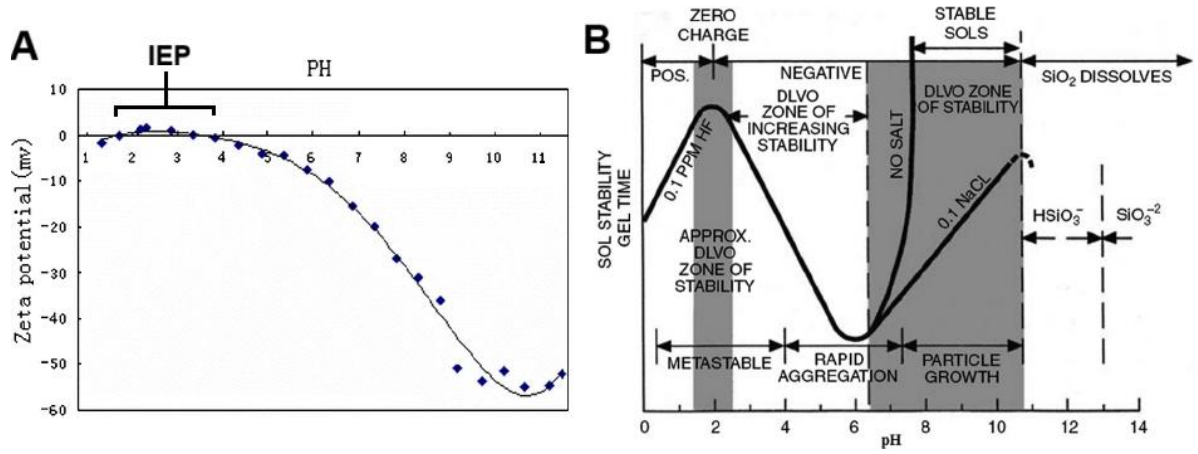

Figure 2.7. *A:* Effect of pH on the zeta potential of CS, from Xu et al. (2006). *B:* Effect of pH on the stability and gel time of CS, from Iler (1979).

2.2.2.4 Effect of electrolyte

Gelation of CS in grouting applications is conventionally induced by mixing with salt solution prior to application (Sögaard, Funehag, & Abbas, 2018). As the electrolyte concentration in CS rises, the number of counter-ions in particle double layers increases, thereby increasing the degree of surface charge screening, and reducing the Debye length of particles (Travesset & Vangaveti, 2009; Zhang et al., 2011). At a particular concentration of an electrolyte, called the critical coagulation concentration (ccc), the

Debye length becomes sufficiently depressed to allow particles to contact, allowing inter-particle bonding to occur and aggregation to proceed. A diagram illustrating this process is provided in Figure 2.8. Increasing electrolyte concentration can be reliably used to reduce CS gel times up to a point, but at very high concentrations, rapid coagulation occurs (Bergna & Roberts, 2006; Sögaard, Funehag, & Abbas, 2018). As well as concentration, the valency of ions in the electrolyte also impacts the rate of CS particle aggregation, as the greater charge of ions with higher valency increases their charge-screening effect (Allen & Matijević, 1969; Bergna & Roberts, 2006).

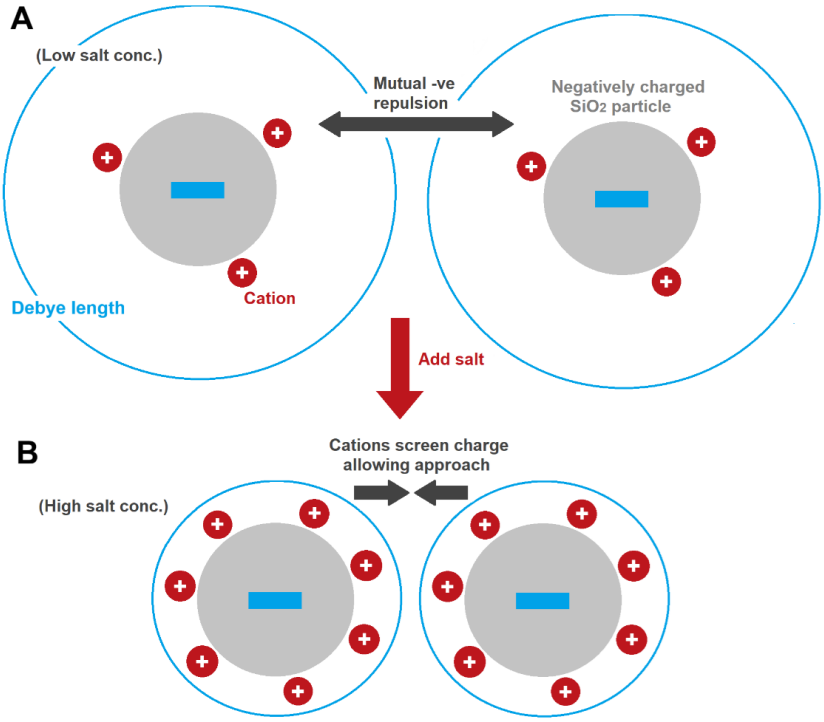

Figure 2.8. *A:* Diagram of CS at low electrolyte concentration, showing negatively charged silica particles with adsorbed cations in their Stern layers. The negative charges dominate, generating sufficient mutual repulsion to prevent particles contacting. Circles with radius of the Debye length, corresponding to the limit of the particles' electric fields, are shown in blue. *B:* After electrolyte concentration is increased, the number of cations in the particles' EDLs rises, increasing charge screening and depressing the Debye lengths, which allows the particles to approach close enough to contact and bind.

In addition to this, the particular species of ions in the electrolyte, beyond simply their concentration and valency, has also been shown to influence the gelling behaviour of CS (MacLachlan et al., 2013; Trompette, 2017; Trompette & Clifton, 2004; Trompette & Meireles, 2003; Van Der Linden et al., 2015; Yotsumoto & Yoon, 1993); this goes against an understanding purely based on DLVO theory. The nature of this ion-specific behaviour is complex and not fully understood, with both counter- and co-ions contributing

(Trompette, 2017). It is thought to depend on the hydration behaviour of the particular ions, as well as the silica surface: that is, how and to what extent they trap and structure surrounding water molecules, which impacts the ability of the ions to adsorb on particle surfaces, and the degree of their charge-screening effect (Sögaard, Funehag, & Abbas, 2018). Monovalent cations have been shown to follow the Hofmeister series in their effect on the stability and gelation of CS at pH well above the pzc (Van Der Linden et al., 2015): that is $NH^{+4} > Cs^{+} > Rb^{+} > K^{+} > Na^{+} > Li^{+}$, in order of least to most hydrated, or the most 'chaotropic' to the most 'kosmotropic', where the chaotropic ions have the greater effect on stability.

2.2.2.5 Silica mass fraction & particle size

Diluting CS grout to reduce its silica mass fraction slows its gelation as the reduced particle density decreases the frequency of inter-particle collisions (Basilio et al., 2025; Bergna & Roberts, 2006; Huang et al., 2017; Hunt et al., 2013; Iler, 1979; Jurinak et al., 1991b; Pedrotti et al., 2017). Contrastingly, reducing particle size accelerates gelation, as it both increases the number of particles, as well as smaller particles having greater kinetic energy in Brownian motion, increasing the likelihood that the potential barrier will be overcome during collisions (Bergna & Roberts, 2006; Huang et al., 2017; Iler, 1979; Jurinak et al., 1991b; Sögaard et al., 2023). Iler (1979) states that the effects of silica mass fraction and particle size are interdependent, with the rate of gelation of CS seemingly being proportional to the surface area per unit volume of the suspension, which both factors contribute towards. If this is true, CS mixtures with the same ratio of silica mass fraction to particle size would be expected to have the same gel times. In practice, it is not possible to use particle size to control the gel time of CS, as this is set by the manufacturer. CS may be diluted to reduce the silica mass fraction and increase gel times, but this also affects the strength of the resulting gel.

2.2.2.6 Temperature

Increasing the temperature of CS increases the average velocity and kinetic energy of silica particles, thereby increasing both the frequency of inter-particle collisions, and the likelihood that the potential barriers between them are overcome (Sögaard et al., 2023). As a result, the influence of temperature on the rate of gelling follows an Arrhenius relationship, with increasing temperature giving shorter gel times (Hunt et al., 2013)(Basilio et al., 2025). It is not generally practical to use the temperature of the grout,

or the ground into which it is injected, to control gel time; but it is an effect which should be accounted for.

2.2.3 Rheology

At the silica particle volume fraction at which most commercial CS is available (0.22-0.51), it behaves as a low-viscosity Newtonian liquid, meaning that its viscosity is independent of shear rate (Di Giuseppe et al., 2012). Shortly after gelling, CS behaves as a viscoelastic solid, meaning it has both viscous and elastic responses to applied shear. The gel becomes increasingly rigid over time, however, with its behaviour approaching that of an elastic solid (Katoueizadeh et al., 2021). Okazaki and Kawaguchi (2008) found higher rigidity of CS gels in the presence of the monovalent cations Li^+, Na^+, and K^+, in order of increasing effect. Under constant shear, CS gel has been observed to exhibit thixotropic behaviour, via shear thinning, which arises as a result of the network being broken (Metin et al., 2014). Once the shear is removed, however, the network has been found to recover (Katoueizadeh et al., 2021).

2.2.4 Gel strength and curing

The number of siloxane bonds which link silica particles is known to be a primary contributor to the strength of CS gels (Depasse & Watillon, 1969; Iler, 1979; Sögaard, Funehag, & Abbas, 2018). After gelation, CS grout continues to increase in strength over time in a process referred to as 'curing' in this work. In the field, CS-grouted soil has been observed to get progressively stronger for at least six months after treatment (Axelsson, 2006; Butrón et al., 2009). Mollamahmutoglu and Yilmaz (2010), Todaro (2021), Terui et al. (2025), Bakhshandeh et al. (2025), Boiero et al. (2026), and Cheng et al. (2022) reported the strength of CS-grouted sand to increase over time, and Pan et al. (2018) showed the same with compression tests on CS grout samples. The rate at which strength increases has been found to depend on the curing environment, with higher temperatures and lower humidities giving faster curing (Jurinak & Summers, 1991a). None of these papers comment on the underlying mechanism behind the strength increase.

In the field of silica-based aerogels, the increase in strength achieved by aging gels in water prior to drying is attributed to a mechanism presented in Iler (1979) (Ahmad et al., 2023; Hæreid et al., 1995; Iswar et al., 2017; Payanda Konuk et al., 2023; Smitha et al.,

2006; Soleimani Dorcheh & Abbasi, 2008). Here, the effect is said to arise from continuous deposition of dissolved silicates at the necks between particles, leading to the formation of additional siloxane bonds at these points, thus strengthening the network. A large part of these free silicates are thought to originate from dissolution of silica at particle surfaces where there is positive curvature, due to higher solubility at these points through the Gibbs-Thomson effect (Hulett, 1926), as well as from smaller particles in a form of Ostwald ripening (Bergna & Roberts, 2006; Iswar et al., 2017; Pantos & West, 1994; Payanda Konuk et al., 2023; Wijnen et al., 1991). The end result of this is that the branched particle chains take on the appearance of tube-like structures, with individual particles no longer apparent, as shown in Figure 2.9.

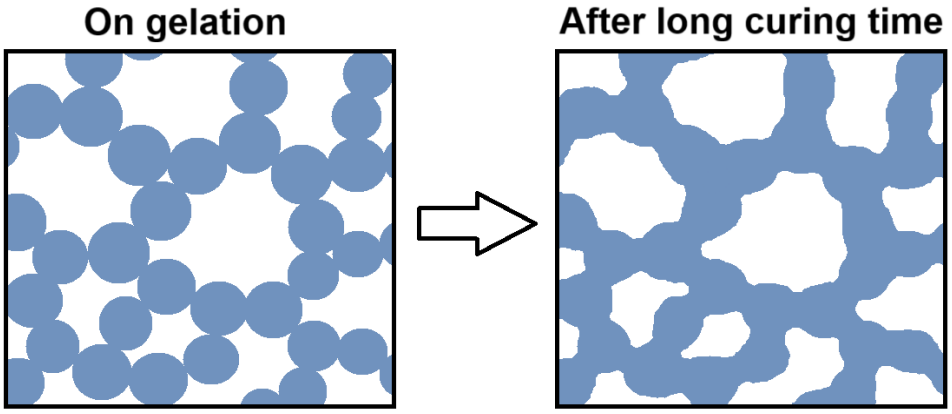

Figure 2.9. CS gel network immediately after gelation, and after a long duration of curing, showing the branched particle chains having taken on tube-like structures, with individual particles no longer as apparent. This occurs through redistribution of silica within the network, as theorised by Iler (1979).

Wijnen et al. (1991) supported this hypothesis by using small angle X-ray scattering (SAXS) to show growth in primary particle size in aged samples. In addition to this, there was a decrease in the fractal dimension of samples over time, which the researchers attributed to a densification of the network through dissolution of peripheral branches in favour of central aggregate kernels.

According to Iler's theory, there should be a maximum strength that a CS gel can reach, at which point no additional siloxane bonding can occur between particles due to exhaustion of all possible bonding sites, and/or no further deposition of silica taking place at particle necks due to absence of dissolved silicates, or deposition no longer being energetically favourable. Currently, no research has demonstrated this limit, however (Sögaard, Funehag, & Abbas, 2018).

2.2.4.1 Effect of silica mass fraction

Higher silica mass fraction gives increased gel strength due to the greater density of the resulting network (Iler, 1979). Persoff et al. (1999) carried out UCS tests on sand grouted with CS of various silica mass fractions. Results recorded compressive strengths of 124 kPa and 417 kPa, using CS of 7.4 wt% and 27 wt% silica, respectively. Similar tests on CS-grouted sand by Gallagher and Mitchell (2002), Mollamahmutoglu and Yilmaz (2010), Bakhshandeh et al. (2025), Terui et al. (2025), and Spagnoli et al. (2024) found CS of higher silica wt% to provide greater strength. Trompette and Clifton (2004) also observed higher silica wt% to produce stronger gels, using rheometer tests.

2.2.4.2 Effect of particle size

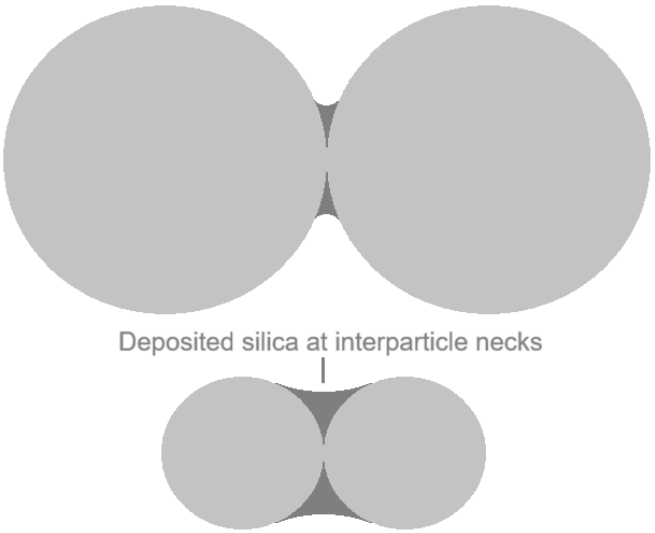

Figure 2.10. Visualisation of the difference in the sizes of necks which form between aggregated CS particles, depending on the size of the particles.

Gels using CS of smaller particle size are expected to be stronger, as such gels exhibit a higher degree of coalescence than those with larger particles (Iler, 1979). This means that comparatively more silica deposition occurs at the necks between particles, making them thicker relative to the overall size of the particles, as shown in Figure 2.10. There is therefore a greater number of siloxane bonds linking particles in the network, thereby increasing its strength. Evidence of this can be seen in Todaro (2021), in which sand samples grouted with CS of particle size 4 nm and 15 wt% of silica exhibited approximately the same compressive strength as samples grouted with CS of 16 nm and 40 wt% of silica, in spite of the smaller particle size grout having much lower silica mass fraction.

2.2.4.3 Effect of electrolytes

As electrolytes are known to promote the dissolution of silica, it may be expected that they also affect the increase in strength of CS grout over time (Bergna & Roberts, 2006; Iler, 1979). Johnsson et al. (2011) found that the use of different electrolytes in the accelerator produced gels with the same fundamental structure, but with slightly different strengths, in the order NaCl > KCl > K_2CO_3. They attributed this effect to more kosmotropic ions polarising water molecules near the silica surface, creating locally more acidic environments, which promote siloxane bond formation. These findings are contrary to earlier work by Johnson et al. (2008), however, which states that CS aggregate stability follows the direct Hofmeister sequence for the cation species inducing gelation ($Cs^+ > Rb^+ > K^+ > Na^+ > Li^+$), which they suggest arises from varying degrees of ion-ion correlation (IIC) interactions. Trompette and Clifton (2004) found that CS gels at high pH aggregated with ammonium (NH_4^+) ions, which are representative of poorly-hydrated so-called 'structure-breaker', or chaotropic ions, were stronger than those made with Na^+, representative of well-hydrated 'structure-maker', or kosmotropic ions.

In grouting application, Cheng et al. (2022) found the compressive strength and erosion resistance of CS-grouted sand samples to be greater when cured in pure water, as opposed to sea water (5% $MgCl_2$ + 5% NaCl), as well as acidic water and air, over durations of 1-365 d. Butrón et al. (2009) found that curing in a high total dissolved solids (TDS) solution of 35 g/L each of Na, Ca, and Cl ions did not significantly affect the strength of CS gel in fall cone, UCS, and triaxial tests over a period of 5 months. Sögaard, Funehag, Gergorić, et al. (2018) showed that the nature of the accelerator salt significantly impacted CS gels' resistance to water erosion, with KCl providing greater resistance than NaCl, suggesting that this also follows the direct Hofmeister series. MacLachlan et al. (2013) conducted shear vane tests on CS grout samples gelled using different electrolytes in the accelerator, finding that, after 7 d, grout made with 0.033 M $CaCl_2$ exhibited higher shear strength (76 kPa) than grout made with 0.29 M NaCl (51 kPa), suggesting that cation valency affects strength gain during curing (divalent Ca^{2+}, compared to monovalent Na^+). Grout made with 0.29 M NH_4Cl, containing monovalent chaotropic NH_4^+ cation, was also stronger (79 kPa), agreeing with the results of Trompette and Clifton (2004).

2.2.4.4 Effect of pH

pH also impacts the rate of dissolution of silica, and so presumably affects the strength of CS gels (Bergna & Roberts, 2006; Dollimore & Heal, 1962; Iler, 1979). Wijnen et al. (1991) found that the fundamental process was the same when aging silica gels at low and high pH, but that pH had a significant effect on the rate of the aging process, which was accelerated in alkaline conditions due to higher solubility of silica. Kaide et al. (2011) showed that the elastic modulus of silica gels aged in solutions at different pHs increased from pH 2 to 6, but was lower at pH 11. In each case the elastic modulus increased over time.

In the context of silica aerogels, it has been found that high pH in the precursor solution gives rise to highly branched, crosslinked networks, leading to greater density and stronger gel structure, with the reverse true for low pH (Payanda Konuk et al., 2023; Venkateswara Rao et al., 1994).

In grouting application, Cheng et al. (2022) observed the compressive strength and erosion resistance of CS-grouted sand samples as being greater when soaked in pure water, compared to acidic water of dilute sulfuric acid at pH 4. Persoff et al. (1999), however, found that immersing CS-grouted sand samples in pH 3 HCl for up to 1 year had no apparent effect on compressive strength compared to water. Furthermore, Butrón et al. (2009) found that curing in pH 11 $NaHCO_3$/NaOH solution did not appreciably affect the strength of CS gel in fall cone, UCS, and triaxial tests. Sögaard, Funehag, Gergorić, et al. (2018) found that higher pH did not have as great an effect as expected on the resistance of silica gel to water erosion due to a buffering effect of surface silanol groups, but they did observe that the gel was less resistant at high pH due to increased solubility of silica.

2.2.5 Hydraulic properties

The porous structure of CS gel acts like a maze, making transmission of water through the gel body very difficult. Very low hydraulic conductivities (below 10^{-10} ms^{-1}) can therefore be achieved in grouted soil samples (Pedrotti et al., 2020). Once CS has gelled, it does not exhibit any syneresis or change in volume, provided it does not dry out, and therefore no significant leakage of fluid occurs from grouted volumes.

One of the primary applications of CS grout is as a hydraulic barrier. Moridis et al. (1996) conducted laboratory and field tests demonstrating significant reduction in hydraulic conductivity of soil after grouting with CS. Other laboratory studies on CS-grouted soils have reported similar results, measuring conductivities of 10^{-9}-10^{-12} ms^{-1} (Durmusoglu & Yavuz Corapcioglu, 2000; Pedrotti et al., 2020; Persoff et al., 1999; Sharma et al., 2021). Butrón et al. (2009) studied the hydraulic conductivity of CS gel, reporting values in the range 10^{-8}-10^{-11} ms^{-1}; they also found a continuous decrease in hydraulic conductivity on increasing applied vertical stress. Tsuji et al. (2017) reported the use of CS for grouting a rock mass, achieving hydraulic conductivity lower than 10^{-9} ms^{-1}.

2.2.6 Drying behaviour

As water evaporates from the surface of CS gel, the gel first shrinks by an amount corresponding to the volume of water lost, which it does in order to keep the interior fully hydrated (Brinker & Scherer, 1990; Iler, 1979). Eventually however, the gel network becomes too compact and stiff to shrink any further, so air begins to intrude into the gel's pore spaces. The resulting completely dried gel is called a 'xerogel'. When CS gel shrinks, its structure is crumpled and folded, with siloxane bonds being broken and reformed in new places as different parts of the network contact each other; this means that the shrinking process is irreversible. Figure 2.11 provides diagrams of the structure of the gel before and after drying to become a xerogel.

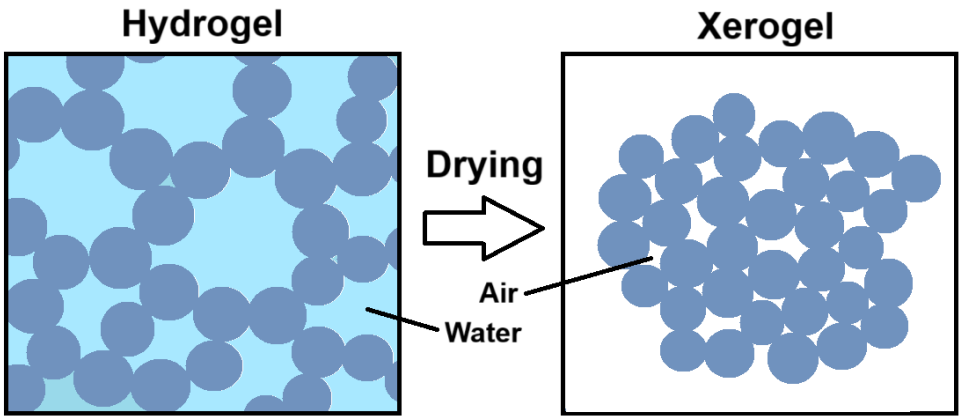

Figure 2.11. The left diagram shows the expansive, branched structure of a CS hydrogel, with water occupying the pore spaces. The right diagram shows the same gel after drying in ambient conditions to become a xerogel. The structure has now collapsed in on itself, with air entering into the contracted pore spaces.

The stresses imparted on the CS gel network during drying and re-wetting can induce cracking. Pedrotti et al. (2020) found that the hydraulic conductivity of CS-grouted sand

exposed to extreme drying conditions (more so than would be found in the field) increased from 5.10^{-10} ms^{-1} to 5.10^{-8} ms^{-1}, due to both nanoscale cracks forming in the gel matrix, as well as meso-scale fissures opening within CS-filled pores due to restrained shrinkage of the grout in the presence of sand grains. This was still over 3 orders of magnitude lower than the conductivity of the sand prior to grouting, however, as the cracks did not form a connected network.

Axelsson (2006) studied the drying shrinkage behaviour of CS gels over a period of six months: samples were stored at 8°C at 75%, 95%, and 100% humidities, with the results showing that most of the shrinkage occurred in the period from 200-1 000 hours, with lower humidities causing greater shrinkage. Butrón et al. (2009) found similar results.

2.2.7 Sorption capacity

The branched network of CS gel presents a large internal surface area onto which complexation of ions may occur. The high pH of the pore water of conventional gelled CS grouts may also further induce cations adsorption. This has led to investigation of CS grout as a chemical barrier for trapping contaminants in soil. However, the high ionic strength of CS grout after mixing with the saline accelerator also results in competition between ions from the accelerator and those of contaminants (Bots et al., 2020; Hakem et al., 1997).

Bots et al. (2020) conducted leaching experiments investigating the sorption capacity of CS-grouted soil for caesium and strontium ions (two bioaccumulating radionuclides commonly found in soil at contaminated nuclear sites). They found that, although accelerator cations compete with Sr^{2+} and Cs^{+} for adsorption sites, CS grouting resulted in an increase in distribution coefficients as a result of both the large silica specific surface area (SSA) where complexation can take place, as well as the high pH of the grout, thereby significantly increasing the immobilisation capacity for Sr and Cs.

Hölttä et al. (2009) found that sorption of Europium onto CS sols significantly depended on pH, with higher pH giving greater sorption. In saline water at pH 10-11, Eu–152 was rapidly sorbed onto CS, such that none was detected still in solution. Batuk et al. (2011) also identified stable sorption of two principal uranium species on CS.

In a field test on CS-grouted soil, Hakem et al. (1997) found less promising results, however, with the calcium ions (Ca^{2+}) of the CS's accelerator competing with Sr^{2+} and Cs^{+}

to result in minimally improved sorption of Cs^{+}, and decreased sorption of Sr^{2+}. Yossapol (2002) also found CS grout to be ineffective at treating chromium-contaminated soil due to high levels of diffusion.

2.2.8 Surface modification

The nature of CS's surface chemistry provides opportunities for modification in order to tailor its behaviour and properties for particular applications. This has been done through both physical blending and chemical modification, although the former provides less stability due to its reliance on transient interactions (Hou & Kang, 2025). Chemical modification using metal ions is often done to control the nature of CS particles' surface charge to improve stability or achieve particular desired behaviours. Aluminium salts have commonly been employed for this, in which tetrahedral vacancies on particle surfaces are substituted with alumina to provide CS with pH-independent negative charge (Gu et al., 2013; Lartiges et al., 1997; Tsai & Wu, 2004); alumina-modified CS grouts have previously been used at scale in civil engineering applications (Funehag & Fransson, 2006; Moridis et al., 1999; Moridis et al., 1997; Moridis et al., 1995). Magnesium (Karami, 2009; Salomão et al., 2023), boride (Clapsadle & Syracuse, 1953; Zelenev et al., 2007), and cerium salts have also been utilised in modifying CS (Tsai et al., 2009), and aluminium nitrate has even been used to produce CS with positive surface charge (Moore, 1973; Moore & Vurlicer, 1976).

Organic modification of CS is also carried out using substances including silane and organic acids to enhance CS's stability, and/or combine it with unique advantages of organic materials to tailor it for particular applications (Alsmaeil et al., 2023; Badley et al., 1990; Fang et al., 2021; He et al., 2013; Liu et al., 2018; Oguz et al., 2019). In this technique, organic functional groups are covalently bonded to CS particles through reaction with surface silanol groups. The most common aim of organosilane-modification is to introduce hydrophobic behaviour to CS (Guo et al., 2023; Hou & Kang, 2025; Liang et al., 2019; Poncet-Legrand et al., 2001; Saadatbakhsh et al., 2020; Wu et al., 2016; X. Zhao et al., 2019).

Hou and Kang (2025) modified CS with polydimethylsiloxane (PMHS) to create a novel, environmentally friendly, superhydrophobic grout with potential for large-scale application in controlling groundwater seepage. PMHS was grafted onto CS particles via

siloxane bonds, reducing the surface energy of the CS, and increasing surface roughness. The superhydrophobic CS grout had enhanced stability with minimal impact on injectability, although with up to 50% reduction in the strength of grouted sand.

2.3 Research and application of CS grout

Research into CS and other colloids began in earnest with the work of Thomas Graham in the 1860s, but it was not until the 1940s that stable concentrated silica sols became available (Bergna & Roberts, 2006; Iler, 1979). Over the following decades, the fundamental technology for the manufacture of CS was fully established, and a variety of CS products were developed. From this time, CS found use in a variety of industrial applications, including in catalyst production, as a ceramic glazing agent, as a coating material, in textiles, and for paper treatment (Bird, 1941). In the 1970s and 80s, however, mass production of CS was achieved, opening the door to large-scale applications, for example, in grouting.

2.3.1 Permeation grouting

When CS grout is applied in soils, it is through the technique of 'permeation grouting': this is when a grout is injected into the ground at minimal pressure to fill free soil porosity, without causing significant movement of soil (Karol, 2003; Warner, 2004). Such grouts are initially low viscosity fluids which then harden after application. Permeation grouting can be used for in situ hydraulic barrier formation using particulate grouts, such as ultrafine cements, or chemical grouts, including CS (U.S. Army Corps of Engineers, 2017). As well as for controlling groundwater flow, permeation grouting can be used to increase the strength and density of soil, giving improved load-bearing capacity, and it can be used to facilitate excavation. The suitability of materials for permeation grouting, and the depth of their penetration through soils, depends on factors relating to both the variety of soil, including its pore size distribution and hydraulic conductivity, and to the grout, such as its viscosity evolution, rheology, particle size, and the applied injection pressure. An illustration of permeation grouting is provided in Figure 2.12A.

2.3.1.1 Injectable barriers

CS grout can be used for in situ formation of hydraulic and chemical barriers in contaminated land remediation and waste management at near-surface applications, with the aim of controlling groundwater flow and immobilising contaminants. Significant

research has been done relating to these applications, including field tests, but full-scale application has been limited, thus far.

Noll et al. (1992) was the first research to report successful application of CS grout for these purposes, achieving a 3-4 order of magnitude reduction in the hydraulic conductivity of sand grouted with CS of 5 wt% silica, and a 30% reduction in the leaching of heavy metals in effluent from grouted samples. Following this, researchers at the Lawrence Berkeley National Laboratory proposed the use of CS grout for injectable barrier formation (Apps et al., 1998; Finsterle et al., 1994; Persoff et al., 1995); although they highlighted concerns regarding the influence of soil chemistry (in particular, the presence of Ca^{2+} ions) on the controllability of the grout's gelation, they also identified strategies to counter this. In field tests, Moridis et al. (1995) found that reasonably uniform alumina-modified CS grout plumes could be formed in spite of significant soil heterogeneity, suggesting that theorised issues regarding preferential flow pathways for the grout could be overcome. A further field trial was done at Brookhaven National Laboratory (Moridis et al., 1999), in which barriers were produced via overlapping bulbs of CS-grout. There was a high degree of variability in hydraulic conductivity measurements of grouted soil samples, however, presumed to arise from high anisotropy of the soil.

Persoff et al. (1995) studied how the soil at Hanford, a nuclear site undergoing decommissioning in Washington, USA, affected the performance of CS grout, finding that it induced premature gelation, although pre-flushing the soil with NaCl solution prior to injection was found to eliminate the issue. In a review, Truex et al. (2011) recommended CS over other grouts for application at Hanford, although this has not been acted upon. In laboratory experiments, Durmusoglu and Yavuz Corapcioglu (2000) produced effective injectable CS grout barriers, again, via overlapping grout bulbs. Similar to (Persoff et al., 1995), they found the gel time of CS grout to be reduced by a third in Vulcan sand. Both studies identified the presence of adsorbed Ca^{2+} and Mg^{2+} ions in the soil as causing the accelerated gelation.

Recent work from the University of Strathclyde has focussed on injectable CS grout barriers for application at nuclear facilities undergoing decommissioning in the UK (Bots

et al., 2020; Lunn et al., 2018; Morrison et al., 2022; Pedrotti et al., 2026; Pedrotti et al., 2020).

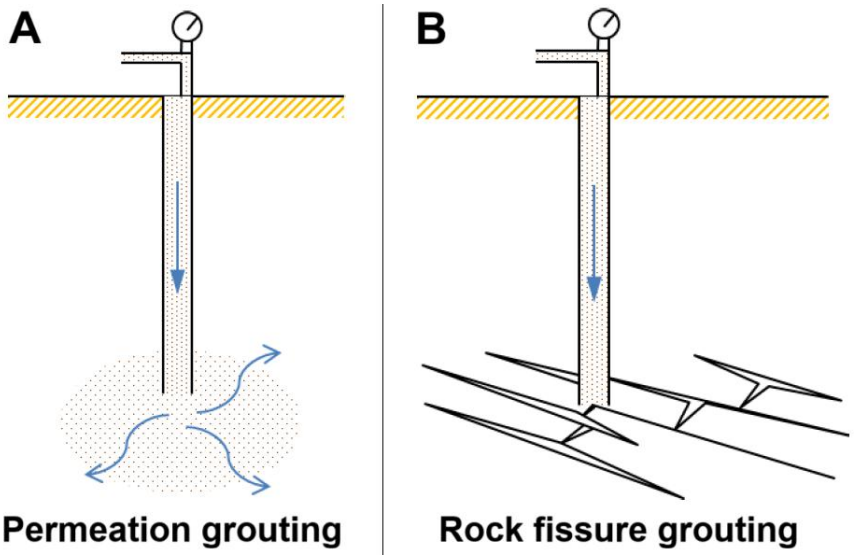

Figure 2.12. Diagrams illustrating permeation grouting (*A*) and rock fissure grouting (*B*): the two primary techniques for applying CS grout, adapted from Wong (2021).

2.3.1.2 Ground improvement

A significant application of CS grout has been in soil stabilisation and liquefaction mitigation. Gallagher (2000) first studied the injection of CS grout into loose sand for stabilisation, citing the appeal of CS's long, controllable gel times and low initial viscosity. In this research, pilot and field tests utilised groundwater flow to transport the grout through the soil, employing CS of low silica mass fraction (< 10 wt%) to allow for long penetration distances before gelation. Gallagher and Mitchell (2002) demonstrated that grouting loose sands with CS increased resistance to deformation from cyclic loading, and that higher silica concentrations gave greater resistance. Field tests performed by Gallagher et al. (2007) also found CS-grouted sand to exhibit reduced settling. In pilot tests, Hamderi and Gallagher (2015) studied the application of low silica wt% CS grout in loose sand, identifying a potential issue involving the grout sinking below the target volume due to gravity before successful transport over the desired distance could be achieved. Injection rates of 1900-7600 mL/min per injection well were found to be required for effective delivery of the grout.

Various more recent studies have since amply demonstrated the viability of CS grout for soil stabilisation and liquefaction mitigation in a variety of soils (Bakhshandeh et al., 2025; Birid & Varak, 2024; Ciardi et al., 2020; Georgiannou et al., 2017; Ghadr et al., 2020;

Huang & Wang, 2016; Kakavand & Dabiri, 2018; Krishnan et al., 2021; Sharafutdinov et al., 2024; Spagnoli et al., 2024; Terui et al., 2025; Todaro, 2021), as well as for increasing friction at soil-pile interfaces (Ali & Aziz, 2021; Boiero et al., 2026; Krishnan et al., 2021; Pamuk et al., 2007).

2.3.2 Rock fissure grouting

Fissure grouting is the injection of grout into joints and fissures in rock, forming a grout curtain, which then fully or partially fills the fissures: this is generally done to reduce the hydraulic conductivity of a rock volume. As part of the injection process, additional hydraulic fractures may be generated to allow further grout penetration. Fissure grouting is commonly employed in tunnelling, dam engineering, mining, and other underground construction projects for mitigating leakage, seepage, and water ingress (Hemphill, 2013). An illustration of fissure grouting is provided in Figure 2.12B.

Several different research groups have proposed CS for application as a fissure grout for tunnelling in hard rock (Butrón et al., 2009; Funehag & Fransson, 2006; Hernqvist et al., 2012), highlighting its ability to penetrate and seal fractures which micro-cements cannot, due to their unfavourable rheology and larger particle size, and because of CS's non-toxicity, which fulfils requirements for use in applications such as deep geological repositories (DGR) for high-level radioactive waste (Tsuji et al., 2017).

Funehag and Fransson (2006) presented the results of field tests conducted at the Äspö Hard Rock Laboratory in Sweden where CS grout was successfully applied to penetrate > 1 m into a rock fracture with hydraulic aperture of 40–50 μm. Initial hydraulic tests showed transmissivity of 10^{-8}–10^{-9} m^2s^{-1}, which was then reduced to 10^{-8}–10^{-10} m^2s^{-1} after grouting with CS. Similar field tests were conducted at the Onkalo DGR in Finland, by Hollmén et al. (2013), and in China, by Xiang et al. (2022), demonstrating CS grout injection in narrow fractured zones. Funehag and Gustafson (2008a) studied the primary factors which impact the behaviour of CS grout in rock fractures at depth, and developed an analytical model for predicting the penetration of the grout. They recommended grouting for a duration of half the estimated gel time of the grout in order to achieve sufficient penetration into fissures in rock.

The use of CS grout for tunnelling and underground construction has become common engineering practice in recent years in some countries, such as Norway (Ashcroft et al., 2025; Haugsand et al., 2025; Holter et al., 2025).

2.3.3 Water shut-off and conformance control

CS grout has additionally been used for water shut-off and conformance control in oil reservoirs; such applications involve diverting, directing, and controlling fluid flow through porous rocks in order to achieve improved oil recovery. Jurinak and Summers (1991a) were amongst the first to investigate CS for this purpose in laboratory and field tests, also applying the grout for repairing leaking well casings. They achieved limited success, with only one of four injection treatments being a success; three out of four casing repairs were successful, however, for a period of at least 6 months. A potential issue highlighted was the need to use fresh water to produce the accelerator for the grout, thereby increasing cost, as sea water gave varying gel time due to the presence of other salts (Jurinak et al., 1991b)

More recent studies, however, have achieved greater success in field tests, demonstrating substantial reductions in water production and enhanced oil output, while reducing operational risks and costs, and eliminating post-treatment complications; this has validated CS grout's effectiveness in oilfield applications, and has positioned it as a promising and flexible new tool (Al-Moshin et al., 2022; Ali, Al Ramadan, & Aljawad, 2024; Ali, Al Ramadan, Aljawad, et al., 2024; Ali, Alabdrabalnabi, et al., 2024; Almoshin et al., 2025; Ghaffari et al., 2022; Huang et al., 2017).

2.3.4 Additive in cementitious materials

Significant research has been conducted on the use of silica nanoparticles, or 'nanosilica', as an additive in various cement-based materials, with aims including improving mechanical performance, durability, and reducing environmental impact (Abhilash et al., 2021; Aggarwal et al., 2015; Ainomugisha et al., 2024; AlTawaiha et al., 2023; Althoey et al., 2023; Barbhuiya et al., 2020; Carneiro et al., 2022; Fu et al., 2022; Hamada et al., 2023; Khan et al., 2022; Paktiawal & Alam, 2020; Singh et al., 2013). Nanosilica is dispersed in cements either directly from a powder, or as a sol, and rather than relying on gelation of silica, it instead enhances cementitious materials via three primary mechanisms: pozzolanic reaction, a nucleation effect, and a filler effect.

Pozzolanic reactions involve the consumption of calcium hydroxide, a by-product of Portland cement hydration, to produce additional calcium silicate hydrate (C-S-H), which is the primary phase responsible for strength development in cementitious materials. Due to its high surface area, nanosilica reacts more rapidly than conventional pozzolanic additives, such as fly ash and silica fume, thereby accelerating secondary C-S-H formation (Buettner et al., 2024; Choobbasti & Kutanaei, 2017; Kashyap et al., 2023; Raveendran & Krishnan, 2025; Tavakoli & Cizer, 2025; Tripathi & Mishra, 2024; J. Wang et al., 2022). The large number of dispersed nanoparticles also provide additional sites for precipitation of hydration products, accelerating hydration kinetics and promoting more uniform C-S-H formation throughout the microstructure (Choobbasti & Kutanaei, 2017; Tavakoli & Cizer, 2025). This effect is particularly pronounced during the early stages of hydration and contributes to improvements in early-age strength and reductions in setting time. The nanoparticles also occupy voids between cement grains, increasing packing density and reducing capillary porosity (Choobbasti & Kutanaei, 2017; Kumar & Rajasekhar, 2022; Mansourghanaei et al., 2024; Raveendran & Krishnan, 2025). This improves the microstructure of cement paste and refines the interfacial transition zone (ITZ) surrounding aggregate particles (Kashyap et al., 2023; J. Wang et al., 2022).

Numerous studies have reported increased compressive, flexural and tensile strength (Alghrairi et al., 2024; Choobbasti & Kutanaei, 2017; Choobbasti et al., 2015; Kumar & Rajasekhar, 2022; Labaran et al., 2024; Mansourghanaei et al., 2024; Nigam & Verma, 2023; Saleh et al., 2023; Tripathi & Mishra, 2024; Zhang et al., 2021), particularly at early ages (Choi, 2025; Moslemi et al., 2013; Potapov et al., 2026; Tavakoli & Cizer, 2025), along with reduced permeability (Labaran et al., 2024), chloride ion ingress (Zhang et al., 2021), and micro-porosity (Al-Mulali et al., 2026; Chiranjeevi et al., 2023; Mansourghanaei et al., 2024; Tavakoli & Cizer, 2025; J. Wang et al., 2022). Improved resistance to sulphate attack and freeze-thaw degradation have also been observed (Kashyap et al., 2023; Moslemi et al., 2013; Raveendran & Krishnan, 2025; Shahrajabian & Behfarnia, 2018; Sharkawi et al., 2018), as well as increased fire resistance (Aziz et al., 2025).

Incorporation of nanosilica presents several practical challenges, however. The high surface area of nanosilica increases the water demand of cementitious mixtures, potentially leading to reduced workability (Nigam & Verma, 2023). Consequently, nanosilica is typically used in conjunction with water-reducing admixtures, such as

superplasticisers, to maintain workability while preserving a low water-to-cement ratio. The nanoparticles also exhibit a strong tendency to agglomerate due to their high surface energy; poor dispersion reduces the surface area available for reaction, diminishing the benefits of the silica (Hendrix et al., 2019). Most investigations report optimum nanosilica concentrations in the range ~1–5 wt% (Kumar & Rajasekhar, 2022; Sharkawi et al., 2018; Tripathi & Mishra, 2024; Zhang et al., 2021), with higher values giving diminishing returns due to agglomeration, increased water demand reducing workability.

2.3.5 Other applications and research

CS grout has also been investigated for other novel applications, such as in grouting fractures in cement and concrete. Sánchez-Moreno et al. (2022) demonstrated the ability of CS grout to penetrate through cracks and gel inside them. Microscopic analysis of a crack indicated that the sealing ability of the grout seemed to result not only from its filling of the crack, but also through chemical interactions with the cement of the crack walls. Pagano et al. (2022a) also successfully demonstrated CS grout for repairing fine-aperture cracks in cement at elevated temperatures and pressures, for application in hydrocarbon wellbores after plug and abandonment (P&A). They found permeability values after treatment to be reduced by three orders of magnitude, confirming the potential of CS grout for this application. Hatami et al. (2021) investigated CS grout for reducing risk of leakage in long-term CO_2 storage, demonstrating that CS gels were stable after 45 d immersed in brine, and for long durations at 60°C.

CS grout has been proposed for inhibiting particulate release during nuclear waste removal and transport operations (Pagano et al., 2022b). Pagano et al. (2023) conducted an experimental investigation, gelling CS grout around objects at 60°C and 120°C to simulate high-level radioactive waste in standard storage conditions, and during loss-of-coolant accident scenarios, confirming that CS grout successfully facilitated safe removal and transport of the simulated heat-generating waste.

2.4 Gaps in literature

2.4.1 Gelation and mechanical properties

Review of literature has shown that, although the gelation of CS grout can be precisely controlled, it is affected by environmental conditions, such as electrolyte content, occasionally leading to premature or unsuccessful gelation. A good understanding of local conditions is therefore important, as well as having accurate models of CS gelation

behaviour. Some such models have been developed (Abdelfatah, 2018; Pedrotti et al., 2017), but they do not yet factor in ion-specific effects on gelation, for example, which are not yet fully understood.

It was not possible to identify any experimental research in a grouting context that addresses the mechanism by which CS grout increases in strength over time, with this instead only being discussed in other fields, focussing on materials such as aerogels. There has also been no conclusive demonstration of the theoretical maximum strength limit attainable from curing. More work needs to be done to confirm whether Iler (1979)'s theories hold in grouting contexts.

Furthermore, there has also been relatively little research on the long-term effects of both electrolyte content and pH on the mechanical properties of CS gel, particularly in a grouting context, where these factors are of particular relevance due to the high variability in electrolyte content and pH in soils, both naturally, and at artificially contaminated sites, as well as the long timescales involved in certain grouting applications. The data that is available is also often contradictory, suggesting that the effects of ions, pH, and the interplay between them on the behaviour of CS grout are complex subjects (Sögaard, Funehag, & Abbas, 2018).

Data on the sorption of various ions and contaminants onto CS and CS-grouted soils and rocks is also often conflicting; the effect clearly depends on various factors, such as the electrolyte content of the grout and the surrounding pH, and it is not well-understood.

The author was not able to identify any research on the ability of CS grout to re-heal after suffering damage, although Katoueizadeh et al. (2021) did note that CS gel recovered its structure after breaking in rheometer tests.

2.4.2 Modification

Section 2.2.8 showed how notable research has been done on the surface modification of CS using materials such as metal ions, silanes and organic acids. However, two materials which have received much less attention for use in modifying CS are clays and polymers.

2.4.2.1 Clays

As clays occur commonly in nature, their material cost is much lower than that of CS when unrefined. Adding clays to CS grout to raise its total mass of solids could therefore provide a way to increase its strength more cost-effectively than by simply increasing the silica

nanoparticle concentration. Similarly, partial replacement of silica particles with clays could reduce cost while preserving mechanical performance. Clays additionally feature certain properties which may be beneficial to CS, such as plastic deformability (Bergaya et al., 2006; Craig, 2004; Guggenheim, 1995), as opposed to the brittle nature of gelled CS, hence potentially increasing resistance to cracking, for example.

One clay with particularly advantageous properties is bentonite, possessing strong cation sorption, high swelling pressure, low permeability, and high water retention (Cho et al., 1999; Lee et al., 2024; Noh et al., 2025; Villar et al., 2010). Bentonite is commonly employed as a hydraulic barrier material (Pedrotti et al., 2020), especially in nuclear decommissioning applications (Alberdi et al., 2000; Alonso et al., 2017; Arcos et al., 2006; Arvidsson et al., 2015; Bish, 1998; Bodvarsson et al., 1999; Dixon et al., 2011; Fernández et al., 2017; Mayordomo et al., 2016; Nazir et al., 2021; SKB, 2010a, 2010b, 2010c; Volckaert et al., 1996; Zheng et al., 2010), and it has the ability to effectively fill voids and self-heal cracks (Dohrmann et al., 2013), in addition to immobilising contaminants (Albarran et al., 2011; Cao et al., 2019; Karnland et al., 2006; Missana et al., 2008). If these beneficial features can be combined with CS's own, it could greatly improve the grout's performance as a hydraulic and chemical barrier and see its application increased as a result, particularly in the key field of nuclear decommissioning.

Although some research has been done on grouting various clayey soils, including bentonite, with CS, and on the structure and mechanical properties of the resulting materials (Aksu & Eskisar, 2023; Baird & Walz, 2006, 2007; Changizi & Haddad, 2015; Holmboe et al., 2011; Mohamadabadi et al., 2019; Roshan et al., 2022; Tomar et al., 2020; Wong et al., 2018), no work was identified which proposes or studies the use of clays as additives in the grout.

2.4.2.2 Polymers

Polymers are long chain molecules and have been used to create hydrogels that are highly customisable, featuring properties such as super-strength, flexibility, and re-healability (Deng et al., 2020; Fan et al., 2020; Tanaka et al., 2005; Zhang & Khademhosseini, 2017). Because of this, as well as their high biocompatibility, polymer hydrogels have been the focus of significant research in medical applications (Caliari & Burdick, 2016; Kondiah et al., 2016; Lee, 2018; Li & Mooney, 2016; Li et al., 2018; Lin & Metters, 2006; Mantha et al.,

2019; Nezhad-Mokhtari et al., 2019; Peppas et al., 2000; Vigata et al., 2020; Zhu & Marchant, 2011). However, polymer gels have generally not been proposed for large-scale engineering contexts, such as in geotechnics, due to high associated costs, challenges in controlling gelation in situ, toxicity of certain reactants (although the final products are usually harmless), and other constraints which hinder scalable deployment (Chirani et al., 2015; Karol, 2003).

If materials and gelation techniques can be identified, however, which address these concerns, and which can be effectively combined with CS grout, then it may allow for incorporation of some of the advantageous and customisable properties of polymer hydrogels into CS, whilst preserving CS grout's own favourable behaviour. This could greatly improve the effectiveness of the grout within its present applications, as well as potentially opening it up to new fields for which it has not previously been considered.

Some research has already been conducted showing successful incorporation of silica nanoparticles into polymer hydrogels, with this giving enhanced performance compared to polymer-only gels (Adibnia & Hill, 2017; Cao et al., 2024; Gaharwar et al., 2013; Gao et al., 2016; Jia et al., 2019; Khedr & Elhady, 2025; Levin et al., 2019; Ma et al., 2024; Mirzababaei et al., 2017; Ren et al., 2025; Rose et al., 2013; Shona Pek et al., 2008; Singh et al., 2024; Yang et al., 2013; Ye et al., 2014). This even been done at scale for applications in oil and gas (Amir et al., 2022; Chen et al., 2018; Cui et al., 2023; Ma et al., 2017; Shamlooh et al., 2019). More information on this research is provided in section 7.2. No work was identified, however, which attempts simultaneous gelation of CS and polymers, or which investigates polymers as an additive for CS grout for application in permeation or rock-fissure grouting.

2.4.3 Gaps addressed in this thesis

Of the research gaps identified here, some are sought to be addressed in this thesis, although not all. Chapters 4 and 5, for example, touch upon the effect of electrolyte content on the gelation of CS grout, although it is not the primary focus of the chapters, rather being done mainly to facilitate later mechanical and other tests. The data obtained, however, can also be used to improve understanding and contribute towards detailed models of the gelation behaviour of CS grout. Electrolyte concentration, valency, and thereby ionic strength are investigated using two salt species: NaCl and $CaCl_2$, as well as

silica particle concentration. The effects of pH, ion specificity, and gelling in different soils were not investigated.

Chapter 4 primarily deals with the strength evolution during curing of CS grout and grouted sandy soil. It seeks to confirm whether Iler (1979)'s theories on the topic hold in a grouting context, and to suggest alternative explanations if not. It further aims to identify any theoretical maximum strength limit, and it investigates the effect of the silica concentration and electrolyte content, both in the grout and the surrounding environment, on the strength evolution, again using NaCl and $CaCl_2$. Chapter 5 also features work on the effect of silica particle size on the strength evolution.

The primary focus of chapter 5, however, is to investigate the ability of CS grout to re-heal after damage, and to propose a theoretical model to describe the behaviour. It additionally studies the effect of electrolyte content on this (again, NaCl and $CaCl_2$), as well as pH, silica particle size and concentration, and re-healing in the presence of additional CS. The mechanical data recorded in chapters 4 and 5 can be used to improve the understanding of the strength evolution of CS grout during curing and re-healing, and can contribute towards detailed models of the behaviour.

Chapter 6 studies the addition of clays to CS grout, including bentonite, exploring the effect this has on viscosity, gelation, mechanical properties, and re-healing. It also assesses the feasibility of using clays to partly replace silica nanoparticles in the grout in order to reduce cost without compromising gelation and/or mechanical performance. No experimental work was done at this time to characterise the sorption properties of the grout, with or without the presence of clays, with this study instead being merely a preliminary proof of concept on adding clays to CS grout.

Chapter 7 investigates the modification of CS grout using polymers, and attempts to combine CS with polymer hydrogels to form nanocomposite gels with advantageous properties. First, polymer hydrogel research is reviewed, aiming to identify polymers and gelation techniques which could be suited for application with CS grout in geotechnical contexts. Candidate polymers are then investigated experimentally by gelling CS grout in their presence and studying the nature of any interaction which occurs, and the properties of the resulting materials. The polymers themselves are then gelled in water

and CS suspension, if possible, with the eventual goal being to simultaneously gel both CS and polymers.

2.5 Conclusion

CS grout shows great potential in a wide range of applications, in particular for the formation of injectable hydraulic and chemical barriers in contaminated land and near-surface waste management; for soil stabilisation and liquefaction mitigation; and for water shut-off and conformance control in oilfields. In spite of a high degree of research interest, large-scale application has remained limited in all applications, however. Contributing to this is the fact that further study is needed to assess key behaviours of the material, such as its long-term stability in soil, and how its gelation and mechanical strength are affected by environmental factors, such as electrolyte content and pH. If these factors can be better understood, it may allow the strength of CS grout to be enhanced or tailored for particular applications. If this, and/or other improvements can be made to the performance of CS grout, via modification using clays and polymers, for example, there is potential that it could be opened up to both large-scale implementation in its conventional fields, as well as to entirely new applications.

Chapter 3: Methodology

3.1 Materials

Master Builders Solutions kindly donated their MasterRoc MP 320 and MP 325 Part A CS for use here. Both CS types were low-viscosity alkaline suspensions of silica nanoparticles, with MP 320 being translucent white, and MP 325 transparent and colourless, due to its smaller particle size and lower silica wt%. Both MP 320 and MP 325 are intended to be used with an accelerator of 1.7 M NaCl solution, at 5:1 volume ratio. Table 3.1 provides technical data for the two CS types from their respective datasheets, along with that of the standard accelerator composition, and the mixed materials, at room temperature (20°C). CS here was diluted with deionised (DI) water of pH ~ 7 if its silica mass fraction needed to be reduced for a particular experiment; this process had negligible effect on the pH.

Table 3.1. Technical data for the standard accelerator (1.7 M NaCl) and CS variants used in this investigation, as well as for the mixed materials, at 20°C, according to the datasheets for the two CS types (Master Builders Solutions, a, b). Values marked with '*' were calculated from the provided data.

Material	*Colour*	*Avg. particle size* (nm)	*Silica wt%*	*Density* (kg/L)	*pH*	*Viscosity* (mPa·s)
Accelerator	Clear	n/a	0	1.07	7	~ 1
MP 320 A	Whitish/clear	15	40 ± 1	1.3	9.5–9.8	~ 10
MP 320 mix			34.2*	~ 1.25	~ 9	~ 5
MP 325 A	Clear	7.5	15 ± 1	1.098	10 ± 1	~ 10
MP 325 mix			0.125*	~ 1.10	~ 9.8	~5

NaCl was purchased from Fisher Scientific in crystalline powder form, and $CaCl_2$ was obtained from Nedmag as solid granules with 96% purity. Using these salts, solutions were prepared at particular concentrations using DI water. The soil used in this investigation was fine-grain washed building sand obtained from Jordanhill Gardening Supplies, and had bulk density 1.62 g/cm^3, and porosity ~ 39% when compacted by hand. 55 mL and 280 mL hexagonal glass jars for shear vane tests were purchased from Ampulla.

3.2 Sample preparation

This section outlines the methods used to prepare CS grout and CS-grouted sand samples for the various tests conducted as part of this investigation. Lists providing more information on samples and their compositions can be found in the appendices.

3.2.1 Note on Terminology

Certain terms used in this chapter require further explanation: here, 'CS' refers to MasterRoc MP 320 or MP 325 part A, 'accelerator' refers to salt solutions that are mixed with CS to initiate gelation, and 'CS grout' to the gelling or gelled mixture of CS and accelerator.

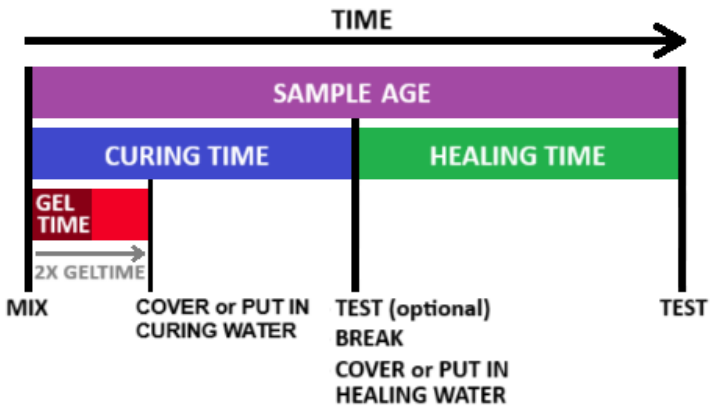

Figure 3.1. Diagram illustrating the meanings of terms used in this investigation.

The time it takes for a particular CS grout sample to gel, as defined here by the protocols in 3.3.1 and 3.3.2, is called the 'gel time'. After gelation, some samples were immersed in particular solutions, termed 'curing water'. For a gelled sample, the 'curing time' refers to the time from when CS and accelerator were mixed, up until the sample is first tested or broken. For samples that were re-healed, the 'healing time' corresponds to the time between breaking and a final test, during which the sample could be immersed in a particular 'healing water' solution, depending on the experiment. The 'sample age' of CS grout or CS-grouted soil corresponds to the total time elapsed since mixing the CS and accelerator, potentially encompassing both curing and healing times. Figure 3.1 provides an illustration of these terms.

3.2.2 CS grout preparation

To prepare CS grout, CS and accelerator were first measured out to desired volumes using measuring cylinders. The volume ratio of CS to accelerator was always 5:1. The accelerator was poured into a beaker, followed by the CS, and the mixture was stirred for 20 s. Preparation was conducted at ambient temperature for the laboratory (~ 20°C). Photographs illustrating the CS grout preparation method are provided in Figure 3.2.

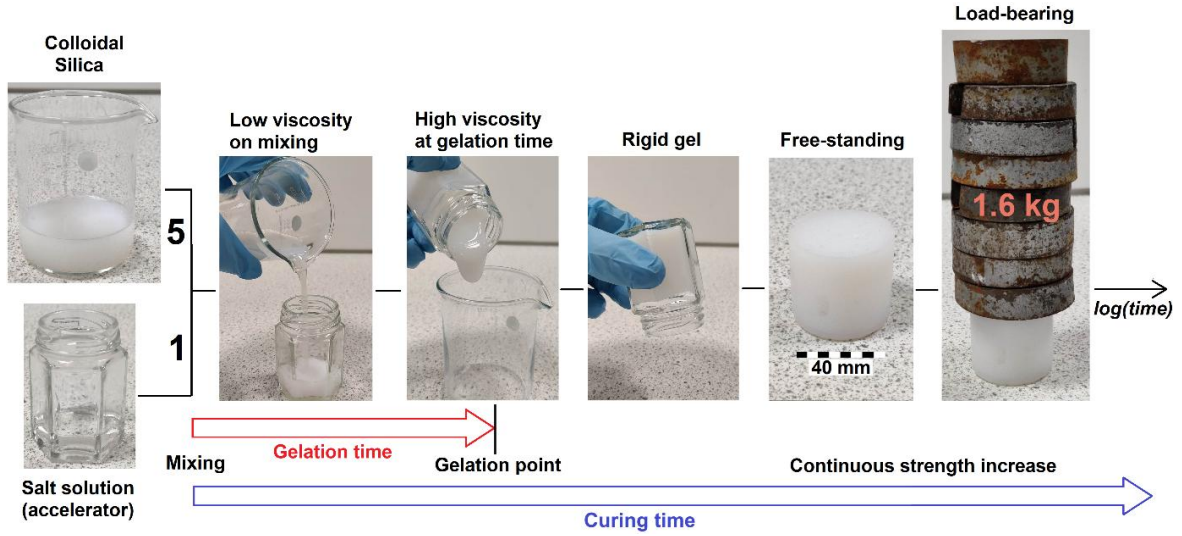

Figure 3.2. Photographs illustrating the CS grout preparation method. *From left:* CS and accelerator at 5:1 volume ratio. The CS is mixed into the accelerator, at this point having very low viscosity, and gelation commences. Around the gel time, viscosity has greatly increased, until later it becomes a rigid gel which continues to increase in strength over time. The horizontal axis corresponds to time and is in an approximately logarithmic scale.

3.2.3 CS grout samples for shear vane test

To create a sample for shear vane test, 42 mL of CS grout was first prepared (see 3.2.2) in a 55 mL hexagonal glass jar; this shape was chosen to minimise slippage between the sample and container walls. After 2× the gel time, as calculated by the method in 3.3.1, the sample was covered with 5 mL of tap water: just enough to cover its surface and prevent evaporation, before it was sealed with the jar lid, and covered with parafilm. The 2× gel time duration was selected as, at this point, the sample was clearly a solid, as opposed to at the gel time itself, at which it was still a viscous liquid. Samples were then left to cure for the desired curing time. Figure 3.3 provides a diagram of this method.

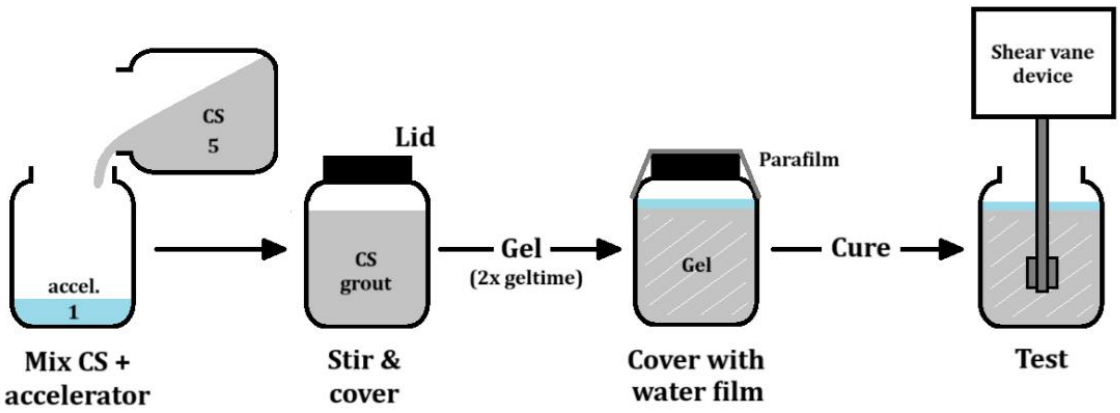

Figure 3.3. Shear vane CS grout sample preparation method.

3.2.4 CS-grouted sand samples for shear vane test

Grouted sand samples for shear vane test were produced by mixing 150 mL of gelling CS grout (190 g) with 300 g of sand, and stirring vigorously for 30 s, until the sand was fully wetted by the grout. The resulting slurry was then poured into a 280 mL hexagonal glass jar and allowed to settle for 1 min, leaving the sand saturated with grout at the bottom of the jar, with around ~ 50 mL of excess grout on the surface which was brown in colour, having some fine soil particles still suspended in it. This grout was syringed off, and the sand was compacted by hand using the plunger of a 60 mL syringe to give a final density of ~ 2.30 g/cm^3. The jar was then sealed and allowed to gel. After the sample was judged to have reached a strength of I on the gel strength code, via the inversion test (see 3.3.2), 25 mL of cold tap water was syringed onto the surface of the now gelled sample, which was then resealed, covered with parafilm, and allowed to cure for the desired duration.

The inversion method was used for determining gelation as the presence of the soil fines caused the grout to gel faster than expected from viscometer-based gel time calculations. Larger jars and sample sizes were used here than in 3.2.3 in an effort to reduce any effect resulting from the size of sand particles relative to the container. Tests were conducted to verify that the change in jar and sample size would not introduce any unexpected effects, the details of which can be found in appendix A.3.2.

3.2.5 Re-healed CS grout samples for shear vane test

Re-healed CS grout samples were prepared by adapting shear vane samples (see 3.2.3). To do this, after the intended curing time of a shear vane sample was reached, it was optionally tested with the vane, before being completely broken up by hand for two minutes using a metal spatula, after which it became a viscous slurry. This was then either covered with another 5 mL film of tap water, or it was placed in a container of 500 mL of a particular healing water. In the former case, the jar was sealed with a lid and parafilm; in the latter, the jar was left open, and the healing water container was sealed with its lid, and parafilm. Samples were then left to heal at ambient temperature for the desired healing time. The preparation method for re-healing samples is depicted in Figure 3.4.

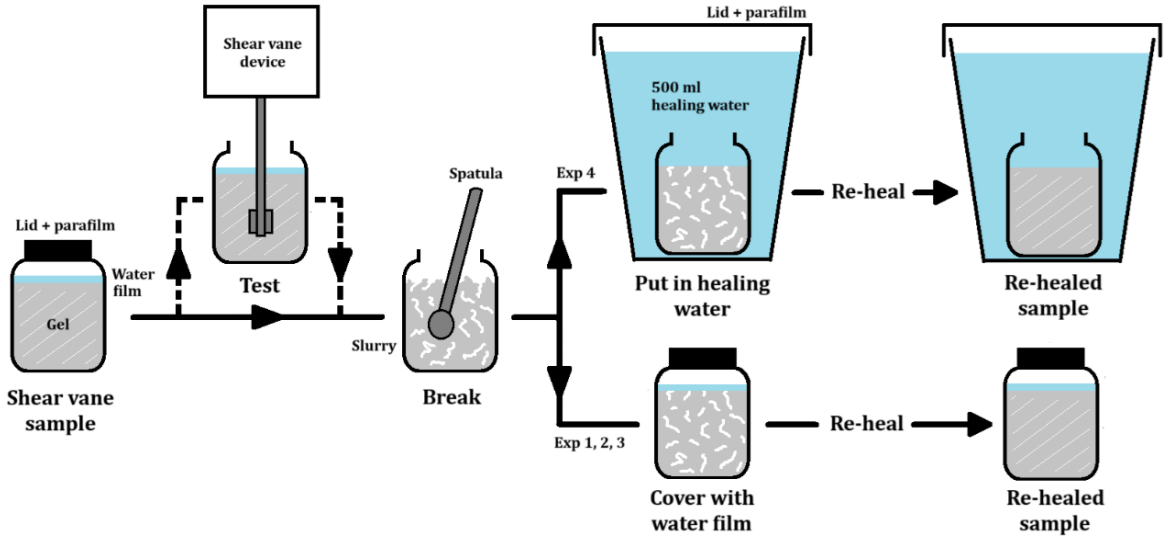

Figure 3.4. Diagram of the preparation methods for re-healed CS grout samples for shear vane test.

3.2.6 Re-healed CS-grouted sand samples for shear vane test

The preparation of re-healed grouted sand samples was the same as that of standard CS grout samples (3.2.5), but adapting from CS-grouted sand shear vane samples (3.2.3). All grouted sand samples were covered with water films for re-healing.

3.2.7 CS-grouted sand samples for UCS test

Sample moulds for UCS tests were produced by cutting plastic pipe into cylinders 64 mm in height and 32 mm in diameter, which were then split lengthwise and secured together. To prepare a sample of CS-grouted sand, a mould was first placed in a 100 mL plastic beaker set upon bench-top scales. 65 g of sand was poured into the mould, enough to fill it to the top, and it was then compacted as much as possible by hand using the plunger of a 25 mL syringe. 100 mL of CS grout (see 3.2.2) was then prepared, per sample. Grout was poured through the sand, eventually filtering out of the bottom of the mould, and filling up around the outside. Once the grout reached the 60 mL mark of the beaker, corresponding to three pore volumes of the sand, the remainder was poured around the outside, over the top of the mould, until it was totally immersed in grout. The surface of the sand was flattened, before covering the beaker with parafilm to limit evaporation as the grout gelled. The sample was left for a duration of 2× the gel time, at which point the parafilm was removed, and the sample weighed, before placing it in a plastic container with 500 mL of a curing water mixture. A diagram of this method is provided in Figure 3.5.

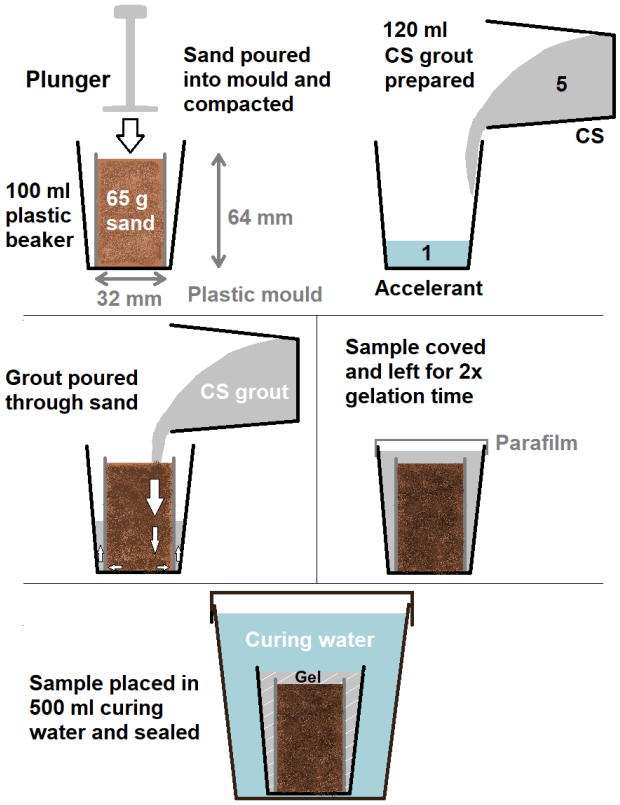

Figure 3.5. Preparation method for columns of CS-grouted sand for UCS test.

3.2.8 CS grout samples for SEM

To prepare CS grout samples for SEM, small fragments (~ 3 mL) of gelled grout (see 3.2.2) were cut out using a spatula. These were then dried for three days in a vacuum chamber. They were then ground into a fine powder using a mortar and pestle, before being dusted onto a carbon sticker attached to a sample pin. They were then gold-coated.

3.2.9 CS grout samples for rheometer test

CS grout samples for rheometer strain and frequency tests were created by preparing 3 mL of grout (see 3.2.2) in 5 mL plastic rheometer cups, which were then sealed with their lid. After 3 h (~ 2× the gel time of the standard CS grout mixture), 0.3 mL of DI water was added onto the surface to limit evaporation, and the cups were resealed and covered with parafilm. Samples for "time-sweeps" were prepared in the same manner, but were tested immediately after mixing the CS and accelerator. Measurements were also attempted on free-standing gel samples (as opposed to using cups), but this method was liable to errors and gave highly variable results.

3.3 Experimental methods

In this investigation, a range of tests, including viscometer and rheometer measurements, shear vane and UCS tests, and SEM imaging were employed to study the properties, behaviour, and structure of CS grout and grouted soil. The following section outlines the different procedures employed in these tests.

3.3.1 Viscometer method for determining gel time

A Cole-Parmer rotational viscometer was used to record the viscosity evolution of CS grout during gelation, and therefore calculate gel times. To do this, the L1 spindle of the viscometer, which facilitated the lowest viscosity measurements, was inserted into a gelling grout sample. The spindle was set to rotate at its maximum speed of 100 rpm, which allowed accurate measurement in the range of 9–57 mPa·s, corresponding to 15–95% of the maximum torque the device could apply to maintain this rotation speed. This spindle and rotation speed were chosen due to the very low viscosity of the CS (~ 10 mPa·s). Measurements were taken every 10 s. A timer was used to measure the duration between mixing the CS and accelerator and commencing viscosity measurement. The experiment was ended once the viscosity exceeded the measurement range. The gel time was defined as the time taken for the grout to exceed 57 mPa·s from the point of mixing.

3.3.2 Solid-state / bottle inversion test method for determining gel time

In some instances, it was not practical to use the viscometer to determine the gel time. In such scenarios, gelation was instead measured by eye using the 'solid-state', or bottle inversion test. Gelling samples prepared in beakers were said to have gelled when they could be inverted without flowing out of the beaker: this corresponded to a gel strength of F in the code proposed by Sydansk and Argabright (1988), provided in Table 3.2.

Table 3.2 Gel strength code from Sydansk and Argabright (1988).

Code	*Description*	*Explanation*
A	No detectable gel	Gel has same viscosity as original mixture and no gel visually detectable.
B	Highly flowing gel	Gel only slightly more viscous than original mixture.
C	Flowing gel	Most obviously detectable gel flows to the bottle top on inversion.
D	Moderately flowing gel	Small portion (5-15%) of gel does not flow to bottle top on inversion.
E	Barely flowing gel	Gel barely flows to bottle top, and a significant portion (> 15%) does not flow on inversion.
F	Highly deformable non-flowing gel	Gel does not flow to bottle top on inversion (flows to a point just short of it)
G	Moderately deformable non-flowing gel	Gel flows half-way down the bottle on inversion.
H	Slightly deformable non-flowing gel	Only gel surface deforms slightly on inversion.
I	Rigid gel	No gel surface deformation on inversion.
J	Ringing rigid gel	Tuning-fork-like mechanical vibration after tapping bottle.

3.3.3 Rheometer test methods

To study the rheology of a gel or gelling sample, the 5 mL rheometer cup containing the sample was placed in the appropriate stage of the rheometer. The cross-shaped vane attachment of the rheometer was then lowered into the sample and set to rotate back and forth at a controlled angular frequency and strain amplitude. For strain tests on gelled samples, the angular frequency of oscillation was kept constant, while gradually increasing the amplitude; for frequency tests, the amplitude was kept constant at a value within the elastic region of the gel being tested, such that the structure would not be broken, while frequency was instead increased; and for time-sweeps, used to study samples during gelation, both frequency and amplitude were kept constant, with the amplitude again at a value which would not damage the structure. To study the viscosity of a liquid sample, 3 mL of liquid was poured onto the rheometer's flat plate stage, and the cone attachment of the rheometer was lowered until making complete contact with the surface of the liquid. The cone was then continuously rotated at an increasing rate. Diagrams of the rheometer setups are provided in Figure 3.6.

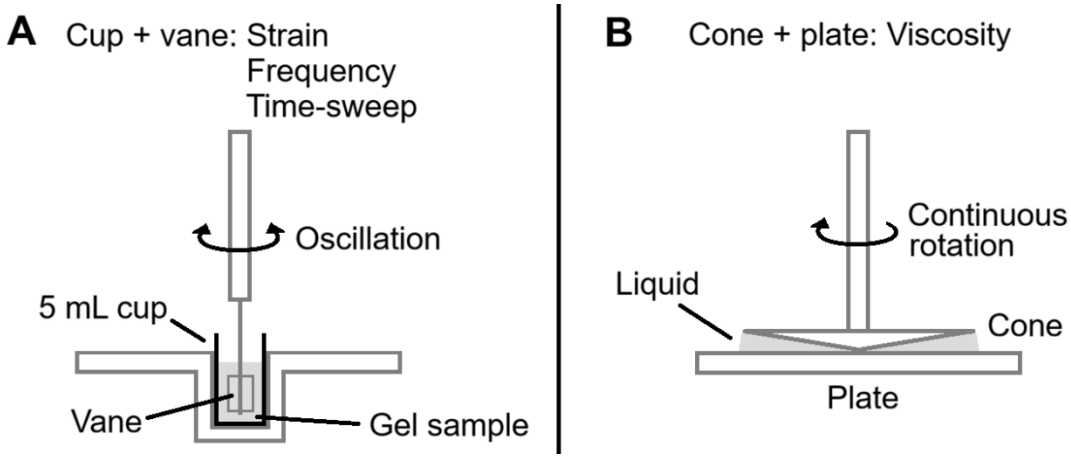

Figure 3.6. *A:* Experimental setup for studying the rheology of a gel (or gelling) sample in a 5 mL cup. The cup was embedded in the appropriate rheometer stage. The rheometer's vane attachment was then inserted into the sample and oscillated with controlled frequency and strain amplitude. *B:* Setup for studying the viscosity of a liquid sample. 3 mL of liquid was poured onto the rheometer's flat stage and the cone attachment was then lowered until making complete contact with the surface of the liquid. The plate was then continuously rotated at an increasing rate.

3.3.4 Shear vane test method

Shear vane tests were used to study the shear response and strength of gelled CS grout. Once the desired curing time was reached, samples (see 3.2.3 – 3.2.6) were uncovered, placed under a shear vane device, and secured in place with tape to prevent them from moving during test. The four-bladed vane of the device was then lowered into the sample, which was further secured with metal weights. When activated, the device would slowly attempt to turn the vane in the sample, and would measure the force required to obtain a particular angular displacement. The device was able to measure shear stresses in a range of ~ 1–167 kPa.

3.3.5 UCS test method

Once the desired curing time was reached, the grouted sand samples (see 3.2.7) were removed from their curing water, weighed, and the moulds were dug out using a metal spatula and detached from the samples. The surface and base of samples were then polished flat using sandpaper, before they were weighed, and their dimensions measured with callipers. When testing a sample, it was placed in a large container which was then filled with DI water until the sample was immersed: this allowed the compression tests to be conducted under water, to ensure the sample remained saturated throughout. The samples were left unconfined during test.

The container holding the sample was placed on the moveable platform of a compression testing machine, and a plastic disk with an embedded metal ball bearing was placed concentrically on top of it. A metal rod and ball were balanced on top of this by hand, and the platform was then moved upwards towards a load cell directly above the sample until the cell, ball, rod, and disk were all in contact, and vertically aligned. The load cell was connected to an acquisition system which plotted the force experienced by the cell. At this point, the platform was set to continue to move upwards, independently, at a constant rate of 10 µm/min, such that the sample was slowly compressed. This very slow rate was chosen to allow for water to gradually drain out of the sample's pore spaces as it was crushed, such that pore pressure would not contribute to the force recorded by the load cell. This rate was chosen as a result of tests outlined in appendix A.1.1. A diagram of the experimental setup is provided in Figure 3.7.

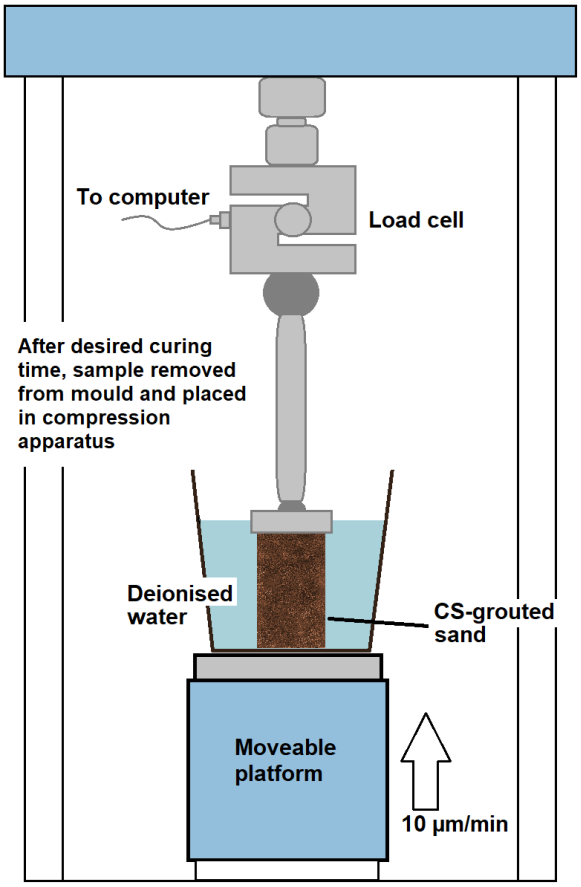

Figure 3.7. Diagram of unconfined drained uniaxial compression test experimental set-up.

3.3.6 SEM imaging method

A Hitachi SU6600 field emission SEM was used to image the micro-structure of CS grout samples (prepared by the method in 3.2.8) at high vacuum. For the smallest-scale images (×150k zoom), a beam energy of 20 keV was used.

Chapter 4: Effect of Grout Composition and Curing Conditions on the Strength Evolution of CS Grout

4.1 Introduction

In spite of its excellent properties, wide-scale application of CS grout has thus far been limited. This may be, in part, due to its cost, calculated as ~ 2.7× greater than cement (Gallagher et al., 2013), its lower strength in comparison to cement, and the lack of a comprehensive understanding of its gelation, transport, and long-term stability in soil (Pedrotti et al., 2026; Pedrotti et al., 2017). In an effort to contribute towards addressing this, the following chapter presents the results of an experimental investigation into CS grout gelation, and the mechanical performance of CS grout and CS-grouted soil, as well as various factors which impact each of them. The factors in question relate to the composition of the grout itself, such as its silica mass fraction and the electrolyte content of its accelerator, as well as to the duration for which it was allowed to cure, post-gelation, and the ionic content of its curing environment. As part of this, viscometer measurements were used to study the gelation of CS grout, and shear vane measurements for its shear strength once gelled. UCS tests were then also conducted to investigate the compressive strength of CS-grouted soil, increasing the relevance of the study to permeation grouting, and providing a point of comparison to the shear vane tests. Finally, SEM was employed to study the micro-structure of certain grout samples.

The aim of the investigation was to improve the understanding of the behaviour and performance of CS grout, and to identify ways of maximising its strength and reducing its cost to facilitate its increased application across fields. Increasing the strength that CS grout imparts in soils would give the hydraulic barriers it produces greater resistance to damage, for example, from seismic events, and would provide soils with improved resistance to settling caused by changes in surface loading; it may also facilitate use of less grout volume, or lower silica mass fraction, whilst maintaining mechanical performance, thereby reducing costs. Significantly increasing the strength of CS grout may also open it up to novel applications with higher strength requirements, such as grouting radioactive waste cannisters, currently done using cement (Pagano et al., 2023).

4.2 Methodology

4.2.1 Materials

Materials used in this investigation included MP 320 CS, NaCl, $CaCl_2$, and fine-grain sand, and equipment included 55 mL hexagonal glass jars: more information on these can be found in section 3.1.

4.2.2 Sample Preparation

4.2.2.1 Terminology, standard parameters, and naming convention

Samples in this study were prepared according to a standardised set of parameters. The standard grout mixture used MP 320 CS (which has 40 wt% silica), and accelerator of 1.7 M NaCl, at 5:1 volume ratio; these gave a silica mass fraction of 34 wt% and NaCl concentration of 0.28 M, after mixing. Gelled grout and grouted sand samples were cured for 7 d, with grouted sand samples cured in 500 mL of DI water. It can be assumed that all samples presented here followed these parameters unless otherwise stated.

Table 4.1. Explanation of the sample naming convention used in chapter 4.

Term order	*Variable*	*Abbreviation*	*Meaning*	*Subscript*
1	Sample type	CS	CS grout	CS silica wt%
		GS	CS-grouted sand	
2	Accelerator salt	N	NaCl	Concentration (M)
		C	$CaCl_2$	
3	Curing time	C	Curing time	Curing time (d)
		/	Group of various ages	–
4	Curing water	DW	DI water	–
		TW	Tap water	
		NW	NaCl solution	Concentration (M)
		CW	$CaCl_2$ solution	

In this chapter, samples are identified according to a bespoke naming convention, the details of which are outlined in Table 4.1. Using this, the standard grout mix (used in viscosity tests) is written CS_{40}-$N_{1.7}$; the standard gelled CS grout sample (for shear vane tests and SEM) is CS_{40}-$N_{1.7}$-C_7; and the standard grouted sand sample (for UCS tests) is GS_{40}-$N_{1.7}$-C_7-DW. The '/' symbol is used to skip the third term and refer to a group of CS-grouted sand samples with different curing times, and a '*' symbol after the fourth term identifies samples whose curing water was regularly replaced. For example:

GS_{40}-$N_{1.7}$-/-TW* refers to a group of standard CS-grouted sand samples cured for various durations in tap water which was regularly replaced.

4.2.2.2 CS grout preparation

CS grout was prepared as described in section 3.2.2, at ambient temperature.

4.2.2.3 CS grout samples for viscometer test

CS grout samples were prepared as described in 4.2.2.2. This was done for samples using CS with 20-40 wt% of silica, as well as those with accelerator NaCl concentrations of 1.3-2.5 M, and $CaCl_2$ of 0.1-0.5 M. A full list of the viscometer samples can be found in appendix A.2.1.

4.2.2.4 CS grout samples for shear vane test

Grout samples for shear vane test were prepared in glass jars by the method described in section 3.2.3. All samples in this investigation were covered with films of tap water during curing. Samples were prepared which were cured for different durations, and which had varying silica wt% and accelerator NaCl concentrations. Equation 4.10 was used to identify accelerator NaCl concentrations needed to ensure the gel time of the grout remained constant where silica wt% was varied. To study the effect of curing water, some jars were opened after 16 d of curing and placed in 500 mL of curing water (either tap water or 1 M $CaCl_2$) to continue curing for a further 48 d. A list of the shear vane samples tested in this study is provided in appendix A.2.1.

4.2.2.5 CS-grouted sand samples for UCS test

Grouted sand samples for UCS test were prepared according to the method in section 3.2.7. A complete list of the UCS samples in this study can be found in appendix A.2.1. Sets of samples prepared via this method are described as follows:

- One set of samples were cured for different durations, from 1-448 d (64 weeks), in DI water.
- Another set used CS of varying silica mass fraction, from 30-40 wt%, each cured for 4 weeks in tap water; equation 4.10 was used to determine accelerator NaCl concentrations needed to ensure the gel time of the grout remained constant. It should be noted that the standard grout mix, which had gel time of ~ 1.70 h, was

not used for the sake of practicality, with all samples instead having gel time of ~ 3.02 h.

- A third set used accelerators with different concentrations of NaCl, and therefore different gel times. These were cured for 1-4 weeks in DI water. Equation 4.5 was used to calculate NaCl concentrations that provided gel times which were multiples of each other. For example, CS_{40}-$N_{1.7}$ had gel time of ~ 1.70 h, which is twice that of CS_{40}-$N_{1.58}$, at ~ 0.85 h, and CS_{40}-$N_{1.92}$ was three times this, at ~ 2.55 h. The purpose of this was to investigate the relative contribution of gel time and curing time to strength: i.e., is a sample which gels twice as fast equivalent to one which has been cured for twice as long?
- A further set was prepared in which samples were cured for 2-4 weeks in either seawater or freshwater analogies (0.6 M NaCl and tap water, respectively). These curing waters were replaced daily, where possible, with their pH and electric conductivity measured; this was done to investigate the movement of ions in and out of samples during curing. 0.6 M NaCl solution is commonly used to imitate sea water, as sea water globally has, on average, around the same concentration of NaCl, and electrical conductivity (~ 50 mS/cm) (Millero et al., 2008; Tyler et al., 2017).
- A last set of samples were cured in two different salt solutions, where one had twice the concentration of the other, which instead used a salt with a cation of twice the valency (1.2 M NaCl and 0.6 M $CaCl_2$, respectively), in order to compare the relative contributions of salt concentration and cation valency to CS grout strength.

4.2.2.6 CS grout samples for SEM

CS grout samples cured for 1 d and 42 d were prepared for SEM imaging to investigate any differences in micro-structure. Two further samples were prepared which were cured for 42 d in 1 M $CaCl_2$ solution and tap water. SEM sample preparation was done according to the method in 3.2.8.

4.2.3 Experimental Procedures

4.2.3.1 CS grout gel time measurement

The viscosity evolution during gelation for various CS grout mixtures was measured using a viscometer, and gel times were calculated from this, according to the method in 3.3.1.

4.2.3.2 Shear vane test method

Shear vane tests were carried out on different gelled CS grout samples to study how shear strength evolves during curing, and how various factors affect the strength. These were done according to the method in 3.3.4.

4.2.3.3 UCS test method

Drained uniaxial compression tests were carried out to study the unconfined compressive strength of sand grouted with various CS grout mixtures. This was done according to the method in 3.3.5.

4.2.3.4 SEM imaging method

SEM imaging was performed on CS grout samples to study their micro-structure. This was done using the method in section 3.3.6.

4.3 Results

Here, the results of the viscometer measurements, shear vane tests, UCS tests, and SEM imaging are presented, showing how the various factors under investigation affected the gelation, strength and structure of CS grout and CS-grouted sand.

4.3.1 Gelation

One way to increase the strength and reduce the cost of CS grout is by changing the nature and quantities of its components; this will also affect its gel time, however, so it is important to understand how and to be able to compensate for it in order to maintain a desired gel time. One such factor is the silica mass fraction of the grout; reducing this quantity could provide significant savings if it can be done without compromising mechanical performance.

Figure 4.1A shows the evolution in viscosity, η, during gelation of CS grouts with 20, 30, and 40 wt% silica. Visible is the characteristic gelation profile of CS grout, which remains low-viscosity for an extended period, before quickly increasing in viscosity. It can be seen that decreasing silica wt% results in longer gel times. The NaCl concentration of the

accelerator also affects the gelation of the grout: Figure 4.1B demonstrates that higher concentrations of NaCl give shorter gel times.

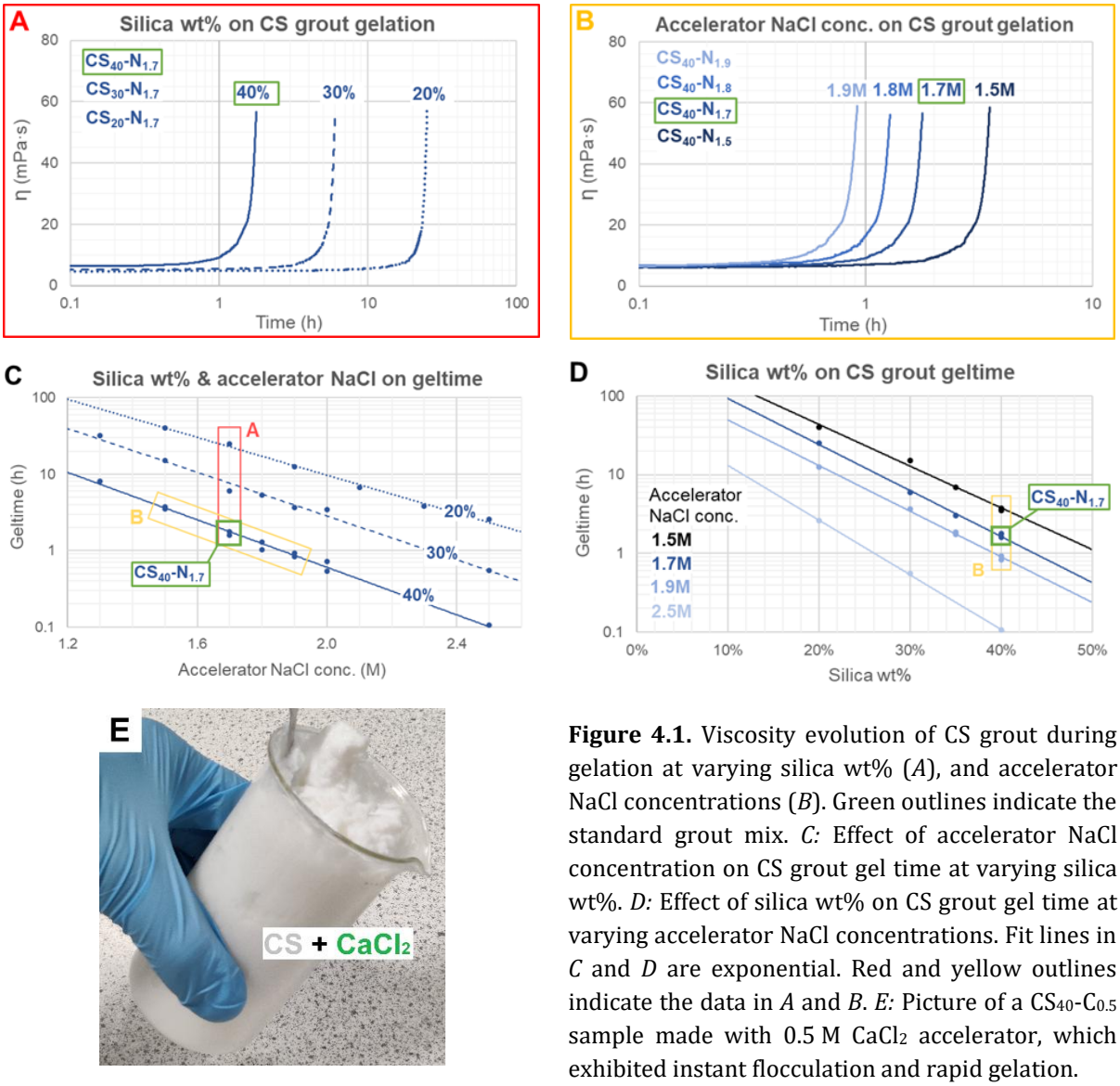

Figure 4.1. Viscosity evolution of CS grout during gelation at varying silica wt% (*A*), and accelerator NaCl concentrations (*B*). Green outlines indicate the standard grout mix. *C:* Effect of accelerator NaCl concentration on CS grout gel time at varying silica wt%. *D:* Effect of silica wt% on CS grout gel time at varying accelerator NaCl concentrations. Fit lines in *C* and *D* are exponential. Red and yellow outlines indicate the data in *A* and *B*. *E:* Picture of a CS_{40}-$C_{0.5}$ sample made with 0.5 M $CaCl_2$ accelerator, which exhibited instant flocculation and rapid gelation.

Figures 4.1C and D show the gel times of CS grouts of 20, 30, and 40 wt% silica with a range of accelerator NaCl concentrations. The relationships between the gel times, t_{gel}, and accelerator NaCl concentrations, c_{NaCl}, in the case of each silica wt% are well-described by exponential decay fits. The reverse is also true for the silica wt%, w_{SiO_2}, at each NaCl concentration. In Figures 4.1C and D, only a selection of the recorded datapoints are displayed, for the sake of clarity. The exponential fit equations have the form

$$t_{gel} = Ae^{Bc_{NaCl}}, \tag{4.1}$$

and

$$t_{gel} = Ae^{Bw_{SiO_2}}, \tag{4.2}$$

respectively, where A is a constant scale factor, $A > 0$, increasing the value of which shifts the fit upwards in the log y-axis, and B is the 'rate constant', with $B < 0$, for which lower values give steeper slopes. Exponential decays intercept the positive y-axis, are asymptotic to the positive x-axis, and appear as straight lines on semi-log axes. Table 4.2 provides the equations for each of the lines in Figures 4.1C and D.

Table 4.2. Exponential fit equations and R^2 values for the lines in Figures 4.1C and D. All values are to three significant figures.

Figure	*Silica wt%*	*Accelerator NaCl conc. (M)*	*Fit equation*	R^2	*Equation no.*
C	20	Varied	$t_{gel} = 2920e^{-2.85c_{NaCl}}$	0.992	(4.3)
	30		$t_{gel} = 2070e^{-3.30c_{NaCl}}$	0.995	(4.4)
	40		$t_{gel} = 775e^{-3.58c_{NaCl}}$	0.995	(4.5)
D	Varied	1.5	$t_{gel} = 499e^{-12.2w_{SiO_2}}$	0.993	(4.6)
		1.7	$t_{gel} = 356e^{-13.5w_{SiO_2}}$	0.999	(4.7)
		1.9	$t_{gel} = 188e^{-13.4w_{SiO_2}}$	0.999	(4.8)
		2.5	$t_{gel} = 64.8e^{-16.0w_{SiO_2}}$	1.000	(4.9)

It is interesting to note that the values of the rate constants in plot C decrease as silica wt% increases; this is also true for the accelerator NaCl concentration. These relationships may be combined to produce a single equation for estimating the accelerator NaCl concentration needed to account for the effect of varying silica wt%, such that gel time is kept constant:

$$t_{gel} = \exp\left(9.49 - 7.09w_{SiO_2} + \left(-3.37w_{SiO_2} - 2.20\right)c_{NaCl}\right). \tag{4.10}$$

Information on the derivation of this equation is provided in appendix A.2.2.

Using a different salt species in the accelerator is another possible way to increase the strength and reduce the cost of CS grout. $CaCl_2$ is an inexpensive and commonly used salt that was investigated here as a potential replacement for NaCl. However, viscometer measurement could not be performed as the $CaCl_2$ was not able to induce controllable gelation of CS grout across any of the accelerator concentrations tested, as shown in Table 4.3. At ≥ 0.5 M $CaCl_2$, there was instantaneous flocculation and gelation of the grout upon mixing; a photograph of such a reaction is displayed in Figure 4.1E. At ≤ 0.15 M, no

gelation occurred, with no change in η measured after 18 h, whilst at intermediate $CaCl_2$ concentrations, significant flocculation occurred, leading to phase separation, where the top portion of the grout gelled very quickly, and the lower part took much longer, if gelling at all. Here, simple visual inspection was used to determine if gelation had occurred or not.

Table 4.3. The effect of accelerator $CaCl_2$ concentration on the gelation of CS grout.

Accelerator $CaCl_2$ conc.	*Effect*	*Gelation*
0.1 M	No effect.	None
0.15 M	Minimal flocculation.	None
0.2 M	Phase separation; ~ 20% flocculation by vol.	Top: ~ 5 min. Bottom: ~ 1 d
0.3 M	Phase separation; ~ 50% flocculation by vol.	Top: ~ 5 min Bottom: ~ 30 min
0.5 M	Total flocculation	Instant

4.3.2 Shear strength

Shear vane tests were used to study the effect of grout components and environmental conditions on the shear strength of CS grout. Figure 4.2A shows shear stress/strain curves for CS grout samples using CS of 20, 30 and 40 wt% silica. Here, τ corresponds to the shear stress resulting from the applied shear strain γ. The gel times of the samples were kept constant by adjusting the concentration of NaCl in the accelerator using equation 4.10. The maximum shear stress samples could withstand before failing, called the ultimate shear strength, is denoted here as τ_{max}. From the figure, it is clear that decreasing silica wt% reduces the τ_{max} of samples. Figure 4.2B shows stress/strain curves for samples of different curing times, demonstrating how CS grout increases in strength over time.

Figure 4.2C combines the data in A and B to show the evolution in τ_{max} of grout samples of different silica wt% over curing time, t_c; this is well-described by sublinear power law relationships, of the form

$$\tau_{max} = \mathrm{a}t_c^b, \tag{4.11}$$

where a is a constant called the multiplier, $a > 0$, and b is another constant called the exponent, in the range $0 < b < 1$. Sublinear power laws pass through the origin and increase continuously, but at an ever slower rate. On log-log axes, power laws appear as

straight lines, with the slope of the line determined by the exponent, and the y-displacement by the multiplier.

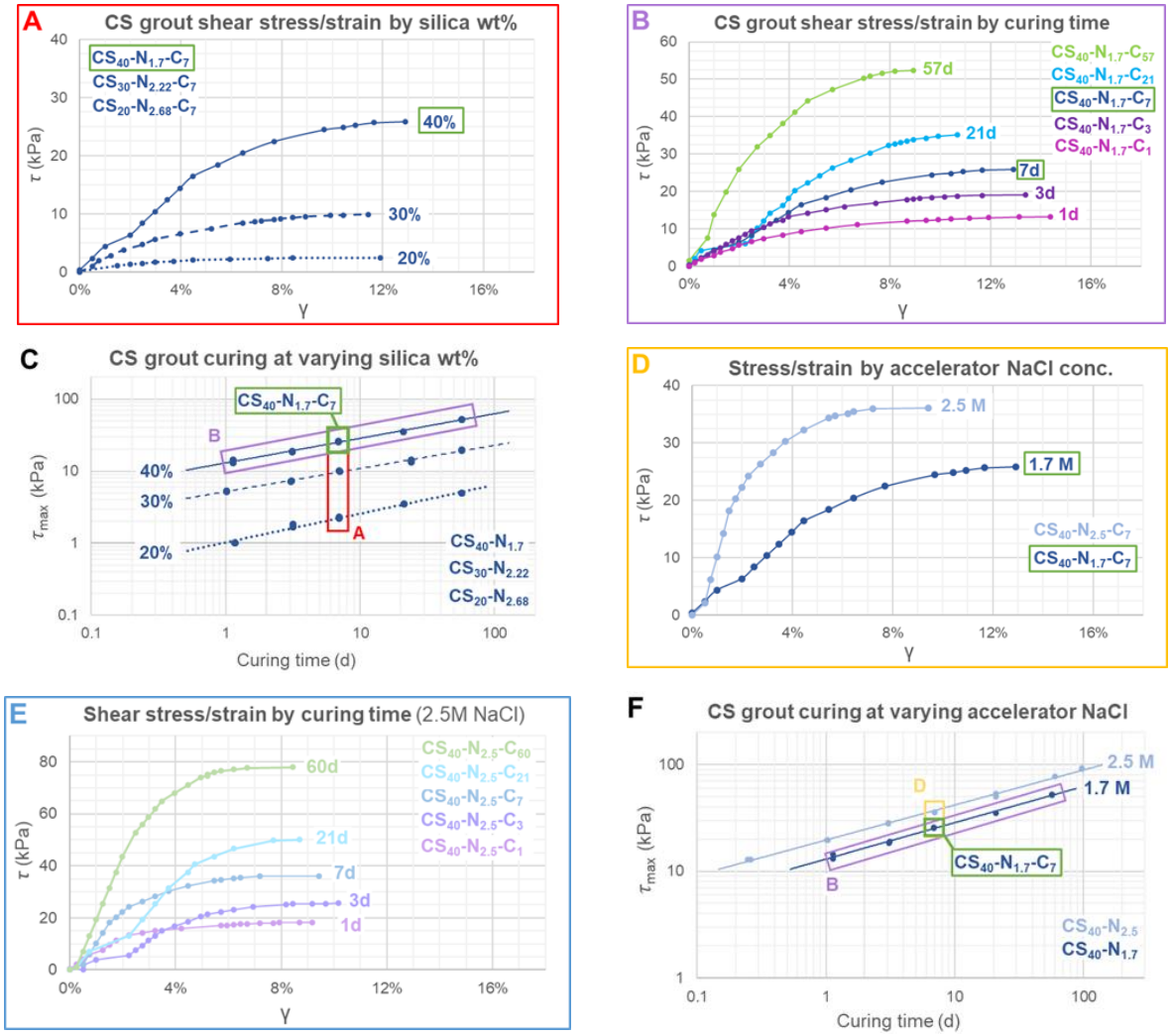

Figure 4.2. The shear response of CS grout of different silica wt% *(A)*, curing time *(B* and *E)*, and accelerator NaCl concentration *(D)*. The evolution in τ_{max} of CS grout of varying silica wt% *(C)* and accelerator NaCl concentration *(F)* during curing. The fits are sublinear power laws. Green outlines correspond to the standard grout mix, and red, purple, and yellow outlines indicate the data in *A*, *B*, and *D*, respectively.

Figure 4.2D shows shear stress/strain curves for CS grout with accelerator NaCl concentrations of 2.5 M, and the standard 1.7 M. From this, it can be seen that the higher NaCl concentration produces greater strength. Figure 4.2E shows stress/strain curves for samples of different curing times, with 2.5 M NaCl accelerator, again showing strength increasing over time. Figure 4.2F combines the data from D and E to demonstrate the effect of accelerator NaCl concentration on the evolution in τ_{max} of the grout during

curing. These are again described by sublinear power laws, of the same form as equation 4.11.

Increasing the accelerator NaCl concentration clearly accelerates the strength gain during curing. For any given curing time, τ_{max} is higher at 2.5 M NaCl than at the standard 1.7 M, and when plotting τ_{max} against the curing time on log-log scales (Figure 4.2F), the two curves are parallel, as if higher NaCl concentration induces an apparent time offset: samples cured at 2.5 M reach the same τ_{max} in a shorter curing time. In other words, increasing the salinity speeds up the bond-formation kinetics without altering the fundamental ageing mechanism.

Table 4.4 provides the fit equations for the power laws in Figures 4.2C and F. The fits all have different multipliers, but approximately equal exponent, with an average of 0.347, making them roughly parallel on the log-log plot, but displaced in the log y-axis.

Table 4.4. Power law fit equations and R^2 values for the lines in Figures 4.2C and F. All values are quoted to three significant figures.

Figure	*Silica wt%*	*Accelerator NaCl conc. (M)*	*Fit equation*	*R^2*	*Equation no.*
C	20	2.68	$\tau_{max} = 1.03 t_c^{0.398}$	0.994	(4.12)
C	30	2.22	$\tau_{max} = 5.20 t_c^{0.321}$	0.991	(4.13)
C, F	40	1.70	$\tau_{max} = 13.0 t_c^{0.341}$	0.997	(4.14)
F	40	2.50	$\tau_{max} = 19.6 t_c^{0.329}$	0.997	(4.15)

In each of the stress/strain graphs in Figure 4.2 (A, B, D, E), the samples can be seen to undergo a period of elastic deformation, followed by plastic deformation until the eventual ultimate strength is reached, at which point measurement stops. In plots B and D it seems as if weaker gels (those cured for lesser durations, and those with lower accelerator NaCl concentrations) undergo greater deformation before reaching their ultimate strength. This is not seen in plots A or E, however.

As well as changing the makeup of CS grout, utilising its curing environment is another potential way to increase its strength. Figure 4.3 shows the results of shear vane tests studying the effect of curing water on the evolution in shear strength of CS grout. The light blue line shows the increase in τ_{max} of a CS_{40}-$N_{2.5}$ sample as it cures. As described in 4.2.2.4, some 16 d cured CS_{40}-$N_{2.5}$ samples were added to containers of either 1 M $CaCl_2$ solution, or tap water, and left to continue curing. The results show how the samples

immersed in 1 M $CaCl_2$ achieved a considerably higher strength than controls by the time of measurement, whereas those cured in tap water were weaker than controls, confirming that the presence of electrolyte in the curing environment of CS grout affects its rate of strength increase, and that diffusion of ions into and out of samples may be an important factor.

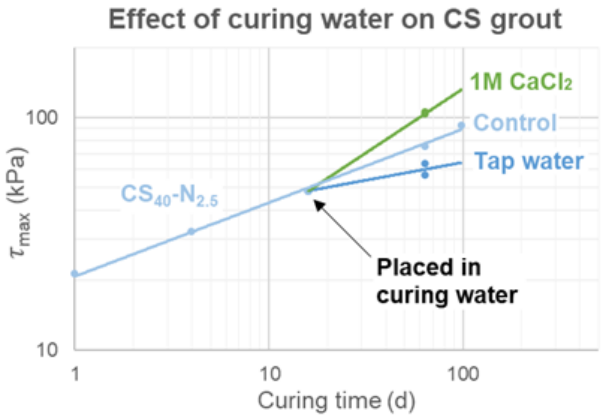

Figure 4.3. Effect of changing the curing water on the τ_{max} evolution of CS grout during curing.

4.3.3 Compressive strength of grouted sand

This subsection describes the results of UCS tests on CS-grouted sand, done to compare and expand on the findings from 4.3.2, to investigate the effect of the presence of sand, and to increase relevance to permeation grouting application.

4.3.3.1 Effect of curing time

Figure 4.4 presents the results of UCS tests on CS-grouted sand samples cured for different durations (GS_{40}-$N_{1.7}$-/-DW). Plot A shows the axial stress/strain curves for the samples during test, where σ is the compressive stress resulting from axial deformation, ε. It is clear that the maximum compressive stress, σ_{max}, that samples could withstand before failure, also referred to as their 'ultimate compressive strength', increased with curing time; the stiffness of the samples (i.e. the gradients of the curves) also increased. The maximum axial deformation that samples endured before failing, or the 'ultimate axial strain', again apparently increased with time, with the exception of the 1 d cured samples, which exhibited a relatively high degree of deformation. Each sample underwent a period of elastic deformation, followed by plastic deformation, during which stress reached a maximum, before it then decreased until eventual failure. Stronger samples (i.e. those with longer curing times) exhibited comparatively less plastic

deformation, and more sudden and brittle failures after their ultimate strength was reached, whereas the 1 d cured sample exhibited more ductile behaviour. Figure 4.4B plots the σ_{max} for each of the samples; as was seen with shear strength in 4.3.2, the increase in σ_{max} during curing is well-described by a sublinear power law, of the form

$$\sigma_{max} = at_c^b. \tag{4.16}$$

In this case, the equation is

$$\sigma_{max} = 20.3t_c^{0.336}, \tag{4.17}$$

with $R^2 = 0.937$. Older and stronger samples tended to fail via axial splitting, with multiple failure planes along the vertical axis, fracturing into several large pieces. An example of this is shown in Figures 4.4C and D. Younger samples instead sheared only along a single plane, splitting into two even pieces, as shown in Figure 4.4E.

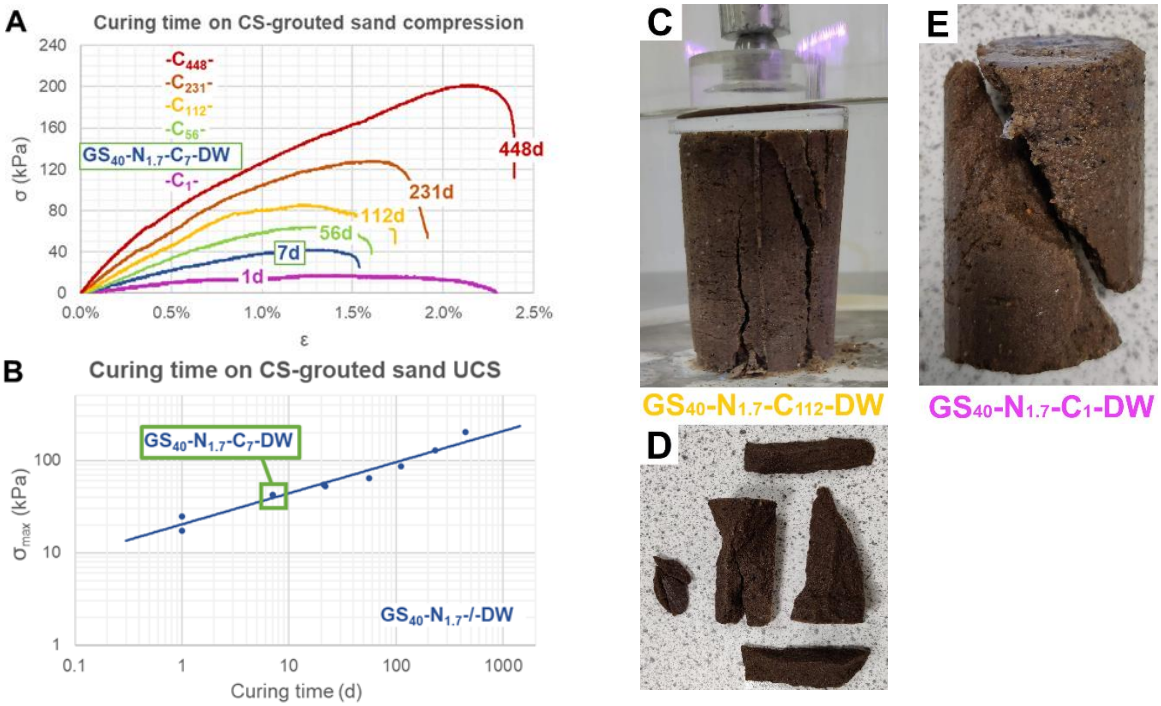

Figure 4.4. *A:* Stress-strain plots for CS-grouted sand samples cured for different durations undergoing unconfined uniaxial compression. *B:* The ultimate compressive strength of each sample against curing time, fitted with a sublinear power law. The standard CS-grouted soil sample composition is highlighted in green. *C:* An older CS-grouted sand sample (GS_{40}-$N_{1.7}$-C_{112}-DW) exhibiting axial splitting as it fails during UCS test, and the resulting fragments, post-failure (*D*). *E:* A young CS-grouted sand sample (GS_{40}-$N_{1.7}$-C_1-DW) which sheared along a single plane.

Electrical conductivity, *K*, and pH measurements were also taken on the curing water of a GS_{40}-$N_{1.7}$-/-DW sample as it was cured. Originally, the DI water had K = (1.14 ± 0.01) µS/cm, but after 13 weeks, it had increased to K = (4.28 ± 0.01) mS/cm,

a 37500% increase, suggesting significant diffusion of ions out of the sample and into the water. A minor increase in pH was also observed.

4.3.3.2 Effect of changing grout components

Figure 4.5A shows the results of UCS tests on samples prepared using grout with CS of 30, 35, and 40 wt% of silica, each cured for 4 weeks in tap water. Equation 4.10 was used to ensure gel time was constant across the samples by varying the concentrations of NaCl in the accelerator. It should be noted that the standard grout mix, which gave a gel time of ~ 1.70 h, was not used, with all samples instead having gel time of ~ 3.02 h. From the plot, it is clear that reducing silica wt% causes a significant decrease in the compressive strength of grouted sand. The relationship between silica wt% and compressive strength is well-described by an exponential fit with positive scale factor and rate constant.

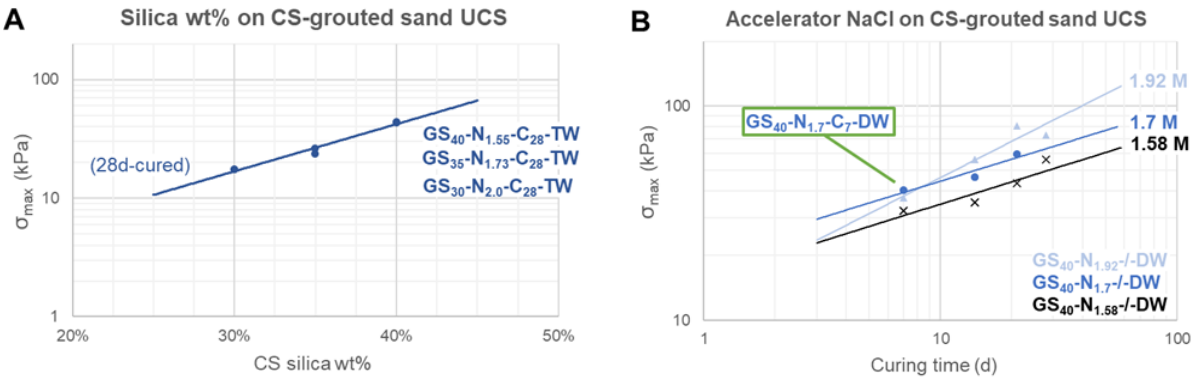

Figure 4.5. *A:* Effect of silica wt% on the compressive strength of CS-grouted sand, with exponential fit shown. *B:* Effect of accelerator NaCl concentration, and by extension, gel time, on the compressive strength of CS-grouted sand. Each of the lines is a sublinear power law fit. The standard CS-grouted sand sample is identified in green.

Figure 4.5B presents the results of experiments investigating the effect of accelerator NaCl concentration, and thereby gelation rate, on the compressive strength of CS-grouted sand. Equation 4.5 was used to calculate NaCl concentrations which would provide gel times that were multiples of each other. As would be expected from the results in 4.3.2, higher accelerator NaCl concentrations, and therefore faster gel times, produced samples with greater compressive strength. Similar to the results presented in Figure 4.2F, when plotting σ_{max} against curing time on log-log scales, the two curves for NaCl concentrations of 1.58 M and 1.7 M are essentially parallel. This suggests that a higher NaCl concentration induces an apparent time offset. In contrast, the dataset for the NaCl concentration of 1.92 M shows a divergent trend instead, which might be caused by an

unexpectedly low σ_{max} value for 7 d cured samples. Table 4.5 provides the power law fit equations for the lines in Figure 4.5B.

Table 4.5. Power law fit equations and R^2 values for the lines in Figure 4.5B. Values are quoted to three significant figures.

Accelerator NaCl conc. (M)	*Gel time (h)*	*Fit equation*	*R^2*	*Equation no.*
1.58	~ 0.85	$\sigma_{max} = 15.7t_c^{0.346}$	0.835	(4.18)
1.70	~ 1.70	$\sigma_{max} = 20.4t_c^{0.339}$	0.911	(4.19)
1.92	~ 2.60	$\sigma_{max} = 12.8t_c^{0.560}$	0.880	(4.20)

4.3.3.3 Effect of curing water properties

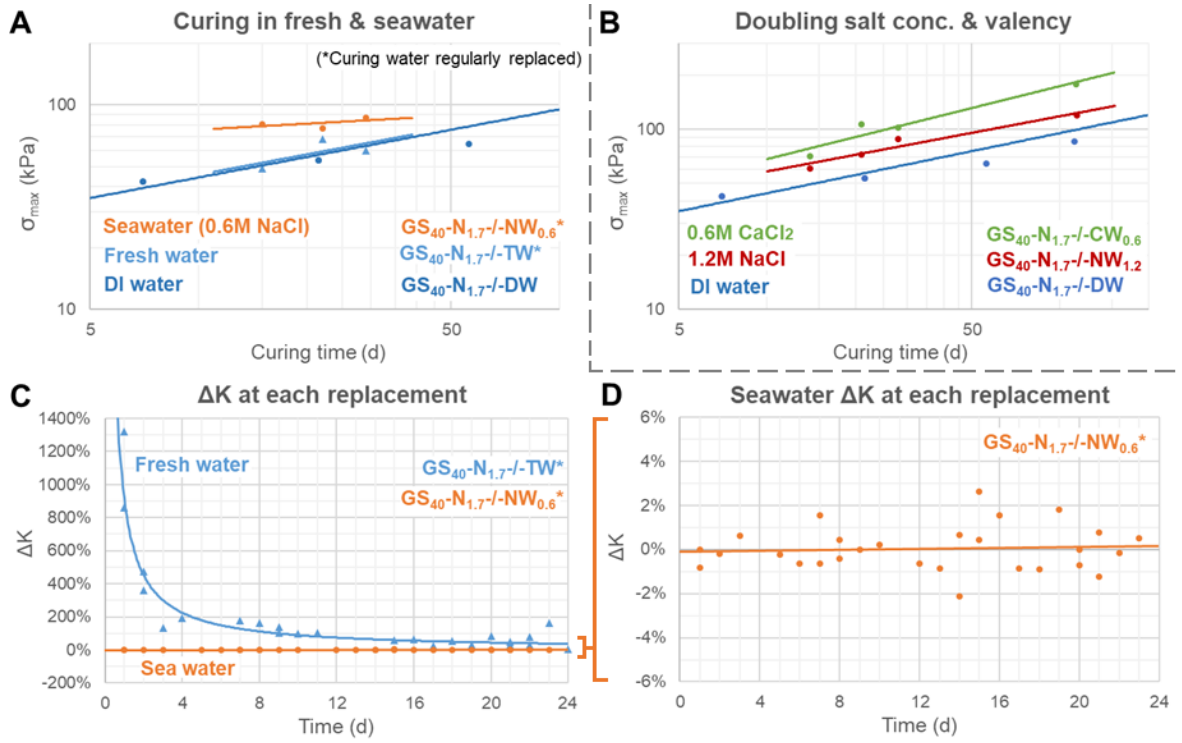

Figure 4.6. *A:* The effect of curing in fresh (tap) water and sea water (0.6 M NaCl) that is continually replaced on the compressive strength evolution of CS-grouted sand, in comparison to control samples cured in DI water, which was not replaced. *B:* The effect of doubling the concentration (1.2 M NaCl), and valency (0.6 M $CaCl_2$), of salt in the curing water, with the same control data as *A*, for comparison. All lines of fit in *A* and *B* are power laws. *C:* The change in electrical conductivity measured each time the curing waters in *A* were replaced. *D:* The saltwater data from *C*, but zoomed in to a smaller percentage range. The blue line in *C* is a power law decay, and the orange lines in *C* and *D* are linear fits.

Figure 4.6A shows the results of UCS tests on samples cured in tap water, and in 0.6 M NaCl, which were analogous to fresh water and sea water. For these samples, the particular curing water was replaced approximately daily. Also present in the figure is the data from 4.3.3.1, as a control: these samples were cured in DI water, which was not

replaced. From Figure 4.6A, samples cured in salt water exhibited significantly higher strength than those cured in fresh water, which were approximately the same as the controls. Notably, the salt water samples began with a higher baseline strength, evidence of greatly accelerated early-age curing, yet their subsequent strength gain was less pronounced compared with the fresh water specimens, and the two curves appear to converge over time.

However, the salt water and fresh water data each suffer from a high degree of random variation, compounded by them only featuring points at three curing times each, meaning that the power law fits describing their increase in σ_{max} with time can be only estimated with a low degree of confidence. Table 4.6 provides the fit equations and R^2 values for each of the lines in Figure 4.6A, with the freshwater and seawater fits having R^2 of only 0.359 and 0.303, respectively, much lower than the control data, at 0.937. This is likely the reason why the salt water fit line is not parallel to the control line on the log-log plot.

Figures 4.6C and D show the percentage change in electrical conductivity, ΔK, of the fresh and salt water, as measured before each replacement. It can be seen that, for the fresh water, large increases in electrical conductivity were observed in the initial replacements, which then decreased towards zero, according to a power law decay, as K approached the value for normal tap water; this suggests that significant movement of ions occurred out of the sample and into the fresh water. For the salt water, however, the electrical conductivity remained virtually constant throughout. It should be noted that the system is not expected to have reached equilibrium each time the curing water was replaced.

Table 4.6. Power law fit equations and R^2 values for the lines in Figures 4.6A and B.

Series	*Curing water salt conc. (M)*	*Curing water salt*	*Replaced?*	*Fit equation*	R^2	*Equation no.*
DI water	0.0	n/a	No	$\sigma_{max} = 20.3t_c^{0.336}$	0.937	(4.17)
Fresh water	0.0	n/a	Yes	$\sigma_{max} = 21.3t_c^{0.331}$	0.359	(4.21)
Salt water	0.6	NaCl	Yes	$\sigma_{max} = 60.5t_c^{0.0978}$	0.303	(4.22)
Double conc.	1.2	NaCl	No	$\sigma_{max} = 28.8t_c^{0.307}$	0.952	(4.23)
Double val.	0.6	$CaCl_2$	No	$\sigma_{max} = 26.9t_c^{0.406}$	0.959	(4.24)

Figure 4.6B shows the results of UCS tests on samples cured in 1.2 M NaCl, double the NaCl concentration of the sea water analogy, and in 0.6 M $CaCl_2$, which has the same concentration, but uses a salt with double the valency of cation (Ca^{2+}, compared to Na^{+}), as well as the same control data as before, in DI water. Unlike with the previous samples,

the curing waters were not replaced here. From plot B, it is clear that both the 1.2 M NaCl- and 0.6 M $CaCl_2$-cured specimens outperformed DI water over time, but they each showed distinct trends. The NaCl-cured specimens began at higher strength and then gained strength at a rate nearly parallel to, or slightly converging toward, the DI-cured curve. In contrast, the $CaCl_2$-cured samples not only exhibited elevated early-age strength, but also sustained a much steeper strength gain throughout the test, rising well above both the DI and NaCl trajectories. Table 4.6 provides power law fit equations for each of the lines in Figure 4.6B. The 1.2 M NaCl and 0.6 M $CaCl_2$ curves have much higher R^2 (0.952 and 0.959, respectively) than the previous data.

4.3.4 SEM imaging

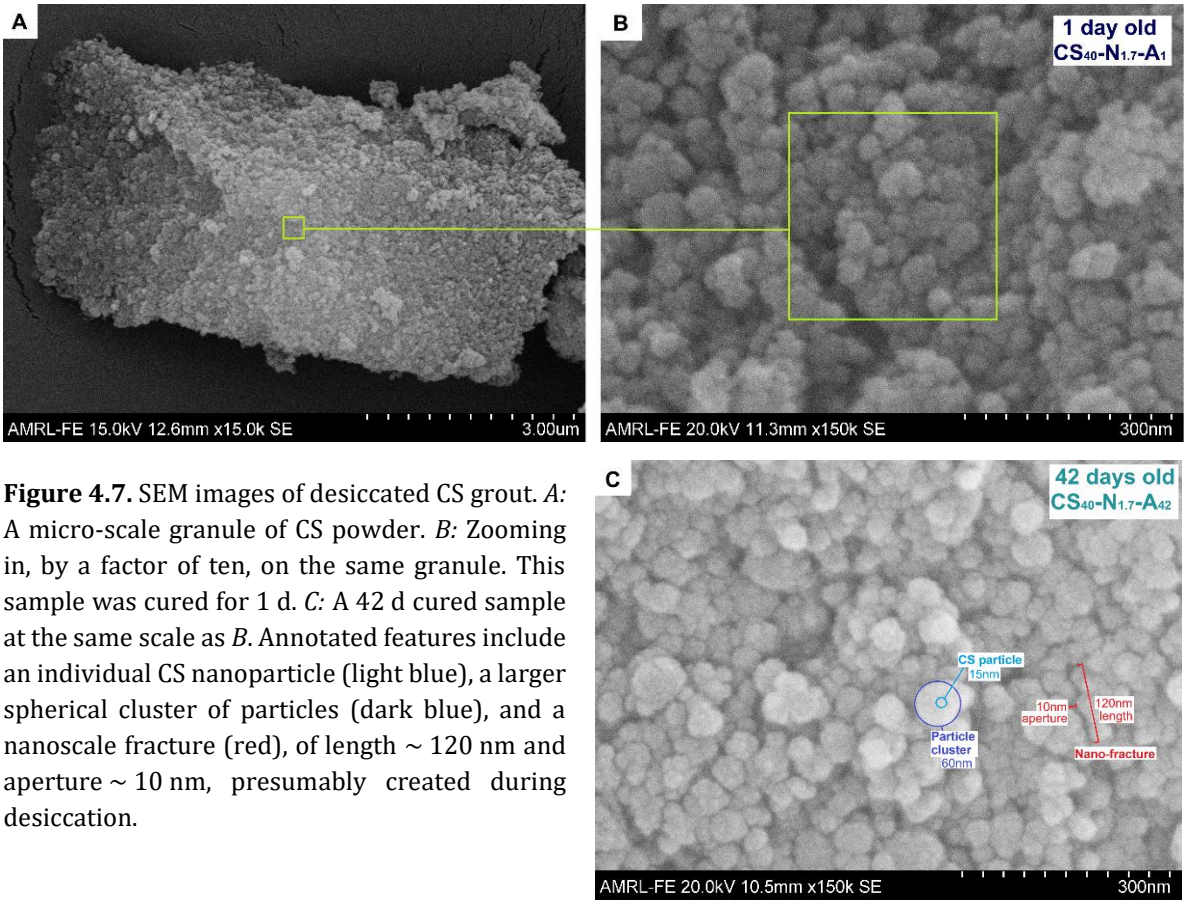

Figure 4.7. SEM images of desiccated CS grout. *A:* A micro-scale granule of CS powder. *B:* Zooming in, by a factor of ten, on the same granule. This sample was cured for 1 d. *C:* A 42 d cured sample at the same scale as *B*. Annotated features include an individual CS nanoparticle (light blue), a larger spherical cluster of particles (dark blue), and a nanoscale fracture (red), of length ~ 120 nm and aperture ~ 10 nm, presumably created during desiccation.

Presented in Figure 4.7 are SEM images taken of desiccated gelled CS grout. Plot A shows a single granule of the resulting powder, several μm in size. Figure 4.7B shows the same granule zoomed in by a further factor of 10. This sample was cured for just 1 d before drying. Figure 4.7C shows another sample, cured for 42 d, at the same magnification as B. From both B and C, the nano-structure of the dried CS grout appears to comprise of tightly

packed, approximately spherical clusters, with diameters ~ 60 nm, consisting of several CS nanoparticles. These clusters are separated in places by nanoscale fractures, presumably resulting from the desiccation process. It does not seem possible to discern any structural differences between the 1 d and 42 d cured samples from these images. Samples were also produced to investigate the effect of curing in 1 M $CaCl_2$ and tap water, but again, no structural difference was observed.

4.4 Discussion

4.4.1 Gelation

The results in section 4.3.1 demonstrate that, for both CS silica wt% and accelerator NaCl concentration, the relationships between each factor and the gel time of CS grout are well-approximated by exponential decay laws, with increasing silica wt% or NaCl concentration giving faster gel time. These results generally agree with observations made by other researchers (Iler, 1979; Jurinak et al., 1991b; Pedrotti et al., 2017), although power law decays have also been used to describe the relationships (Van Der Linden et al., 2015). As described in section 2.2.2, increasing the electrolyte concentration increases the number of cations which adsorb on the surface of CS particles, strengthening the charge screening effect and depression of the EDL; this causes faster gelation by allowing more collisions between particles (Bergna & Roberts, 2006). Higher silica wt% also gives faster gel times, as there are more CS particles to collide.

In 4.3.1, it was found that $CaCl_2$ salt could not be reliably deployed in the accelerator in place of NaCl. The reason for this is that Ca^{2+} ions have double the valency of Na^{+} ions (2 to 1), meaning they also have twice the charge, and are therefore more effective at screening the surface charge of CS particles, causing them to clump together rapidly and densely, such that they coagulate out of suspension rather than gradually forming a gel network. Other studies have had success using $CaCl_2$ accelerator, although these have mostly been either at neutral or acidic pH (Pedrotti et al., 2017), or have used alumina-stabilised CS (Funehag & Fransson, 2006; Moridis et al., 1995), both of which reduce the screening effect of cations by reducing the extent of their adsorption on CS particles (Iler, 1979). MacLachlan et al. (2013) was able to gel MP 320 CS at alkaline pH using 0.033 M $CaCl_2$, but noted significant heterogeneities in samples, with large aggregates and layers,

presumably making it unsuitable for grouting. It can be concluded that $CaCl_2$ is therefore not suitable to use in the accelerator for MP 320 CS grout at alkaline pH.

Different applications for CS grout have their own requirements in terms of gel time, but in permeation grouting, CS grout generally needs sufficient time to spread away from the injection point before gelling to ensure proper coverage, and to avoid blocking the injection apparatus. However, it also needs to gel quickly enough to avoid excessive dilution and being transported out of the target volume by gravity and groundwater flow, as happened in Hamderi and Gallagher (2015). Soil conditions have also been seen to greatly affect the gelation of CS grout, and by extension, its effectiveness in its applications. It is clear, therefore, how having a good understanding of the ways in which different factors affect the gelation of CS grout is vital to its successful application. The data in 4.3.1 adds to this understanding, and could be used in designing a comprehensive model for predicting the viscosity evolution and gel time of CS grout.

4.4.2 Strength and curing

4.4.2.1 Effect of curing time

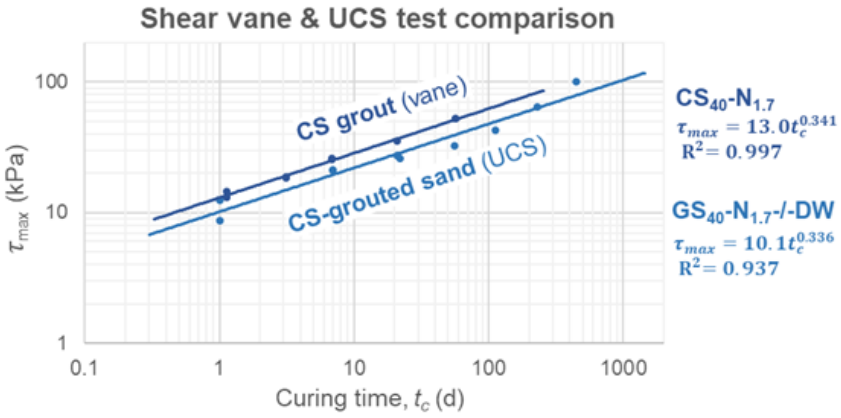

Figure 4.8. Comparison of τ_{max} measured in shear vane tests on CS grout and UCS tests on CS-grouted sand. On the right are shown the power law fit equations and R^2 values.

Figure 4.8 plots the evolution in shear strength of CS grout (CS_{40}-$N_{1.7}$), from section 4.3.2, and CS-grouted sand samples (GS_{40}-$N_{1.7}$-/-DW), from section 4.3.3.1, each cured for increasing durations; this allows for a comparison of the shear vane and UCS methods. For unconfined uniaxial compression, τ_{max} can be determined by dividing σ_{max} by 2 (i.e., $\tau_{max} = \sigma_{max} / 2$) (Craig, 2004). The increases in shear strength seen in each test are well-described by power laws of approximately equal exponents, but different multipliers,

such that they are parallel on the log-log plot, but with the shear vane data shifted up in the y-axis. The reason for the shear vane data giving greater shear strength is likely that it did not use curing water, as opposed to the grouted sand samples, which were cured in DI water, and therefore experienced some diffusion of ions out of the sample, as evidenced by the electric conductivity measurements in 4.3.3.1. However, the fact that the exponents of the fits are approximately equal implies that both tests effectively measure the curing process. The UCS data has notably higher R^2 than the shear vane data, implying it suffers from a greater degree of random variation; this is likely due to minor inconsistencies in the densities, grain sizes, and grout penetration of the grouted sand samples.

As described in section 2.2.4, it is thought that the increase in strength of CS grout during curing is due to ongoing deposition and condensation of dissolved silicates at the joining points between CS particles, where there is negative curvature, thickening the 'necks' which formed when the particles first linked together (Iler, 1979). The additional covalent siloxane bonds created by this process increase the strength and rigidity of the network: an effect which may then continue for long durations after gelation. The increased strength and rigidity is likely what causes the failure mechanism of CS-grouted sand to change from a single failure plane, to one of axial splitting as curing progresses.

Iler (1979) says that the thickening of necks in the CS gel network, as well as dissolution from areas of positive curvature, can cause the network to take on a 'tubular' structure (see Figure 2.9). The SEM images in 4.3.4 were not able to demonstrate the formation of necks or tubular structures in CS grout cured for 49 d, however. This could be due to a variety of factors: in particular, the fact that the relative maximum width of inter-particle necks is thought to depend inversely on the particle size, such that MP 320 CS particles may be too large for the necks to be visible (see Figure 2.10). Other contributing factors could include insufficient SEM resolution, or allowed curing duration.

With regard to practical application, the results show that as long a curing time as possible should be allowed to achieve maximum strength in CS grouted soils; this is particularly true where grouted volumes are expected to come under mechanical stress, such as if construction/deconstruction operations are to commence on the surface above

them, or if CS grout is being used to facilitate excavation of contaminated soils, for example.

4.4.2.2 Effect of grout components

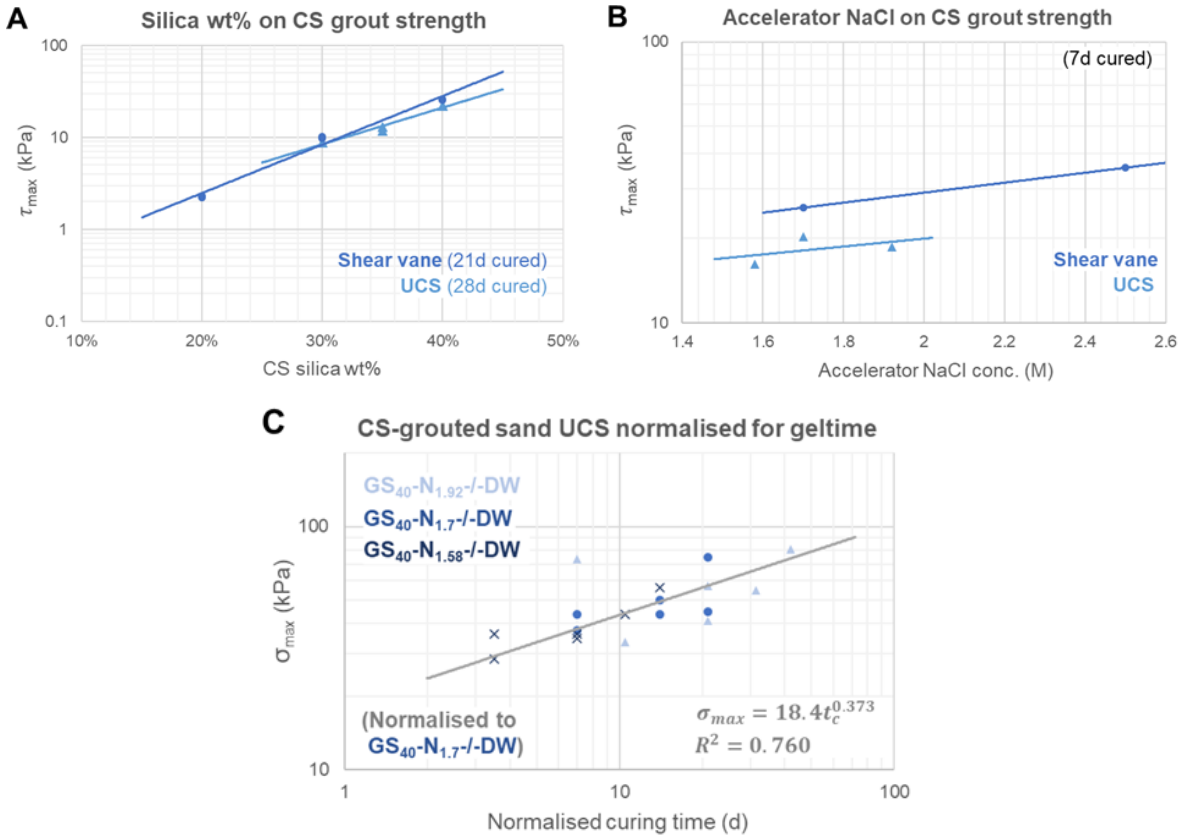

Figure 4.9. Effects of silica wt% (*A*) and accelerator NaCl concentration (*B*) on the shear strength of CS grout and CS-grouted sand, with exponential fits shown. *C:* The data from Figure 4.5B, but with the curing times of points normalised for the gel times of the grout mixtures used, such that they are all equivalent to GS_{40}-$N_{1.7}$-/-DW. The line is a sublinear power law fit, with associated equation and R^2 value shown.

The results in 4.3.2 and 4.3.3.2 show that both higher silica mass fraction and accelerator NaCl concentration give greater strength in CS grout and CS-grouted sand. Figures 4.9A and B show how, in each case, the relationships are well-described by exponential fits, with similar results in both the shear vane and UCS tests. It makes sense that CS of greater silica wt% would produce denser networks, and therefore stronger gels, and that having a greater concentration of dissolved silicates in the solvent would accelerate the curing process.

Regarding the effect of salt concentration, it is known that dissolved salts, such as NaCl, promote dissolution of silica (Iler, 1979), so it may be that higher electrolyte

concentration accelerates the redistribution of silica to inter-particle necks, thereby accelerating curing. The effect may also arise from greater numbers of adsorbed kosmotropic Na^+ ions at particle surfaces increasingly polarising surrounding water molecules to create local areas of acidity, which promote siloxane bond formation, as suggested by Johnsson et al. (2011). Adsorbed Na^+ ions could also be contributing to strength via electrostatic interactions, either acting as bridges between particles, or through ion-ion correlation interactions, as described by Johnson et al. (2008).

Figure 4.9C shows the data from Figure 4.5B, normalising the curing times of points according to the gel times of the grout mixtures used, such that they are all equivalent to the standard GS_{40}-$N_{1.7}$-/-DW. The result is well-described by a sublinear power law fit, with equation similar to that of equation 4.17, which used the same grout mix, but with much lower R^2 (0.760 compared to 0.937). This suggests that it may be possible to equate curing times and gel times in terms of how they affect the strength of CS grout, which in turn suggests that salt ions play a similar role in curing as they do during the gelation process, although the confidence in this conclusion is not high.

By combining the relationships in table 4.4, it is possible to calculate the accelerator NaCl concentration needed to account for the decrease in strength of CS grout as its silica wt% is reduced, as described by the equation

$$c_{NaCl} = 0.0442\, w_{SiO_2}^{-4.041}, \tag{4.1}$$

where c_{NaCl} is the accelerator NaCl concentration in M, and w_{SiO_2} is the CS silica wt%. This could be used to reduce the cost per unit mass of CS grout by diluting it, whilst maintaining its mechanical strength using increased salt concentration. However, the NaCl concentrations required to compensate for the strength reduction quickly become unpractically high as silica wt% decreases (e.g., 20 wt% silica requires $c_{NaCl} \sim 29$ M, with corresponding gel time of t_g = 0.002 s), so this technique could therefore only reasonably be used for small reductions in silica wt%.

4.4.2.3 Effect of the curing environment

The results in 4.3.2, and 4.3.3 show how increasing salt content in the curing water of CS grout gives samples greater strength, and accelerates their curing. The reverse was also found, with samples cured in fresh water having reduced strength, and exhibiting slower curing than samples cured in their own pore water (i.e., with just a thin film of water to

cover them and prevent drying). When samples were cured in fresh water, or DI water, significant movement of ions out of samples and into the curing water was detected, reinforcing the assertion that the presence of ions continues to play a key role throughout the curing process via the same potential mechanisms as described regarding the accelerator salt concentration in 4.4.2.2.

In addition to this, doubling the cation valency of the salt used (from NaCl to $CaCl_2$) was found to give a greater effect than doubling the concentration. This is likely due to the higher charge density of Ca^{2+} ions having a greater screening effect than simply increasing the number of Na^+ ions (Döpke et al., 2019). Ionic strength is a measure which combines both the concentrations and charges of ions in a solution, and is defined by the formula

$$\mathrm{I} = \frac{1}{2}\sum_i c_i z_i, \tag{4.2}$$

where z_i is charge of ion i, c_i is its molar concentration, and the sum is taken over all ions in the solution. From this, 0.6 M $CaCl_2$ has higher ionic strength than 1.2 M NaCl (1.8 M to 1.2 M), so it may be that the effect on strength and curing simply depends on the ionic strength. Future experiments should be done to identify whether the increase in strength provided by the $CaCl_2$ is simply due to its higher ionic strength, or if there are ion-specific factors involved, as some studies have suggested (Bischoff et al., 2021; Szymanek et al., 2021).

These results demonstrate that CS grout can be expected to impart greater strength in soils, and cure faster, where local ground water is more saline, for example at coastal or contaminated sites, and particularly where $CaCl_2$ is present, in comparison to NaCl. Where ground water is fresher in character, and especially where it is regularly replaced with new fresh water, the strength of grouted volumes can be expected to be reduced, with slower curing, due to the diffusion of ions from the accelerator out of the grout and into the environment. With this in mind, a possible way to improve the strength and accelerate the curing of grouted volumes after they have been prepared could be to perform secondary injections of $CaCl_2$, or other salt solutions.

4.5 Conclusion

In this chapter, viscometer tests found that both the silica mass fraction of CS grout, and the concentration of NaCl in its accelerator, affected its gel time according to exponential

relationships, with lower silica wt% and NaCl concentrations giving longer gel times. These relationships were combined to derive an equation for estimating the gel time of MP 320 CS grout with any silica wt% or accelerator NaCl concentration. Using $CaCl_2$ in the accelerator, however, was found to be an unreliable method for inducing gelation in MP 320 CS grout at alkaline pH, with it instead causing rapid coagulation and phase separation. NaCl is instead recommended over $CaCl_2$ for application with this CS. Cations from salts induce gelation of CS by screening the negative surface charge of particles, depressing the EDL, and allowing them to approach close enough to bond. The higher charge of Ca^{2+} ions compared to Na^{+} is too effective in this, however, causing CS particles to rapidly aggregate into dense clumps which cannot stay in suspension, as opposed to gradually forming a gel network. Having precise control of gel times is of great importance in the application of CS grout, particularly if grout properties are to be varied to produce different effects. The data presented here contributes to the understanding of the gelation of CS grout and could be used as part of a comprehensive model for predicting the viscosity evolution and gel times of CS grout.

Shear vane and UCS tests found that the strength of CS grout and CS-grouted soil increased with curing time according to sublinear power law relationships. This is thought to arise from continuous deposition and condensation of dissolved silicates at the joining points between CS particles in the gel network. The additional siloxane bonds resulting from this process cause the network to become stronger and more rigid over time. SEM imaging was not able to demonstrate this effect, however, for several possible reasons. It is important to allow as long a duration as possible, therefore, before conducting operations on or above volumes of CS-grouted soil, to maximise their strength and integrity.

It was also found that silica wt% and accelerator NaCl concentration affect the strength of CS grout according to exponential relationships, with higher silica wt% and NaCl concentrations giving greater strength. By combining these relationships, an equation was derived which allowed for calculating the concentration of NaCl needed to offset the decrease in strength resulting from reducing the silica wt% of CS grout. This could be useful for reducing the material cost of the grout without compromising on mechanical performance. However, this method can only be used for small reductions in silica wt%,

as the NaCl concentrations required quickly become impractically high. Normalising curing times by assuming proportionality with gel times gave apparently valid results, suggesting that ions play a similar role in the curing process to that which they have in gelation. Possible reasons for the strength increase caused by increased electrolyte concentration could be due to it promoting the redistribution of silica in the network towards the joining points between particles; due to cations facilitating additional siloxane bond formation between particles; or due to the electrostatic interactions of adsorbed cations.

Finally, it was shown that the salt content of the surrounding water in which CS grout cures also affects its strength, with higher concentrations of NaCl giving greater strength. Using $CaCl_2$, which has double the cation valency of NaCl, was found to give a greater strength increase than doubling the NaCl concentration due to the higher charge density of Ca^{2+} ions. In contrast, samples cured in fresh water were found to have reduced strength compared to controls. In such cases, diffusion of ions out of samples and into the fresh curing water was detected through electric conductivity measurements. These results are important for understanding how the ground water properties and electrolyte content of the soil at a site can impact the strength and curing of grouted volumes. Utilising this effect, a potential way to increase the strength of CS-grouted volumes after installation is to employ secondary injection of a saline solution, such as $CaCl_2$.

Chapter 5: The Re-healing Ability of CS Grout

5.1 Introduction

During the course of this investigation on CS grout, it was observed that samples which had been broken and left for a time were able to re-heal the damage sustained. This previously unknown property of CS grout gives it a key advantage over conventional grouting materials, such as cements, by providing it with added resilience and adaptability in all potential applications. For instance, regarding its use as an injectable hydraulic barrier, cracking and other damage has been shown to greatly reduce the effectiveness of such barriers, so the ability to self-repair in situ would be a highly desirable property for a barrier material, as it could potentially remove the need for future interventions after installation to shore up or replace barriers which have become damaged. The same benefit would also exist for grout used in soil stabilisation: reducing or avoiding the need for potential repeated treatments would provide significant cost savings. To the author's knowledge, no literature currently exists on the re-healing ability of CS grout.

Presented in this chapter is the first experimental study on CS grout re-healing, demonstrating that it occurs both in the grout itself and in CS-grouted soil, and aiming to identify which properties of the grout and the surrounding environment affect re-healing, and how they can be manipulated to enhance it. The study focusses on mechanical tests of the shear strength of CS grout and CS-grouted sand before and after suffering damage to observe how the strength of samples recovers over time, and to what extent it does so. Explanations for the underlying mechanism behind the re-healing process, and how it is impacted by various factors, are then discussed. Five experiments were conducted as part of this study, examining the effects of curing and healing times; breaking and re-healing multiple times; grout properties; and healing water properties on the re-healing of CS grout, as well as demonstrating that re-healing occurs in CS-grouted sand.

5.2 Methodology

5.2.1 Materials

Materials used in this study include MP 320 and MP 325 CS, NaCl, $CaCl_2$, and fine-grain sand, and equipment used includes 55 mL and 280 mL hexagonal glass jars: more information on all of these can be found in section 3.1.

5.2.2 Sample preparation

5.2.2.1 Sample naming convention

Table 5.1 outlines the naming convention used for samples in this investigation. Using this, for example, a sample named CS_{40}^{320}-$N_{2.5}$-C_{14}-H_{14}-$NW_{0.6}^{9}$ would refer to a one which used MP 320 CS grout with 40 wt% of silica, and accelerator of 2.5 M NaCl, which was cured for 14 d, and re-healed for 14 d in healing water of 0.6 M NaCl at pH 9.

Table 5.1. Explanation of the re-healing sample naming convention used in chapter 5.

Term order	*Variable*	*Abbreviation*	*Meaning*	*Subscript*	*Superscript*
1	Sample type	CS	CS grout	CS SiO_2 wt%	CS type
		GS	CS-grouted sand		
2	Acc. salt	N	NaCl	Conc. (M)	-
3	Curing time	C	Cur. time	Cur. time (days)	-
4	Healing time	H	Heal. time	Re-heal. time (days)	-
5	Healing water	TW	Tap water	-	pH
		NW	NaCl sol.	Conc. (M)	
		CW	$CaCl_2$ sol.		
		SW	MP 320 CS	-	

5.2.2.2 CS grout preparation

CS grout was prepared as described in section 3.2.2: the standard grout mix used MP 320 CS mixed at 5:1 volume ratio, with accelerator of 2.5 M NaCl. The resulting composition of such samples by mass was 64% water, 34% silica, and 1.9% NaCl. Other silica mass fractions and accelerator NaCl concentrations were also used, as well as MP 325 CS.

The gel time of the grout used was determined using a viscometer, according to the method in 3.3.1. Gel time data for MP 325 CS grout with different accelerator NaCl concentrations was collected, and can be found in appendix A.3.1. Similar data on MP 320 was previously collected in chapter 4. From this, the NaCl concentration needed to give MP 320 CS grout the same gel time as MP 325 CS grout could be determined, using the formula

$$c_{320} = 0.354 + 0.667 c_{325}. \quad (5.1)$$

This suggests that an NaCl concentration of ~ 2.0 M would give MP 320 CS the same gel time as MP 325 grout with 2.5 M NaCl.

5.2.2.3 CS grout shear vane samples

CS grout samples for shear vane test were prepared by the method described in section 3.2.3, by pouring the selected grout into a 55 mL hexagonal glass jar and letting it cure for a set time. All samples in this study were covered with films of tap water during curing. As well as the standard 55 mL jars, one set of tests was conducted using 280 mL jars: 210 mL of CS grout was prepared for each jar, with 25 mL for the water film.

5.2.2.4 CS-grouted sand shear vane samples

CS-grouted sand samples for shear vane test were prepared according to the method in 3.2.4, by pouring a slurry of sand and CS into a 280 mL hexagonal glass jar and allowing it to cure for a set time.

5.2.2.5 Re-healed CS grout samples

Re-healed CS grout samples were prepared as described in section 3.2.5, by adapting from CS grout shear vane samples (see 5.2.2.3). After the intended curing time of a shear vane sample was reached, it was optionally tested with the vane before being completely broken up by hand for two minutes using a metal spatula, after which it became a viscous slurry and was left to re-heal.

5.2.2.6 Re-healed CS-grouted sand samples

The preparation of re-healed CS-grouted sand samples was the same as that for CS grout samples (5.2.2.5), but by instead adapting from CS-grouted sand shear vane samples (5.2.2.4). All grouted sand samples were covered with water film for healing.

5.2.3 Experimental methods

5.2.3.1 Shear vane tests

The method for shear vane test of CS grout and CS-grouted sand samples was the same as that described in section 3.3.4.

5.2.3.2 Description of experiments

This part gives descriptions of the five experiments conducted in this study. Tables are provided which list all samples prepared. In all cases, doublets were made and tested for each sample, where possible.

Effects of curing and healing times. Four sets of CS_{40}^{320}-$N_{2.5}$ shear vane samples were prepared (see 5.2.2.3): samples in set 1 were cured for different durations (from 6 h to 98 d), and then healed for 98 d; set 2 samples were cured for 6 h and then healed for different durations (18 h – 116.75 d). Set 3 samples were cured for different durations (6 h – 98 d) and healed for 16 d. Set 4 samples were cured for 16 d and then healed for different durations (6 h – 98 d). Samples in sets 1 and 3 were tested at the end of their curing times, before being broken and healed: these were for investigating the effect of curing time. Set 2 and 4 samples, however, were not tested after curing, but were directly broken and healed; these were for studying the effect of healing time. Samples in all sets were covered in water films for re-healing. Table 5.2 provides details of the experiment, and Figure 5.1A presents a graphical representation. Further information on each sample can be found in appendix A.3.3.

Table 5.2. Samples in experiment 1, testing the effect of curing time and healing time on CS grout re-healing.

Set	*Grout used*	*Test at break?*	*Cur. time (d)*	*Heal. Time (d)*
1	CS_{40}^{320}-$N_{2.5}$	Y	Varied	98
2		N	0.25	Varied
3		Y	Varied	16
4		N	16	Varied

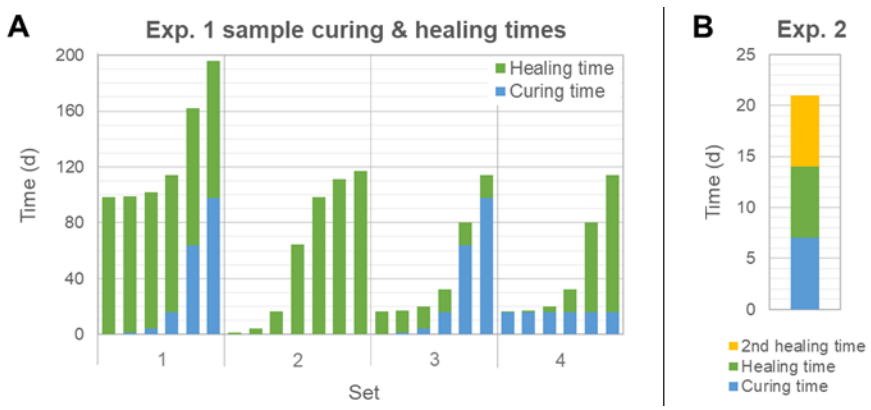

Figure 5.1. Curing and healing times of samples in experiment 1 (*A*) and 2 (*B*).

1) *Double-breaking and re-healing.* A CS_{40}^{320}-$N_{2.5}$ grout shear vane sample was cured for 7 d before testing and breaking. It was then healed for 7 d before testing and breaking again. Finally, it was healed for a further 7 d and tested once more to observe whether re-healing could still occur over multiple breaking/healing cycles, and if so, to what extent. Samples were covered in water films for re-

healing. Table 5.3 summarises this, and Figure 5.1B provides a graphical representation.

Table 5.3. Experiment 2 sample, testing the effect of two breaking and healing samples on CS grout re-healing.

Grout used	*Test at break?*	*Test at 2nd break?*	*Cur. time (d)*	*Heal. Time (d)*	*2nd heal. time (d)*
CS_{40}^{320}-$N_{2.5}$	Y	Y	7	7	7

2) *Effect of grout properties.* To test the effect of the CS type, two sets of CS_{15}^{325}-$N_{2.5}$ shear vane samples were prepared, which used MP 325 CS. One set was cured for different durations and then tested; the other was cured for 16 d before breaking and re-healing for different durations. Two sets of CS_{40}^{320}-N_2 samples, which had the same gel time as CS_{15}^{325}-$N_{2.5}$, but using MP 320 CS (calculated from equation 5.1), were also prepared and tested in the same way. All samples were covered in water films for re-healing. Table 5.4 summarises this. Further information on each sample can be found in appendix A.3.3.

Table 5.4. Experiment 3 samples, testing the effect of the grout properties, including CS type and accelerator NaCl concentration, on CS grout re-healing.

Set	*Grout used*	*Test at break?*	*Cur. time (d)*	*Heal. Time (d)*
1	CS_{15}^{325}-$N_{2.5}$	Y	Varied	-
2		N	16	Varied
3	CS_{40}^{320}-N_2	Y	Varied	-
4		N	16	Varied

3) Effect of healing water properties. Nine CS_{40}^{320}-$N_{2.5}$ shear vane samples were prepared; after curing for 14 d and breaking, each sample was placed in a different healing water and healed for 14 d before testing. The healing waters included tap water at pH 7 and 9; NaCl solutions at 0.5, 1.0, and 2.0 M; $CaCl_2$ solutions at 0.25, 0.5, and 1.0 M; and MP 320 CS. The salt solutions and MP 320 were adjusted to pH 9 using 1 M HCl. Table 5.5 summarises this information.

Table 5.5. Experiment 4 samples, testing the effect of healing water properties on CS grout re-healing.

Grout used	*Test at break?*	*Cur. time (d)*	*Heal. time (d)*	*Heal. Water*	*pH*
CS_{40}^{320}-$N_{2.5}$	N	14	14	Tap	7
				Tap	9
				0.5 M NaCl	9
				1 M NaCl	9
				2 M NaCl	9
				0.25 M $CaCl_2$	9
				0.5 M $CaCl_2$	9
				1 M $CaCl_2$	9
				MP 320 CS	9

4) *Re-healing in CS-grouted sand.* Two sets of grouted sand shear vane samples were prepared (see 5.2.2.4): one used CS_{40}^{320}-$N_{2.5}$ and was cured for 6 h; the other used CS_{20}^{320}-$N_{2.68}$, which had the same gel time but lower silica wt%, and was cured for 3 d. Each set was healed for 7 d. Control samples of each grout without sand were also prepared. All samples were covered in water films for re-healing. Table 5.6 summarises this.

Table 5.6. Experiment 5 samples, testing re-healing in CS-grouted sand.

Set	*Grout used*	*Test at break?*	*In sand?*	*Cur. time (d)*	*Heal. Time (d)*
1	CS_{40}^{320}-$N_{2.5}$	Y	Y	0.25	7
			N	0.25	7
2	CS_{20}^{320}-$N_{2.68}$	Y	Y	3	7
			N	3	7
C	H_2O	Y	Y	-	-

5.3 Results

5.3.1 Effect of curing and healing times

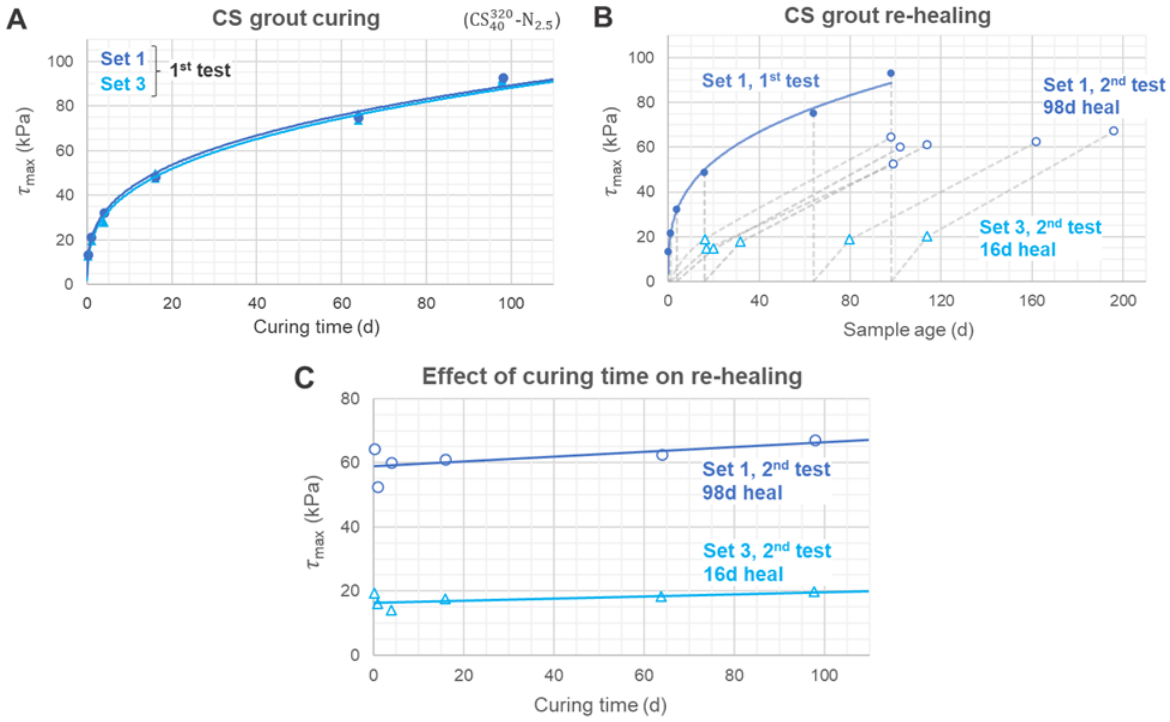

Figure 5.2. *A:* Results of the first shear vane test for samples from sets 1 and 3, showing the τ_{max} of CS_{40}^{320}-$N_{2.5}$ increasing continuously with curing time, according to a sublinear power law. Sets 1 and 3 are identical at the first test. *B:* The τ_{max} of the samples from sets 1 and 3 after breaking and re-healing for 98 d and 16 d, respectively, also with the test 1 data from set 1, for comparison. Dotted lines illustrate the assumed evolution in τ_{max} after breaking for each curing time tested. *C:* The re-healing data from *B* now plotted with curing time on the x-axis, and linear fits applied, showing no clear relation between curing time and the degree of re-healing.

This subsection presents the results of experiment 1, which focussed on the curing and re-healing of CS_{40}^{320}-$N_{2.5}$ grout. Figure 5.2A shows the results from the first shear vane tests for sample sets 1 and 3, prior to any re-healing. These are displayed as points and crosses on the plot, respectively, with different colours representing different curing times. Given the two sets were the same at this point, they exhibited identical behaviour, as would be expected. For both, the maximum shear stress, τ_{max}, recorded before failure can be seen to increase with curing time, t_c, according to a sublinear power law relationship (the solid and dashed blue lines in the plot, for sets 1 and 3, respectively), meaning it has the form

$$\tau_{max} = a t_c^b, \tag{5.2}$$

where a is the multiplier, and b is the exponent, in the range $0 < b < 1$. τ_{max} can be thought of as a measure of the shear strength of the grout.

Plot B shows the data from the second tests for sets 1 and 3, after having been broken and re-healed for 16 d and 98 d, respectively, along with the test one data for set 1, for comparison. From the plot, the 98 d healed samples exhibited greater strength than the 16 d healed samples with the same curing time, and in four of six cases, the 98 d healed samples had healed to such a degree that they were stronger than at their first test, prior to breaking. The dotted lines in the plot illustrate the presumed evolution in τ_{max} of the samples after breaking, for each tested curing time, assuming that the break reduces the strength of the grout to zero. This demonstrates the re-healing ability of CS grout and suggests that increased healing time gives greater strength recovery. Also apparent in the plot is that all samples healed for the same duration appear to recover the same amount of strength, regardless of the curing time at which they were broken. Plot C demonstrates this by presenting this data again with curing time on the x-axis, rather than sample age, such that the 16 d and 98 d re-healing data sets are aligned; linear fit lines are applied, which appear approximately horizontal.

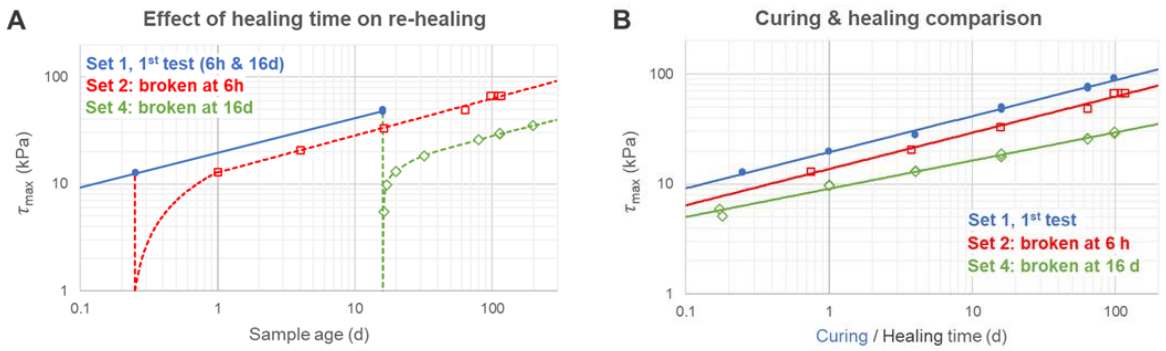

Figure 5.3. *A:* The increase in τ_{max} during re-healing of CS_{40}^{320}-$N_{2.5}$ grout broken after 6 h (red, set 2) and 16 d (green, set 4) of curing, with curing data (blue, set 1, test 1) for comparison. The dotted lines are guides illustrating the assumed evolution in τ_{max} of samples *B:* A comparison of the curing and re-healing of CS_{40}^{320}-$N_{2.5}$ grout. For the curing data, the x-axis is curing time; for the healing data, it is healing time. The solid lines are power law fits. Log-log axes are used in both *A* and *B*.

Figure 5.3A shows the τ_{max} measurements for sets 2 and 4, which were cured for 6 h and 16 d, respectively, before breaking and healing for different durations. In each case, longer healing times gave increased strength according to sublinear power law relationships, with the 6 h samples eventually surpassing their original strength at breaking. The 6 h and 16 d points from set 1, test 1, are also plotted for comparison.

Plot B compares the power law relationships obtained for the curing of CS_{40}^{320}-$N_{2.5}$ grout (set 1), and its healing after breaking at 6 h and 16 d (sets 2 and 4). Here, the x-axis for

the curing data is curing time, and for the healing data it is healing time, such that the two datasets are aligned. The fit equations are provided in table 5.7, where t_h is healing time. The curing and 6 h re-healing lines are roughly parallel on the log-log axes as their fits have similar exponents (0.328 and 0.330), but the exponent for the 16 d data is slightly smaller (0.256). Each of the lines are also displaced along the y-axis, having different multipliers: the curing fit has the highest (19.5), followed by the 6 h (13.7), and then the 16 d (9.05). From this result, it can be said, therefore, that the re-healing samples increased in strength slower than the curing samples, and that the samples broken after 16 d healed slower than those broken at 6 h.

Table 5.7. Power law fit equations from Figure 5.3B, on the curing and re-healing of CS_{40}^{320}-$N_{2.5}$ grout.

Sample set	*Description*	*Fit equation*	*Equation no.*
1	Curing	$\tau_{max} = 19.5 t_c^{0.328}$	(5.3)
2	Re-healing after breaking at 6 h	$\tau_{max} = 13.7 t_h^{0.330}$	(5.4)
4	Re-healing after breaking at 16 d	$\tau_{max} = 9.05 t_h^{0.256}$	(5.5)

5.3.2 Double breaking and re-healing

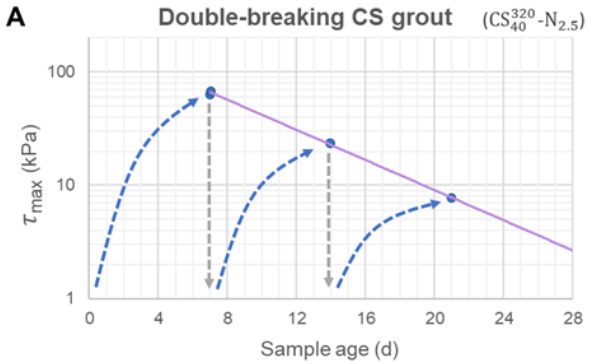

Figure 5.4. τ_{max} data for a CS_{40}^{320}-$N_{2.5}$ sample cured for 7 d, broken, healed for 7 d, broken again, and re-healed for a further 7 d. The blue arrows represent curing and re-healing, and the grey arrows represent breaking. The purple line is an exponential fit.

Figure 5.4 shows the results of experiment 2, in which CS_{40}^{320}-$N_{2.5}$ samples were broken and re-healed twice. From the figure, it can be seen that CS grout is indeed still able to re-heal after being completely broken up for a second time, but that it does so to a lesser extent than on the initial re-heal. The purple line represents an exponential decay fit, which allows for predicting the τ_{max} of samples on successive breaking and 7 d re-healing cycles, assuming the observed trend continues.

5.3.3 Effect of grout components

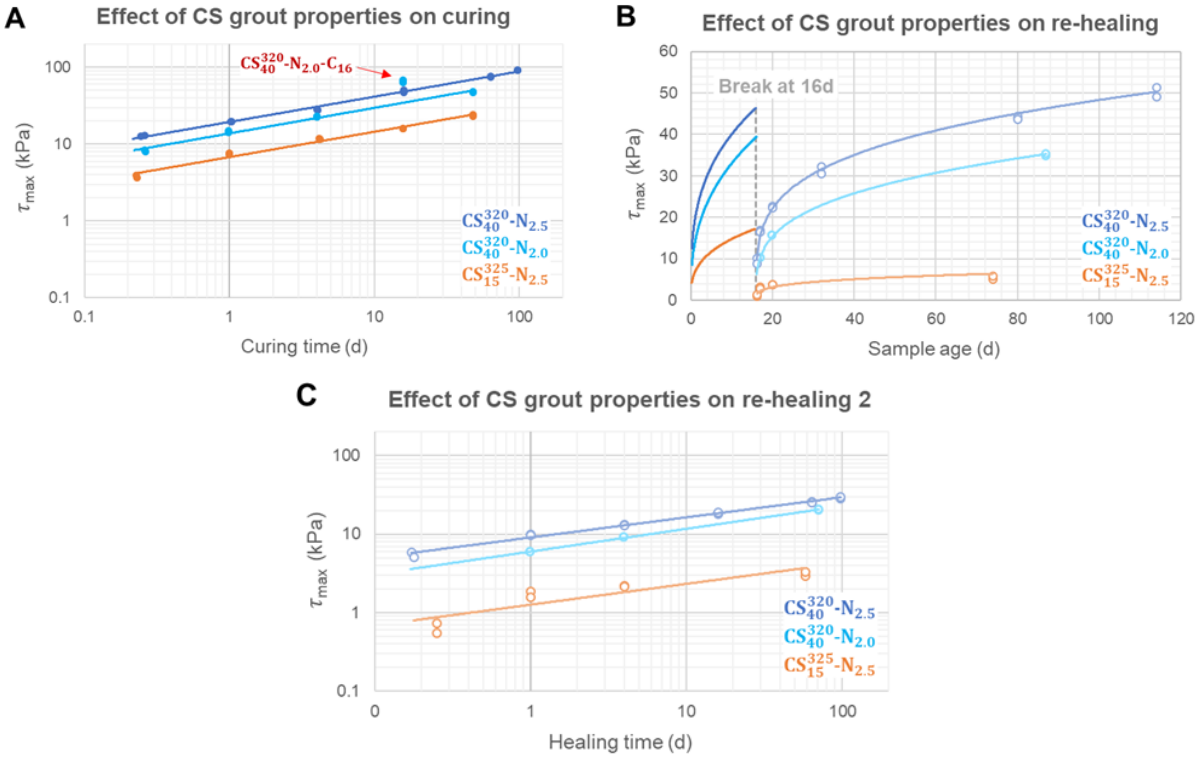

Figure 5.5. *A:* The effect of CS type and accelerator NaCl concentration on the curing of CS grout, with log-log axes. The lines are sublinear power law fits and correspond to CS_{40}^{320}-$N_{2.5}$ (dark blue), CS_{40}^{320}-$N_{2.0}$ (light blue), and CS_{15}^{325}-$N_{2.5}$ (orange) grouts. The red arrow highlights outlying points. *B:* The effect of CS type and accelerator NaCl concentration the re-healing of CS grout. The grey dotted line represents the samples being broken at 16 d. *C:* The re-healing data plotted again on log-log axes, with healing time on the x-axis.

Figure 5.5 illustrates the effect of CS type and accelerator NaCl concentration on the curing and re-healing of CS grout. The solid orange lines in the plots correspond to CS_{15}^{325}-$N_{2.5}$, which features MP 325 CS with 2.5 M NaCl accelerator. The blue lines are standard MP 320 CS, also using 2.5 M NaCl (CS_{40}^{320}-$N_{2.5}$, dark blue), as well as 2.0 M NaCl (CS_{40}^{320}-$N_{2.0}$, light blue), which had the same gel time as CS_{15}^{325}-$N_{2.5}$. The CS_{40}^{320}-$N_{2.5}$ data is that of set 1 in experiment 1. Plot A shows the increase in τ_{max} of the three grout varieties during curing. It can be seen that reducing the accelerator NaCl concentration used with MP 320 CS from 2.5 M to 2.0 M gave lower τ_{max} values, such that its fit line is shifted downwards in the log-log axes, with lower multiplier (13.8 compared to 19.5), but while remaining parallel, with effectively unchanged exponent (0.333 to 0.329). The CS_{15}^{325}-$N_{2.5}$ data had reduced τ_{max} values compared to both sets of MP 320 data: again, it had lower multiplier (6.78), but equal exponent (0.329). This was despite having the same accelerator NaCl as CS_{40}^{320}-$N_{2.5}$, and the same gel time as CS_{40}^{320}-$N_{2.0}$. This suggests that

neither NaCl concentration nor gelation are the determining factors in the strength of CS gelled grout.

It should be noted that the CS_{40}^{320}-$N_{2.0}$-C_{16} points (highlighted with a red arrow) appear to be outliers from the rest of the data and so are not included in the CS_{40}^{320}-$N_{2.0}$ fit line; the reason for this difference could be that these samples were produced using a new batch of CS, which would have experienced less precipitation of silica due to aging, and so would have a greater wt% of dispersed CS particles, meaning its gel would be stronger.

Table 5.8. Fit equations from Figure 5.5, for data on the curing and re-healing of CS grouts of different grout properties.

Grout	*Curing*		*Healing*	
	Fit equation	*Equation no.*	*Fit equation*	*Equation no.*
CS_{40}^{320}-$N_{2.5}$	$\tau_{max} = 19.5t_c^{0.329}$	(5.3)	$\tau_{max} = 9.05t_h^{0.256}$	(5.5)
CS_{40}^{320}-$N_{2.0}$	$\tau_{max} = 13.8t_c^{0.333}$	(5.6)	$\tau_{max} = 5.99t_h^{0.289}$	(5.9)
CS_{15}^{325}-$N_{2.5}$	$\tau_{max} = 6.78t_c^{0.329}$	(5.7)	$\tau_{max} = 1.26t_h^{0.265}$	(5.10)

Plot B shows the re-healing of the three grout varieties after 16 d curing, with similar results to those seen in plot A, each described by a sublinear power law relationship. This reinforces the assertion that curing and re-healing are related processes. Plot C presents this data again with log axes. The CS_{40}^{320}-$N_{2.5}$ data is that of set 4 in experiment 1. Table 5.8 provides each of the fit equations in Figure 5.5; the curing fits all have effectively equal exponents, with an average of 0.330 for the three grout variants, but differ in their multipliers. The same is true for the re-healing fits, with an average exponent of 0.270. The re-healing fits notably each have smaller exponents than the curing fits.

5.3.4 Effect of healing water

Figure 5.6A shows the effect of different healing water compositions on the re-healing behaviour of CS_{40}^{320}-$N_{2.5}$ grout. The heights of the bars in the plot represent the τ_{max} the samples reached after they were cured for 14 d, broken, and re-healed for a further 14 d in particular healing waters. Plot B shows the difference in τ_{max} of the samples in comparison to that achieved using healing water of tap water at pH 9. From the plots, it can be seen how increasing concentration of either NaCl or $CaCl_2$ in the healing water increases the degree to which samples re-heal, with $CaCl_2$ also providing greater re-healing than NaCl at the same concentration. It should be noted that Ca^{2+} and Na^{+} have valencies of 2 and 1, respectively. This implies that increasing either the concentration or cation valency of salt in the healing water increases the degree of healing achieved. The

pH 9 water also gave slightly greater τ_{max} than the pH 7. Finally, MP 320 CS at pH 9, which contains ~ 0.1 M NaCl, gave greater re-healing than either water at pH 9, or NaCl solutions of higher molarity (0.5 M and 1.0 M, but not 2.0 M), implying that the presence of additional CS in the healing water also increases re-healing.

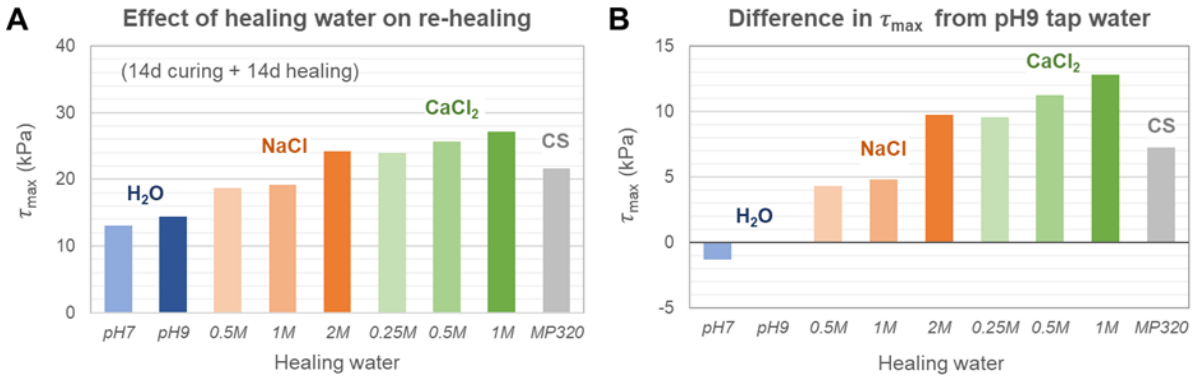

Figure 5.6. *A:* The effect of different healing water properties on the τ_{max} of re-healed CS samples: these include tap water at pH 7 and 9, NaCl and $CaCl_2$ solutions of different concentrations, at pH 9, and MP 320 CS, also at pH 9. *B:* The difference in τ_{max} between each sample and that which used pH 9 tap water.

5.3.5 Re-healing in CS-grouted sand

Figure 5.7 presents the results of shear vane tests on the curing and re-healing of CS-grouted sand. On the left of plots A and B, in darker colours, are the τ_{max} values achieved by CS-grouted sand samples (brown), and control samples with CS grout only and no sand (blue), each cured for the same duration. On the right of each plot, in lighter colours, are the τ_{max} values for the same samples after having been broken and re-healed for 7 d. The samples in plot A used CS_{40}^{320}-$N_{2.5}$ and were cured for 6 h. Attempting longer curing times with this grout, however, produced samples which were above the measurement limit of the shear vane device; hence for the second set of tests, presented in plot B, a weaker grout was used (CS_{20}^{320}-$N_{2.68}$), allowing a curing time of 3 d to be reached, to provide a point of comparison with A.

In both sets of tests, all samples were observed to recover τ_{max} after re-healing, thereby confirming that re-healing occurs in CS-grouted sand. In both cases, the grouted sand samples prior to breaking exhibited far greater τ_{max} than the controls. This implies that the high strength of the CS-grouted sand samples does not simply arise from the presence of sand, but that there exists some favourable interaction between the CS and sand particles. This effect is also apparent in the re-healed GS_{20}^{320}-$N_{2.68}$-C_3-H_7 sample in plot B,

but not so for the GS_{40}^{320}-$N_{2.5}$-$C_{0.25}$-H_7 in plot A, which has similar τ_{max} to the control sample. The reason for this discrepancy is not yet understood.

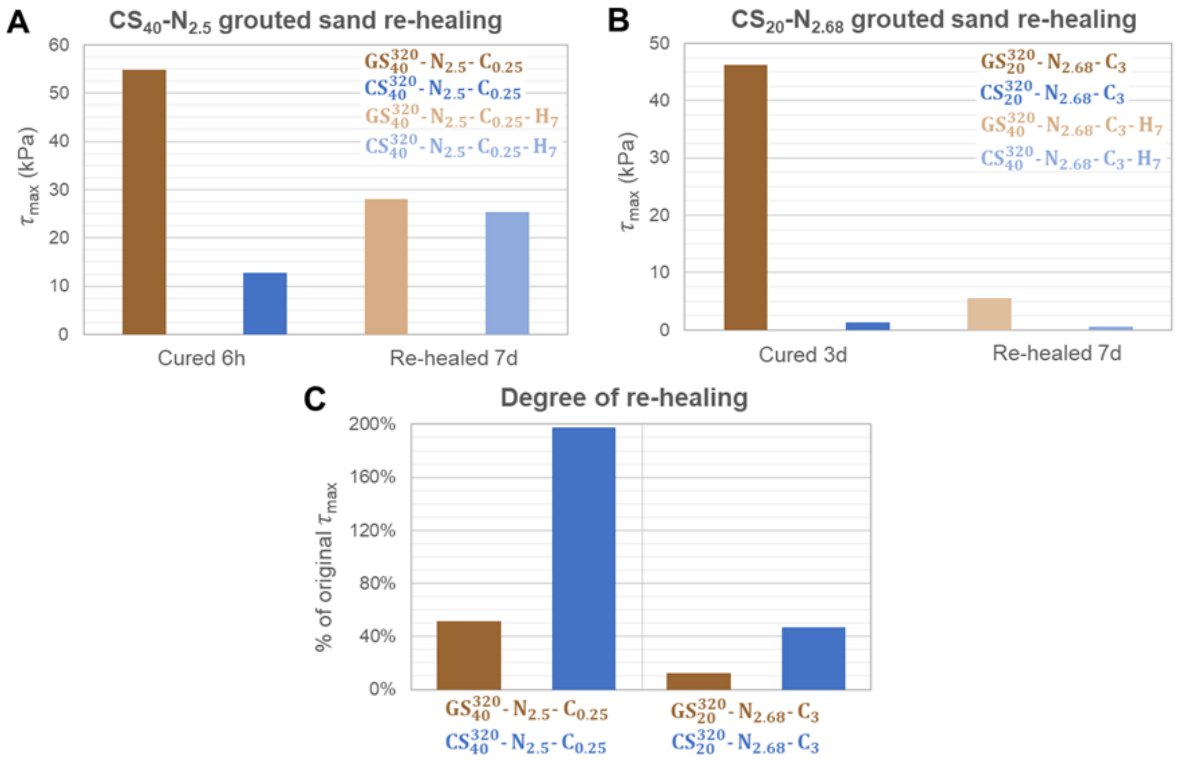

Figure 5.7. *A:* The dark brown bar shows the τ_{max} of sand grouted with CS_{40}^{320}-$N_{2.5}$, cured for 6 h, and the light brown bar shows it again after breaking and re-healing for 7 d. The dark blue and light blue bars are equivalent control samples without sand. *B:* The dark brown bar shows the τ_{max} of sand grouted with CS_{20}^{320}-$N_{2.68}$, cured for 3 d, and the light brown bar shows it again after breaking and re-healing for 7 d. *C:* The degree of re-healing achieved by each of the samples in the experiment, in terms of the τ_{max} of the re-healed samples as a percentage of the τ_{max} of the samples prior to breaking.

Figure 5.7C shows the degree of re-healing achieved for each of the samples in terms of the re-healed samples' τ_{max} as a percentage of their original τ_{max} values, prior to breaking. These results suggest that the CS-grouted sand samples are able to recover relatively much less of their original strength in comparison to the CS grout samples. This implies that the favourable interaction between CS and sand particles is much less prevalent in re-healed samples than unbroken samples.

5.4 Discussion

5.4.1 Nature and mechanism of CS grout re-healing

Given that the increases in strength of CS grout during both curing and re-healing are described by sublinear power law relationships, it leads to the question of whether the two phenomena are governed by the same underlying process, with re-healing simply being a continuation of the same effect which was interrupted by the breakage. This can

be evaluated by comparing the rate of strength increase from both curing and re-healing, considering only the total age of samples. Figure 5.8 does this, showing samples from sets 3 and 4 in experiment 1, which each have the same range of total ages, but which experienced different durations of curing and re-healing. Using information from the inset table, in plot A it can be seen that samples which experienced more curing than healing always exhibited greater total strength gain. This suggests that re-healing is a slower process than curing, even though the pore water chemistry was kept constant throughout. The implication of this is that, if the two processes are indeed governed by the same mechanism, the difference in rate is likely influenced by the particular particle arrangements and geometries in cured and re-healed grout samples.

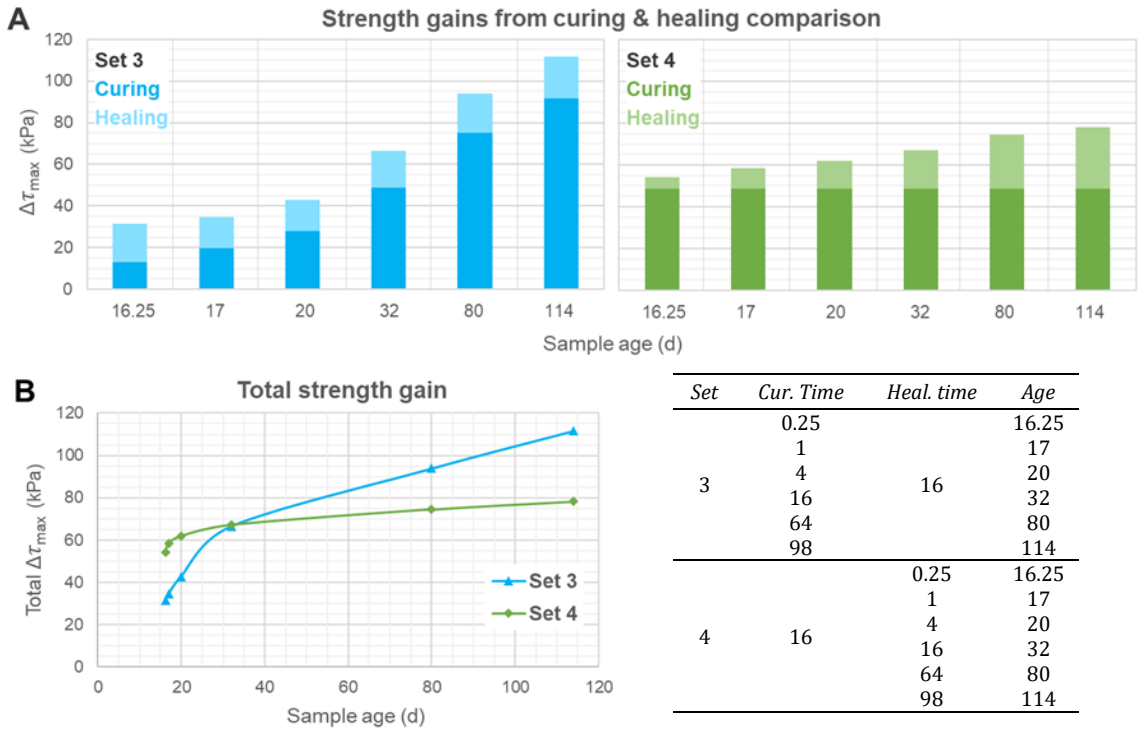

Set	*Cur. Time*	*Heal. time*	*Age*
3	0.25	16	16.25
	1		17
	4		20
	16		32
	64		80
	98		114
4	16	0.25	16.25
		1	17
		4	20
		16	32
		64	80
		98	114

Figure 5.8. *A:* Comparison of the strength gained from curing and healing for two sets of samples with the same range of total ages, but which were cured and healed for different durations. The data is from sets 3 and 4 in experiment 1. The darker coloured bars represent the $\Delta\tau_{max}$ from curing, and the lighter bars the $\Delta\tau_{max}$ from healing. *B:* The total strength gain by age for the two sets, including a table showing the durations each sample was cured and healed for.

A different interpretation of the relationship is that re-healing power law fits are the same as their curing equivalents, but shifted down in log-log axes, such that they have lower multipliers, but the same exponents. The re-healing power laws in Figure 5.5C challenge this, however, as each has somewhat lower exponent than its corresponding curing power law. Figure 5.9 illustrates the difference in exponent for curing and re-healing of

CS_{40}^{320}-$N_{2.5}$ grout broken at 16 d. Similar data in Figure 5.3B is less clear, with 6 h cured CS_{40}^{320}-$N_{2.5}$ grout's fit having roughly equal exponent to its respective curing data. More work is needed to determine if the difference in exponent is genuine, or the product of some experimental error.

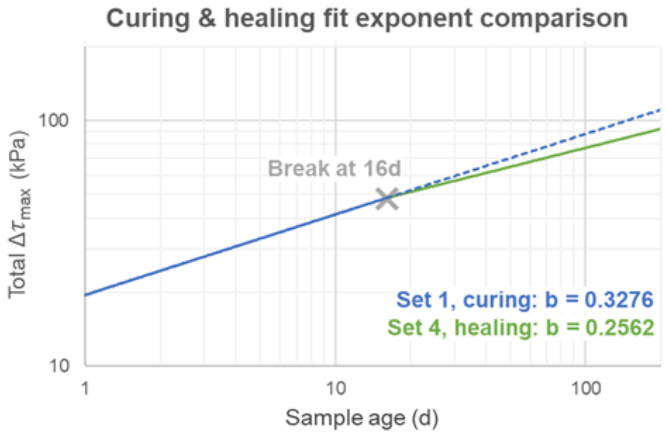

Figure 5.9. Comparison of the power law exponents from the curing of CS_{40}^{320}-$N_{2.5}$ grout and its re-healing after breaking at 16 d.

A sign of re-healing being an extension of curing would be if there were curing time dependence on the degree of re-healing achieved, as samples broken earlier would be expected to heal faster. The difference between the 6 h and 16 d cured data in Figure 5.3B supports this conclusion, but Figure 5.2C counters it, showing no curing time dependence on the re-healing of 16 d and 98 d healed samples. It seems likely, though, that the 6 h cured data are outliers; however, more tests are needed to be certain.

Figure 5.4 showed that samples recover less strength on successive curing and re-healing cycles. This would be expected if re-healing were an extension of curing, and were dependent on curing time. If this is not the case, it may be that the break itself causes the decreased ability to re-heal.

It is assumed that breaking gelled CS grout reduces it to a suspension of small gel fragments, each featuring networks of linked silica particles, rather than reverting it entirely to a dispersion of individual nanoparticles. This explains the observed higher viscosity of broken grout relative to the original. The resulting suspension appears stable, with no precipitation of gel fragments observed. The conditions which initiated the original gelation, such as increased ionic strength in the suspension, are presumably still present. Although element mobility is reduced due to the higher viscosity, at least some network fragments remain mobile enough to be attracted to others, allowing them to

reform a fully encompassing network. Alternatively, individual suspended nanoparticles, which were never part of the original network, are still present, and condense onto the network fragments, bridging them together.

If curing and re-healing are indeed related processes, it may be assumed that, as described in relation to curing in section 4.4, after the initial re-forming of the fully expansive gel network, re-healing of CS grout proceeds via the ongoing formation of additional siloxane bonds in the silica network, and by continuous condensation of dissolved silicates into the necking points between CS particles (see Figure 2.9). Additional nano-structural analysis must be done in order to verify this. If there is a transition from one process to another during re-healing, this is not observed in the τ_{max} data, however, which obeys a consistent power law throughout. It may be that the initial network formation occurs very quickly: faster than 6 h, at least, which was the shortest healing time measured in this study.

5.4.2 Effect of electrolyte

Section 5.3.3 demonstrated that higher accelerator NaCl concentration gives greater strength in both curing and re-healing of CS grout. This agrees with previous results in 4.3.2. Similarly, in section 5.3.4, it can be seen that increasing the NaCl concentration of healing water also increased the degree of re-healing. Furthermore, using $CaCl_2$, a salt with cation valency of 2, gave even greater re-healing. This is comparable to the results for curing water in 4.3.3.3. The fact that electrolyte content impacts re-healing in a similar manner to how it does to the curing adds to the argument that the two processes are related.

The measure of ionic strength, defined in equation 4.2, can be used to combine the concentrations and charges of the ions in a solution. Employing this, the ionic strength of healing water on the shear strength of the CS grout samples from 5.3.4 is presented in Figure 5.10, showing how increased ionic strength gives greater strength gain, according to a linear relationship. As described in section 4.4, relating to curing, increasing ionic strength presumably increases some combination of the rate of siloxane bond formation, or the rate of condensation of dispersed silicates during the re-healing of CS grout.

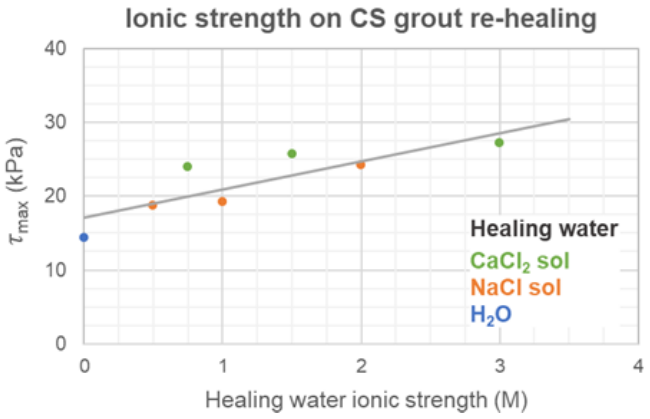

Figure 5.10. The effect of healing water ionic strength on the shear strength of CS grout samples cured and re-healed for 14 d each. All healing waters were pH 9. The colour of points corresponds the healing water used, with points from $CaCl_2$ sol being green, NaCl sol points being orange, and water being blue.

5.4.3 Effect of pH

Like ionic strength, pH also impacts the electrostatic environment of a solution, so it may also be expected to affect curing and re-healing. The data in Figure 5.6 shows that a CS grout sample re-healed in pH 9 water had greater strength after 14 d than a sample healed in pH 7 water. This may be due to the fact that, although alkaline pH causes deprotonation of silica surface groups in the gel network, and on any remaining dispersed particles, it also increases the rate of sorption and desorption processes which are required for new siloxane bond formation (Iler, 1979; Pedrotti et al., 2017).

5.4.4 Effect of additional silica

Section 4.4 describes the theory that the curing phenomenon arises in CS grout as a result of continuous siloxane bond formation in the network, and condensation of dissolved silicates at the necks between particles. From this, it is postulated that the slowing down of the rate of strength increase over time, described by a sublinear power law, is the result of continuously decreasing concentrations of dispersed silicates that are free to condense onto the network. It follows then that re-healing CS grout in the presence of additional CS would cause increased strength gain beyond that which would be otherwise expected.

The data presented in Figure 5.6 seems to support this, with a CS grout sample re-healed in MP 320 achieving higher shear strength, at 21.6 kPa, than one re-healed in tap water at the same pH (14.4 kPa). It should be noted that MP 320 CS contains ~ 0.1 M NaCl, but that this is not sufficient to explain the observed effect, as, using the fit in Figure 5.10, which describes the impact of the healing water's ionic strength on the strength achieved, it would be expected that a 0.1 M solution give τ_{max} of only 17.5 kPa; the actual value of

21.6 kPa would be expected from a 1.2 M NaCl solution. Future experiments could focus on the size of dispersed silica particles, or even the use of dissolved silicate molecules, in healing water to give a more complete picture of the processes involved in CS grout re-healing.

5.4.5 Effect of surface area per unit volume

The reason why silicates are expected to condense particularly at the joining points between particles is that this reduces the surface area of the network, bringing the system to a lower energy state (Iler, 1979). The surface area per unit volume of the two CS types may therefore be expected to affect their relative rates of curing and re-healing. MP 325 CS has lower silica wt% and smaller particle size than MP 320 (15 wt% and 7.5 nm compared to 40 wt% and 15 nm). Using this, the surface area per unit volume of the two CS types can be calculated via the equation

$$A_v = \frac{6w_{SiO_2}}{\rho d}, \tag{5.11}$$

where ρ is the density of the silica particles, d is the particle size, and w_{SiO_2} is the silica wt%. Assuming ρ = 2.2 g/cm^3 for both suspensions yields surface areas per unit volume of 72.7 m^2/cm^3 for undiluted MP 320, and 54.5 m^2/cm^3 for MP 325, with a ratio of ~ 4/3.

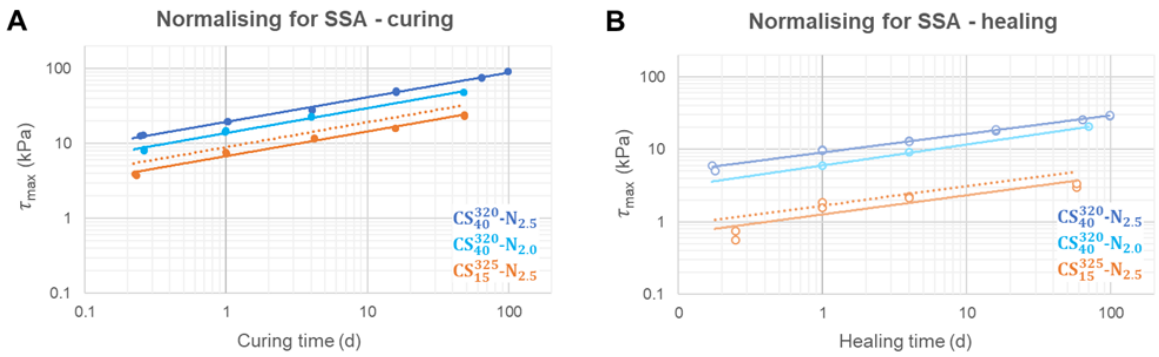

Figure 5.11. Normalising the CS_{15}^{325}-$N_{2.5}$ curing (*A*) and re-healing (*B*) data from Figures 5.5A and C to account for the difference in surface area per unit volume of MP 325 and MP 320 CS. The dotted orange lines are the fit lines of the normalised data; the points are not plotted, for clarity.

Figure 5.11 shows the curing and re-healing data from Figures 5.5A and C, respectively, but with the CS_{15}^{325}-$N_{2.5}$ data normalised, using the 4/3 ratio, to account for the difference in surface area per unit volume of the two CS types. As can be seen, the normalisation does not make up for the difference in strength between the MP 325 and MP 320 datasets.

There must therefore be other factors as of yet unaccounted for which impact the curing and re-healing of MP 325 grout with respect to MP 320.

5.5 Conclusion

This study is the first to investigate the re-healing behaviour of CS grout. Here, shear vane tests demonstrated the ability of CS grout to re-heal after being completely broken up. Similar to its curing behaviour, CS grout was seen to increase in shear strength continuously during re-healing, according to sublinear power law relationships. The multipliers of re-healing power laws were greatly reduced compared to their curing equivalents, but their exponents were only slightly reduced, if at all. The results suggest that the curing time prior to breaking did not affect the degree of re-healing achieved, although more data is needed to confirm this.

Re-healing was observed still to occur in samples broken for a second time, although to a lesser extent than at the first re-heal, with the reduction in strength after each curing and re-healing cycle defined by a negative exponential relationship.

Higher NaCl concentration in the accelerator was found to increase the strength of CS grout in a similar way in both curing and re-healing. Higher ionic strength in the healing water was also found to increase the degree of re-healing achieved, according to a linear relationship; this is analogous to earlier findings on the effect of curing water. Healing water at pH 9 gave increased re-healing relative to pH 7 water.

Employing MP 320 CS as healing water also gave increased healing relative to water of the same pH: this is thought to be due to the presence of additional dispersed silica, which may condense onto the existing CS network in the grout, thereby increasing strength.

Using MP 325 CS grout, which has smaller particle size and lower silica wt%, in place of MP 320 reduced the strength of the grout in a similar way in both curing and re-healing. The MP 325 had lower strength than MP 320 of both the same gel time, and the same accelerator NaCl concentration. Normalising for the difference in surface area per unit volume still did not account for the difference, implying that there are additional, unaccounted factors at play.

Re-healing was confirmed to occur in CS-grouted sand. However, whereas the grouted sand was extremely strong prior to breaking, this was mostly lost in the re-healed samples, such that they recovered relatively much less strength than control grout

samples, despite being stronger. The strength of unbroken grouted sand samples was much greater than that of CS grout alone, implying that there exists a complementary interaction between the CS and sand grains.

The fact that re-healing is defined by a similar sublinear power law relationship to curing, and that it is affected by properties such as ionic strength and CS type in similar ways, leads to the conclusion that curing and re-healing are related phenomena governed by similar physical processes. However, it is thought that the relationship is more complex than re-healing simply being an extension of curing, as re-healing was observed to give a slower increase in strength than curing, and its power laws had lower exponents. Therefore, if the two processes are governed by the same mechanism, differences in particle arrangement and geometry between curing and re-healing samples likely affect the rate of strength increase.

Breaking is presumed to reduce gelled CS grout to a suspension of gel fragments, which are then able to re-link, either on their own, or through bridging by previously un-coagulated CS nanoparticles, as a result of the continued presence of the conditions which originally initiated gelation. After this, it is thought that, as with curing, re-healing continues as a result of ongoing siloxane bond formation in the network, and condensation of dissolved silicates into the necks between CS particles. No evidence of a transition between two distinct processes has been observed thus far in the shear vane data.

Chapter 6: Adding Clay to CS Grout

6.1 Introduction

As has been mentioned in previous chapters, a possible barrier to wide-scale application of CS grout is its relatively low strength in comparison to cements, and its somewhat greater cost (Gallagher et al., 2013). One potential way to increase the strength of CS grout would be to increase the mass of solids present; adding clays to the grout prior to application could be a way to achieve this in a more cost-effective manner than simply increasing the silica nanoparticle mass fraction. Should addition of clays increase the strength of the gelled grout, it would likely provide it with greater resistance to damage, and a longer lifespan when employed as a hydraulic barrier, as well as improving its performance as a soil-strengthening agent. Ideally, the inclusion of any additives should not greatly affect the low viscosity of CS grout, however, since its injectability at minimal pressure into soil is one of its key advantages.

Due to the abundance of clayey soils in nature, they are significantly more affordable than CS when unrefined. Replacing some of the mass of silica in CS grout with clays could therefore be a way to reduce its cost whilst maintaining mechanical performance. Clays also possess a range of properties which may provide additional benefits to CS grout. For example, clays generally exhibit plastic deformability (Bergaya et al., 2006; Craig, 2004; Guggenheim, 1995), which stands in contrast to the brittle nature of CS gel; imparting this behaviour into CS grout could reduce the likelihood of performance-compromising cracks forming in CS hydraulic barriers.

Bentonite clay in particular has very useful properties, such as strong cation sorption, high swelling pressure, low permeability, and good water retention (Cho et al., 1999; Lee et al., 2024; Noh et al., 2025; Villar et al., 2010). These have helped it find extensive use as a hydraulic barrier material, installed via excavation (Pedrotti et al., 2020), and it has notably been commonly employed in nuclear decommissioning applications (Alberdi et al., 2000; Alonso et al., 2017; Arcos et al., 2006; Arvidsson et al., 2015; Bish, 1998; Bodvarsson et al., 1999; Dixon et al., 2011; Fernández et al., 2017; Mayordomo et al., 2016; Nazir et al., 2021; SKB, 2010a, 2010b, 2010c; Volckaert et al., 1996; Zheng et al., 2010), where it is favoured for its ability to fill voids and self-seal cracks caused by damage (Dohrmann et al., 2013), as well as for trapping radioactive contaminants in soil

(Albarran et al., 2011; Cao et al., 2019; Karnland et al., 2006; Missana et al., 2008). Nuclear decommissioning is an area of particular concern for the UK, with the Nuclear Decommissioning Authority estimating the total cost of the process at £121 billion for the country, with activities continuing over a duration of 120 years (Mulholland et al., 2019). If the highly beneficial properties of bentonite can be combined with those of CS grout, it could significantly improve the grout's effectiveness as a hydraulic and chemical barrier, and hence see its application greatly increased, particularly in the field of nuclear decommissioning, in which engineers are already familiar with the use of bentonite.

In this chapter, two clayey soils, rich in kaolin and bentonite, respectively, were added to CS grout to explore the effects this had on viscosity, gelation, mechanical properties, and re-healing. It was not possible within the timeframe of this PhD to also assess changes to the sorption capacity in the clay/CS grout mixtures. Bentonite was selected for this purpose due to its advantageous properties and established utility, described previously; kaolin, on the other hand, was chosen simply as a reference clay for comparison, which did not possess bentonite's swelling behaviour, and which was low-cost and readily available in the laboratory. Although there has previously been research on using CS to grout clayey soils, including kaolin and bentonite, and the resulting effect this has on structure and mechanical properties (Aksu & Eskisar, 2023; Baird & Walz, 2006, 2007; Changizi & Haddad, 2015; Holmboe et al., 2011; Mohamadabadi et al., 2019; Roshan et al., 2022; Tomar et al., 2020; Wong et al., 2018), the present investigation represents the first work known to the author which proposes and studies the use of clays as additives in the grout. In the following experiments, the feasibility of using kaolin and bentonite to partly replace the mass of silica in CS grout without compromising its gelation and mechanical performance is assessed. To do this, viscometer and shear vane tests were carried out on CS/clay grout samples, and UCS tests were performed on CS- and CS/clay-grouted sand samples.

6.2 Background

Clays are a variety of fine-grained soils which, at the microscopic scale, feature plate-like particles, comprised of layers featuring 2D sheets of tetrahedrally arranged silica (SiO_2), and octahedrally arranged alumina (Al_2O_3) (Figures 6.1A and B). When clays are sufficiently wet, thin molecular films of water exist between the particles. Hydrogen

bonding between the water molecules and the particles allows the plates to slide past each other upon pressure, but hold their shape when released; this gives the hydrated clay plasticity at the macro-level (Guggenheim, 1995).

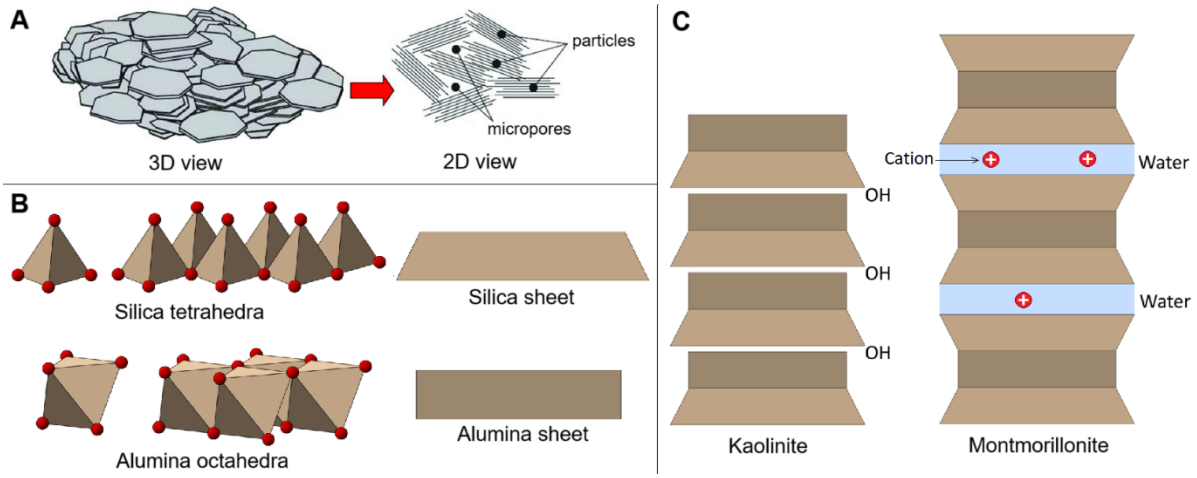

Figure 6.1. *A:* Representation of the microscopic arrangement of plate-like clay particles and their layered composition, adapted from Yang (2013). *B:* Schematic of the atomic structure within silica and alumina sheets. C: Schematics of kaolin and montmorillonite clay structures, showing montmorillonite's swelling behaviour and sorption of cations.

Kaolin clay primarily consists of kaolinite: a 1:1 layer clay mineral, whose layers feature one sheet of silica and one of alumina (Figure 6.1C, left). The layers in kaolin are tightly packed together as a result of strong hydrogen bonding between flat basal surfaces. The basal surfaces also have very low permanent charge due to minimal occurrence of isomorphous substitution in kaolinite. These features give kaolin clay relatively low sorption capacity and ability for cation exchange. Bentonite clay, however, is primarily composed of smectites, such as montmorillonite, a 2:1 layer clay mineral with layers consisting of two sheets of silica sandwiching one of alumina (Figure 6.1C, right). In montmorillonite, layers are held together by weak van der Waals forces and exchangeable cations, which allows water and ions to enter between layers. The basal surfaces also have permanent negative charge due to isomorphous substitution (e.g. Mg^{2+} replacing Al^{3+}). As a result of this, bentonite has high sorption capacity and ability for ion exchange, and it exhibits swelling upon hydration (Bergaya et al., 2006). These properties make it useful as a barrier material, where its swelling ability allows it to fill fractures and voids on installation, providing low hydraulic conductivity, and it can also self-seal cracks upon later damage. Its sorption properties are useful in fields such as nuclear

decommissioning for trapping radioactive cations in contaminated soil (Albarran et al., 2011; Cao et al., 2019; Karnland et al., 2006; Missana et al., 2008).

In both kaolin and bentonite, the edges of layers feature hydroxyl groups: aluminol, (AlOH) on alumina sheets, and silanol (SiOH) on silica sheets. As with the surface silanols of CS particles (2.2.1), these groups increasingly deprotonate to AlO^- and SiO^- at high pH, such that layer edges acquire negative charge in alkaline conditions.

6.3 Methodology

6.3.1 Materials

Materials used in this study included MP 320 CS, NaCl, and fine-grain sand, and equipment included 55 mL hexagonal glass jars; more information on these can be found in section 3.1. A kaolin-rich clay in dried powder form was also used, which was cream in colour, as well as a bentonite-rich clay, also a dried powder, of dark grey/green colour. For convenience, these are henceforth referred to in this chapter as simply 'kaolin' and 'bentonite'.

6.3.2 Sample preparation

6.3.2.1 Sample naming convention

Table 6.1. Explanation of the sample naming convention used in chapter 6.

Term order	*Variable*	*Abbreviation*	*Meaning*	*Subscript*
1	Sample type	CS	CS grout	Silica wt% / clay wt%
		CS/K	CS/kaolin grout	
		CS/B	CS/bentonite grout	
		GS	CS-grouted sand	
		GS/K	CS/kaolin grouted sand	
2	Accelerator salt	N	NaCl	Concentration (M)
3	Curing time	C	Curing time	Curing time (d)
4	Healing time	H	Healing time	Healing time (d)

A particular naming convention was used to identify samples in this chapter, the details of which are provided in Table 6.1. Using this information, for example, a sample named CS_{40}/K_{16}-$N_{1.7}$-C_7-H_7 would refer to a CS/kaolin grout sample created using CS of 40 wt% silica, with 16 wt% of kaolin clay added to it; it would use 1.7 M NaCl accelerator solution

and be cured for 7 d, before being broken and re-healed for 7 d. The resulting composition of the grout by weight would be 57% water, 30% silica, 12% kaolin, and 1.1% NaCl. Lists detailing all of the samples produced for this study can be found in appendix A.4.4.

6.3.2.2 Addition of clay to CS

To add clay to CS, a quantity of CS was placed in a beaker on a magnetic stirrer, and a measured amount of clay powder was slowly added to the edge of the vortex produced in the liquid by stirring. The beaker was then covered with parafilm and left until the powder had fully dispersed in the CS. For kaolin, 1 h was allowed for this, with the end result being a liquid which was cream in colour, somewhat more viscous than previously (depending on the amount of kaolin added), and of uniform consistency. For bentonite, the process took much longer, and the beaker had to be left stirring overnight for full dispersion of the powder. The eventual result was a liquid that was dark grey/green in colour, of slightly increased viscosity, and uniform in consistency. CS/clay mixtures prepared in this manner were stable against gelation and could be stored for long durations at room temperature; over such durations, small quantities of clay could fall out of suspension, but were easily re-dispersed by stirring. Something to note is that the addition of clays caused a small increase in the volume of the CS/clay mixture relative to the original CS (due to a decrease in the bulk density of solid, when silica mass is replaced by clay), depending on the amount and type of clay added; this effect was not tracked as part of this investigation.

As part of the first experiment in this study, using the method described here, CS/clay samples were produced with different wt% of kaolin and bentonite added to measure the effect this had on viscosity.

6.3.2.3 CS grout and CS/clay grout preparation

CS grout was prepared as described in section 3.2.2. CS/clay grout was prepared in the same manner, but using CS/clay mixtures, produced according to 6.3.2.2, in place of CS. For the second set of experiments in this study, CS/clay grout samples were created with different wt% of kaolin added, different accelerator NaCl concentrations (each with 16 wt% kaolin and 5 wt% bentonite added), and replacing mass of silica with kaolin while keeping the total mass of solids constant with respect to standard CS grout; this was done

by adding kaolin to CS diluted with DI water. This set of experiments was carried out to investigate the effect of each factor on the gelation of CS/clay grouts.

6.3.2.4 CS/kaolin grout shear vane samples

CS/kaolin grout samples for shear vane test were prepared in the same manner as standard CS grouts, described in section 3.2.3, but using CS/kaolin mixture (see 6.3.2.3) in place of CS. All samples were covered with films of tap water during curing. Each sample used CS_{25}/K_{25}-$N_{2.3}$, meaning they were prepared with CS of 25 wt% silica, and adding 25 wt% of kaolin, resulting in the CS/clay mixture being 20 wt% of both silica and kaolin, such that it had half the silica content of standard CS_{40}, but the same total mass of solids. The CS/clay suspensions were then mixed with 2.3 M NaCl accelerator, which gave the same gel time as standard CS_{40}-$N_{1.7}$, calculated via equation 6.4, and were cured for different durations.

6.3.2.5 Re-healed CS/kaolin grout shear vane samples

CS/kaolin grout re-healing samples for shear vane test were prepared in the same manner as for standard CS grouts, described in section 3.2.5, but by instead adapting CS/kaolin grout shear vane samples (see 6.3.2.4). Each sample used CS_{25}/K_{25}-$N_{2.3}$ grout and was cured for 16 d. They were then healed for different durations.

6.3.2.6 CS- and CS/kaolin grouted sand UCS test samples

Unlike in previous studies, a bespoke method was used to prepare CS-grouted sand and CS/kaolin-grouted sand samples here for UCS tests. The reason for this difference was due to the increase in viscosity caused by the addition of the kaolin, which, at higher wt%, made it difficult to simply pour grout through the fine-grain sand as it was gelling. To prepare a sample by the method here, 100 mL of CS grout or CS/kaolin grout was mixed with 65 g of sand in a beaker and stirred thoroughly with a spatula until the sand was fully saturated. After leaving to settle for 30 s, the result was the saturated sand at the bottom of the beaker, with a layer of grout above. The sand was scooped out with the spatula into a cylindrical plastic mould (the same as in 3.2.5) in a 100 mL beaker, and was then compacted by hand with the plunger of a 25 mL syringe. The quantity of sand was chosen to exactly fill the mould on compaction. The remainder of the grout in the original beaker was then poured around the sides of the mould until it was fully immersed. The beaker was then covered with parafilm while the grout gelled. At 2× the gel time, as

calculated via the method in 6.3.3.1, the parafilm was removed and the sample was placed in a container with 500 mL of DI water in which to cure. The container was then sealed with its lid and parafilm. The samples were cured at ambient temperature. This method of grouting was shown to produce equivalent results to the usual 'penetration' method, described in 3.2.5, allowing results obtained via the two techniques to be compared; a comparison of the two methods can be found in appendix A.4.3.

Using this method, in the third experiment, samples were prepared using CS, and CS/kaolin with 11 wt% and 25 wt% added, such that the resulting CS and CS/clay mixtures had 0, 10, and 20 wt% of kaolin, respectively. These were each mixed with 1.7 M NaCl accelerator and cured for 4, 6, or 12 weeks.

6.3.3 Experimental methods

6.3.3.1 Gel time calculation method

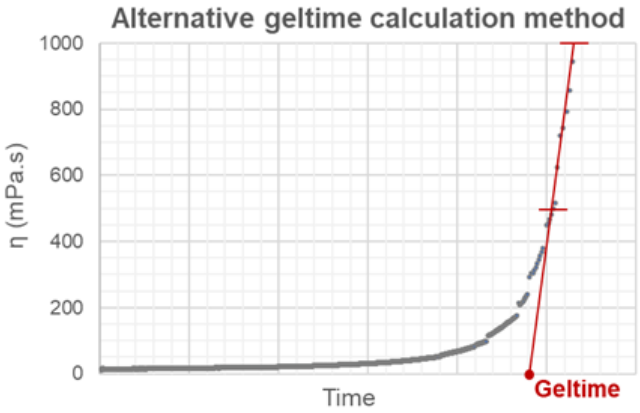

Figure 6.2. Diagram illustrating the alternative method used to calculate gel time in this study.

The method outlined in section 3.3.1 for determining the gel time of CS grout bears the underlying assumption that the initial viscosities of the grouts used are effectively unchanging. However, the addition of clay to CS grout caused an increase in viscosity related to the type and wt% of clay added, so an alternative method for calculating gel time was used here. For the method in 3.3.1, the viscometer's spindle was set to 100 rpm, and the time the grout took to reach a viscosity of 57 mPa·s (95% of the spindle's tolerance in torque) provided the gel time. In this method, however, measurement was continued past this viscosity by reducing the rpm during test. This, hypothetically, allowed for viscosities up to 20 000 mPa·s (at 0.3 rpm) to be recorded, although measurement was usually ceased below 2 000 mPa·s, as the rate at which measurements

could be taken became impractically slow compared to the rate of change of viscosity past this point. To determine the gel time, the data was plotted, and all points in the range of 500–1 000 mPa·s were used to plot a line to the x-axis. The intercept of this line was used for the gel time. A diagram of this method is provided in Figure 6.2, where η is viscosity.

6.3.3.2 Shear vane test method

Shear vane tests on CS grout and CS/kaolin grout were carried out according to the method in 3.3.4.

6.3.3.3 UCS test method

Drained UCS tests on CS-grouted sand and CS/kaolin-grouted sand samples were carried out according to the method in 3.3.5.

6.4 Results

6.4.1 Adding clays to CS grout

6.4.1.1 Effect on viscosity

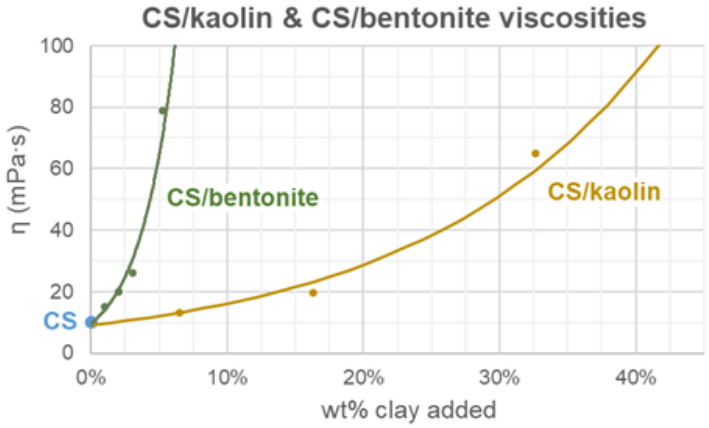

Figure 6.3. Effect of the wt% of added clay, including kaolin (green) and bentonite (yellow), on the viscosity of CS/clay mixtures. Fit lines are exponential. The blue point represents CS.

Figure 6.3 shows the effect of adding kaolin and bentonite to MP 320 CS on the viscosity of the resulting CS/clay mixture. No mass of silica was replaced, so the total mass of solids increased with the wt% of clay added. No accelerator was present for this test, so the mixtures were not gelling. As the wt% of kaolin, w_k, and bentonite, w_b, added to CS increased, they each caused exponential increases in viscosity, η, described by the equations

$$\eta = 9.07e^{5.76w_k}, \tag{6.1}$$

and

$$\eta = 9.56e^{38.1w_b}, \tag{6.2}$$

for kaolin and bentonite, respectively. Also from the plot, it is clear that the addition of bentonite caused a significantly greater increase in viscosity than did kaolin.

6.4.1.2 Effect on gelation

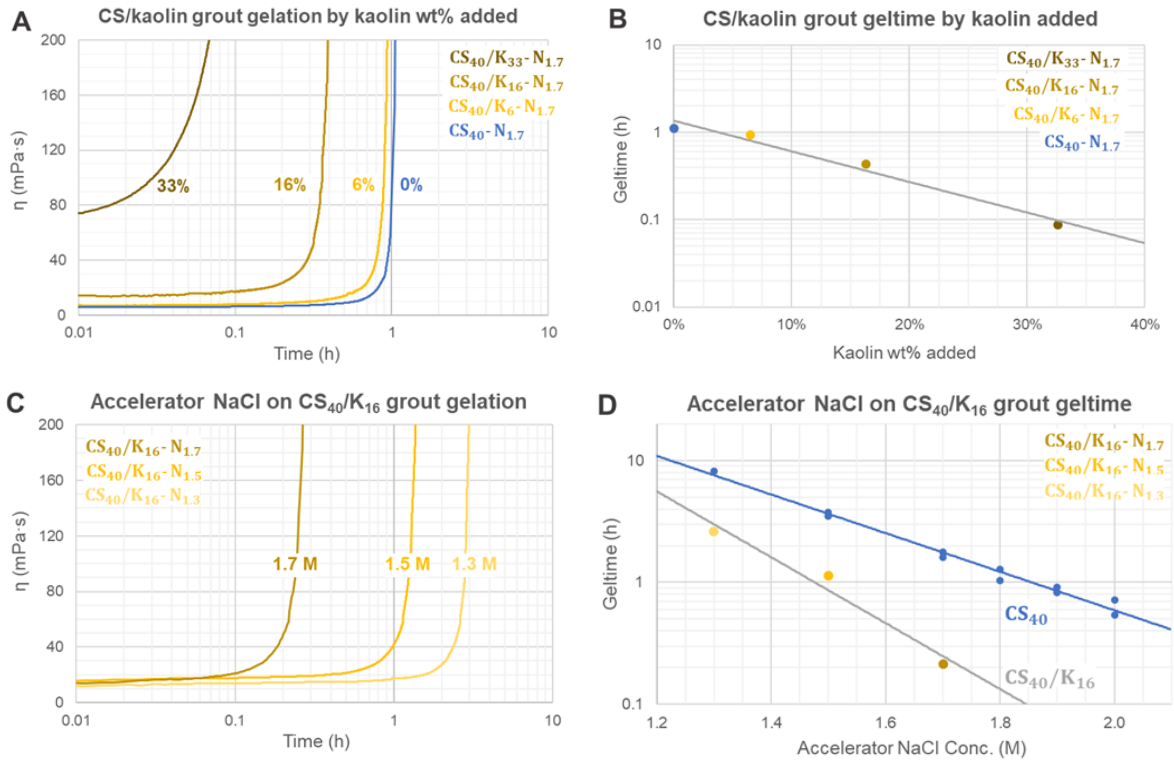

Figure 6.4. *A:* Evolution of viscosity during gelation of CS/kaolin grout with varying wt% of added kaolin, using 1.7 M NaCl accelerator. *B:* Effect of added kaolin wt% on the gel time of CS/kaolin grout, using 1.7 M NaCl accelerator, with exponential fit applied. *C:* Evolution of viscosity during gelation of CS_{40}/K_{16} grout at various accelerator NaCl concentrations. *D:* Effect of accelerator NaCl concentration on the gel time of CS_{40}/K_{16} grout, with exponential fit. Data for standard CS grout (CS_{40}), from section 4.3.1, is provided for comparison, in blue.

Figure 6.4A shows the effect of the wt% of kaolin added to CS grout on its viscosity evolution during gelation, and B shows the effect on the resulting calculated gel times. From the plots, it is clear that the presence of kaolin causes gelation to accelerate, resulting in an exponential decrease in gel time with increasing wt% of kaolin added, according to the formula

$$t_g = 1.35e^{-8.07w_k}, \tag{6.3}$$

for t_g in hours. Figure 6.4C shows how the concentration of NaCl in the accelerator solution affects the viscosity evolution during gelation of CS_{40}/K_{16} grout, and D shows the effect this has on the gel time, with data for standard CS grout, from section 4.3.1,

provided for comparison. Like with the standard CS grout, increasing accelerator NaCl concentration, c_{NaCl}, accelerates gelation, resulting in a decrease in gel time described by an exponential decay law, of equation

$$t_g = 9860e^{-6.23c_{NaCl}}. \quad (6.4)$$

The CS_{40}/K_{16} fit line is somewhat steeper than that of the CS_{40}, however.

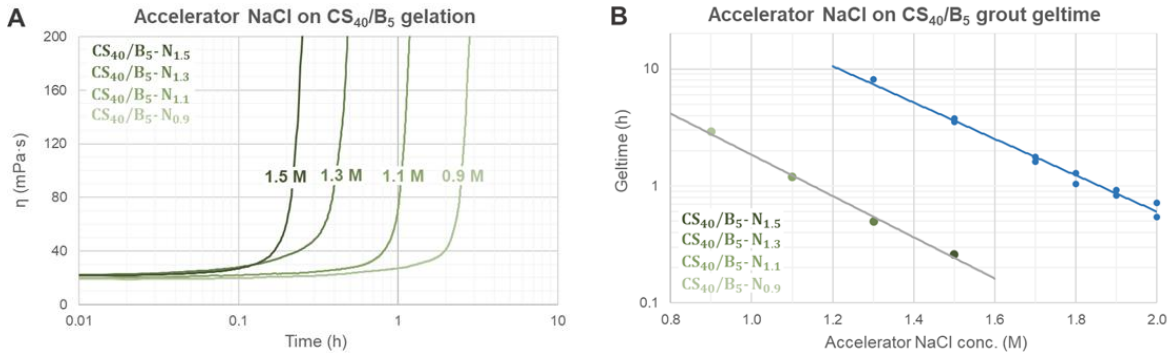

Figure 6.5. *A:* Evolution of viscosity during gelation of CS_{40}/B_5 CS/bentonite grout at various accelerator NaCl concentrations. *B:* Effect of accelerator NaCl concentration on the gel time of CS_{40}/B_5 grout, with exponential fit, and CS_{40} data for comparison.

Figure 6.5A shows how accelerator NaCl concentration affected the viscosity evolution during gelation of CS_{40}/B_5 grout, and B shows the effect on gel time, with CS_{40} data for comparison. Only 5 wt% of bentonite was added here, as opposed to 16 wt% for the kaolin, as gelation would occur too rapidly to measure with the viscometer at this wt% of bentonite. For the same reason, NaCl concentrations above 1.5 M could also not be used. Like for CS/kaolin, the addition of bentonite accelerated the gelation of CS grout, and increasing accelerator NaCl concentration resulted in a decrease in gel time according to an exponential decay law,

$$t_g = 107e^{-4.06c_{NaCl}}. \quad (6.5)$$

In this case, the gradient of the fit line for the CS/bentonite is roughly equal to that of the CS grout. Due to time restraints on this investigation, CS/bentonite grout was not investigated further, with experiments focussing only on CS/kaolin, as it was easier to work with.

6.4.1.3 Effect on strength

Figure 6.6 presents data from UCS tests on sand samples grouted with standard CS_{40}-$N_{1.7}$ grout, and CS/kaolin grouts; the CS/kaolin grouts were CS_{40}/K_{25}-$N_{1.7}$ and CS_{40}/K_{11}-$N_{1.7}$, which had 11 wt% and 25 wt% of kaolin added, respectively. Each grout used 1.7 M NaCl

accelerator, meaning that the CS/kaolin grouts had faster gel times than the CS_{40} grout. Figure 6.6A shows the stress response of samples cured for 28 d. Each of the samples endured a comparable amount of strain, ε, before failing, with increasing wt% of kaolin added increasing the maximum compressive stress, σ, recorded. Figure 6.6B plots the maximum compressive stress, referred to here as the compressive strength, for all of the samples, over their curing times. The plot shows an increase in strength over time described by power law relationships, for each of the grout mixes. Adding 11 wt% of kaolin gave a significant strength increase over standard CS-grouted sand, but further increasing to 25 wt% kaolin gave little additional benefit. Each of the power law fits had roughly equal gradient on the log-log axes.

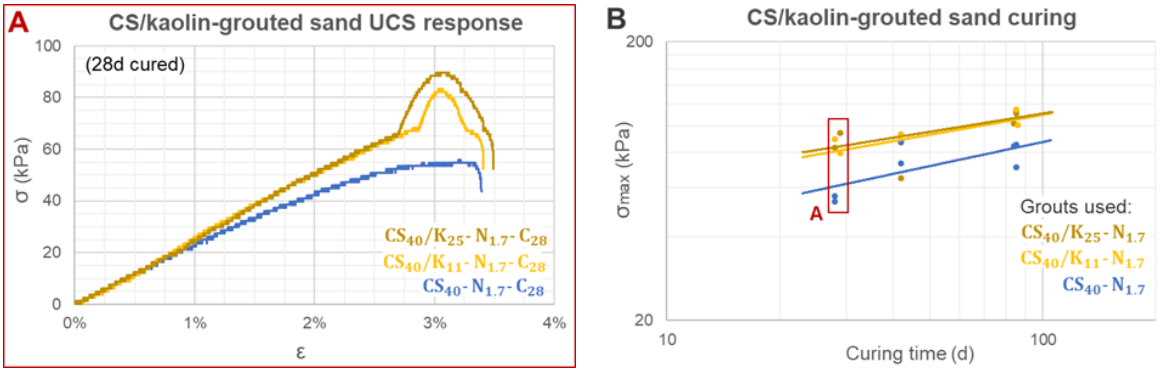

Figure 6.6. *A:* Stress response of CS- and CS/kaolin-grouted sand samples with different wt% of kaolin added (blue and yellow, respectively), to UCS test. Each sample was cured for 28 d and used 1.7 M NaCl accelerator. *B:* Compressive strength of CS- and CS/kaolin-grouted sand samples with different kaolin wt% increasing over curing time, with power law fits shown. The data from *A* is highlighted in red in *B*.

6.4.2 Replacing mass of silica with kaolin

6.4.2.1 Effect on initial viscosity and gelation

Instead of simply adding clay to CS grout, mass of silica could instead be replaced with clay, such that the total mass of solids remained the same. Figure 6.7 shows the effect of accelerator NaCl on the viscosity, gelation, and gel time of grouts in which different amounts of kaolin were used to replace corresponding masses of silica. Two such grouts were employed: CS_{33}/K_{11} and CS_{25}/K_{25}, which used CS/kaolin mixtures of 30/10 wt% and 20/20 wt% silica/kaolin, respectively. Plots A and B show the viscosity evolution duration gelation for the two grout variants. The initial viscosities of the CS_{25}/K_{25} grouts (Figure 6.7B) appeared to vary somewhat with accelerator NaCl, whereas they were constant for the CS_{33}/K_{11} (Figure 6.7A). Figure 6.7C plots the initial viscosities with accelerator NaCl concentration, with standard CS_{40} grout for comparison. From this, the

CS_{40} and CS_{33}/K_{11} had near-identical initial viscosity, which did not vary with accelerator NaCl: (6.29 ± 0.08) mPa·s and (6.62 ± 0.12) mPa·s, respectively. The CS_{25}/K_{25}, however, had higher initial viscosity, which apparently increased exponentially with NaCl concentration: its average was (10.9 ± 1.7) mPa·s. Figure 6.7D shows the gel times of the grout mixes in A and B, as well as for CS_{40} grout. In each case, as may be expected, increasing accelerator NaCl concentration caused a decrease in gel time according to exponential decay laws, for CS_{33}/K_{11} and CS_{25}/K_{25}, respectively,

$$t_g = 718e^{-3.33c_{NaCl}}, \tag{6.6}$$

and

$$t_g = 2380e^{-3.39c_{NaCl}}. \tag{6.7}$$

These equations allowed the gel times of CS_{33}/K_{11} and CS_{25}/K_{25} to be precisely controlled using the accelerator NaCl concentration. The concentrations which would give equal gel time to standard CS_{40}-$N_{1.7}$ were estimated at 1.8 M and 2.3 M for CS_{33}/K_{11} and CS_{25}/K_{25}, respectively.

Figures 6.7E and F compare the gel time data for CS_{33}/K_{11} and CS_{25}/K_{25} grouts with CS grouts of the same silica wt% (CS_{30} and CS_{20}, respectively, again from section 4.3.1), as well as CS_{40}, which had the same total wt% of solids. Unlike the CS/kaolin grout in Figure 6.4D (CS_{40}/K_{16}), the gradients of the CS/kaolin grout fit lines here were roughly equal to those of the standard CS grout. In both cases, the CS/kaolin grout gave faster gel times than CS grout with the same silica wt%, but slower than the CS_{40} with the same total wt% of solids. This suggests that kaolin content has less effect on gel time than silica content.

As shown in Figure 6.7G, for any particular NaCl concentration, increasingly replacing the mass of silica in CS grout with kaolin, whilst keeping the total mass of solids constant, caused an increase in gel time described by the formula $y = a(1 - x)^{-b}$, where a and b are constants. The example in Figure 6.7E is for 1.7 M NaCl.

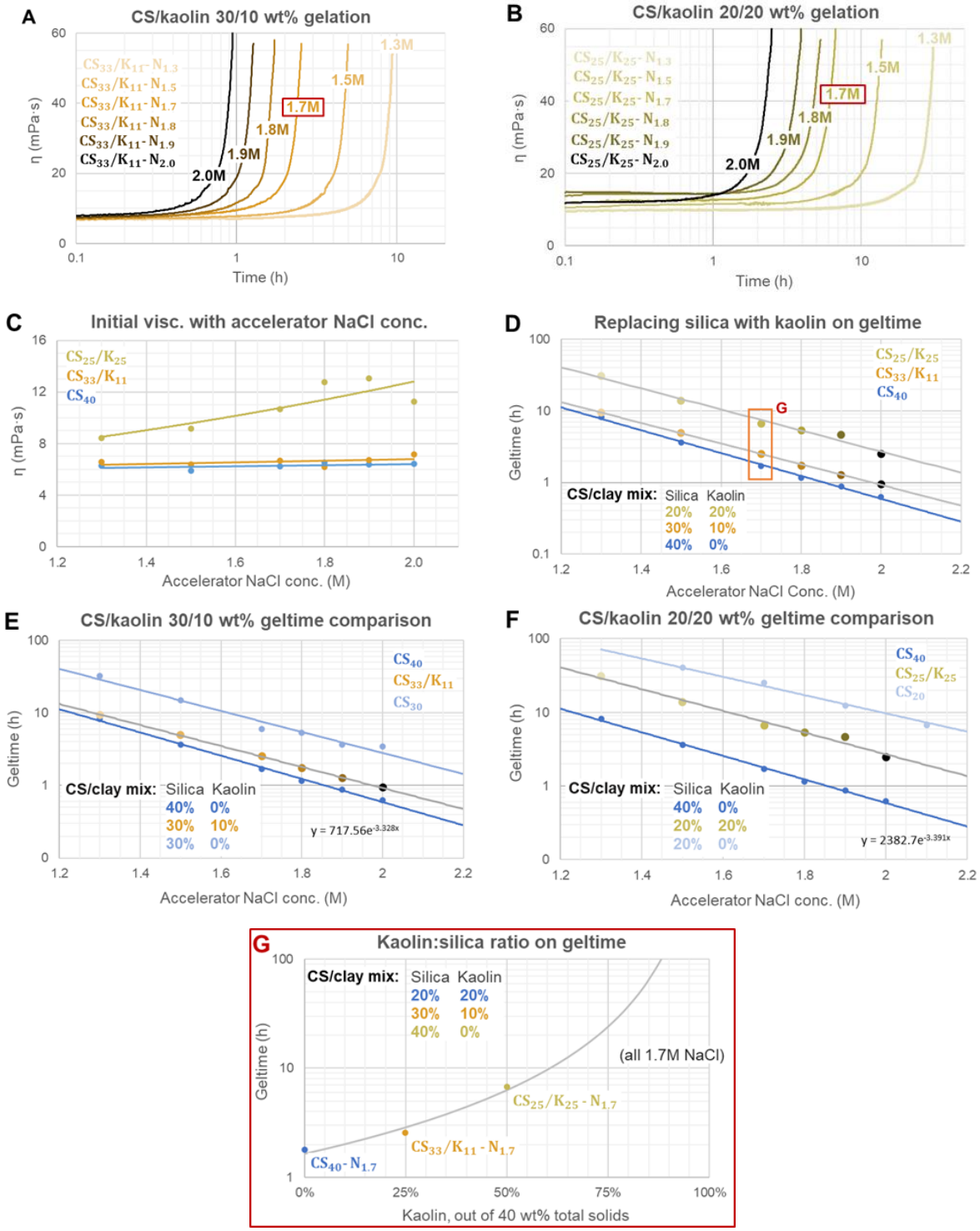

Figure 6.7. Viscosity during gelation of CS_{33}/K_{11} (*A*) and CS_{25}/K_{25} (*B*) grouts at different accelerator NaCl concentrations. *C:* Initial viscosities of the grouts, plus standard CS_{40}, with accelerator NaCl concentration. CS_{25}/K_{25} has an exponential fit applied. *D*: Gel times of the grouts with accelerator NaCl concentration. The lines are exponential fits. *E:* Comparison of the gel times of the CS_{33}/K_{11} grouts with data for CS_{30} and CS_{40}, which, respectively, had the same silica wt% and total mass of solids. *F:* The same for CS_{25}/K_{25} grout, with CS_{40} and CS_{20} for comparison. *G*: The effect of kaolin/silica ratio on the gel time of CS/kaolin grout, for mixes with 40 wt% total mass of solids, and 1.7 M NaCl accelerator. Fit is of form $y = a(1 - x)^{-b}$.

6.4.2.2 Effect on strength and re-healing

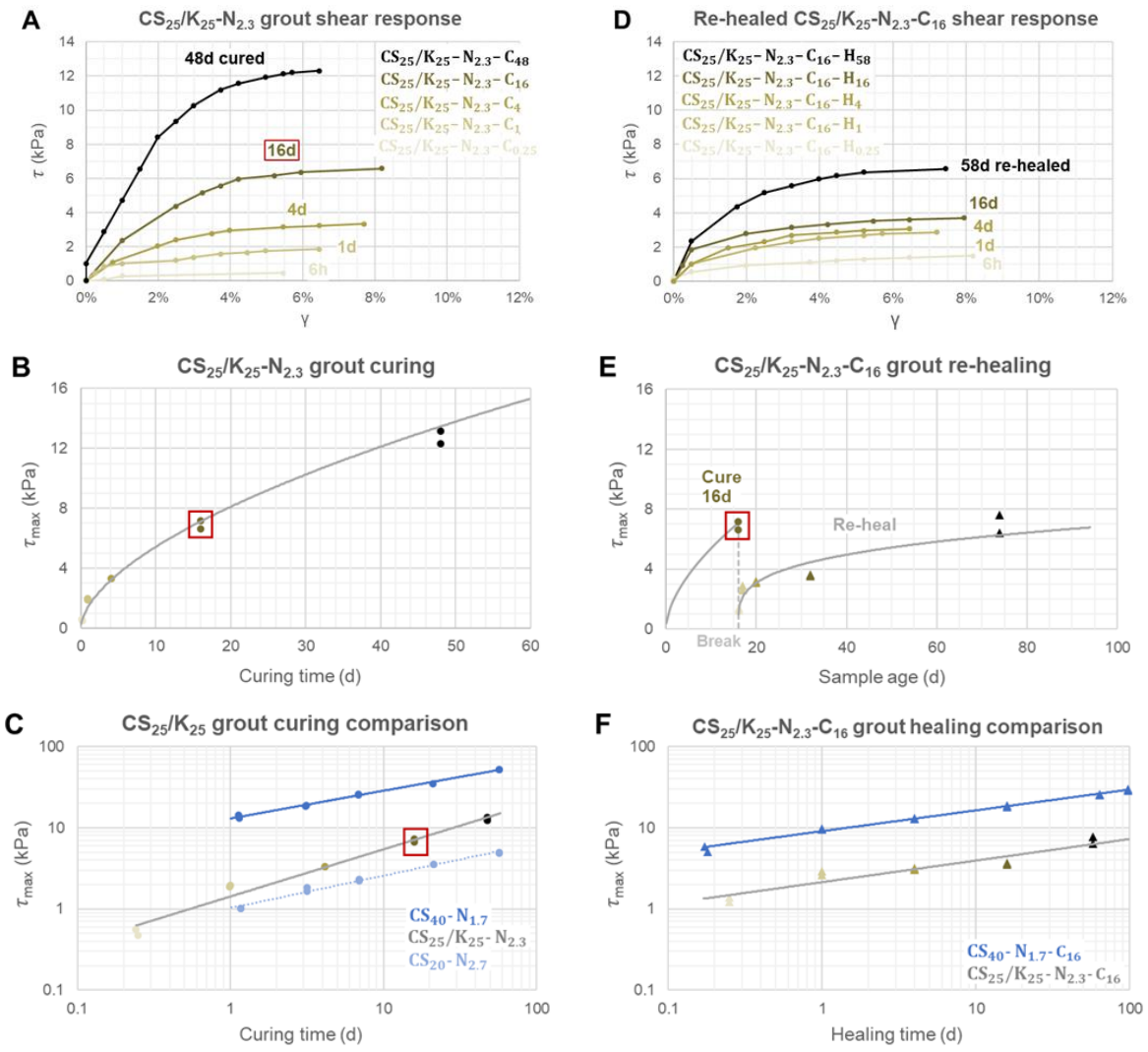

Figure 6.8. *A:* Shear stress response of CS_{25}/K_{25}-$N_{2.3}$ grout, cured for different durations, to increasing shear strain, imparted by a shear vane. *B:* The maximum shear stress values for the CS_{25}/K_{25}-$N_{2.3}$ samples, over curing time, with power law fit shown. *C:* Data from *B* with log-log scales, and corresponding data for CS_{40}-$N_{1.7}$ and CS_{20}-$N_{2.7}$ grouts, which have the same gel time, but no kaolin. *D:* Shear response of CS_{25}/K_{25}-$N_{2.3}$-C_{16} grout, which was broken after 16 d curing and healed for different durations. *E:* The maximum shear stress values for the CS_{25}/K_{25}-$N_{2.3}$-C_{16} samples, over the total sample age, with power law fit. The dotted line illustrates the break at 16 d, assuming total loss of strength. *F:* Data from *E* plotted over healing time, with log-log axes, and corresponding CS_{40}-$N_{1.7}$-C_{16} data. Red boxes identify the same CS_{25}/K_{25}-$N_{2.3}$-C_{16} data point in different plots.

Figure 6.8A shows the response of CS_{25}/K_{25}-$N_{2.3}$ CS/kaolin grout samples cured for different durations to increasing shear strain, generated using a shear vane, where τ is the shear stress imparted by the vane to achieve strain γ. Shear vane tests were used here over UCS, as in 6.4.1.3, as it was found that they provided results with less random variation, and they also allowed simple measurement of re-healing behaviour, via

previously established methods. Figure 6.8B plots the maximum stress value, τ_{max}, for each of the curves in A; this can be interpreted as the failure stress of the samples, and is a measure of shear strength. Plot B therefore shows how, as for standard CS grout (see section 4.3.2), the shear strength of CS_{25}/K_{25}-$N_{2.3}$ grout increases with curing time according to a sublinear power law relationship. Figure 6.8C plots the increase in shear strength again with log-log axes, and corresponding data for CS_{40}-$N_{1.7}$ and CS_{20}-$N_{2.7}$ grouts, from 4.3.2; the CS_{40}-$N_{1.7}$ has the same total mass of solids, and CS_{20}-$N_{2.7}$ the same silica wt% as the CS_{25}/K_{25}-$N_{2.3}$, but both are silica only, with no kaolin. All three grouts had the same gel time, achieved by using different accelerator NaCl concentrations. For CS_{25}/K_{25}-$N_{2.3}$, equation 6.7 was used to calculate the concentration needed. From plot C, the strength of the CS_{25}/K_{25}-$N_{2.3}$ samples seemed to fall between those of the CS_{40}-$N_{1.7}$ and CS_{20}-$N_{2.7}$, suggesting that adding kaolin to CS grout increased its strength, but not to the extent that increasing silica wt% by the same amount does. The fit line for the CS/kaolin grout also has slightly steeper gradient than those of the silica-only grouts.

Figures 6.8D-F demonstrate the ability of CS/kaolin grout to re-heal after damage. Plot D shows the shear response of CS_{25}/K_{25}-$N_{2.3}$-C_{16} grout samples, which were cured for 16 d before being broken and re-healed for different durations. Figure 6.8E plots the maximum shear stress for each sample over their total age, showing, as was seen with standard CS grout (see section 5.3.1), an increase in strength described by a power law. Plot E also shows the evolution in strength during the 16 d of curing, and for the break, where complete loss of strength is assumed. Figure 6.8F plots the maximum shear stress values again on log-log axes, against healing time, with corresponding data for CS_{40}-$N_{1.7}$-C_{16} grout. It was not possible to obtain CS_{20}-$N_{2.7}$-C_{16} within the timeframe of the study. From plot F, the CS/kaolin grout appears to re-heal slower than the silica-only grout with the same total mass of solids. In this case, the fit lines have roughly equal gradient.

6.5 Discussion

6.5.1 CS/clay viscosity

The results in section 6.4.1.1 give an idea of the limits of kaolin and bentonite which may be added to MP 320 CS whilst remaining usable as a permeation grout. It is clear from the data in Figure 6.3 that significantly more kaolin can be added to CS than bentonite while maintaining low viscosity. Although the viscosity of grout which may be used for

permeation grouting depends on various factors, such as the rheology of the grout, and the nature of the soil, applying an arbitrary limit of 100 mPa·s, for example, which is typical of urethane grouts used with loose sands and gravel (U.S. Army Corps of Engineers, 1995), allows up to 42 wt% of kaolin to be added, compared to just 6 wt% of bentonite. It should be noted that mixing with the accelerator solution also affects viscosity. The quantity of clay which can be added is important as, if addition of clay does provide benefits such as improved mechanical or sorption properties, then it may be beneficial to include as much clay as possible whilst keeping viscosities at practical levels, and this is more easily done with kaolin than bentonite.

Although adding kaolin to CS increased its viscosity, from Figure 6.7C, it can be seen that the CS_{33}/K_{11} grout, which used CS/kaolin of 30 wt% silica and 10 wt% kaolin, had only negligibly higher initial viscosity than standard CS_{40} grout. This suggests that, at least for smaller quantities of kaolin, the clay had no greater effect on viscosity than the silica wt%. The CS_{25}/K_{25} grout, however, which used CS/kaolin of 20 wt% each of kaolin and silica, did have higher initial viscosity, which increased exponentially with accelerator NaCl concentration. It may be that the electrolyte interacts with the kaolin particles in some way, causing viscosity to increase, but that this effect only becomes apparent once a certain quantity of kaolin is present. In spite of this, however, the viscosity of all the samples remained low, with none higher than 13 mPa·s, demonstrating that replacing mass of silica with kaolin does not significantly increase viscosity.

The addition of bentonite to CS did notably increase viscosity, however, due to the swelling behaviour of bentonite, previously described in section 6.2, in which bentonite particles expand as their layers are pushed apart by intrusion of water.

6.5.2 CS/clay grout gelation

In section 6.4.1.2, both kaolin and bentonite were observed to accelerate the gelation of CS grout, with increasing wt% of kaolin giving an exponential decrease in gel time. Data for only one wt% of bentonite was recorded, but it may be assumed to behave similarly. Figure 6.9 combines the data on the effect of accelerator NaCl concentration on the gel times of CS_{40}/K_{16} and CS_{40}/B_5 grouts, with standard CS_{40} for comparison. The gradient of the CS_{40}/B_5 fit is roughly equal to the CS_{40}, whereas for CS_{40}/K_{16} it is noticeably steeper. This difference likely arises simply due to there being a high degree of variation in the

data, and few datapoints available for the CS_{40}/K_{16}, due to time constraints. It is clear here though that, although the addition of both clays caused reductions in the gel time of CS grout, the bentonite had a much greater effect than the kaolin, even though the quantity added was over three times less.

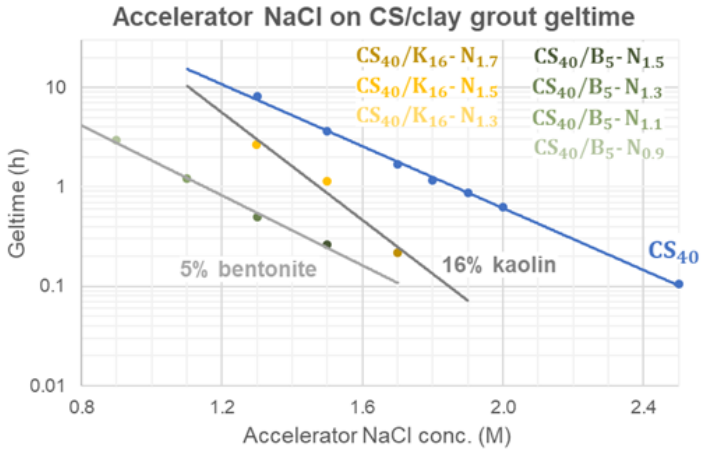

Figure 6.9. Effect of accelerator NaCl concentration on the gel times of CS/kaolin (CS_{40}/K_{16}) and CS/bentonite (CS_{40}/B_5) grouts, with standard CS_{40} grout for comparison, and exponential fits applied.

The reason for bentonite's large effect on CS grout gelation may be again due to its swelling behaviour, which traps water within clay particles, reducing the volume available for CS particles to move in, thereby increasing the frequency of collisions between particles, accelerating gelation.

In section 6.4.2.1, it was shown that replacing the mass of silica in CS grout with kaolin slowed gel times, meaning that, although adding kaolin accelerates gelation, it has less of an effect than the wt% of silica present in the grout.

Kaolin's acceleration of CS grout gelation could be due to it trapping water molecules needed to dissolve it. Similar to the proposed effect of bentonite, in which the frequency of inter-particle collisions is increased by reducing the volume of available water, but to a much lesser extent due to the lack of swelling. Alternatively, it may be that the clay particles actively take part in CS network formation by providing additional bonding sites, but not to the extent that CS particles themselves do. As mentioned in 6.2, the edges of layers in both kaolin and bentonite feature aluminol and silanol groups, which could potentially form aluminosilicate (Al-O-Si) and siloxane (Si-O-Si) bonds with CS. The aluminol and silanol groups could also act as nucleation points for CS polymerisation by hydrogen bonding with CS particles, facilitating close approach and bond-formation

between them. The clays may also affect the zeta-potential or local pH of the CS to facilitate gelation.

Although both clays accelerated the gelation of CS grout, NaCl accelerator was always required to induce gelation. CS/clay mixtures by themselves would remain stable to gelation for long durations, although some settling of the clay out of suspension could occur.

6.5.3 CS/kaolin grout mechanical performance and re-healing

The data in section 6.4.1.3 showed that addition of 11 wt% of kaolin to CS grout increased the strength of grouted sand samples in UCS tests, but that there was little added benefit when increasing this to 25 wt% kaolin. This could be due to kaolin particles actively participating in the CS gel network through their surface silanol and aluminol groups, forming covalent bonds with CS particles; they may also reinforce the network through transient interactions, such as hydrogen bonds. Even just the physical presence of the comparatively large, solid clay particles could make the gel stronger and more rigid by taking up space which would otherwise be occupied by pore water.

A possible reason for the reduction in strength gain when increasing to 25 wt% kaolin added is that the CS content of the grout is technically being reduced. As mentioned in 6.3.2.2, when kaolin is added to CS, it somewhat increases the volume of the grout, which is an effect not accounted for in this investigation. This means that the same volume of CS/kaolin grout contained slightly less silica than standard CS grout: increasingly so with more kaolin added. In 6.4.1.3, it was seen that, although addition of kaolin increased the strength of CS grout, it had less effect than the silica wt% of the grout, so eventually, the reduction in silica content could begin to nullify the gain in strength provided by the addition of kaolin.

Section 6.4.1.3 also showed that CS/kaolin increases in strength during curing, and re-heals in a similar manner to standard CS grout, suggesting that the same underlying processes explain CS/kaolin's curing and re-healing, and that the kaolin does not hinder these. Although for curing the gradient of the CS/kaolin fit line was steeper than those of the standard CS grout, this is again likely due to a high degree of variation in the data, and a need for more measurements, as in the case of re-healing, the CS/kaolin and standard CS grout fit lines had roughly equal gradient.

6.6 Conclusion

Here, the effect of the addition of kaolin and bentonite clays to CS grout on its viscosity, gelation, and mechanical properties was investigated. The goals of this were to assess the feasibility of the CS/clay grouts for use in permeation grouting, to see if clays could increase the strength of CS grout, and to investigate whether clays could be used to replace the mass of silica in the grout without compromising mechanical performance, in order to reduce the cost of the grout. Increasing the strength and reducing the cost of CS grout would extend its range of application, and if bentonite clay can be used with CS, it could impart it with various beneficial properties, such as high sorption capacity and self-sealing behaviour, which would be very useful for application as a barrier material.

Viscometer tests showed how addition of both kaolin and bentonite gave exponential increases in the viscosity of CS with increasing wt% of clay added, but that bentonite had a much greater effect than kaolin; this meant that much larger quantities of kaolin than bentonite could be added to the grout whilst keeping viscosities useably low. Kaolin had about the same impact as the silica wt% of the grout, such that 10 wt% of silica could be replaced with kaolin with effectively no change in viscosity. Replacing 20 wt% of the silica with kaolin did increase viscosity somewhat, and an effect appeared where viscosity increased exponentially with accelerator NaCl concentration, although the viscosity was still very low.

Both kaolin and bentonite were found to accelerate the gelation of CS grout, with bentonite again having a much greater effect. Increasing wt% of kaolin was found to give an exponential decrease in gel time, although kaolin had less impact on than the wt% of silica in the grout. The NaCl concentration of the accelerator could be used to control the gel time of both CS/kaolin and CS/bentonite, with the effects defined by exponential relationships. Bentonite's large impact on CS grout's viscosity and gelation is likely due to its swelling behaviour removing water for the CS particles to move in, increasing the frequency of particle collisions. Several possible explanations were discussed regarding kaolin's effect on viscosity and gelation.

UCS tests on sand grouted with CS and CS/kaolin grouts showed that adding 11 wt% of kaolin to the grout gave a significant increase in strength, but increasing this to 25 wt%

produced only a minor improvement on this; the reduction in strength gain may have been the result of an experimental error, however.

In shear vane tests, CS/kaolin grout was seen to increase in strength during curing and re-healing after breaking according to power law relationships, in a similar manner to standard CS grout. The presence of kaolin was found to increase the strength of the grout, but it had less effect than the wt% of silica. Several explanations were proposed regarding kaolin's effect on CS grout's mechanical properties.

Chapter 7: Combining CS Grout with Polymers

7.1 Introduction

This chapter features an investigation on the combination of CS grout with polymers to form so-called 'nanocomposite hydrogels'. Polymer hydrogels are highly modifiable, and can be customised for super-strength, flexibility, and re-healability (Deng et al., 2020; Fan et al., 2020; Tanaka et al., 2005; Zhang & Khademhosseini, 2017). Due to their tuneable mechanical properties and biocompatibility, polymer hydrogels are materials which have been the object of intensive research in medical applications, such as drug/cell culture delivery (Caliari & Burdick, 2016; Lee, 2018; Li & Mooney, 2016; Lin & Metters, 2006; Peppas et al., 2000; Vigata et al., 2020), and tissue engineering (Kondiah et al., 2016; Li et al., 2018; Mantha et al., 2019; Nezhad-Mokhtari et al., 2019; Zhu & Marchant, 2011). However, despite this surge in medical-focused innovation, they have rarely been considered for large-scale engineering application. This is largely attributed to high material costs, challenges in in situ gelation control, and constraints in scalable deployment that hinder widespread use in geotechnical or infrastructural contexts (Chirani et al., 2015). These limitations are particularly pronounced in field applications where polymer hydrogels must be injected into soil and rock, which necessitates precise control over viscosity, gel time, and crosslinking dynamics. Without predictable rheological behaviour and reliable gelation mechanisms, deployment becomes challenging. As such, while polymer hydrogels present compelling functional properties, their translation to large-scale engineering systems remains constrained by processing complexities and materials handling requirements.

Incorporating the desirable and tailorable properties of polymer hydrogels into CS grout, which itself features a highly controllable gelation mechanism, could significantly enhance its effectiveness within existing applications, and potentially unlock new uses in domains where it has not traditionally been considered. This work represents the first time that CS-nanocomposite gels have been investigated for use in permeation grouting.

A brief review of polymer hydrogel research is first provided here, highlighting and evaluating particular polymers and gelation techniques which may be suitable for grouting application alongside CS. The sections which follow then describe experimental investigations into three candidate polymers: polyethylene glycol (PEG), polyacrylamide

(PAM), and polyvinyl alcohol (PVA), and their combination with CS grout. Here, the nature of any interaction between the polymers and CS was first studied, forming conventional CS gels in the presence of the polymers. Polymer gels themselves were then created in water or CS if possible, with the aim of eventually achieving simultaneous CS and polymer gelation to form double networks. Initial evaluations of samples were carried out by solid-state test. For gels identified as having potential for application, mechanical properties were also studied using a rheometer.

7.2 Literature review

This section presents the results of a literature review on polymer hydrogel research. First, theoretical background is provided on polymers and hydrogels; then, criteria are identified which candidate polymers should fulfil in order to be combined effectively with CS grout in permeation grouting. Three polymers which potentially meet these criteria (PEG, PAM, and PVA) are then described, and associated gelation techniques for them are discussed.

7.2.1 Hydrophilic polymers

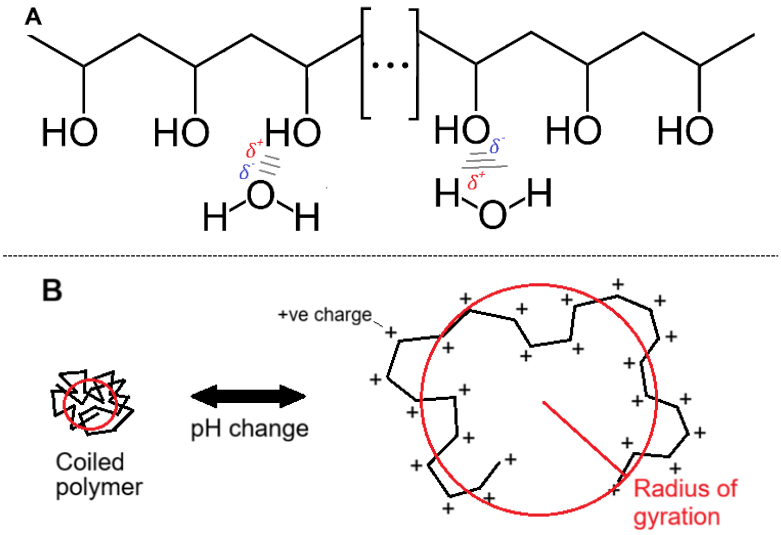

Figure 7.1. *A:* The hydrophilic polymer PVA, featuring polar OH groups on each monomer which interact with water molecules to allow dispersion. *B:* A hydrophilic polymer whose monomers become charged on changing pH. Like-charges repel each other, and the polymer extends out as a result.

Polymers are long chain molecules comprised of many repeating units called monomers (Gargallo & Radić, 2009; Schaller, 2025). For hydrophilic polymers, such as that depicted in Figure 7.1A, the monomers feature hydrophilic polar or electrically charged groups which interact with water molecules to allow stable dispersion of the polymer. Similar to

CS's silanol groups (see 2.2.1), polar groups of hydrophilic polymers can dissociate in dispersion to acquire charge, depending on the pH and the nature of the polar group. When these groups are mostly undissociated, having neutral charge, polymer segments can easily approach one another, and so the chain takes on a coiled conformation. As they become charged, however, the groups begin to repel each other, such that the polymer expands and extends. A diagram of this effect is provided in Figure 7.1B. By varying solvent properties, such as pH and ionic strength (which screens polymer charges), the behaviour of dispersed polymers can be controlled, allowing them to be extended or contracted accordingly, which in turn affects a range of properties of the solution, such as its viscosity. A polymer's radius of gyration is the root-mean-square distance of all its segments from its centre of mass, and it can be used to describe the polymer's effective size in dispersion.

7.2.2 Polymer hydrogels

Polymer hydrogels are composed of networks of hydrophilic polymers in a solvent, such as water (Odian, 2004). Some use chemicals called crosslinkers to form permanent, covalently bonded links between polymers via chemical reaction, often in combination with a reaction initiator and/or a catalyst. Others instead utilise transient physical interactions to link polymers together, such as network entanglements or salt bridges. Chemically crosslinked gels generally have the advantage of stiffness, but they are non-recoverable, meaning that the gel is permanently altered by deformation or damage to its network, as is the case for gelled CS grout. So called 'physical hydrogels' do often exhibit recoverability, however. A diagram of a chemically crosslinked hydrogel is shown in Figure 7.2A).

Polymer hydrogels have been the focus of an extensive and ever-growing body of research in recent years, particularly in medical applications, such as drug/cell culture delivery, and tissue engineering (Caliari & Burdick, 2016; Chirani et al., 2015; Kondiah et al., 2016; Lee, 2018; Li & Mooney, 2016; Li et al., 2018; Lin & Metters, 2006; Mantha et al., 2019; Nezhad-Mokhtari et al., 2019; Peppas et al., 2000; Vigata et al., 2020; Zhu & Marchant, 2011). Novel gelation mechanisms have been developed to produce gels with highly desirable properties, such as super-strength, super-flexibility, and re-healability (Deng et al., 2020; Fan et al., 2020; Tanaka et al., 2005); examples of such gels are provided in Figure 7.2B. Successful incorporation of any of these properties into CS grout

could greatly benefit its performance in a range of fields, and open it up to new applications.

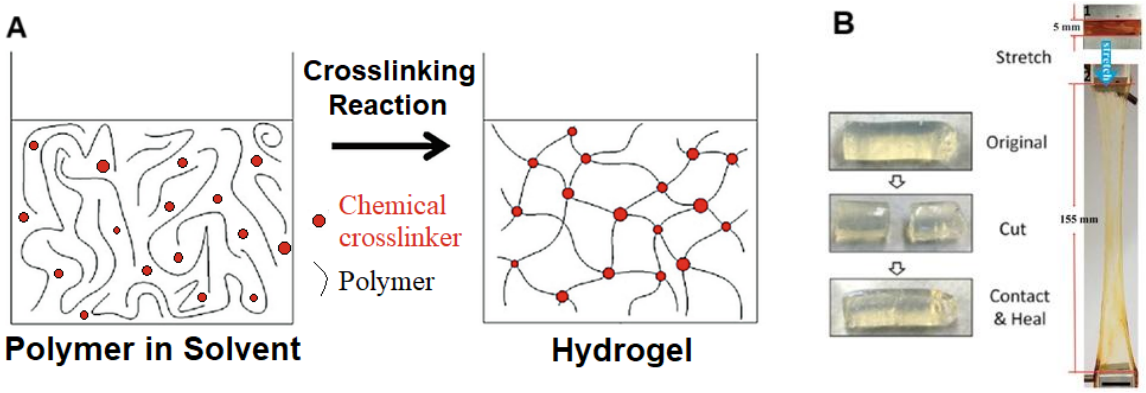

Figure 7.2. *A:* Formation of a chemically crosslinked hydrogel from a polymer solution. *B:* Re-healable and super-stretchable hydrogels from Han et al. (2017) and Wang and Gao (2016).

7.2.3 CS/polymer nanocomposite hydrogels

To best incorporate the advantageous properties of polymer hydrogels into CS grout without sacrificing CS's own beneficial features, it follows that composite gels should ideally feature both CS and crosslinked polymer networks, as depicted in Figure 7.3. Gels which utilise two independent networks are termed double network hydrogels and are known for their high strength and blending of properties (Chen et al., 2015). However, simple addition of polymer to CS grout, i.e. without crosslinking, may also produce samples with interesting and potentially useful modifications to their properties. For example, transient interactions between the respective hydrophilic groups of CS particles and polymers may act as a source of added flexibility and/or partial recoverability. Nanocomposite gels of both kinds were studied in this investigation.

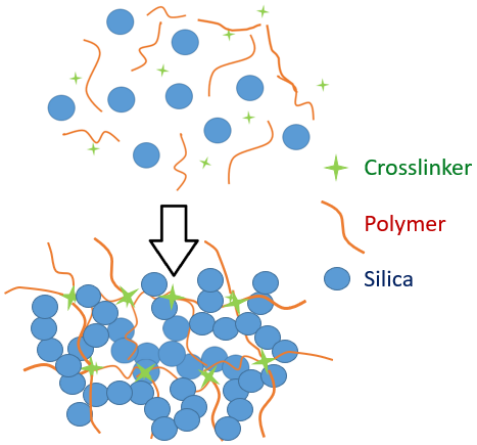

Figure 7.3. Hypothetical representation of the formation of a CS/polymer double network.

7.2.4 Choice of polymer and gelling system

As there is a large body of literature on polymer hydrogels, it was important to first establish key search criteria for identifying candidate polymers and gelation techniques for use in combination with CS grout. The criteria for candidate gel behaviour were as follows:

- Not overly interacting with CS to compromise its stability and/or gelation.
- Being cheap enough for production on large scales, here defined as being within one order of magnitude of the cost of CS at expected concentrations of the materials in question.
- Having the ability to gel in situ.

If gels are to be used for permeation grouting application, they must also exhibit the following further properties:

- Having the ability to gel in subterranean conditions.
- Having low enough viscosity for injection, ideally as low as possible, to minimise injection pressures and maximise soil penetration. An arbitrary upper bound for this was set at ~ 100 mPa·s.
- Being non-toxic, to prevent environmental contamination. Given this, it was decided to only consider gel systems which build up from pre-formed polymers, as opposed to those which build up directly from monomers, as the latter generally have high toxicities.

7.2.5 Polyethylene glycol

Polyethylene glycol (PEG), also known as polyethylene oxide (PEO), is the most common polymer used for biomedical hydrogels (Bakaic et al., 2015; Lin & Anseth, 2009), and PEG gel variants have been produced which have excellent mechanical properties and self-healing (Anindita et al., 2023; Bernal-Chávez et al., 2023; Mao et al., 2019; Nguyen et al., 2019; Z. Wang et al., 2022; Zheng et al., 2025). There have also been isolated examples of PEG composite gels with embedded silica nanoparticles which give them improved mechanical properties (Gaharwar et al., 2013; Ma et al., 2024; Shona Pek et al., 2008). PEG is unusual amongst hydrophilic polymers in that it does not contain a true polar (or charged) group, but rather simply ether oxygen atoms within each monomer which have sufficient slightly negative (δ^-) charge to interact with water molecules and allow

solubility that would otherwise not be expected (Figure 7.4A). As there is no polar group present to dissociate, PEG is not affected by changing pH.

Lin and Anseth (2009) categorised PEG crosslinking techniques as follows (Figures 7.4B-D):

- Chain growth: cost-effective, but requires initiation from energy sources, such as light or heat. Redox reaction initiators, such as ammonium persulfate, can instead be used, but they have high toxicity.
- Step growth: can take place under ambient conditions and has low toxicity, but requires chemically modified multi-arm PEG molecules, which are expensive to produce.
- Mixed mode: a combination of the two systems occurring simultaneously.

Given this, if PEG were to be combined in CS grout, compromises would need to be made regarding either cost or environmental compatibility.

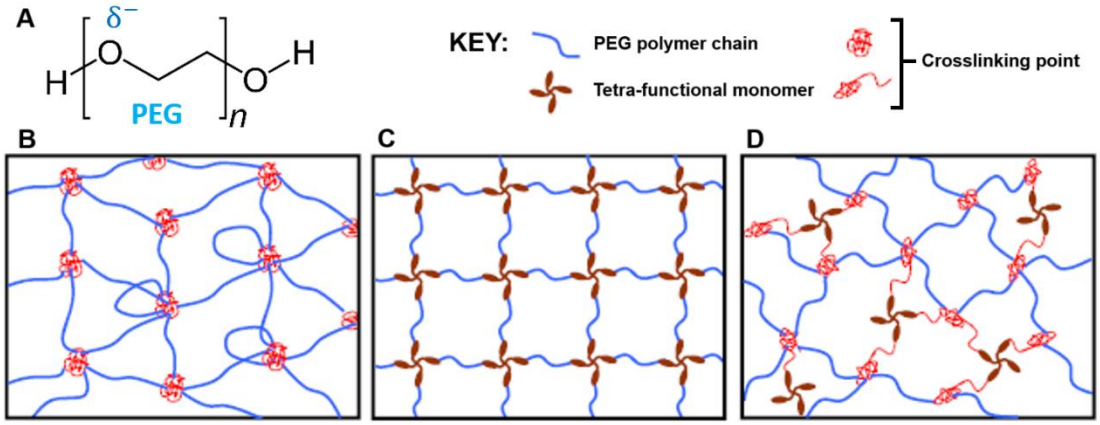

Figure 7.4. *A:* Structural formula of PEG. Also shown are diagrams illustrating the structures of chain growth (*B*), step growth (*C*), and mixed mode (*D*) PEG hydrogels, and a key. Adapted from Lin and Anseth (2009).

PEG was selected for use as, due to it not featuring true polar groups, it was thought it was less likely than other polymers to interact with CS to disrupt its stability or gelation. The fact that PEG has bio-compatible gelation techniques also contributed, although due to cost concerns, these were not attempted in this study. It was decided instead to first simply add PEG to CS grout in the hope that it may increase the water retention of the resulting gel and improve its mechanical properties by adding flexibility due to the

polymer's chain structure, or recoverability through secondary interaction of PEG's ether groups with CS silanol groups, post-gelation.

7.2.6 Polyacrylamide

Polyacrylamide (PAM) is a rare example of a polymer whose gel has found large-scale engineering application in the form of water shut-off and conformance control in oil reservoirs (Amir et al., 2018; Garcia Cordeiro Tessarolli et al., 2018; Lei et al., 2022; Lu et al., 2023; Mohamed & Mohyaldinn, 2025; Moradi-Araghi, 2000; Pinho De Aguiar et al., 2020). Its monomers feature polar amine groups (NH_2) which tend to dissociate to NH_3^+ in aqueous solution. Some interaction between these positive groups and the negatively charged dissociated silanol groups (SiO^-) on silica particle surfaces may therefore be expected. Under high temperatures, and at high pH, PAM has a tendency to undergo hydrolysis, with its amine groups being converted to anionic carboxylate (COO^-), which can affect its behaviour in a complex variety of ways (Jia et al., 2010). Most modern use of PAM in the oil industry is done alongside the non-toxic crosslinker polyethyleneimine (PEI) (Anyaezu et al., 2023; Gao et al., 2026; Ghriga et al., 2019; Ghriga et al., 2021; Marques et al., 2023; Martinez et al., 2025; Qin et al., 2020; Wang et al., 2024). The structural formulae for PAM and PEI are shown in Figures 7.5A and B, respectively.

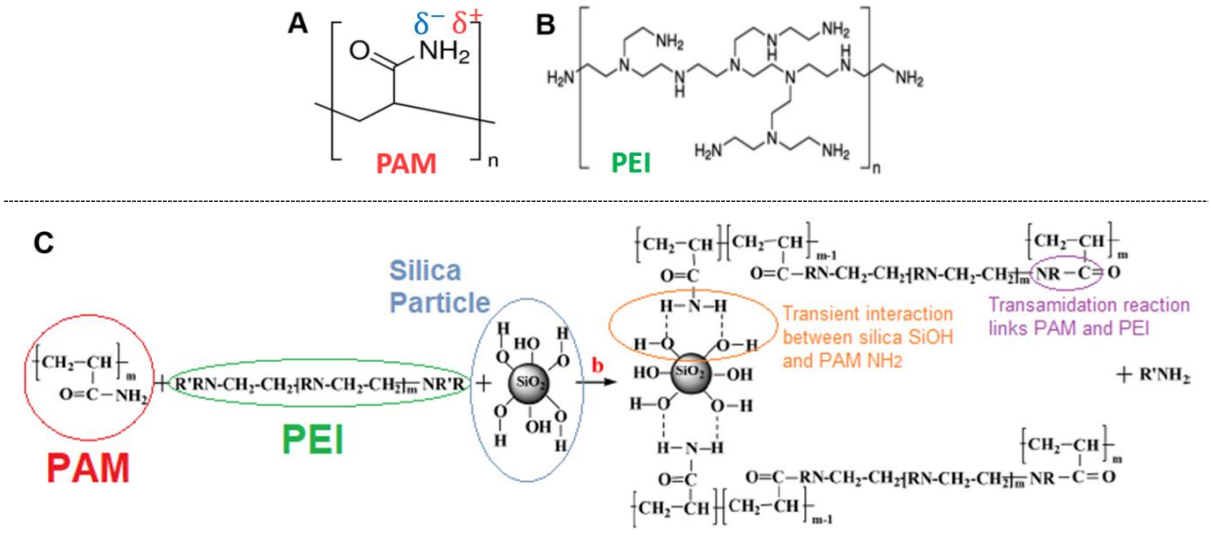

Figure 7.5. *A:* Structural formula of PAM. *B:* Structural formula of the crosslinker PEI. *C:* Diagram of the reaction which binds PAM and PEI together via PAM's NH_2 group. The transient interaction between PAM's NH_2 and a CS particle's SiOH is also shown. Adapted from Chen et al. (2018).

There has already been research carried out by the industry on adding CS into PAM-based gels, with CS particles found to act as anchor points adsorbed to the polymer network,

adding strength and increasing flexibility as a result of transient interaction between the PAM's amine and carboxylate groups and the silanol groups on CS particle surfaces, as depicted in Figure 7.5C (Amir et al., 2022; Chen et al., 2018; Cui et al., 2023; Ma et al., 2017; Shamlooh et al., 2019).

PAM Gels derived from acrylamide monomer were previously commonly used in permeation grouting, usually in combination with the crosslinker methylene-bis-acrylamide (MBAm) (Karol, 2003; Warner, 2004), and nanocomposite variants of PAM gels produced in this way have been created in combination with silica nanoparticles which feature excellent properties, such as super stretchability and flexibility (Jia et al., 2019; Rose et al., 2013; Yang et al., 2013), very high compressive strength and toughness (Adibnia & Hill, 2017; Gao et al., 2016; Levin et al., 2019; Ye et al., 2014), and self-healing (Shi et al., 2016). However, both acrylamide and MBAm are highly toxic and so are no longer preferred for civil engineering applications.

PAM was chosen for the study due to it already being used at large scales in engineering applications in combination with an environmentally friendly crosslinker in PEI, and because it is known to be enhanced in combination with silica. It was hoped that double network PAM/PEI/CS gels could be produced with enhanced strength and toughness due to secondary transient interactions of PAM and silica.

7.2.7 Polyvinyl alcohol

Polyvinyl alcohol (PVA) is unusual amongst polymers in that it does not require any additives to form a hydrogel; the polymer chains instead may entangle together under certain conditions to form self-crosslinks, as shown in Figure 7.6B (Bercea et al., 2013). It is assumed that this occurs when PVA solutions reach a specific concentration threshold, which can be brought on by drying (Stoks et al., 1988), or by freezing, during which the formation of ice crystals can push chains together to form areas of locally high concentration where quasi-crosslinks form (Bercea et al., 2013; Liu et al., 1995). Polar hydroxyl (OH) groups are the source of PVA's solubility and inter-molecular interaction, as depicted in Figure 7.6A. PVA/silica nanocomposite gels have been produced with enhanced mechanical properties and self-healing through freeze-thaw (Luo et al., 2019; Mahamoud et al., 2025; Tan et al., 2024), drying (Dadache et al., 2025; Quan et al., 2009; Sabr et al., 2021; Takeno et al., 2021), and chemical crosslinking methods (Zhang et al.,

2018; Zhang & Ye, 2014). PVA solutions are also already injected into soils for soil stabilisation, and have been used in combination with silica nanoparticles to improve soil mechanical properties (Cao et al., 2024; Khedr & Elhady, 2025; Mirzababaei et al., 2017; Ren et al., 2025; Singh et al., 2024).

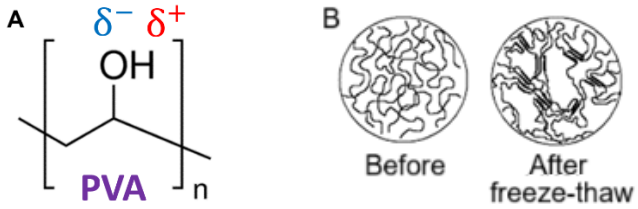

Figure 7.6. *A:* Structural formula of PVA. *B:* Formation of self-crosslinks in PVA upon freeze-thawing. Adapted from Bercea et al. (2013).

PVA was selected for use here due to its ability to gel without complex, expensive, or toxic crosslinkers, with it instead able to produce gels with excellent mechanical properties and self-healing properties simply through physical interaction. It was hoped that CS/PVA nanocomposite gels could be created with improved strength and toughness, enhanced re-healing, and which would be resistant to cracking from drying and wetting cycles, which is currently an area of concern for CS grout (Pedrotti et al., 2020).

7.3 Methodology

This section outlines the materials, sample preparation, and experimental methods employed in the study. Here, different combinations of CS, NaCl, polymer, and crosslinker were mixed to study if and how they would interact and gel. Three types of investigations were carried out:

1. Polymers were added to CS, which was then gelled using NaCl solution, or by lowering pH, in order to study the nature of any interaction, and to identify any gel variants with potential for application. This was done with all of the polymers.
2. Polymer hydrogels were formed in water, or in very dilute CS. This was done for PAM/PEI and PVA.
3. Polymer hydrogels were formed in undiluted CS, aiming to produce double network gels. This was done with CS/PAM/PEI and CS/PVA.

Initial characterisation of samples was conducted using solid-state test to evaluate gel strength and gel time. For some promising samples, a viscometer was used to study viscosity evolution during gelation, or on increasing polymer concentration; selected gels

were also dried to investigate their water-retention capabilities; mechanical and rheological properties of samples of interest were additionally investigated using a rheometer.

7.3.1 Materials

Materials used in this study included MP 320 CS, NaCl, 1 M HCl solution, and fine-grain building sand: more information on these can be found in section 3.1. PEG of average molecular weight 6 kg/mol was purchased from Sigma Aldrich in the form of solid flakes. 5 000 kg/mol PAM was purchased in granule form, and 150 kg/mol PAM was obtained from Sigma Aldrich in powder form. PEG-6000, PAM-5m, and PAM-150k were used to refer to each of these, respectively. 10 kg/mol branched PEI was obtained from Alfa Aesar in the form of a very viscous liquid. 31-50 kg/mol PVA, 98-98.8% hydrolysed, was procured from Fischer Scientific in granule form.

7.3.2 Sample preparation

7.3.2.1 Dissolving the polymers

Each of the polymers behaved differently regarding their requirements for dissolving in water and/or CS. To ensure proper dissolution, therefore, different mixing procedures were adopted for each. PEG and PAM did not react with CS when mixed, so they could be readily added to beakers containing either CS or water, depending on the experiment:

- PEG was added to the wall of the vortex created by stirring the solvent to ensure that the polymer beads were fully wetted. Stirring was then continued for 5 min.
- PAM needed a longer time to dissolve. After addition during stirring, the mixture was covered with parafilm to prevent evaporation, and was left on a magnetic stirrer until the solution became a consistent liquid with no visible undissolved polymer. This took 6-12, h depending on the PAM concentration.

PVA and PEI interacted strongly with CS, so they were only dissolved in water or NaCl solution:

- PEI was simply stirred into water by hand for 5 min.
- PVA required high temperatures to dissolve. After mixing with water, the beaker was covered and placed on a heated magnetic stirrer at 90°C until all the polymer was dissolved, usually taking ~ 1 h. Aluminium foil was used to cover the beaker

to limit evaporation. The mass of the mixture was measured before and after heating to track the amount of water lost, which was then replaced.

7.3.2.2 Measuring and adjusting pH

The polymers PAM, PEI, and PVA each had an effect on pH due to them featuring polarisable groups, so pH was always measured and/or adjusted when using these polymers. pH was measured using a Jenway 3510 pH meter. With each use, the pH meter was calibrated following a 2-point calibration (pH 4 and 7). Before every measurement, the probe was rinsed with DI water. If the pH of a solution was to be adjusted, 1M HCl solution was added dropwise to it from a 5 mL syringe, intermittently stirring and re-measuring until the desired pH was reached.

7.3.2.3 CS/polymer grout

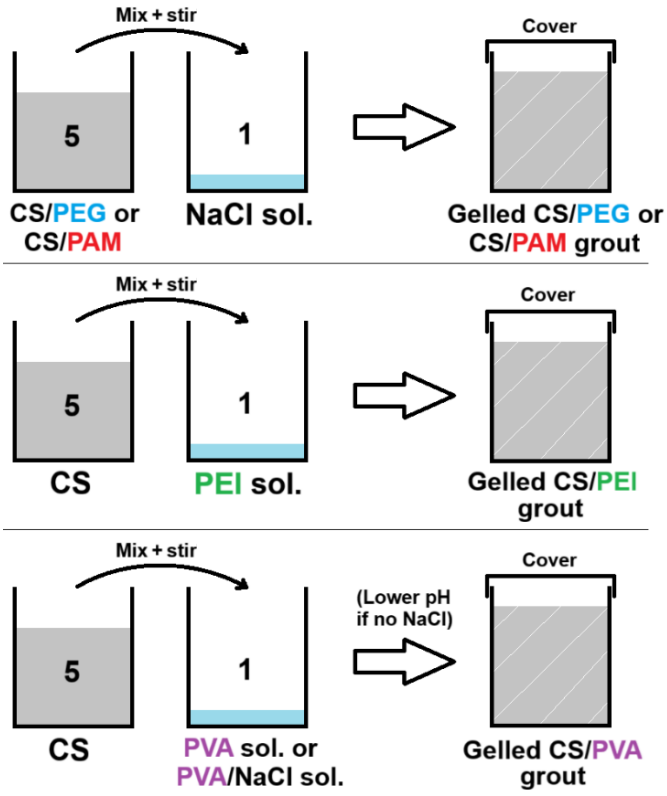

Figure 7.7. CS/polymer grout preparation methods.

This subsection describes the methods used in the first type of investigation, where polymers were added to CS that was then gelled conventionally with NaCl solution (see 3.2.2), or by lowering pH. This was done for each of the polymers in this investigation. Such samples are referred to as 'gelled CS/polymer grouts' to differentiate them from hydrogels created through crosslinking of polymers. Once prepared, all grout samples

were covered with parafilm. Figure 7.7 illustrates the different CS/polymer grout preparation methods.

- CS/PEG and CS/PAM grouts were prepared by first dissolving the desired quantity of PEG or PAM in CS, via the methods in 7.3.2.1. The mixture was then added to NaCl accelerator solution at a volume ratio of 5:1, and stirred.
- To create CS/PEI grout, PEI was first dissolved in water by the method in 7.3.2.1. CS was then added to this at a 5:1 ratio, and it was stirred. No NaCl was needed due to PEI's strong interaction with CS.
- CS/PVA grout was prepared by first dissolving PVA in either water or NaCl solution by the method in 7.3.2.1. CS was then added to this at a 5:1 ratio and stirred. If no NaCl was used, gelation was instead induced by subsequently lowering the pH.

7.3.2.4 PAM/PEI and CS/PAM/PEI gel

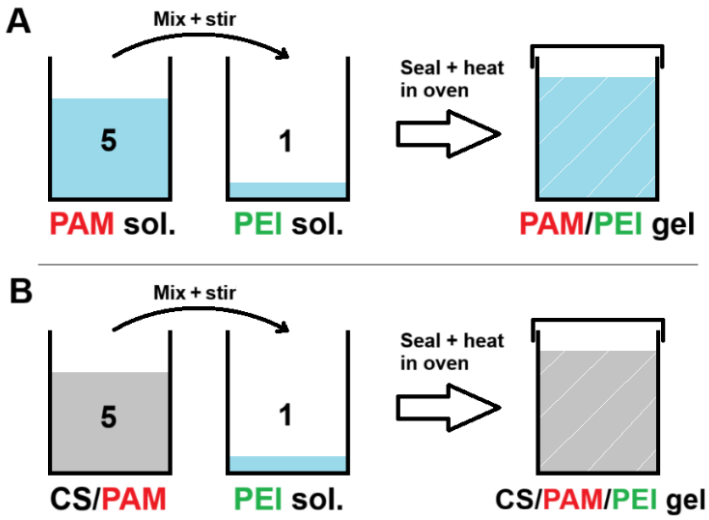

Figure 7.8. *A:* PAM/PEI gel preparation method. *B:* CS/PAM/PEI gel preparation method.

To prepare crosslinked PAM/PEI gels, PAM solutions were first prepared in DI water, or in very low silica wt% CS, created by adding a small amount of CS to DI water. PEI solutions were also prepared in DI water. The PAM and PEI solutions were then mixed at a volume ratio of 5:1, and stirred for 30 s, before being transferred to a sealed container and placed either in an oven (60°C or 100°C), or left out at ambient temperature (~ 20°C). Solid-state tests were used to assess whether samples had gelled (and estimate the strengths of those gels) over the following days. The same method was used to

prepare CS/PAM/PEI gels, but using CS/PAM in place of PAM solution. Diagrams of the two methods are provided in Figure 7.8.

7.3.2.5 PVA and CS/PVA gel

Self-crosslinked PVA gels were created via both air-drying and freeze-thaw methods. For air-drying, PVA solution was prepared and transferred to a petri dish which was left out in ambient conditions and weighed intermittently. This method is shown in Figure 7.9A.

For the freeze-thaw method, PVA solutions were first prepared in DI water; these were poured into plastic falcon tubes and sealed with parafilm. They were then placed in a freezer at -20°C for 1 d before being removed and allowed to thaw at ambient temperature. This process was repeated several times. To investigate the effect of the magnitude of temperature change on gelation, one tube was first poured into a glass container, covered with aluminium foil, and heated in an oven at 90°C for 1 h, before quickly being transferred to a falcon tube and frozen whilst still hot. This sample was weighed to ensure that negligible water loss had occurred during heating. CS/PVA gels were also prepared using the freeze-thaw method by starting with CS/PVA mixture, as opposed to PVA solution. Diagrams of the freeze-thaw methods are provided in Figures 7.9B and C.

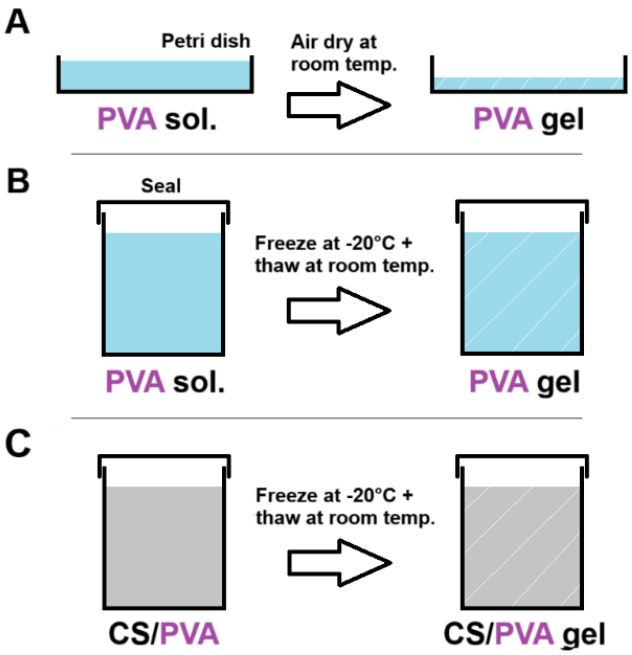

Figure 7.9. *A:* Air-dry method of PVA gel preparation. *B:* Freeze-thaw method of PVA (*B*) and CS/PVA (*C*) gel preparation.

7.3.2.6 Rheometer sample preparation

Freeze-thaw PVA and CS/PVA gel samples were prepared as in 7.3.2.5, but in 5 mL plastic rheometer cups. Standard CS grout rheometer samples were also prepared in cups by the method described in 3.3.3, along with CS/PEG and CS/PAM grout samples (PEG-6000 and PAM-5m), described in 7.3.2.3.

7.3.2.7 PAM/PEI gel grouted sand samples for compression test

100 mL of PAM/PEI mixture was prepared, using either 2.5 wt% PAM-5m and 1.3 wt% PEI, or 6.5 wt% PAM-150k and 0.8 wt% PEI. The solution was then mixed with 65 g of fine-grain sand, and was stirred by hand for 30 s. The PAM/PEI mixture containing the sand was then poured into a cylindrical plastic mould (the same as in 3.2.7), which had been attached to the base of a 280 mL glass jar using silicone sealant. The mixture was then compacted using the plunger of a 25 mL syringe. A tin cap was placed on the mould, and the jar outside the mould was filled up with tap water to just below the top of the mould in an effort to limit evaporation without submerging the gel, which risked diffusion of the gellants. The jar was then sealed with its lid, and it was placed in an oven at 85°C for 1 week.

7.3.3 Experimental methods

7.3.4 Viscosity measurements

A Cole-Parmer rotational viscometer was used to record the viscosity evolution of two CS/PEG grout samples during gelation, as well as a control CS grout sample, according to the method in 3.3.1. The CS/PEG grouts contained 1 wt% and 5 wt% of PEG, respectively. The viscometer was also used to measure the viscosity of PAM solutions of different PAM wt%, and upon increasing shear rate.

7.3.4.1 Measuring gelation with solid-state test

The method in 3.3.2 was used to measure the gelation and strength of various gels in this investigation via solid-state test and Sydansk and Argabright (1988)'s associated gel strength code. Gel time was defined as the time required for a sample to reach a strength of F on the gel strength code.

7.3.4.2 Measuring water retention with air-drying

Air-drying was used to measure the water retention of gelled CS/PEG grouts. Samples were uncovered and weighed before being left to dry in ambient conditions (~ 20°C and

~ 45% relative humidity). At the same time over the following days, weights were again recorded. Measurements continued until a clear trend, or lack thereof, was observed.

7.3.4.3 Studying cracking with oven drying

Oven drying was used to completely desiccate gelled CS/PEG grout samples to study how they crack. For this, wet samples were first weighed, before being set on a metal plate and placed in the oven at 100°C overnight. They were then allowed to cool in ambient conditions and weighed again.

7.3.4.4 Rheometer measurements

The methods outlined in section 3.3.3 were used to study the rheology of gel and liquid samples. Strain sweeps and steady shear sweeps were performed in this investigation, using the vane and cone-and-plate geometries, respectively.

7.3.4.5 PAM/PEI gel grouted sand UCS test method

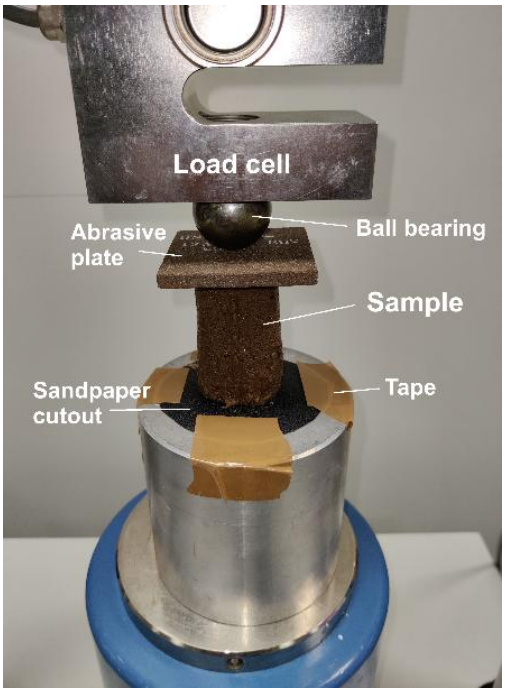

Figure 7.10. PAM/PEI gel grouted sand UCS test setup.

Gelled PAM/PEI grouted sand samples were removed from the oven and allowed to cool to ambient temperature. The water around the mould was removed, and the sample was extracted from the jar and mould and weighed. PAM/PEI gel grouted sand samples were much more flexible than standard CS-grouted sand samples, so they required a bespoke method for UCS test. In this, the sample was first placed on a sandpaper cutout which was

taped to the moving platform of the compression device: the purpose of this was to prevent slippage during test. It was ensured that the sample was aligned directly in the centre of the platform before an abrasive plate was set on top of the sample, which was then connected to the compression device's load cell via a large ball bearing. The device was then set to compress at a rate of 0.1 mm/min, and measurement was commenced.

The PAM/PEI grouted sand samples were very 'slippery', which made them difficult to keep stable whilst submerged in water; this issue was avoided by testing samples outside of water. To reduce the amount of evaporation that could occur during test, a compression rate which was 10x faster than that used for standard CS grout (see 3.3.5) was chosen to speed up the test, and samples were intermittently sprayed with water every ~ 10 min. A photograph of the setup is provided in Figure 7.10.

7.4 Results

7.4.1 Adding PEG to CS grout

7.4.1.1 Interaction of PEG and CS

PEG-6000 readily dissolved in CS at ~ 20°C up to very high wt% (50+ wt%) with no observed interaction, other than an increase in viscosity. It also had no effect on solution pH. However, upon mixing CS/PEG with NaCl solution to induce gelation of the CS, different varieties of gel were produced, depending on the wt% of PEG present. Images of these are provided in Figure 7.11A.

- CS/PEG mixtures with $\lesssim 1$ wt% of PEG produced a large degree of flocculation instantly upon mixing with NaCl solution. When stirred, this disappeared to leave a consistent, opaque white liquid, which gelled much quicker than standard CS grout (Figure 7.11A, centre). The resulting gels had a plasticity and mouldability that standard CS gels do not (see Figure 7.11B).
- Mixes with $\gtrsim 1$ wt% of PEG produced a small degree of flocculation which dissolved on stirring without causing colour change; they eventually gelled, but at slower rates than standard CS grout. The gels formed did not exhibit plasticity, and they were more predisposed to cracking than controls on oven drying (Figure 7.11A, right).

In another experiment, the pH of CS/PEG mixtures with 0.25 wt% of PEG-6000 was lowered from their initial value of 9.6 to observe the effect of pH on the interaction of CS

and PEG; no NaCl solution was added for this. It was noted that small quantities of flocculant appeared with each drop of HCl when passing through pH 9 and 8, which could be quickly stirred away. However, at pH ~ 7.5, a great increase in flocculation was observed, along with rapid gelation, producing an effect similar to that observed when adding NaCl solution.

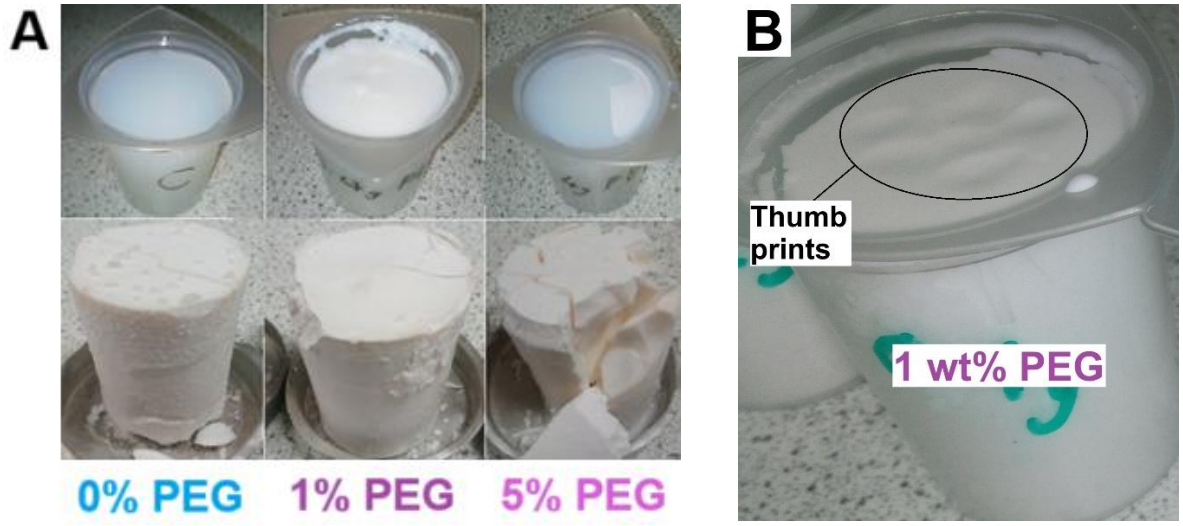

Figure 7.11. *A:* CS/PEG gels of different PEG wt% before (*above*) and after (*below*) drying for 1 h in an oven, at 100°C. *Left:* 0 wt% PEG; *centre:* 0.25 wt%; *right:* 2.5 wt%. *B:* Thumb prints left in 1 wt% PEG CS/PEG grout, demonstrating its plastic behaviour.

7.4.1.2 CS/PEG grout gelation

Figure 7.12A shows how PEG-6000 wt% affects the gel time of CS/PEG grout, as estimated by solid-state test. After a rapid decrease in gel time for low PEG wt% compared to standard CS grout (blue in the plot), there followed a gradual increase in gel time with PEG wt%, eventually exceeding that of standard CS grout at ~ 3.5 wt% PEG. For all grout mixtures, 1.7 M NaCl accelerator was used at 5:1 volume ratio. The lines in plot A are purely visual guides, and the coloured points correspond to mixtures chosen for further investigation with the viscometer, the data from which is presented in plot B. Viscometer measurements could not be done for all samples, as some gelled too quickly to be effectively measured by this method.

Figure 7.12B shows the evolution in viscosity, η, during gelation of the standard CS grout, as well as CS/PEG grouts containing 1 and 5 wt% of PEG-6000, as measured with the viscometer. As expected, the 1 wt% PEG mixture gelled faster than the control with no PEG, and the 5 wt% PEG mixture gelled slower. For both CS/PEG grouts, the initial

viscosity was higher than the standard CS grout, but, there was little difference in initial viscosity between the 1 and 5 wt% PEG samples.

Figure 7.12C shows the effect of reducing accelerator NaCl concentration on the gel time of CS/PEG grout with 0.25 wt% of PEG-6000, as measured by solid-state test. The aim of this was to see if the flocculation and rapid gelation observed at this PEG wt% could be controlled by reducing NaCl concentration. The gel times of the grouts did indeed rise as NaCl concentration was reduced, according to a negative exponential law, and furthermore, the visual and physical properties of the gels became more similar to control samples, as can be seen in the photos in Figure 7.12D.

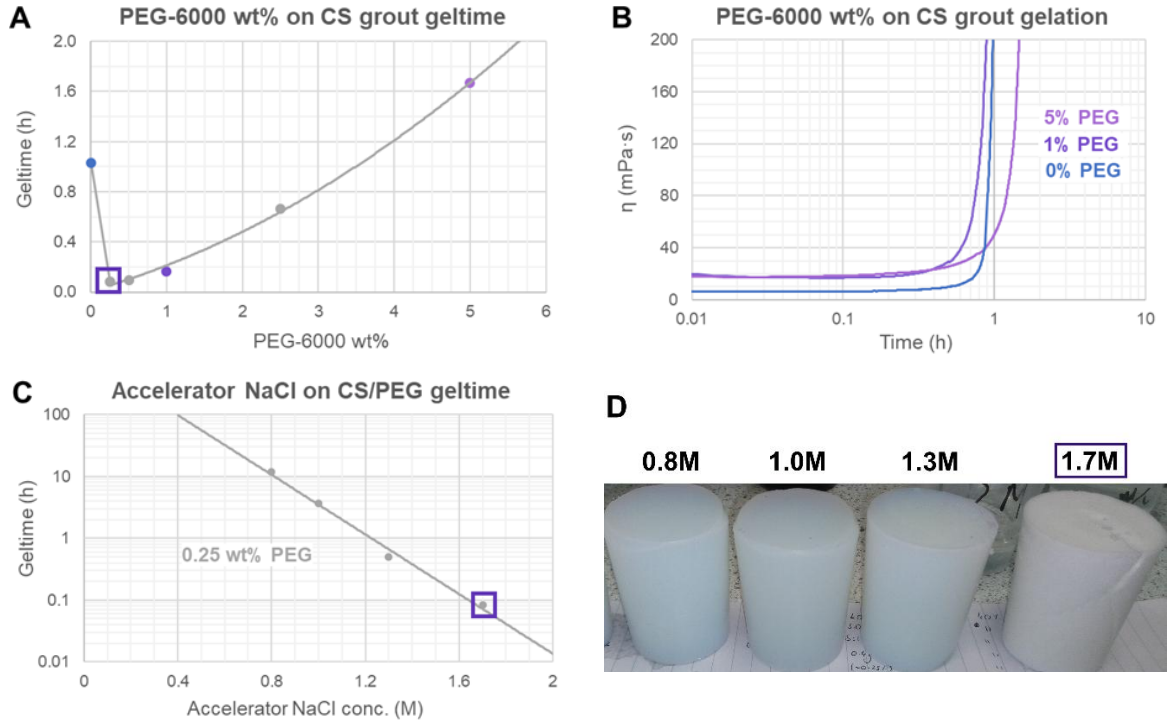

Figure 7.12. *A:* Effect of PEG-6000 wt% on CS/PEG grout gel time; coloured points correspond to the grout mixes in *B*. A point common to both *A* and *C* is highlighted with a purple square. *B:* The viscosity evolution during gelation of CS grout (blue) and CS/PEG grouts containing 1 and 5 wt% of PEG-6000. *C:* Effect of accelerator NaCl concentration on the gel time of CS/PEG grout with 0.25 wt% PEG-6000, with negative exponential fit applied. *D:* Photos of the grouts from *C*.

7.4.1.3 CS/PEG grout water retention

Figure 7.13B shows the effect of PEG-6000 wt% on water retention in CS/PEG gels after 8 d air-drying at ~ 20°C and ~ 45% relative humidity, with the percentage change in mass, Δm, of water during this time plotted. From the figure, gels with higher PEG wt% ($\gtrsim$ 2 wt%) can be seen to increasingly retain water better than standard CS grout, in spite

of these gels being observed to crack more than controls, which exposes greater surface area to air. Gels with low PEG wt% ($\lesssim$ 2 wt%), however, seem to instead exhibit poorer water retention than standard CS grout; these are the gels which are white, plastic, and fast gelling, as can be seen in the corresponding photos in A.

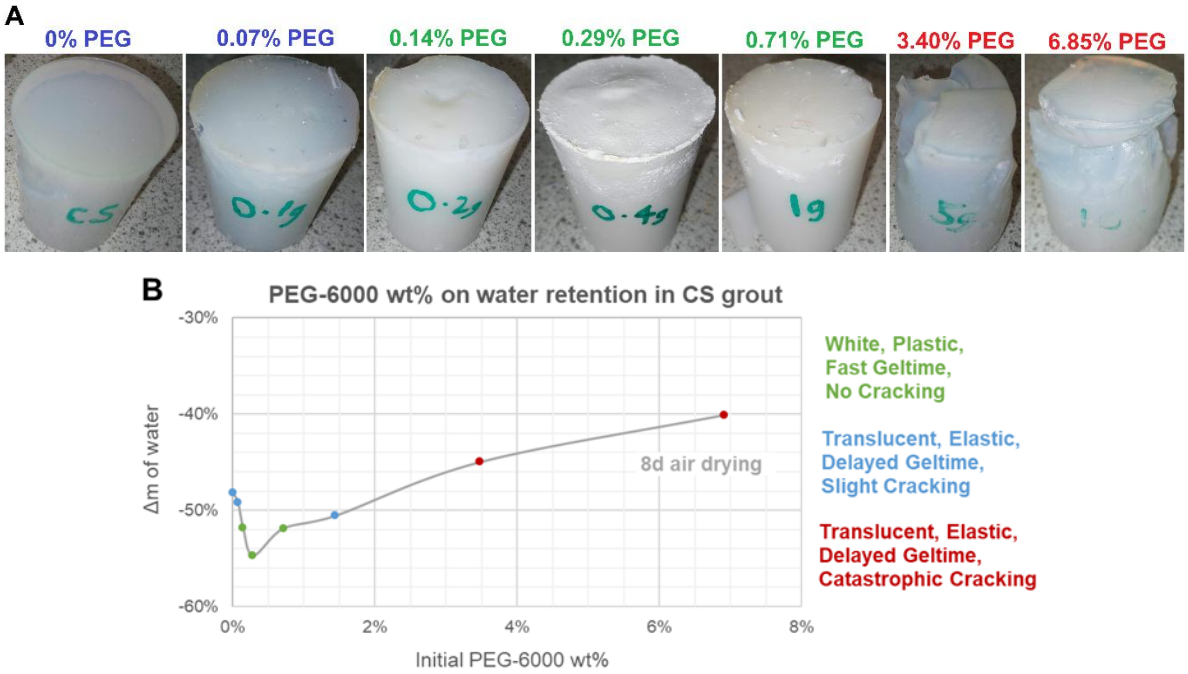

Figure 7.13. *A:* Photos of CS/PEG grout samples with different wt% of PEG-6000, which have been air-dried for 8 d and removed from their beakers. *B:* Effect of PEG-6000 wt% on water retention in gelled CS/PEG grout. The percentage change in mass of water in the gels after 8 d air-drying at 20°C is shown. The natures of each of the gels, which depend on the wt% of PEG, are described and colour coded.

7.4.1.4 Rheology of CS/PEG grout

Figure 7.14A shows the storage, G', and loss, G'', moduli of gelled CS/PEG grout with 0.25 wt% of PEG-6000, and standard CS grout, under increasing strain amplitude, γ_0, as induced using a rheometer with vane geometry, at angular frequency of 10 rad/s^{-}. Both gels were cured for 1 d and used 1.7 M NaCl accelerator. Figures 7.14B, C, and D show the shear stress, τ_0, against strain, the shear stress against phase angle, δ, and the strain against phase angle for the same tests.

From the plots, the gelled CS/PEG grout appears to have slightly higher G' than the control, implying greater stiffness, but it has a much lower yield point in terms of both the degree of stress and strain it can endure before breaking. For the CS/PEG grout, failure (the peak in the curve in Figure 7.14C) occurs much earlier than the flow point (δ = 45°), and at a smaller strain than for the control (~ 5%, compared to ~ 20%). After

24 h curing, gelled CS grout forms a stiff, percolated silica network that resists deformation (delayed δ increase). Adding 0.25 wt% PEG breaks up that tight network, reducing the peak stress and introducing an early viscoelastic transition. This is consistent with the reported plastic behaviour of such samples, in which thumbprints may be left when compressing by hand: here, the gel flows instead of rebounding, trapping the imprint like a wax. Further information on rheology and rheometers, and the definitions of terms used here, can be found in appendix A.5.1.

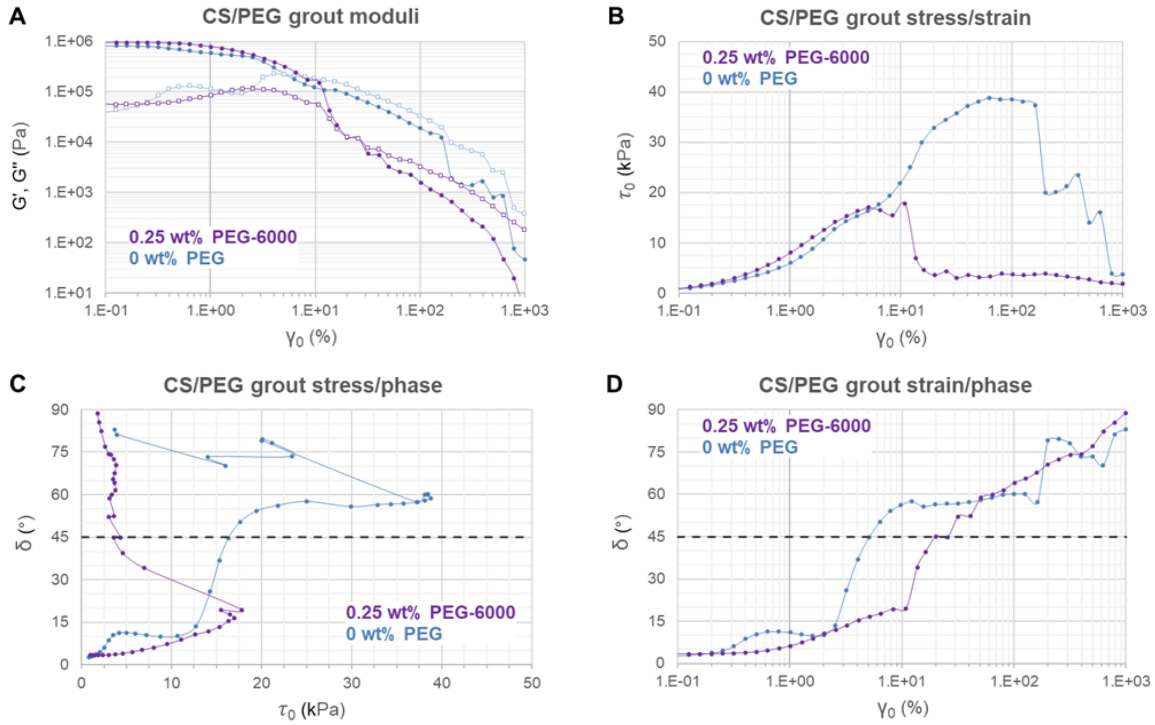

Figure 7.14. *A:* Storage and loss moduli of CS/PEG grout with 0.25 wt% of PEG-6000 and standard CS grout, under increasing strain amplitude at angular frequency 10 rad/s; both gels were aged 1 d and used 1.7 M NaCl accelerator solution. Other plots show stress/strain (*B*), stress/phase angle (*C*), and strain/phase (*D*) angle from the same tests.

7.4.2 PAM and PEI

This subsection outlines the results of experiments investigating PAM and its crosslinker PEI. The viscosity of PAM solutions was first studied; then, the nature of the reaction between PEI and CS was characterised for different PEI wt% and water chemistries, via solid-state test. Solid-state tests were again conducted on crosslinked PAM/PEI gels in water and CS, for both PAM-5m and PAM-150k. Rheometer measurements were also performed on a CS gel with PAM-5m added.

7.4.2.1 Viscosity of PAM solutions

In this study, different molecular weights of PAM were used: 5 000 kg/mol and 150 kg/mol. Figure 7.15 shows the results of viscometer measurements carried out on solutions of these two polymers in DI water. PAM-5m solutions had very high viscosities, even at low wt%; approaching 10 wt%, the mixtures effectively became a viscous gel upon mixing. For PAM-150k solutions, however, viscosities remained much lower.

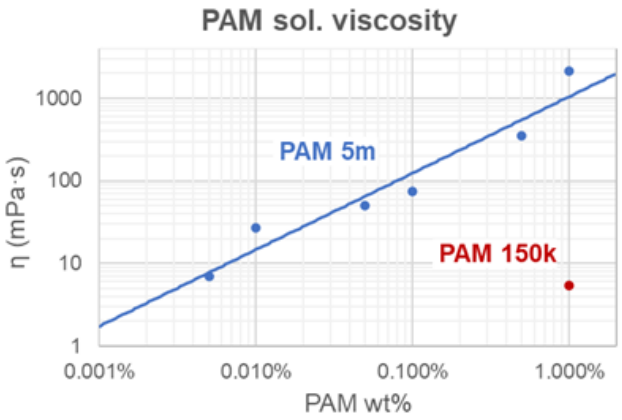

Figure 7.15. Viscosity of PAM-5m and PAM-150k solutions in DI water, at ~ 20°C, with power law fit shown.

Figure 7.16A demonstrates the shear thinning behaviour of PAM-150k solutions in both water and MP320 CS, at 7.2 wt% PAM, with the viscosity of the solutions decreasing with shear rate, according to a power law relationship. Figure 7.16B shows how increasing shear rate, $\dot{\gamma}$, produces an exponential increase in the shear stress induced in the solutions. These measurements were also taken with the viscometer.

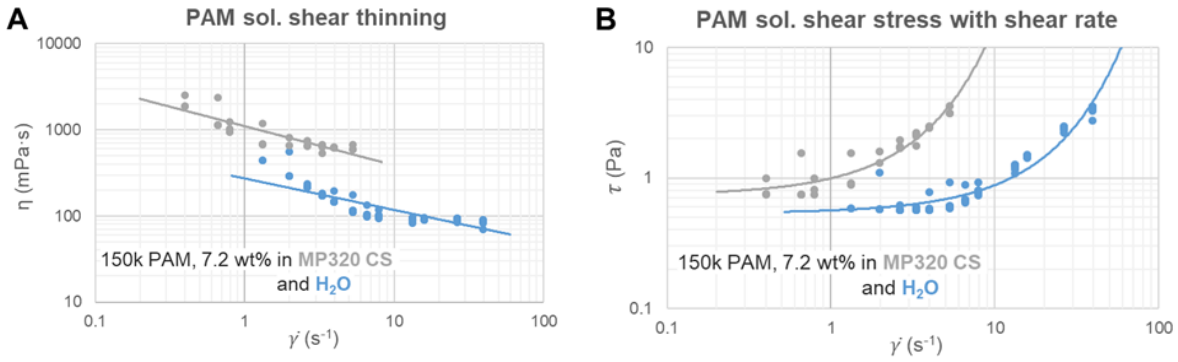

Figure 7.16. *A:* Effect of shear rate on the viscosity of PAM-150k solutions, demonstrating shear thinning behaviour. Solutions were in both water and MP320 CS, for 7.2 wt% PAM. Power law fits are applied. *B:* The shear stress generated by shear rate for the same solutions, with exponential fits applied.

A further demonstration of the shear thinning of PAM solutions, in comparison to CS, is provided in Figure 7.17A, in which the viscosity of 1.5 wt% PAM-5m solution decreases

with increasing shear rate, again according to a power law; in contrast, after a small initial decrease, the viscosity of MP320 CS remains constant. Plot B shows the increasing shear rate producing increasing shear stress in the two mixtures, although now the increases appear to be power laws rather than exponentials. These measurements were taken using the rheometer.

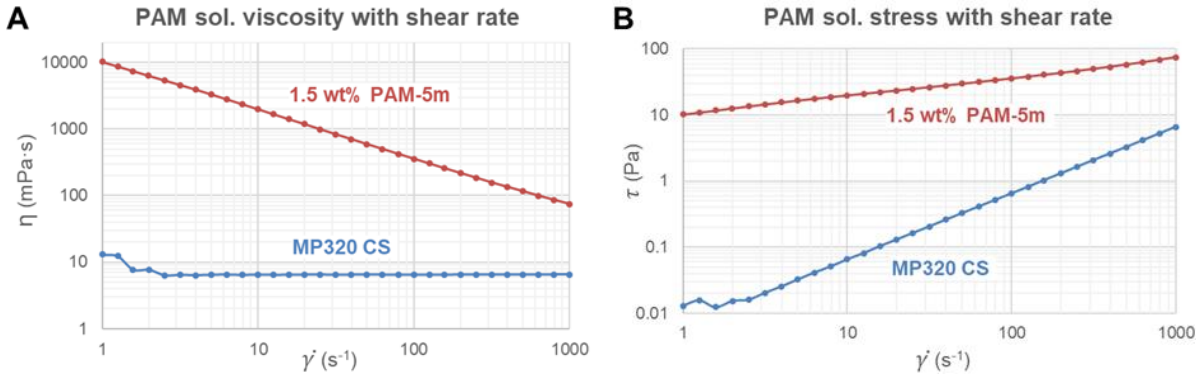

Figure 7.17. *A:* Viscosity of 1.5 wt% PAM-5m solution and MP320 CS with increasing shear rate. *B:* Shear stress of the same mixtures with increasing shear rate. This data is from rheometer measurements.

7.4.2.2 Interaction of PEI with CS

Whereas PAM could be readily added to CS without effect beyond increasing viscosity, PEI exhibited strong interaction with CS on mixing, which has the potential to interfere with both CS's gelation, as well as that of PEI's own with PAM. It was therefore important to understand the nature of the reaction if PEI were to be used in making double-network gels. PEI readily dissolved in room temperature water at pH 7, and had minimal effect on viscosity; it acted as a weak base, raising pH after dissolution by an amount dependent on its wt%.

The effect of pH on the interaction of PEI with CS was studied using solid-state tests. CS/PEI mixture was prepared by the method in 7.3.2.3, containing 1 wt% PEI, an amount reflective of those commonly used for crosslinking with PAM in the literature (Ma et al., 2017). When CS was added to PEI solution at 5:1 volume ratio, the mixture immediately turned white due to flocculation. Unlike what was seen in section 7.4.1.1 with PEG, however, the mixture was not consistent in texture, but clearly had floating particulate. Over a period of days, this began to separate out, with loose sediment forming at the bottom of the container.

When lowering pH, the white liquid turned into a thick paste, indicating an intensification of the reaction as pH decreased. The mechanically strongest paste was observed at pH 5. Images of samples adjusted to different pHs can be seen in Figure 7.18, after leaving for 7 d. Table 7.1 shows the details of the experiment.

Table 7.1. 1 wt% PEI in CS grout at different pHs, left for 7 d.

CS pH	*pH after adding PEI*	*Gel?*	*Comments*
9.6	10.0	X	White low-viscosity liquid with floc. Sediment formed after 1 d.
7	9.9	X	Viscous flowing white paste.
5	9.2	?	Firm solid white paste.
1	8.8	?	Soft solid white paste.

Figure 7.18. 1 wt% PEI in CS at pH 1, 5, 7 and 9.6, from left to right, left for 7 days. No NaCl accelerator solution was used.

7.4.2.3 PAM/PEI hydrogels (PAM-5m)

Experiments were conducted to produce PAM/PEI gels using PAM-5m, whose gelation was characterised using solid-state tests over a period of several days. Some gels were also made with low silica wt% CS present. Gels were prepared by first progressively increasing the polymer content to identify the point of maximum strength (samples 1-4 in Table 7.2), followed by a stepwise increase in CS silica wt%, with the aim of forming a potential double network (samples 5- 8).

The base gel composition was that of sample 1 in Table 7.2: 1.5 wt% PAM, 0.8 wt% PEI. These concentrations were recommended as ideal values in similar experiments by (Ma et al., 2017). Table 7.2 details the exact concentrations used for each sample, and comments on the gels produced from these. 'Day 0' represents a gel strength taken 6 h after mixing, still at ambient temperature. Subsequent measurements were after having been cured in an oven at 60°C. The pH of each sample was measured, but not adjusted, to avoid the effect seen in 7.5.2.2, where PEI formed a paste with CS when pH was adjusted down to 7.

Sample 2 in Table 7.2 had the same PEI wt% as 1, but more PAM (2.5%, 0.8%). This sample gelled faster and ended up stronger than 1. Sample 3 had the same increased PAM concentration as 2, but also added PEI, to keep the same concentration ratio as 1 (2.5%, 1.3%). This gelled faster than 1 and 2, and was also stronger. Sample 4 had the same PEI concentration as 3, but the original PAM concentration (1.5%, 1.3%). This sample successfully gelled, but after about a month, syneresis was observed, with liquid being ejected from the gel. This suggests that a high crosslinker to polymer ratio causes syneresis.

Table 7.2. Results of solid-state tests of gels formed by PAM-5m and PEI, with and without CS. Samples were heated in an oven at 60°C. The letters (e.g. G, H, I, J) refer to the gel strength code of Sydansk and Argabright (1988) (see Table 3.2).

Sample	*pH*	*PAM wt%*	*PEI wt%*	*Silica wt%*	*Gel?*	*Days*				*Comments*
						0	*3*	*4*	*5*	
1	10.2	1.5	0.8	-	✓	G	I	J	J	Colourless gel.
2	10.3	2.5	0.8	-	✓	I	J	J	J	
3	10.4	2.5	1.3	-	✓	H	J	J	J	Colourless gel. Strongest.
4	10.4	1.5	1.3	-	✓	G	J	J	J	Colourless gel. Eventual syneresis
5	10.2	1.5	0.8	0.5	✓	G	I	I	J	Gel. Increasing white colouring
6	10.2	1.5	0.8	1.0	✓	G	J	J	J	with concentration.
7	10.8	1.5	0.8	10.0	✓	-	-	-	-	Thick white paste in appearance. Later found to be gel after removal from tube.
8	-	1.5	0.8	16.8	X	-	-	-	-	Formed a viscous white liquid.
9	10.0	-	-	16.8	X	-	-	-	-	No change
10	5.9	3.0	-	-	X	-	-	-	-	No change

Samples 5 and 6 had the same concentration ratio as 1, but also featured 0.5 wt% and 1 wt% of CS, respectively. This gave them a slightly white appearance (see Figure 7.19A), but it was not clear if their mechanical properties were improved by the presence of the silica. Sample 7, with 10 wt% silica, seemed to have formed a thick white paste, and so was assumed not to be gelling; however, on later removal from its tube it was in fact found to have gelled. Sample 8, with 16.8 wt% silica, failed to gel, however, producing only a viscous white liquid. There, therefore, seems to be a limit as to the silica wt% which can be included in PAM/PEI gels without compromising gelation.

Samples 9 and 10 were controls containing only CS and PAM solution, respectively. These were each found not to have gelled after being left in the oven (see Figure 7.19A), showing that additional additives are necessary in each case.

The PAM/PEI gels created here were stronger, with much greater flexibility, than conventional gelled CS grout, as shown in Figure 7.19B. Standard gelled CS grout manipulated as shown in the figure would crumble and not flex. Furthermore, as seen in Table 7.2, some PAM/PEI gels were able to form on 'day 0', before being placed into the oven, suggesting that heating may not always be necessary for practical application of PAM/PEI gels.

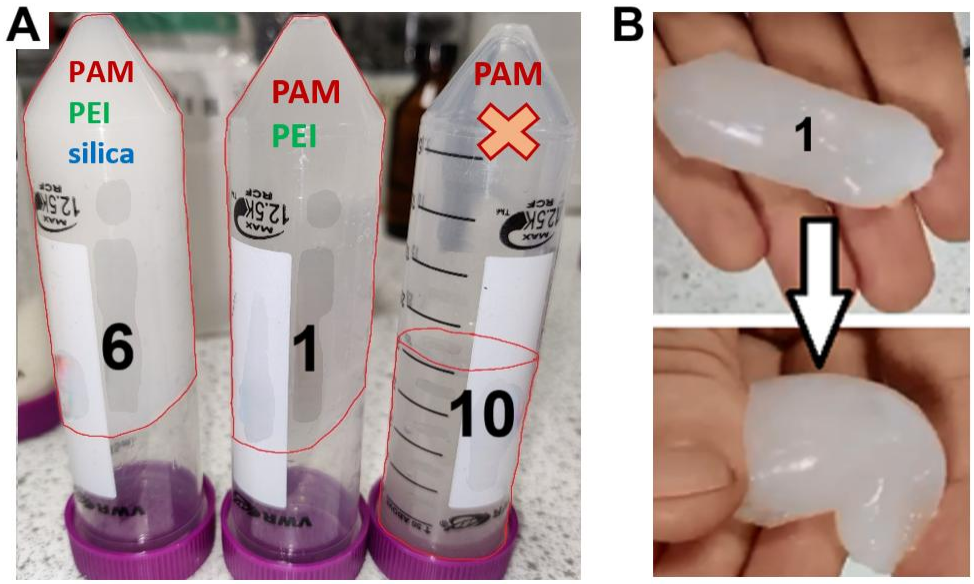

Figure 7.19. *A*: Falcon tubes containing CS/PAM/PEI gel (sample 6: 1.5 wt% PAM, 0.8 wt% PEI, 1 wt% silica), PAM/PEI gel (sample 1: 1.5 wt% PAM, 0.8 wt% PEI), and a PAM solution (sample 10: 3 wt% PAM), which has not gelled. Red lines identify the outline of the materials. *B*: Sample 1 gel demonstrating high flexibility compared to standard gelled CS grout. PAM-5m was used here.

7.4.2.4 PAM/PEI hydrogels (PAM-150k)

Similar experiments to those in 7.4.2.3 were conducted with PAM-150k, which gave viscosities more suitable for injection in soil. PAM-150k did not gel as readily as PAM-5m, requiring either increased concentration and/or increased temperature to gel at a similar rate. The standard PAM/PEI mixture here, therefore, used a higher PAM concentration (6.5 wt%) than was used with PAM-5m in 7.4.2.3, and they were cured at 100°C, rather than 60°C. The PAM-150k gels tended to be mechanically more rigid and brittle than the PAM-5m gels. The gels were prepared according to the method in section 7.3.2.4.

Table 7.3 details the composition of the samples tested, and Table 7.4 shows the results of solid-state tests after various curing durations. Sample 1 used 6.5 wt% and 0.4 wt% PEI, and successfully formed a rigid gel after 1 d in the oven. This low PEI wt% was chosen to reduce risk of syneresis. Sample 2 used the same concentrations of PAM and PEI, but

was prepared in 40 wt% silica CS. This sample solidified to form a wax-like substance after 1 d curing. Sample 3 was the same as 2, but without PEI crosslinker; this formed a similar waxy substance after 1 d, however, implying that the substance in sample 2 is produced primarily via an unexpected interaction between the PAM and silica, without the PAM and PEI necessarily gelling. Sample 4 was a control sample of just 40 wt% silica CS, and it did not noticeably change after being in the oven. Samples 1-4 can be seen in Figure 7.20.

Table 7.3. Results of experiments to create gels from PAM-150k, PEI, and CS.

Sample	*PAM wt%*	*PEI wt%*	*Silica wt%*	*pH*	*Temp (°C)*	*Gel?*	*Result*
1	6.5	0.4	-	9.9	100	✓	Transparent gel after 1 d
2	6.5	0.4	40	10.2	100	✓	White waxy substance
3	6.5	-	40	9.5	100	✓	White waxy substance
4	-	-	40	9.6	100	X	No change
5	6.5	0.8	-	7	100	✓	Transparent gel after 1 d
6	6.5	3.5	-	7	20	✓	Transparent gel after 2 months

Table 7.4. Results of solid-state tests on the gels in table 7.3, measured with the gel strength code.

Sample	*Solid-state test after x days*			
	0	*1*	*2*	*7*
1	A	I	I	I
2	A	I	I	I
3	A	I	I	I
4	A	A	A	A
5	A	H	J	J
6	A	A	A	A

Samples 5 and 6 were adjusted down to pH 7 to see if PAM/PEI would still gel at neutral pH. Sample 5 used a higher PEI concentration (0.8 wt%) to encourage gelation, and was cured in the oven at 100°C, successfully forming a rigid gel within 1 d. Sample 6 was given an even higher wt% of PEI crosslinker (3.5 wt%) to see if this would allow it to gel at ambient temperature, but after a week it showed no change in viscosity. At that point, it was placed in the oven at 100°C for 20 min before being left out again at ~ 20°C. The aim of this was to investigate whether pre-heated PAM/PEI mixture could still gel whilst cooling down, for example, after application in soil, without having to be continuously heated. However, sample 6 took approximately a further two months to gel, so higher concentrations of either PAM and/or PEI are likely needed to gel at ambient temperature

within a practical duration, at least for neutral pH. None of the samples in this experiment exhibited any syneresis.

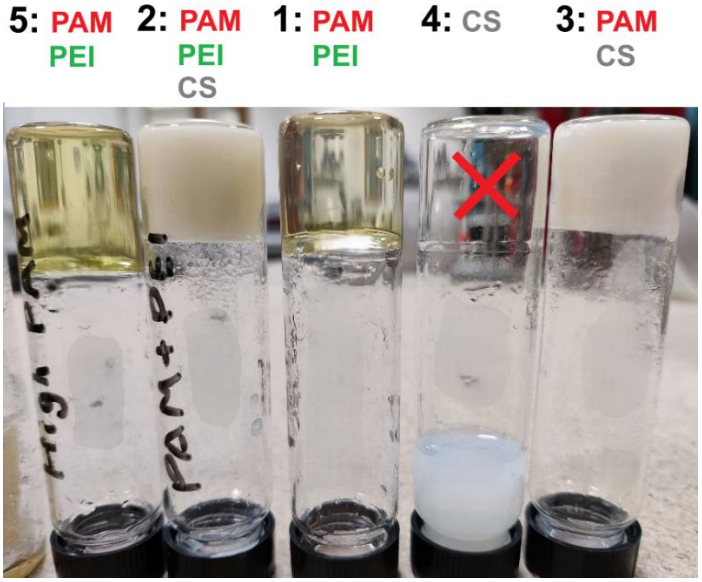

Figure 7.20. Glass tubes featuring different combinations of PAM-150k, PEI and CS after heating in an oven at 100°C for 1 d. Sample names and contents are shown on the tubes. The red X highlights that sample 4 did not gel.

7.4.2.5 PAM/PEI gel grouted sand UCS tests

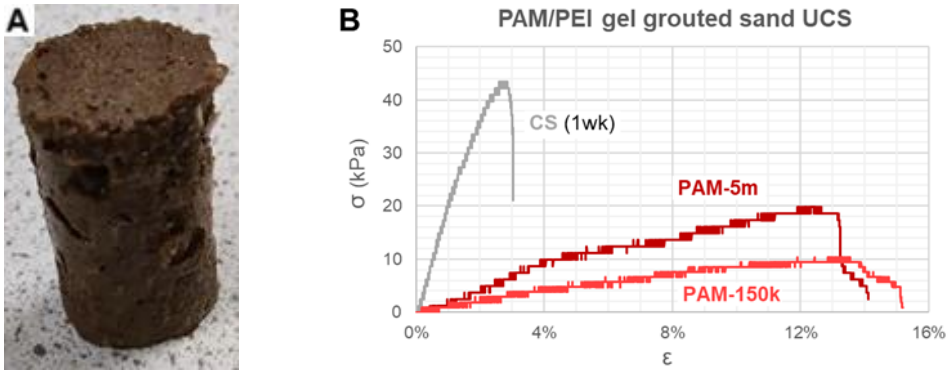

Figure 7.21. *A:* PAM-150k/PEI gel grouted sand sample. *B:* Stress/strain plots from UCS tests on PAM/PEI gel grouted sand samples using mixtures of 2.5 wt% PAM-5m and 1.3 wt% PEI, and 6.5 wt% PAM-150k, and 0.8 wt% PEI, respectively. A 1 wk cured standard CS-grouted sand sample is shown for comparison.

Figure 7.21B shows the stress/strain curve for PAM/PEI grouted sand samples undergoing UCS test. The samples used PAM-5m (2.5 wt% PAM, 1.3 wt% PEI) and PAM-150k (6.5 wt% PAM, 0.8 wt% PEI). From the plot, the PAM-5m sample had higher yield stress than the PAM-150k sample, but slightly lower yield strain. The stress/strain curve for a 1 week cured standard CS-grouted sand sample (from 4.3.3.1) is also shown for

comparison, demonstrating how the PAM gels have much greater flexibility than CS grout, but lower compressive strength.

7.4.3 PVA

This subsection outlines the results of experiments on PVA. Firstly the nature of the interaction of PVA with CS was studied using solid state tests; then, PVA polymer gels were produced via air-drying and freeze-thaw methods, and preliminary rheometer measurements were taken on PVA and CS/PVA gels.

7.4.3.1 Interaction of PVA with CS

Figure 7.22. On the left is standard gelled CS grout; on the right is gelled CS/PVA grout, containing 1 wt% PVA. These were each prepared with 1.7 M NaCl accelerator, at 5:1 volume ratio. In the case of the CS/PVA grout, the PVA was dissolved in the accelerator. The upper layer of water which formed from phase separation has been removed from the gelled CS/PVA grout here.

The interaction of PVA with CS and NaCl was investigated to optimise the mixing procedure. The goal was to prepare CS/PVA grout with a 5:1 volume ratio of CS to 1.7 M NaCl, and a final PVA concentration of 1 wt%. First, a sample without NaCl was prepared: PVA was dissolved in DI water, which was then mixed with CS at 5:1 ratio. In this case, no visible interaction occurred, and the mixture remained translucent and homogeneous. The mixture had pH of 9.3, compared to 9.6 for a control sample of CS and DI water, suggesting that the PVA was very slightly acidic. For another sample, PVA was dissolved in 1.7 M NaCl solution and mixed with CS at 5:1 ratio. On mixing, the suspension immediately turned white, indicating that the NaCl induces interaction between the PVA and CS. The mixture could be stirred back to a uniform, low-viscosity white liquid. After ~ 1 h, phase separation occurred, with a soft, plastically deformable gel forming at the bottom of the beaker, and a colourless liquid layer appearing above. Figure 7.22 shows a

side-by-side comparison of the gelled CS/PVA grout with 1 wt% PVA compared to standard gelled CS grout. The liquid layer has been removed in the image.

Another experiment explored how pH affects the interaction of CS and PVA. Here, CS suspensions containing 1 wt% of PVA were first prepared by adding CS to PVA solution in DI water, at 5:1 ratio. The pHs of these mixtures were then adjusted down different amounts between 1 and the original 9.3. As pH was lowered past 5, samples became increasingly white in colour, hinting at an increasing interaction between CS and PVA. Figure 7.23 shows pictures of the different samples. In a similar pattern to that seen with CS alone (see appendix A.6.1), the pH 5 sample formed a gel the fastest, within 1 d, followed by pH 3 after 2 d, and pH 7 after 1 week. The pH 1 sample, however, quickly exhibited phase separation, with a firm, compact gel forming at the bottom after 1 d, beneath a layer of colourless liquid. The pH 3 sample also exhibited a small degree of separation, with a thin layer of liquid at the surface.

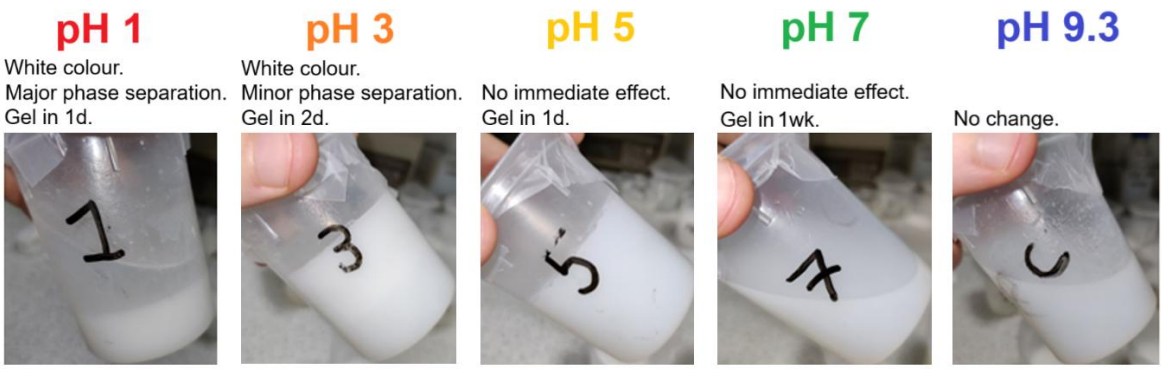

Figure 7.23. CS/PVA with 1 wt% PVA, at different pHs. No NaCl is present.

7.4.3.2 PVA hydrogels: air-dry method

A solution of PVA dispersed in DI water was prepared at 10 wt% and allowed to desiccate on a petri-dish, with the total mass recorded at regular intervals. As water evaporated, and the solution became more concentrated, it gradually transitioned from a liquid to a gel. The gel strength increased progressively with rising PVA concentration. On tilting the dish, similar to the solid-state test method, the solution ceased to flow with gravity at ~ 30 wt% PVA, presumably having formed a gel.

The PVA gel produced by this method was found to be very strong and flexible (as seen in Figure 7.24). As desiccation continued, and the PVA approached ~ 95 wt%, the gel became noticeably more brittle, and it was possible to break it by hand into two pieces.

On re-wetting one of these dried gel pieces by immersing it in 100 mL DI water, it swelled, increasing in volume, softening, and becoming highly flexible, but not reverting back to a liquid solution. Notably, under the geometrical and boundary conditions tested, the swelling process did not result in any visible cracking.

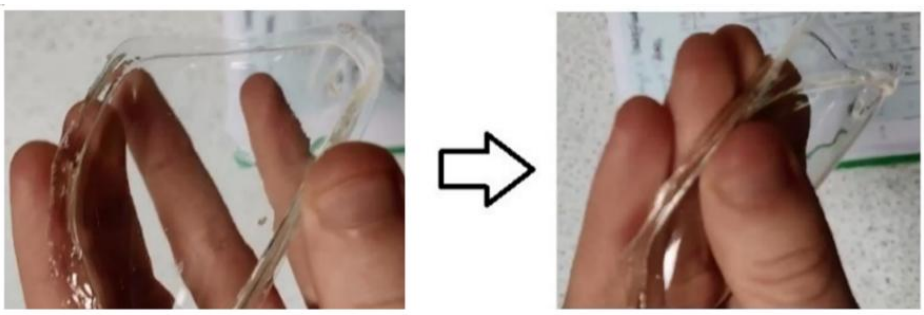

Figure 7.24. PVA gel formed in a petri dish by desiccation of PVA solution. The sample is ~ 90 wt% PVA.

7.4.3.3 PVA hydrogels: freeze-thaw method

Table 7.5. Gel strength code values for samples containing different PVA concentrations exposed to different numbers of freeze-thaw cycles.

Number	*Sample*	*Gel strength after x freeze-thaw cycles*			
		1	*2*	*3*	*4*
0	DI water	A	A	A	A
1	5% PVA	A	B	C	H
2	10% PVA	B	H	H	I
3	15% PVA	I	I	-	-
4	20% PVA	I	I	-	-
5	10% PVA at 90°C	H	I	-	-

Another experiment focussed on forming PVA gels using the freeze-thaw method (see 7.3.2.5). Here, PVA solutions of different concentrations in DI water were frozen at -20°C for 1 d, before leaving to thaw at ~ 20°C, again for 1 d. Table 7.5 shows how the strength of the gels continues to increase with repeated freeze-thaw cycles, but that good mechanical strength can be achieved after even just one cycle. Sample 5 was first heated to 90°C before being placed in the freezer while still hot: this sample formed a strong gel with fewer freeze-thaw cycles than the standard sample of equivalent concentration. It should be noted that this sample was sealed while heating and had negligible water loss. After two cycles, sample 5 was once again heated to 90°C, but this caused the gel to return to a solution. Figure 7.25 shows gels 1-3, which were formed from different PVA concentrations after two freeze-thaw cycles. Unlike the air-dried gel in Figure 7.24, which

was colourless, the freeze-thaw PVA gels were translucent, and increasingly white in colour at higher PVA concentrations.

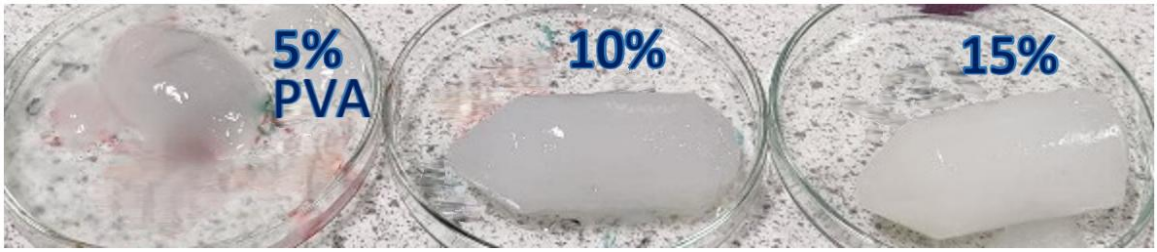

Figure 7.25. Freeze-thaw PVA gels formed from solutions of varying PVA wt%, after 2 freeze thaw cycles.

7.4.4 Freeze-thaw PVA gel rheology

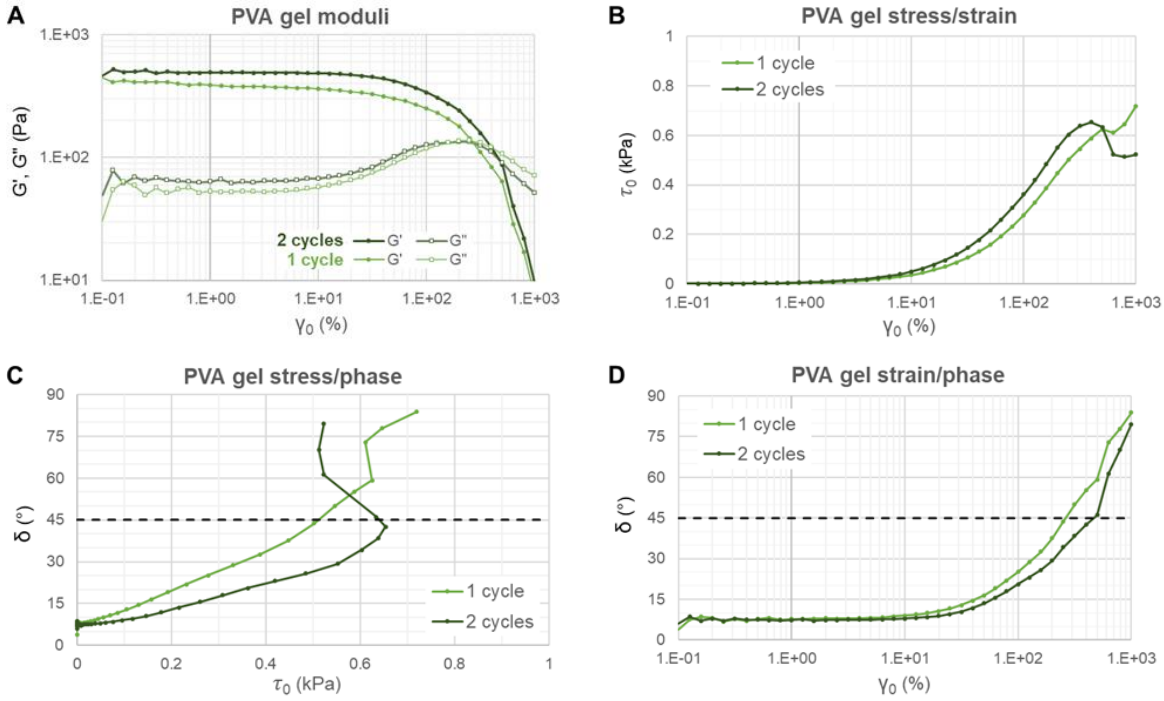

Figure 7.26. *A:* Storage and loss moduli of PVA gel (15 wt% PVA in water) under increasing strain amplitude at angular frequency 10 rad/s, for gels prepared from one and two freeze-thaw cycles. Other plots show stress/strain (*B*), stress/phase angle (*C*), and strain/phase (*D*) angle from the same tests.

Figure 7.26 shows the results of rheometer tests on a PVA gel sample formed via the freeze-thaw method, tested after one cycle, and then again after a second. The sample had 15 wt% of PVA. The freeze-thaw method was chosen over air-drying, for this, as samples could be easily prepared directly in rheometer cups, whereas creating suitable air-dried samples would have been more difficult. From the plots, the 2-cycle gel had higher storage modulus than the 1-cycle gel, indicating greater stiffness, and it also reached its flow point at higher stress and strain. This was in spite of it previously having been

broken during the first test. This demonstrates that both successive freeze-thaw cycles improve the mechanical properties of PVA gel, and also that it possesses the ability to recover after damage through additional freeze-thaw cycles.

The freeze-thaw method also allowed successful preparation of a CS/PVA gel, as described in 7.3.2.5. Figure 7.27 shows the results of rheometer tests on the CS/PVA gel after 1 freeze-thaw cycle, alongside that of the 15 wt% PVA gel from Figure 7.26, as well as a 1 d cured standard CS grout sample. The CS/PVA mixture was created by adding 15 wt% PVA solution to CS at a volume ratio of 3:1, such that the resulting composition was 11 wt% PVA and 11 wt% silica, whereas the standard CS grout has ~ 34 wt% silica after mixing with its accelerator. From the plots, the CS/PVA gel exhibits roughly an order of magnitude higher storage and loss moduli than the PVA, implying much greater stiffness, and its yield stress is far higher than the PVA, meaning it is stronger, in spite of having lower PVA concentration. It also requires higher stress and strain to reach its flow point, maintaining its solid behaviour for longer. It certainly appears, therefore, that addition of CS to PVA gel improves its mechanical properties.

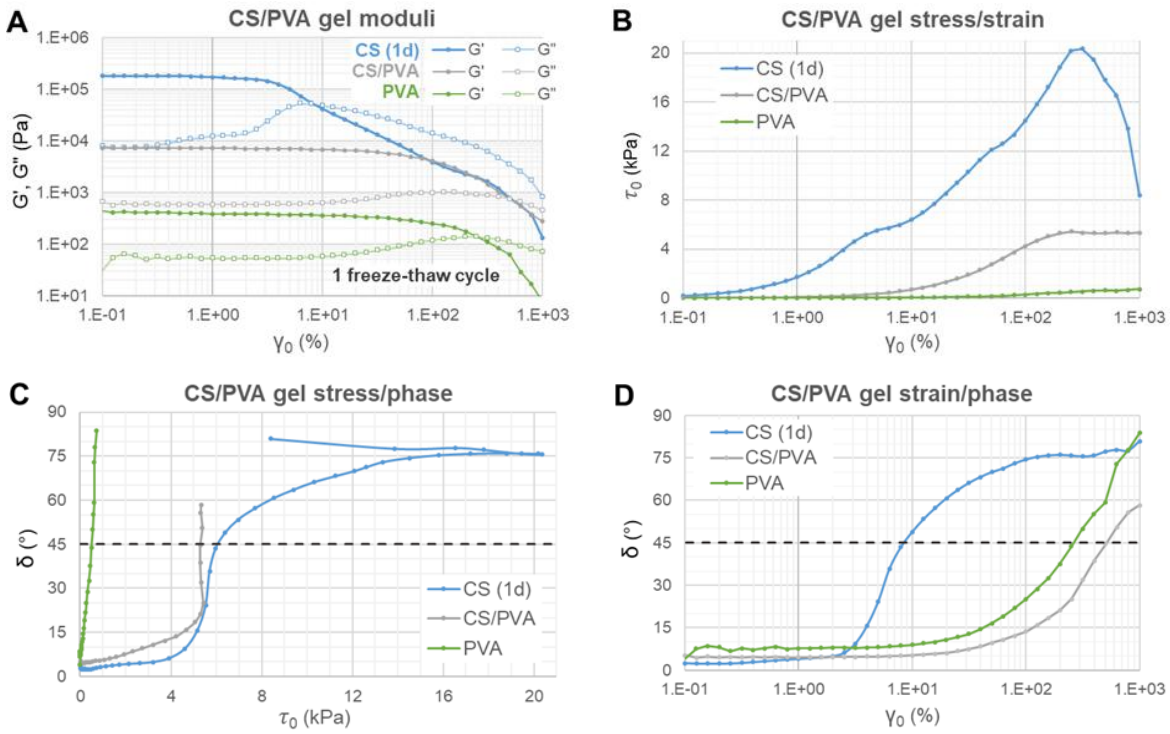

Figure 7.27. *A:* Storage and loss moduli of PVA gel (15 wt% PVA in water), CS/PVA gel (11 wt% PVA and 11wt% silica), and 1 d cured standard CS grout, under increasing strain amplitude at angular frequency 10 rad/s. The PVA and CS/PVA gels were each prepared from one freeze-thaw cycle. Other plots show stress/strain (*B*), stress/phase angle (*C*), and strain/phase (*D*) angle from the same tests.

The profiles of the PVA and CS/PVA gel data in Figure 7.27 closely resemble each other, implying similar behaviour, whereas the standard CS grout has very different shape in each plot. According to the data, the standard CS grout is stiffer, with higher yield stress than the PVA and CS/PVA gels, but it is much less flexible, reaching its flow point at a far lower strain. With this in mind, it seems likely that an encompassing silica network was not formed in the CS/PVA sample, but rather that the CS particles reinforced the PVA network in some way. In order to achieve the hoped-for increased strength and toughness from combining PVA with CS grout, therefore, additional steps should be taken, or additives included, to ensure that a CS network forms, perhaps prior to commencing the freeze-thaw cycles. This was not done at this stage due to efforts to avoid the phase separation of CS/PVA seen in 7.4.3.1 caused by addition of NaCl. However, lowering pH was shown to be a viable alternative to this.

7.5 Discussion

7.5.1 PEG

7.5.1.1 Gelation of CS/PEG grout

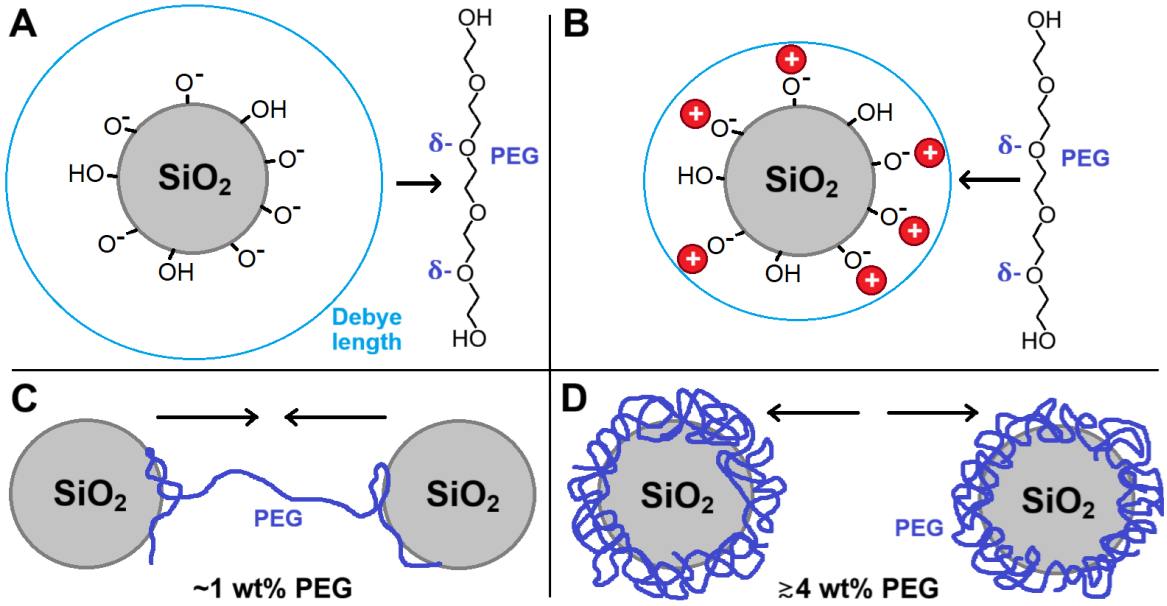

Figure 7.28. *A:* Mutual repulsion between negatively charged CS particles and PEG's slightly negative ether groups prevents adsorption of PEG. *B:* The presence of cations in CS particles' double layers from the addition of salt screens the negative charge, shrinking the Debye length such that PEG molecules can approach close enough to adsorb onto the CS particles through a combination of electrostatic attraction, hydrogen bonding, and hydrophobic association. *C:* Two CS particles pulled together by a PEG polymer molecule acting as a bridge between them. *D:* Two CS particles coated with PEG repelling each other via steric repulsion.

Rubio and Kitchener (1976) suggest that interaction between PEG and CS is the result of adsorption of the polymer on the surface of CS particles. At high pH, there is initially no reaction between PEG and CS as there is sufficient repulsion between negatively charged CS particles and the slightly negative ether groups of the PEG. Upon addition of NaCl, however, the screening of CS particles' charge by adsorbed Na^+ ions (see 2.2.2.4) shrinks the Debye length enough to allow PEG to adsorb onto CS particles via a combination of electrostatic attraction and hydrogen bonding through PEG's ether oxygen groups, as well as hydrophobic association through its CH_2-CH_2 groups; this then leads to the observed macro-scale interactions. Diagrams of this effect are provided in Figure 7.28A and B. A similar result is obtained on lowering the pH of CS. As pH decreases, ionised SiO^- groups at particle surfaces increasingly protonate to become SiOH (see 2.2.2.3), thereby decreasing the negative charge of particles, while the increased density of SiOH groups provides more hydrogen bonding sites for the PEG. Both of these effects promote greater adsorption of the polymer.

As seen in Figure 7.12, CS/PEG grout with low PEG wt% (~ 1 wt%) gels faster than standard CS grout. This is thought to be the result of a 'bridging' effect, in which polymer chains link multiple particles and pull them together, thereby greatly accelerating gelation (Figure 7.28C). At higher PEG wt% however, gelation is increasingly slowed relative to standard CS grout. This is probably the result of steric repulsion created by the elevated presence of PEG chains on CS particle surfaces, whereby loops of the adsorbed polymer resist compression when coming into contact with those on the surface of other particles (Figure 7.28D). The reduced strength and increased degree of cracking seen in high-PEG gels (see Figure 7.11), presumably arises from fewer siloxane bonds being able to form between CS particles due to the presence of adsorbed PEG blocking contact points.

As shown in 7.4.1.2, the gel time of CS/PEG grout can be controlled by reducing the NaCl concentration of the accelerator, but the desired plasticity property appears to phase out as NaCl concentration is reduced.

7.5.1.2 Water retention of gelled CS/PEG grout

As seen in 7.4.1.3, gelled CS/PEG grout with high PEG wt% has improved water retention over standard CS grout. This is likely due to the added number of hydrophilic groups in

the form of PEG's ether oxygens: these bind water molecules and make it more difficult for them to evaporate. Gelled CS/PEG grout with low PEG wt% does not exhibit improved water retention with respect to standard CS grout, however. A possible explanation for this was proposed by Martin et al. (2001), who suggest that it arises from PEG impacting the structure of CS gel by generating large clusters of silica particles and polymer during gelation as a result of its bridging action, and the rapid aggregation it induces. This in turn produces larger pore sizes in the resulting gel network. The increase in air entry value associated with the higher porosity would allow for faster evaporation, balancing the improved water retention from PEG's ether groups. Changes in pore size are also known to affect the colours of gels; when pore diameter approaches the wavelength range of visible light (~ 400 nm), gels often turn opaque as a result of increased scattering of light within gel pore-spaces. This may explain the white colour of these gels. Alternatively, the increased scattering could be caused by the large particle-polymer clusters which themselves approach the wavelength of light, or by a change in the shape of the polymer. Micro-structural evaluation is needed to explore these hypotheses.

7.5.1.3 Potential application of CS/PEG grout

As demonstrated by the differing behaviour observed at low and high PEG concentrations, there is potential to fine-tune PEG content, or adjust its molecular weight, to balance injectability with cured-state rigidity for specific field applications. PEG acts as a "lubricant", reducing network connectivity and stiffness by introducing microdomains that yield under low stress. This results in a gel that retains its shape (residual elasticity), but deforms plastically around imprints. Water retention experiments and rheological analyses further support this observation: at low PEG concentrations, injectable gels can be formed with reduced mechanical strength and an early viscoelastic transition. On desaturation, these gels transform into xerogels without exhibiting cracking. This behaviour highlights a promising avenue for the development of injectable hydraulic barriers, where the naturally low hydraulic conductivity of CS grout can be paired with near-zero diffusion coefficients. Once water is fully removed, the resulting xerogel remains intact, potentially offering a robust and impermeable sealing material through which contaminants cannot migrate, either by advection or diffusion.

7.5.2 PAM and PEI

7.5.2.1 Viscosity of PAM solutions

As seen in 7.4.2.1, the large size of PAM-5m molecules compared to PAM-150k causes more intermolecular interaction during flow, thereby increasing viscosity (see appendix A.5.1). PAM-5m is representative of the molecular weights commonly used in the oil industry, where high viscosity is a desirable trait for applications such as conformance control. However, these viscosities are likely unworkable for permeation grouting. PAM-150k does exhibit more suitable viscosity, though.

PAM solutions do, however, exhibit shear thinning, as seen in Figures 7.16 and 7.17. The reason for this is that, when at rest, polymer chains are randomly coiled and entangled, facilitating interactions which resist flow at low shear; at higher shear, however, the chains begin to align with the flow direction, reducing the number of entanglements and decreasing intermolecular interaction, leading to lower viscosity (Akbari et al., 2017; Chandler, 2019; Navaie et al., 2022; Sun et al., 2025; Tie et al., 2019). This effect could potentially allow the use of relatively high viscosities of PAM in grouting applications. For example, Figure 7.17 shows how a 1.5 wt% PAM-5m was reduced from ~ 10 000 mPa·s to < 100 mPa·s (within the limit set for injection in 7.2.4) by increasing shear rate from 1 s^{-1} to 1 000 s^{-1}. The increased pumping velocity needed to produce this shear rate would require higher injection pressures, however.

7.5.2.2 Interaction of PEI with CS

As presented in 7.5.2.2, PEI exhibits a strong interaction with CS, dependent on the wt% of PEI present. The result of the reaction is described as forming a 'paste' rather than a gel. In this case, the transition from liquid to solid was effectively instant, as opposed to delayed gelation, and the texture was grainy and not smooth and consistent, indicating the presence of large quantities of coagulant.

The reason for PEI's strong interaction with CS is likely due to the highly branched structure of PEI, with many amine groups which protonate to NH_3^+ in aqueous solution, providing ample electrostatic bonding sites for the negatively charged CS particles, and facilitating the formation of dense clumps of particles and polymer which coagulate, rather than gradually forming a gel network.

7.5.2.3 PAM/PEI and CS/PAM/PEI gels

The PAM/PEI gels produced in 7.4.2.3 and 7.4.2.4 exhibit much higher flexibility than standard CS gels. This is a result of the long polymer chains that comprise the gel, which are able to bend and flex to a far greater extent than the rigid network of particles in a CS gel network. Following this same logic, gels produced with the longer PAM-5m molecules have greater flexibility than those using PAM-150k.

From 7.4.2.3, there exists an apparent limit to the wt% of silica which can be included in PAM/PEI gel; this is presumably a result of the strong interaction between CS and PEI. Hypothetically, there will be a minimum wt% of MP 320 CS for which it is possible to create a coherent gel network. Therefore, to create a double network hydrogel, there must be at least this quantity of silica present in the mixture. For samples 5 and 6 in 7.4.2.3, which are PAM-5m gels with low silica wt%, it is assumed that CS particles acted as discrete anchor points to strengthen the PAM network, rather than forming their own CS network. It is unknown if samples 7 and 8 (10 wt % and 16.8 wt% silica) contained sufficient silica to form CS networks; however, due to these gels behaving more like PAM gels than CS gels, it is unlikely that double networks were formed in these samples.

Section 7.4.2.4 saw the production of waxy PAM-150k 'gels' with significant quantities of silica present, both with and without the presence of PEI (PAM = 6.5 wt%, PEI = 0 or 0.8 wt%, silica = 40 wt%). Further work is needed to study the nature of these materials.

PAM/PEI mixtures were shown to gel at room temperature (although this took a very long time for PAM-150k), but gelled much faster at higher temperatures. It can therefore be said that increased temperature accelerates the PAM/PEI gelation reaction. In contrast, the interaction between CS and PAM which occurred at high temperature in 7.4.2.4 was never observed at ambient temperature, with CS/PAM suspensions produced as part of this study remaining stable over long durations. It is therefore thought that temperature initiates the CS/PAM reaction rather than accelerating it.

From the UCS tests on sand grouted with PAM/PEI gel, the PAM-5m sample exhibited lower yield strain than the PAM-150k (see Figure 7.21). This was unexpected as, in 7.4.2.3 and 7.4.2.4, PAM-5m/PEI gels were observed to be more flexible than PAM-150k/PEI gels. It is therefore possible that there is some interaction between the gel and the sand, or an effect of the quality of grouting achieved, which may have impacted the result.

7.5.2.4 Potential application of PAM/PEI and CS/PAM/PEI gels

One issue regarding the use of PAM/PEI gel for grouting application is its reliance on high temperatures. In the oil industry this is not an issue, as deep subterranean oil reservoirs naturally provide sufficiently high temperature for timely gelation of PAM/PEI; this effect was reproduced here using an oven. Such high temperatures are not present and presumably are not practical to induce in near-surface grouting applications, however, meaning that gel times may be impractically long. There may be ways around this, though, such as pre-heating the grout prior to injection, or utilising some catalyst to increase reaction rate. Furthermore, in other applications, such as for grouting radioactive waste cannisters, there may well be sufficient heat available for timely crosslinking of PAM/PEI.

7.5.3 PVA

7.5.3.1 Interaction of PVA with CS

The interaction between PVA and CS is influenced by pH, ionic strength, and the chemical nature of both components. PVA's solubility and intermolecular interactions are primarily governed by its polar hydroxyl (OH) groups, which are very weakly acidic, only dissociating to a minimal extent in solutions of pH < 12 (Morariu et al., 2023). This explains why the presence of PVA minimally impacted the gelation of CS in the pH range 3-9.3, in 7.4.3.1. However, at pH 1 there was significant interaction, with phase separation occurring. At this pH, CS particles' silanol groups increasingly begin to protonate to SiO_2^+; presumably this change in surface charge facilitates adsorption of PVA onto CS particles. This suggestion is supported by studies which have found increasing adsorption of PVA on CS at decreasing pH (Chu et al., 2007; Kim et al., 2009; Wiśniewska et al., 2016). At low pH, adsorbed PVA molecules likely act as bridges to quickly form dense clusters of CS and polymer which then settle out of suspension. However, unlike for CS/PEI, where sediment remained unchanged, the CS/PVA coagulant seemingly was able to bond together to form a compact gel network. While such low pH conditions are not suitable for in-soil applications, the pH 1 sample here is of interest, as its greater density may give it reduced hydraulic conductivity and increased mechanical strength compared to standard CS grout. This was not explored further within the scope of this study, however.

The presence of NaCl also facilitated interaction between CS and PVA, with phase separation occurring even at pH 9.3. The mechanism differed from that seen with CS/PEG, however, as there was no rapid acceleration in gelation; instead, the NaCl prompted

phase separation, and gradual formation of a softer gel than standard CS grout, which could deform plastically. Due to the complication of the phase separation, no rheology measurements were conducted on such samples, but these effects may offer opportunities for tailoring gel structure and performance. As described with PEG, the negative surface charge of CS particles is screened by cations from the salt, presumably allowing adsorption of PVA, which causes the coagulation via a bridging effect. After settling, the coagulant is then able to continue to form a gel. The plastic deformability of the gel likely arises due to hydrogen bonding of the PVA's hydroxyl groups and CS particle surfaces. This property could be useful in creating barriers which are resistant to cracking from damage.

7.5.3.2 PVA and CS/PVA gel

As mentioned in 7.2.7, PVA is able to produce gels without any additives due to its ability to form self-crosslinks when the polymer is brought to high (or locally high) concentration. It makes sense, therefore, that the relative strength of the gels in 7.4.3.2, from either the air-drying or freeze-thaw methods, increases with PVA wt%, as more polymer chains are pushed into contact where they can form crosslinking points. The number of freeze-thaw cycles also increases gel strength by the same effect, as ice crystals force more polymer molecules to contact and create additional crosslinking points, but without needing to increase the overall PVA concentration of the solution.

PVA gel also possessed the ability to recover after breaking through an additional freeze-thaw cycle, demonstrating the reversible nature of its physical self-crosslinks. This would be a useful property to impart into CS grouts.

A large increase in strength was also produced by addition of CS, as seen in Figure 7.27. This is true even though the CS/PVA gel had lower PVA concentration (11 wt%, compared to 15 wt%). As no accelerator solution was added, it is assumed that the CS did not form its own independent network, but rather acted as anchor points in the PVA network, adding strength, as has been observed in other works (Khedr & Elhady, 2025). This hypothesis is further supported when comparing the rheology of the PVA and CS/PVA gels to the 1 d aged standard CS grout sample. The profiles of the PVA and CS/PVA gel data closely resemble each other, although they have different values, implying that they

have fundamentally similar structure (i.e., a crosslinked PVA network). The standard CS grout, however, looks very different in each plot in Figure 7.27.

7.5.3.3 Potential application of PVA and CS/PVA gels

The application of freeze-thaw PVA gels in civil engineering may be possible through artificial ground freezing (AGF), for example, which is a technique currently employed to create temporary hydraulic barriers in soils. Here, cryogens, such as liquid nitrogen, are piped through soil in order to induce freezing of the soil's pore water (Alzoubi et al., 2020; Joudieh et al., 2024; Park et al., 2024; Teng et al., 2025; Wagner & Yarmak, 2012). The suitability of this method for forming PVA gels remains to be seen, however. There exists also the risk of inducing ground heave at the surface when freezing soil, due to the expansion of water ice as it freezes (Joudieh et al., 2024; Park et al., 2024; Teng et al., 2025).

The fact that PVA forms a hard gel when it dries, and can easily return to a soft state upon re-wetting, may help it combat the effects of cracking seen in CS gels upon repeated drying and wetting cycles, if the two gels can be combined (Pedrotti et al., 2020). Indeed, PVA solutions have already been investigated for injecting into soil to prevent cracking from both wet-dry and freeze-thaw cycles (Ren et al., 2025). Air-dried PVA gel could also potentially be used as a spray coating to capture contaminated dust particles on the surfaces of structures, for example, in nuclear decommissioning.

7.6 Conclusion

This chapter has presented the results of experiments on the combination of polymers with CS grout, investigating polymer hydrogels, and attempting to form CS/polymer double-network nanocomposite gels, with the aim of creating novel grouts and gels with potential for application in civil engineering. In research for other applications, polymer hydrogels have been made which are customisable to be ultra-strong, flexible, or re-healable, so incorporation of properties such as these into CS grout, whilst retaining its own beneficial properties, could be highly advantageous.

Preliminary investigations into the polymers PEG, PAM, and PVA, their interaction with CS grout, and how they can be combined in different ways, were conducted, and a range of different grout and gel variants with novel properties were identified. Two varieties of CS grout with added PEG were observed, depending on the wt% of PEG present. At low

PEG wt%, fast-gelling samples, which featured plasticity and mouldability not found in standard CS grout, were formed. These could be used as grouts which resist damage from cracking. At higher PEG wt%, gels exhibited greatly improved water retention over controls, but at the cost of weakened structure.

Crosslinked PAM/PEI gels were produced, using PAM-5m, which had improved flexibility over standard CS grout, and several examples of these were created with low wt% of CS present. However, this molecular weight of PAM had much higher viscosity than CS grout. Gels with higher wt% of silica were made using PAM-150k, which were rigid and wax-like. These formed from interaction of PAM and CS; the structure of such samples is not yet known.

Adding PVA to CS grout created a soft, plastically-deforming gel, which could be used as a grout which does not crack upon damage. Another CS/PVA grout sample was created at pH 1 which formed a dense, compact gel, with potentially lower hydraulic conductivity and increased strength compared to standard CS grout. PVA polymer hydrogels were also produced, with excellent strength and flexibility, by both air-drying and freeze-thaw methods. Adding CS to freeze-thaw PVA gel further improved mechanical properties.

Additional work is needed to investigate the structures of the novel gels created here to determine if CS/polymer double networks were formed.

Chapter 8: Discussion

8.1 Introduction

In this work, the effects of various factors on the gelation and strength evolution during curing of CS grout have been investigated, as well as its ability to re-heal, and the effects of adding clays and combining it with polymers. Here, the results from chapters 4-7 are compared and evaluated, exploring how they relate to the theoretical understanding of CS, and their implications for its practical application in grouting.

8.2 Gelation

The rate of gelation of CS grout depends on the frequency of inter-particle encounters, the probability that encounters lead to particles contacting, and the probability that contact results in sticking and bond formation (Iler, 1979). Each of these in turn are affected by a variety of sub-factors, several of which were investigated in this work, including the particle size and silica mass fraction, and the electrolyte species and concentration in the accelerator. A detailed description of the gelation mechanism of CS grout can be found in section 2.2.2.

8.2.1 Silica concentration and particle size

The results in section 4.3.1 found that silica wt% affects the gel time of MP 320 CS grout according to an exponential decay relationship, such that lower silica mass gives longer gel times. This is generally consistent with the findings of other studies (Agapoulaki & Papadimitriou, 2018; Hatami et al., 2021; Huang et al., 2017; Iler, 1979; Jurinak et al., 1991b; Metin et al., 2014; Pedrotti et al., 2017; Trompette, 2017), although some have modelled the relationship as a power law decay (Hunt et al., 2013; Trompette & Clifton, 2004; Trompette & Meireles, 2003; Van Der Linden et al., 2015). From Smoluchovsky theory on the collisions of particles in Brownian motion (Hunter, 1981), the rate of collisions per unit volume is proportional to the square of the number density of particles, N,

$$Collisions/vol. \alpha\, N^2. \tag{8.1}$$

Decreasing the silica concentration reduces the number of particles, and therefore the frequency of particle collisions, contributing to slower network formation.

In chapter 5, gel time data was also collected for MP 325 CS grout, which has particle size half that of MP 320 (7.5 nm comparted to 15 nm), and uses lower silica wt% (15 wt%

compared to 40 wt%): this data is presented alongside equivalent MP 320 data in Figure 8.1, showing the geltimes of the grouts at different accelerator NaCl concentrations (more information can be found in appendix A.3.1). Using equation 4.10, it is possible to predict the gel times of a grout created using MP 320 CS at 15 wt% of silica for comparison with MP 325, which is also shown in the plot. As can be seen, the MP 325 samples gelled much faster than these predictions, demonstrating how smaller particle size gives faster gel time for CS grout. This has also been found in other studies (Huang et al., 2017; Jurinak et al., 1991b; Sögaard et al., 2023). The MP 325 data also has a shallower gradient than the MP 320 lines on the semi-log axes. The reason for this is difference is not known: it could be due to differences in surface chemistry between the two CS types, or in how Na^+ adsorbs with CS particle size.

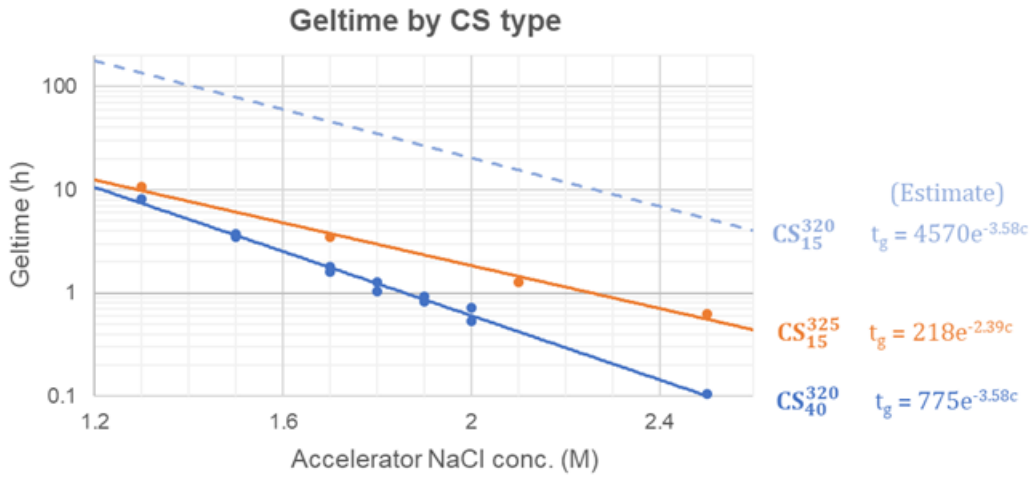

Figure 8.1. Comparison of the gel times of MP 320 (dark blue) and MP 325 (orange) CS grout with accelerators of different NaCl concentration. Fit lines are exponential decays. The dotted blue line is a prediction for MP 320 grout with only 15 wt% of silica, the same as MP 325 has.

As particle size, d, decreases, for constant wt%, the number density of particles increases cubically,

$$N \propto \frac{1}{d^3}. \tag{8.2}$$

By equation 8.1, this means that the rate of collisions per unit volume increases by a power of 6 for decreasing particle size, contributing to faster gelation. Furthermore, in Brownian motion, smaller particles have greater kinetic energy, increasing the likelihood of overcoming the potential barrier between particles (Hunter, 1981). The greater velocity of smaller particles is not expected to increase the frequency of collisions,

however, as it is balanced by smaller collision cross-sections, according to Smoluchovsky theory.

Both silica concentration and particle size contribute to the surface area per unit volume of CS, which may be calculated using equation 5.11. Combining the datasets for MP 320 and MP 325 allows for estimating the effect of the surface area of particles per unit volume, A_v, of grout on the gel time, shown in Figure 8.2. For the MP 320 data, there is a negative exponential relationship between the surface area per unit volume and the gel time. The MP 325 appears to outlie this trend, however, implying that surface area alone may not be sufficient to explain the difference in gel times of MP 320 and 325 grouts. More MP325 data is needed to further investigate this, however. This finding would be counter to Iler (1979), which states that "sols having the same ratio of concentration to particle diameter gel at about the same rate" (p. 367). As mentioned previously, other factors, such as differences in surface chemistry or Na^+ adsorption, may impact the gelation of the two CS types.

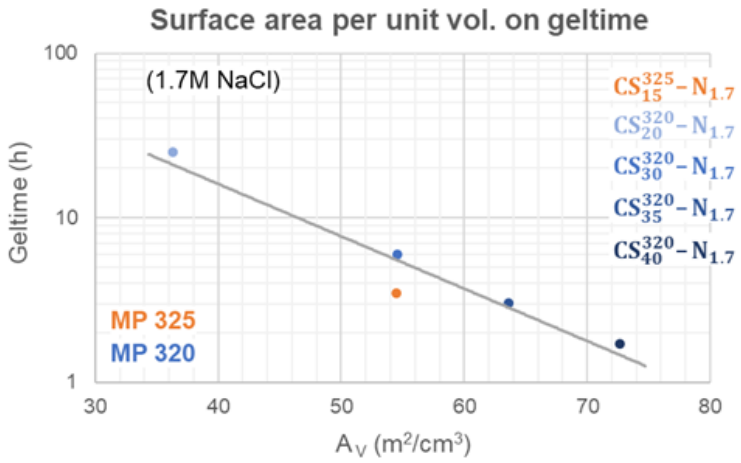

Figure 8.2. Effect of silica surface area per unit volume on the gel time of CS grout, using two types of CS. An exponential fit line is shown. 1.7 M NaCl accelerator was used for all samples. Shades of blue are used to represent samples produced using MP 320 CS, and orange is used for MP 325.

8.2.2 Electrolyte

In section 4.3.1, it was found that the NaCl concentration in the accelerator affected the gel time of MP 320 CS grout according to an exponential decay relationship, with higher NaCl concentration giving faster gel time. This is generally consistent with the findings of other studies (Agapoulaki & Papadimitriou, 2018; Basilio et al., 2025; Hatami et al., 2021; Huang et al., 2017; Iler, 1979; Jurinak et al., 1991b; Metin et al., 2014; Pedrotti et al., 2017; Shen et al., 2017; Trompette, 2017), although the relationship has also been described as

a power law (Van Der Linden et al., 2015). A wider range of NaCl concentrations would be needed to be more certain about the nature of the relationship. The same was also found to be true for MP 325, as was shown in Figure 8.1. The cause of this is that higher electrolyte concentrations result in a greater number of cations adsorbing onto CS particles, increasing the surface charge screening and further depressing particles' EDLs; this accelerates gelation by permitting more successful particle collisions (Bergna & Roberts, 2006).

In 4.3.1, $CaCl_2$ salt, however, was found to not be able to gel CS grout in a controllable manner, inducing phase separation and rapid coagulation. The underlying cause of this is the higher valency of Ca^{2+} ions compared to Na^{+} (2 to 1), and their corresponding greater charge density, which is more effective at screening CS particles (Döpke et al., 2019), causing them to rapidly aggregate into dense clusters which fall out of suspension rather than gradually forming into a branched network. Although $CaCl_2$ has been successfully employed in other research, it has generally been at either neutral or acidic pH (Pedrotti et al., 2017), or in combination with alumina-stabilised CS (Funehag & Fransson, 2006; Moridis et al., 1995), both of which lessen the effect of cations on stability by reducing the degree to which they adsorb at particle surfaces (Iler, 1979). It can be said here then, that $CaCl_2$ is not suitable for use in the accelerator of MP 320 CS grout at alkaline pH.

8.2.3 Application

The ability to precisely control the gelation of CS grout is one of its primary advantages (Pedrotti et al., 2017; Yates, 1990), and each application for CS has its own gel time requirements. In permeation grouting, the grout generally needs enough time to travel away from the point of injection before it gels, to ensure effective coverage of the target volume, and to prevent blockage of injection equipment. It must, however, gel fast enough to not be excessively diluted or transported away from the target volume by gravity and groundwater flow, as Hamderi and Gallagher (2015) observed. Subterranean environmental conditions, such as the presence of adsorbed cations in soil, have also been found to greatly affect the gelation of CS grout, and thereby its performance in application, although pre-flushing soil with saline solution has been successfully used to counter this (Durmusoglu & Yavuz Corapcioglu, 2000; Persoff et al., 1995). It is therefore apparent how achieving a thorough understanding of the impact of grout components and environmental factors on the gelation of CS is important for its successful application.

This research has added to the understanding of CS grout gelation, and it could be used to help design a comprehensive model to predict viscosity evolution and gel times.

The results here have confirmed that CS grout's gel times can be precisely tailored through the concentration of a suitable electrolyte in the accelerator. NaCl is recommended as one such electrolyte, whereas $CaCl_2$ may only be used under particular circumstances, such as at neutral or acidic pH, or with alumina-modified CS. The effect of varying other grout components on the gel time, such as the silica concentration, may be controlled for by using this method. The silica mass fraction of the grout also allows tailoring of gel times and can be easily done through dilution, but this also impacts the strength of the grout, and the silica content cannot easily be raised above the initial value set by the manufacturer. It is not practical to use the particle size to control gelation, as this too is set by the manufacturer.

8.3 Curing and re-healing

Due to the assumed related nature of the curing and healing phenomena, discussion of their mechanisms, and the impact of different factors on these, are grouped together in this subsection.

8.3.1 Curing mechanism

In chapter 4, it was found that the strength of CS grout increased continuously over time according to a power law. This is consistent with other studies (Axelsson, 2006; Bakhshandeh et al., 2025; Boiero et al., 2026; Butrón et al., 2009; Cheng et al., 2022; Jurinak et al., 1991b; Mollamahmutoglu & Yilmaz, 2010; Pan et al., 2018; Todaro, 2021), although the relationship has also been described as logarithmic (Terui et al., 2025). It is thought that the origin of this strength increase is the mechanism described by Iler (1979), involving ongoing deposition of dissolved silicates at the necks joining CS particles in the gel network, at which there is strong negative curvature. New siloxane bonds then form through condensation reactions, strengthening the network, and increasing its rigidity.

By combining all the curing data from chapters 4 and 5, and performing an ordinary least-square fit in log-log space, it is possible to produce a single equation for the shear strength, τ_{max}, of CS grout, in terms of its particle size, d, silica mass fraction, w_{SiO_2}, accelerator NaCl concentration, c_{NaCl}, and curing time, t_c:

$$\tau_{max} = 4 \times 10^7 d^{-4.34} w_{SiO_2}^{4.12} c_{NaCl}^{1.04} t_c^{0.341}, \quad (8.3)$$

assuming the final relationship is a multivariate power law. This is a very preliminary effort at modelling the system, however, and considerably more data is needed to increase accuracy.

8.3.2 Re-healing mechanism

Chapter 5 showed that CS grout was able to re-heal after suffering damage, before recovering and increasing its strength again via a power law. No other research has been identified which studies this phenomenon, although Katoueizadeh et al. (2021) did observe CS gel to recover its structure after breaking in rheometer tests. Because of the similarity of this strength increase to that seen during curing, it is proposed here that the two phenomena are related. The healing of samples was shown to be slower than their original curing, however, with fit lines shifted down in log-log plots of strength against time, and having apparently shallower gradients. Assuming that curing and healing are fundamentally the same process, then the distinct particle arrangements and geometries in broken and unbroken samples presumably causes the difference in rate of strength gain.

Surprisingly, no dependence on curing time was found in the degree of re-healing achieved by samples, meaning that samples broken soon after gelation seemingly do not heal any faster than those broken after long durations of curing. Samples broken for a second time, however, were found to re-heal more slowly than the first time they were broken.

It is assumed that, on breaking, CS gel is reduced to a suspension of gel fragments, each comprised of a network of bonded silica particles, thus explaining the higher viscosity of the grout after breaking, compared to its original value. Because the conditions which first initiated gelation are still present (for example, the added salt from the accelerator), the fragments are able to link back together to re-form a fully-encompassing network, before presumably continuing to gain strength via the same redistribution of silica as described by Iler (1979) regarding curing. A diagram showing the evolution in strength of CS grout during curing, breaking and re-healing is provided in Figure 8.3, with the assumed structure of the network at various points depicted.

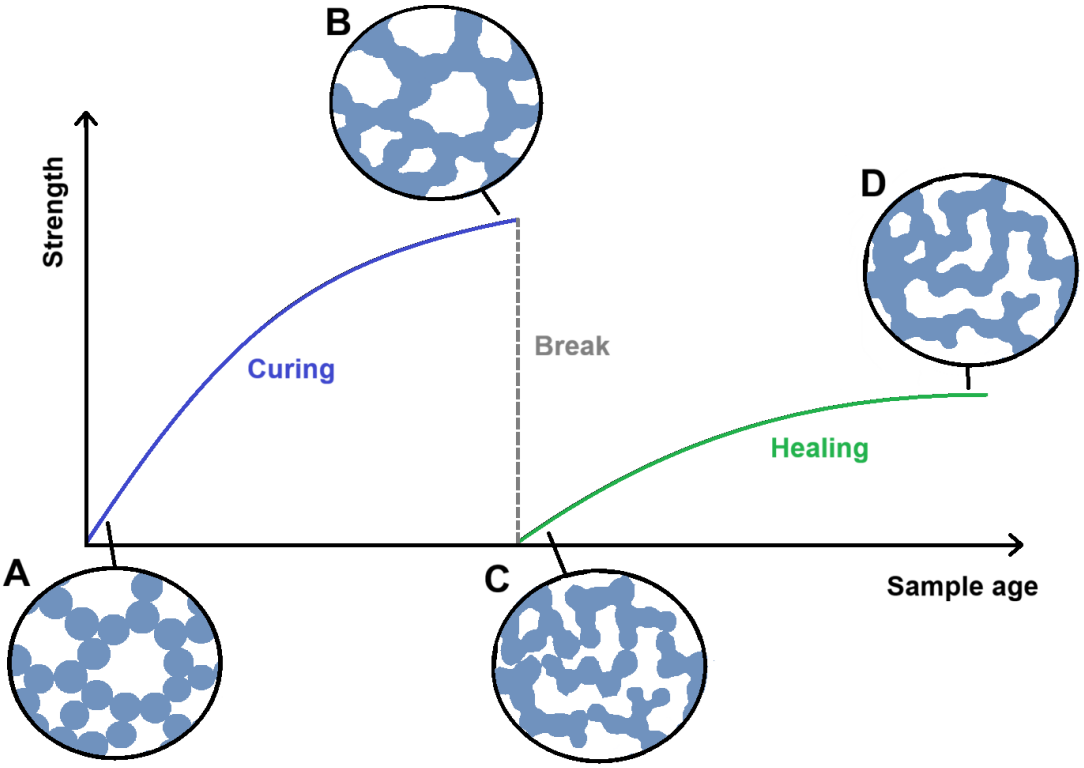

Figure 8.3. Representation of the strength evolution of CS grout during curing, breaking, and re-healing, with diagrams of the CS network at various points, based on Iler (1979)'s mechanism. *A:* The network of distinct CS particles shortly after gelation. *B:* After a long curing duration silica has been redistributed to particle necks, leading to a tubular structure. *C:* Network fragments quickly reconnect after breaking. *D:* Further redistribution of silica occurs during re-healing.

8.3.3 Effect of silica concentration and particle size

It was shown in chapter 4 that raising the silica concentration of CS grout exponentially increased its strength. This makes sense, as CS with higher mass of silica should produce denser networks, and therefore stronger gels, and more silica would be available to re-distribute around the network, accelerating the curing and (presumably) re-healing processes. These results are generally in agreement with other research (Gallagher & Mitchell, 2002; Jurinak et al., 1991b; Mollamahmutoglu & Yilmaz, 2010; Persoff et al., 1999; Trompette & Clifton, 2004), although the increase in strength has also been described as both linear (Persoff et al., 1999; Terui et al., 2025), and a power law (Persoff et al., 1999; Trompette & Clifton, 2004).

In chapter 5, it was shown that MP 325 CS grout increased in strength during both curing and re-healing according to power laws with equal exponents to MP 320 equivalents, implying that the same processes occur in both CS varieties. The difference in strength was significantly greater in re-healing, however, for unknown reasons. Figure 8.4 shows

how the strength of MP 325 CS grout during curing was significantly greater than that predicted for MP 320 CS grout with the same gel time and silica wt%, as calculated via equations 4.10 and 8.3; this demonstrates how smaller particle size gives stronger gels. This would be expected, as the greater surface area provided by smaller particles presents more sites where siloxane bonds can form. However, normalising to account for the different surface areas per unit volume did not make up for variance in strength between the two grouts, in either curing or re-healing. As was mentioned in 8.2.1 regarding gelation, there may, therefore, be other factors contributing to the difference in strength between the two CS types, such as differences in surface chemistry or Na^+ sorption with particle size.

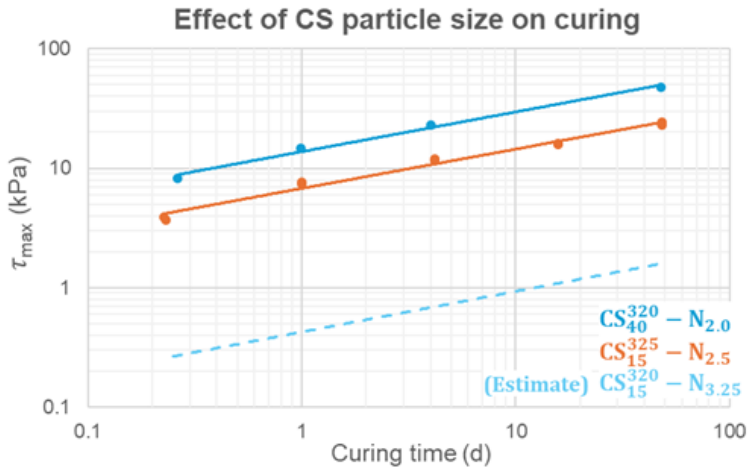

Figure 8.4. MP 325 CS grout (15 wt% silica, 7.5 nm particle size) strength gain during curing compared to MP 320 CS grout with the same gel time (40 wt% silica, 15 nm particle size). The dotted line is the estimated strength gain for MP 320 CS grout with 15 wt% at the same gel time, for comparison.

Re-healing CS grout in the presence of additional colloidal silica was found give greater strength recovery than healing in water of the same pH, and with equivalent salt content. This makes sense, as it provides an additional source of silica to be dissolved and be redeposited onto the existing network, leading to its densification and reinforcement, and with additional siloxane bond formation. Alternatively, the additional CS particles may simply diffuse into the sample and bond onto the network as discrete particles, without initial dissolution. This effect could be further investigated by using a solution containing pre-dissolved silicate.

8.3.4 Effect of electrolyte

It was shown in chapters 4 and 5 that higher NaCl concentration in the accelerator exponentially increased the strength of CS grout during curing and re-healing. It was also found that higher electrolyte concentrations in curing and healing water increased the strength of the grout. Diffusion of ions between samples and the surrounding water was identified, and is assumed to contribute to the differences in strength.

Doubling the cation valency of the salt in curing and healing water, from NaCl to $CaCl_2$, produced a greater effect than doubling the NaCl concentration, presumably as a consequence of the higher charge density of Ca^{2+}. Plotting healing water ionic strength against sample shear strength gave a proportional relationship, suggesting that ionic strength is the determining factor in the effect of electrolyte on curing and re-healing. However, more data using other salts is needed to determine if there are ion-specific factors at work. For example, Ca^{2+} ions have been found to produce a far greater screening effect than simply increasing N^{+} concentration to the same ionic strength (Döpke et al., 2019).

It has been established that the presence of electrolyte in solution, including NaCl, can accelerate dissolution of silica (Iler, 1979). It may therefore be the case that higher salt concentrations in CS grout encourage greater redistribution of silica towards inter-particle necks, speeding up the curing and healing processes. A mechanism proposed by Johnsson et al. (2011) could also be responsible, in which additional kosmotropic ions, such as Na^{+}, adsorb onto particles, increasingly polarising associated water molecules to create areas of local acidity where siloxane bond formation is more favourable. Cations could also contribute towards strength through electrostatic interactions, by bridging particles, or via ion-ion correlation interactions, such as those outlined in Johnson et al. (2008).

In section 4.4.2.2, it was shown that curing times can be equated with gel times, such that a sample cured for twice as long can be taken as equivalent to one which gels at twice the rate. This suggests that electrolytes play similar roles in both gelation and curing. The degree of error in this experiment was quite high, however.

8.3.5 Effect of pH

Re-healing in alkaline aqueous solution at pH 9 was found to give greater strength recovery than neutral pH 7. Higher pHs are known to cause increasing dissolution of silica (Bergna & Roberts, 2006; Dollimore & Heal, 1962; Iler, 1979), and Wijnen et al. (1991) found that alkaline pH accelerated the redistribution of silica and reinforcement of the gel network because of the increased solubility, with other studies reaching similar conclusions in the context of aerogels (Payanda Konuk et al., 2023; Venkateswara Rao et al., 1994). This effect may explain the greater strength achieved by re-healing at high pH, and would also suggest that the same would be true for curing.

It is likely that there is a limit to the pH that can be used for curing and healing CS gel, however, as very high pH could cause the network to dissolve entirely (Iler, 1979). Furthermore, the increased solubility of silica at high pH could make CS gels more vulnerable to water erosion, as was observed by Sögaard, Funehag, Gergorić, et al. (2018).

8.3.6 Application

Regarding practical application, as long a time as possible should be allowed for CS grout to cure or re-heal after damage in order for it to obtain its highest strength; this is especially the case, for example, where CS-grouted soils are likely to experience mechanical stress, such as from construction or deconstruction operations being carried out on the surface above the grouted volume, or if CS grout is being used to assist in excavating contaminated soils.

It was shown here that the strengthening effect of electrolyte on CS grout could be used to offset the decrease in strength brought about by reducing the silica mass fraction, via equation 4.1. This could allow for reducing the cost of CS grout, through dilution, whilst preserving its mechanical strength. However, the NaCl concentrations needed for this quickly become impractically high as the silica wt% decreases, meaning that this method could only feasibly be used for small reductions in silica.

CS grout can be expected to cure and re-heal faster, reaching greater strengths, in areas with more saline conditions: for example, in coastal regions, or at contaminated sites. This will additionally affect the gelation of the grout, however. CS grout should also presumably cure and heal faster in areas with alkaline groundwater, as opposed to neutral. The impact of acidic pH has yet to be conclusively determined. Furthermore,

given that CS grout was found to heal faster in the presence of additional silica, it may be that soils with higher silica content, or which are more prone to dissolution, could increase the strength of the grout by providing additional silica to be redistributed onto the gel network. Given these findings, potential ways to accelerate the curing and re-healing of CS-grouted volumes in situ could be to conduct secondary injections of saline solutions, such as $CaCl_2$, at alkaline pH, or even to inject additional CS or other silicious solutions.

The previously unknown ability of CS grout to re-heal provides it with a key benefit over conventional grouting materials, such as cements, and gives it added resilience and adaptability in all potential applications, which has not thus-far been considered. Considering hydraulic barrier application, for example, the formation of fissures through cracking is known to significantly reduce barrier effectiveness; the ability to self-heal in situ is therefore a highly desirable property for barrier materials, reducing the likelihood that future interventions are needed to restore or replace damaged barriers. The same would also be true for grout used for soil stabilisation and liquefaction mitigation, as well as various other applications. Avoiding the need for potential repeated treatments would provide significant cost savings.

8.4 Addition of clays

8.4.1 Viscosity and gelation

In chapter 6, it was shown that adding either kaolin or bentonite clays to colloidal silica caused exponential increases in viscosity, but that bentonite had a much more pronounced effect than kaolin. This is due to the swelling property of bentonite, caused by its smectite layers being pushed apart due to the intrusion of water, such that its particles increase in size. The result of this is that much more kaolin can be added to CS than bentonite whilst keeping viscosities low enough for use as a permeation grout. Replacing the mass of silica in CS with kaolin was found to have very little effect on viscosity. At 1:1 ratio of silica to kaolin, a slight viscosity dependence on salt concentration could be measured, but overall, the viscosity remained very low throughout.

Both kaolin and bentonite caused acceleration of the gelation of CS grout, with increasing wt% of kaolin added resulting in an exponential decrease in gel time (the same is

presumed to be true for bentonite). Again, bentonite had a much greater effect on the gel time than kaolin. In each case, however, the gel time could be controlled using the NaCl concentration in the accelerator, and varied according to an exponential relationship, just as for standard CS grout. When plotting the gel time against the NaCl concentration on semi-log axes, the CS/bentonite grout's fit line was shifted down in gel time, but had equal gradient to standard CS grout; the CS/kaolin had a steeper gradient, but this could be due to experimental factors. Replacing the mass of silica in CS grout with kaolin caused slower gelation, meaning that kaolin has less of an effect on gelation than silica.

The reason the clays accelerate the gelation of CS grout could be that they trap water molecules when the clay dissolves, decreasing the volume available for CS particles to move in, and thereby increasing the frequency of inter-particle collisions, and accelerating gelation. It may also be the case that clay particles actively partake in network formation, providing their own bonding sites. The edges of kaolin and smectite mineral layers feature aluminol and silanol groups, which could form aluminosilicate and siloxane bonds with CS particles. Furthermore, these groups could act as nucleation points for CS network growth by hydrogen bonding with CS particles, facilitating contact and bond formation. The clays could also affect the zeta-potential or local pH of the CS to promote aggregation. The reason bentonite has a greater effect on gelation than kaolin is presumably due to its swelling behaviour, which sequesters additional water within its expanded clay particles, further reducing the space available to CS particles, and thereby increasing collision frequency.

Although both clays accelerated the gelation of CS grout, NaCl accelerator was needed to induce gelation. The CS/clay mixtures themselves remained mostly stable for long durations, although small amounts of clay could settle out of suspension, which could be redispersed through stirring.

8.4.2 Strength, curing, and re-healing

In chapter 6, it was demonstrated that the addition kaolin increased the strength of CS-grout (at least up to a point). This added strength could arise from kaolin particles taking part in the CS gel network through their silanol and aluminol groups covalently bonding with CS particles, or simply reinforcing the network through transient interactions, such as hydrogen bonds, or electrostatic interactions. The idea of some interaction between

the clays and CS is supported by observations of CS adsorbing onto both kaolin and bentonite particles (Baird & Walz, 2006; Holmboe et al., 2011; Wong et al., 2018). Simply the physical presence of the comparatively large, solid clay particles, where there would otherwise be porewater, could give added resistance to the gel, through friction with the CS network. It was also found that replacing the mass of silica with kaolin caused a reduction in strength, but not as much as simply removing that amount of silica. It can be said, then, that kaolin adds to the strength of CS grout, but does not contribute as much as the silica itself.

CS/kaolin grout was shown to both increase in strength during curing, and to re-heal after suffering damage, in a similar manner to standard CS grout, implying that the same underlying physical processes take place. When plotting strength against time on log-log axes, the CS/kaolin grout's fit line has a steeper gradient than standard CS grout; this was not true for re-healing, however, where it had the same gradient as standard CS. It may be that, during curing, the kaolin provides an additional source of silica to dissolve and redistribute to joining points in the CS network, making the strength gain faster than expected. Why this does not occur for re-healing, though, is not known.

8.4.3 Application

The strength increase provided to CS grout via the addition of clays like kaolin could increase its resistance to damage, and give it longer lifespan when used, for example, as a hydraulic barrier; it would also improve its effectiveness in soil stabilisation and liquefaction mitigation. Replacing part of the mass of silica in CS grout with clays, which are much cheaper materials, could also provide a way of reducing the cost without overly compromising mechanical performance.

Clays have various other properties which could be of benefit in combination with CS grout. For instance, clays tend to deform plastically, in contrast with CS gel, which is more brittle in nature. Imparting this behaviour into CS grout could reduce the incidence of fracture formation, which can compromise hydraulic barrier performance. Bentonite has particularly useful properties, such as its high swelling potential, which could facilitate better void filling and self-healing of fractures in situ. It also has high sorption capacity, which could help CS in application as a chemical barrier for trapping contaminants, for example in soil at nuclear sites.

Significant quantities of kaolin can be added to CS grout while keeping viscosities low enough for permeation grouting, and replacing mass of silica with kaolin has very little impact on viscosity. Only smaller quantities of bentonite can be used with CS grout, however.

8.5 Combination of CS grout with polymers

8.5.1 PEG

The interaction of PEG with CS presumably arises due to adsorption of the polymer onto silica particle surfaces, via the mechanism proposed in Rubio and Kitchener (1976). At alkaline pH, the mixture is initially stable, as there is enough repulsion between negatively charged CS particles and PEG's slightly negative ether groups. Upon adding electrolyte, however, the screening of CS particles' surface charge by adsorbed cations sufficiently contracts the EDL to allow PEG to adsorb onto the silica particles via electrostatic attraction and hydrogen bonding of the polymer's ether groups, in addition to hydrophobic association through PEG's CH_2-CH_2 groups; this leads to the macro-scale effects observed in chapter 7. Similarly, if pH is lowered, the magnitude of CS particle surface charges reduces as ionised silanol groups protonate, and the higher density of SiOH groups at surfaces provides more sites for PEG to hydrogen bond with. These effects each promote the adsorption of PEG.

At low PEG concentration in CS grout, gelation is accelerated by PEG's adsorption. This is presumably due to a bridging effect, in which PEG chains link multiple particles and bring them together because of the polymer's tendency to coil up in solution. These gels deform plastically when hydrated due to the transient nature of the bonds between the PEG and CS particles, although they become brittle when dried, implying that the transient bonds disappear or are replaced by permanent covalent bonds. Such gels are white in colour, and have slightly reduced water retention compared to standard CS grout, probably as a result of greater pore sizes arising from the presence of large flocs during gelation, as suggested by Martin et al. (2001). The larger pore diameters approach the wavelength of light, which increases scattering to produce the white colour, and the associated higher air entry value of the larger pores allows for faster evaporation. The gel time of these grouts can be slowed to practical rates by decreasing the electrolyte concentration of the accelerator, but this causes the plastic behaviour and white colour to phase out, due to reduced PEG adsorption. During desiccation, these gels apparently crack to a lesser

degree than standard CS, likely due to the increased pore sizes producing less build-up of capillary pressure.

Above a certain PEG concentration, gelation is instead increasingly slowed with respect to standard CS grout, due to steric repulsion from loops of adsorbed PEG chains resisting compression, and preventing CS particles contacting, which decreases the number of successful collisions. The resulting gels crack more than standard CS gel, likely as a result of fewer siloxane bonds forming between CS particles, because of adsorbed PEG molecules blocking contact points between particles. These gels have higher water retention that standard CS grout due to PEG's hydrophilic ether groups binding water molecules, thereby inhibiting their evaporation.

8.5.2 PAM and PEI

In chapter 7, it was found that PAM could be dissolved in CS with practically no effect, beyond increased viscosity. The large sizer of PAM-5m molecules compared to PAM-150k results in more intermolecular interaction during flow, causing it to have a greater effect on viscosity. Both PAM varieties exhibited shear thinning in CS, however, as, when at rest, the polymer chains are coiled and entangled, causing a high degree of friction and resistance to flow; whereas at high shear, the chains start to align with the flow direction, reducing entanglements and decreasing the resistance to flow, thereby leading to lower viscosity (Akbari et al., 2017; Chandler, 2019; Navaie et al., 2022; Sun et al., 2025; Tie et al., 2019).

On the other hand, PEI, the crosslinker used here with PAM, had little effect on viscosity, but exhibited strong interaction with CS, depending on their respective concentrations, and on the pH. The result of the reaction was instantaneous flocculation, which, at high pH, lead to a delayed phase separation, and at lower pH, formed a solid white 'paste' which deformed plastically. In both cases, PEI presumably adsorbs onto CS particles and has a bridging effect: under alkaline conditions, dense polymer-particle clusters are formed which fall out of suspension, whereas at lower pH, the bridging causes rapid acceleration of CS's gelation, with the mechanical behaviour of the resulting material possibly arising from transient interactions between PEI's amine groups and CS surface silanol groups. The cause of the strong interaction is likely PEI's highly branched structure, with many amine groups, which protonate to NH_3^+ in solution, providing

numerous bonding sites for CS silanol groups. The protonation of PEI's amine groups also gives it a basic effect on pH.

The rate of gelation of PAM/PEI mixture, and the strength and stability of the resulting gel, was found to depend on the temperature, the molecular weight of PAM, and the concentrations of PAM and PEI. The strength of PAM/PEI gels also increased with aging. Higher concentrations of PAM allowed faster gelation, due to the increased number of crosslinking amine groups, and they produced stronger and more stable gels because of the denser networks formed, with more crosslinking points (Ma et al., 2017). Higher PEI concentration also gave faster gelation, but only increased strength up to a critical concentration, above which syneresis occurred due to excessive crosslinking pulling the network in on itself and ejecting liquid (Ma et al., 2017). The value at which this happens depends on the particular gel system. PAM was found not to gel in the absence of any PEI. PAM of higher molecular weight gelled more readily and gave stronger and more flexible gels, but at the cost of much higher initial viscosity. The long chain nature of PAM polymers gives PAM/PEI gels greater flexibility than standard CS gels as the polymers are able to bend and flex, as opposed to the rigid nature of CS particles. By the same logic, gels made with PAM of higher molecular weight are more flexible. The reason why higher molecular weight gives greater strength is thought to be due to the higher hydrodynamic volumes of such polymers in solution, which leads to more entanglements, and therefore stronger gels (Ghriga et al., 2021; Ma et al., 2017). Higher temperatures increase the rate of gelation and strength gain by accelerating the transamination reaction between PAM and PEI, but they can also lead to syneresis, due to hydrolysation of PAM (Moradi-Araghi, 2000).

Counter to expectation, UCS tests on sand grouted with PAM/PEI gel found higher molecular weight PAM-5m to give lower yield strain than PAM-150k. This could be due to the nature of the how the sand and gel interact, and/or be due to the quality of grouting achieved with the different PAM varieties.

Small amounts of CS could be added to PAM-5m/PEI without greatly affecting the gel behaviour. 0.5 wt% of silica was found to slightly retard gelation, although this effect disappeared at higher silica wt% (1.0 wt%). Other authors have reported similar variable results, implying that the CS/PAM/PEI relationship is complex (Amir et al., 2022). Other

research has observed silica nanoparticles to increase the strength of PAM/PEI gel (Amir et al., 2022; Chen et al., 2018; Li et al., 2022; Liu et al., 2017; Ma et al., 2017; Shamlooh et al., 2019), although no effect on final gel strength was apparent here for low silica wt%. More complex mechanical testing is needed to evaluate this. The proposed mechanism for the strength increase is the adsorption of silica nanoparticles onto the PAM matrix via hydrogen bonding between CS's silanol and PAM's amide groups, whereupon they act as strengthening anchor points, without forming their own coherent network. Addition of larger quantities of silica greatly retarded (10.0 wt%), and eventually prevented gelation altogether (16.8 wt%). Ma et al. (2017) also found that higher silica wt% slowed gelation, and that excess silica loading beyond a critical concentration reduced strength, with this attributed to agglomeration of CS interfering with the flexibility of polymer chains, and with the PAM/PEI gelation reaction. There is, therefore, possibly a practical limit to the amount of CS which can be added to PAM/PEI, although this may depend on many factors, such as CS particle size, PAM molecular weight, etc.. Surface modification has been successfully used as to reduce the agglomeration of CS in PAM/PEI gel (Li et al., 2022).

Large quantities of silica (~ 40 wt%) could be added to PAM-150k solution and produced a waxy substance, both with and without the presence of PEI, when heated in the oven. The resulting materials were not like PAM/PEI or standard CS gels. It seems, therefore, that high temperature induces a reaction between the silica and PAM. This interaction was never observed at ambient temperature (~ 20°C), with CS/PAM suspensions in this study remaining stable over long durations, reinforcing the idea that temperature initiates the rection, rather than simply accelerating it. Additional analysis is needed to investigate the structure and mechanical properties of these materials.

8.5.3 PVA

Interaction between CS and PVA is affected by the pH, ionic strength, and chemical nature of the materials. PVA could be dissolved in CS using high temperature, and had minimal effect on pH. It did not significantly affect the behaviour of CS in th pH range 3-9.3, but at pH 1 phase separation occurred, with a condensed gel forming underneath a supernatant liquid layer. The increasing protonation of CS surface silanol groups at low pH presumably facilitates adsorption of PVA onto CS particles, where they act as bridges to form dense clusters of CS and polymer, which then settle out of suspension. Other studies have confirmed increased adsorption of PVA on silica at low pH (Chu et al., 2007; Kim et

al., 2009; Wiśniewska et al., 2016). However, the CS particles and/or polymer remain mobile enough to continue to form bonds and produce a gel network after settling. Further investigation is needed to determine the structure and mechanical properties of the condensed CS/PVA gels.

Adding NaCl also induced interaction of CS and PVA, causing delayed phase separation, and the formation of a soft, plastically-deforming gel beneath a small supernatant layer. This effect presumably arises from the NaCl screening the negative surface charge of CS particles, facilitating PVA adsorption, with coagulation and settling occurring through a bridging effect. As before, a gel then proceeds to form during, or soon after settling. The mechanical properties of the gel suggest the presence of transient interactions between the polymer and silica, such as hydrogen bonding of PVA's hydroxyl groups and CS's silanol groups.

PVA is also able to produce gels from solution without any additives by self-crosslinking at high concentrations brought about by drying, or locally high concentrations produced through freezing, in which ice crystals push polymer chains together. Through air-drying, ultra-strong, flexible, plastic-like gels were produced, although as PVA concentration approached 100 wt%, these became brittle, presumably due to excessive crosslinking limiting the movement of polymer chains. Through freeze-thaw cycling, strong flexible gels were created, with additional cycles giving improved mechanical properties as more crosslinking points are generated. Freeze-thaw PVA gels could also recover strength after being broken by undergoing an additional freeze-thaw cycle, thereby demonstrating the reversible nature of its physical crosslinking mechanism. In both air-drying and freeze-thaw methods, increased PVA concentration gave higher gel strength, due to increased crosslink density.

Freeze-thaw gels were also be produced from CS/PVA mixtures with 11 wt% of silica, giving much greater strength than PVA-only equivalents. As no electrolyte was used, it is assumed that the CS did not form its own gel network, but rather acted as anchor points in the PVA network, as has been proposed in other research (Khedr & Elhady, 2025). This conclusion is supported by rheometer tests showing the CS/PVA gel produced here to have far more similar behaviour to PVA-only gel than to standard CS gel.

8.5.4 Application

The variable behaviour of PEG at low and high concentrations in CS grout could allow for fine-tuning of PEG concentration (plus possibly molecular weight) to balance injectability, and end-state rigidity, for particular applications. At low wt%, PEG reduces network stiffness through the introduction of microdomains which yield under low stress, resulting in gel that retains its shape, but deforms plastically. On desaturation, these gels transition to xerogels without displaying any cracking, hence providing a promising avenue of research for injectable hydraulic barrier application, in which the near-zero diffusion coefficients could be combined with CS's low hydraulic conductivity. CS/PEG xerogels have the potential to act as robust and impermeable sealing materials, through which contaminants cannot migrate, neither through diffusion nor advection.

PAM/PEI gel's high flexibility compared to standard CS gel could give it significant advantages in certain applications, particularly if it can be successfully combined with CS grout's own beneficial properties. However, PAM/PEI's reliance on high temperature to gel makes it difficult to use in near-surface permeation grouting application. There are possible solutions to this, though, such as pre-heating the grout prior to injection, or utilising a catalyst or a more reactive crosslinker to increase reaction rate at low temperatures. Other applications, such as in grouting radioactive waste cannisters, could also provide sufficient heat on their own for PAM/PEI gelation to occur within a practical timescale.

Regarding PVA, the condensed CS/PVA gel produced at pH 1 is of interest, as its higher density could provide it with lower hydraulic conductivity and greater mechanical strength than standard CS grout, although it should be noted that such low pH conditions are not suitable for near-surface applications in soil. The soft, plastically deforming gel produced by addition of NaCl also could be useful in creating barriers which are resistant to cracking from damage. In either case, the variation with pH and salt content offers opportunities for tailoring gel structure and properties.

PVA gels had excellent mechanical properties, showed recoverability, and could be successfully made with high concentrations of silica through the freeze-thaw method. Such gels could be potentially be employed in grouting application through artificial ground freezing, a technique currently used for producing temporary hydraulic barriers

in soil by piping cryogens, such as liquid nitrogen, through the ground to freeze pore water (Alzoubi et al., 2020; Joudieh et al., 2024; Park et al., 2024; Teng et al., 2025; Wagner & Yarmak, 2012). This method can risk inducing ground heave at the surface, however, due to the expansion of water as it freezes (Joudieh et al., 2024; Park et al., 2024; Teng et al., 2025).

The fact that PVA solutions also form strong and flexible gels on drying, and return to a softer gel without dissolving on rewetting, could help them combat the effects of cracking in CS gels on repeated drying and re-wetting cycles (Pedrotti et al., 2020). PVA solutions are indeed already injected into soils to prevent cracking from both wet-dry and freeze-thaw cycles (Ren et al., 2025). Air-dried PVA gel could also possibly be employed as a spray coating to capture contaminated dust particles on surfaces, for example, in nuclear decommissioning.

Chapter 9: Conclusion

CS is a novel, low-cost, environmentally friendly, non-toxic permeation grout with significant advantages over conventional materials. It has water-like initial viscosity, nano-scale particle size, and precisely controllable gel times, allowing it to be injected with minimal pressure to fill free pore-spaces in soil, and penetrate deep into fissures in rock. The rigid hydrogel product of the grout also has very low hydraulic conductivity and exhibits good sorption of contaminants. These exceptional properties have led to significant research and some application of CS grout across a variety of fields, including as an injectable barrier for contaminated land remediation and waste management; preventing water ingression and seepage in tunnelling and underground construction; stabilising loose soils and mitigating against liquefaction; and for water shut-off and conformance control in oilfields. In spite of its excellent potential, however, wide-scale application of CS grout has thus far been limited, possibly due to its lower strength compared to cements, its somewhat higher material cost, and the lack of comprehensive models for describing its gelling behaviour, transport, and long-term stability in soils.

This thesis has reported on experimental investigations into factors controlling the strength evolution of CS grout during curing, and the physical mechanism which drives it; its ability to re-heal after suffering damage; and its combination with clays and polymers. The findings of these investigations are summarised in the following sections, along with potential ways in which this research could be continued and expanded upon in future.

9.1 Summary

9.1.1 Gelation

Viscometer tests showed that higher silica mass fractions and NaCl concentrations in CS grout exponentially accelerated its gelation and could be used to precisely control gel times. Smaller particle sizes also gave faster gelation. $CaCl_2$ was determined to be unsuitable for gelling MP 320 CS grout, however, as it caused rapid coagulation and phase separation, due to the higher charge density of Ca^{2+} compared to Na^{+} being too effective at screening CS particle surface charges.

9.1.2 Curing and re-healing

Shear vane and UCS tests found that the strength of CS grout and grouted soil increased with curing time according to power law relationships, attributed to continuous deposition and condensation of silicates at the joining points between particles in the gel network. SEM imaging was not able to demonstrate this effect, however. CS grout and grouted soil were also found to re-heal after breaking, before gaining strength again via power laws, although at a slowed rate compared to their curing. The similarity of the two phenomena led to the assumption that they are governed by the same effect. It is proposed that breaking reduced CS gel to a suspension of network fragments, which then quickly re-connected due to the ongoing presence of the conditions which initiated gelation. The gel then continues to gain strength via the same redistribution of silica as described for curing. As long a duration as possible should be allowed for CS grout to cure or re-heal, therefore, before conducting operations on or above grouted soil volumes, in order to ensure maximum strength.

Higher silica mass fraction and NaCl concentration both exponentially increased the strength of CS grout. It was also shown that the NaCl concentration could be used to offset the strength decrease from small reductions in silica content to lower cost without compromising mechanical performance. Smaller particle sizes were also found to increase the strength of CS grout during curing and re-healing, although the difference in surface area was not sufficient to explain the variation, implying that there may have been confounding factors relating to the particular grout varieties used (MP 320 and 325).

Higher salt concentrations in surrounding water accelerated the curing and re-healing of the grout, with $CaCl_2$ having a greater effect than doubling NaCl concentration. In the case of healing, the effect was proportional to the ionic strength. Samples cured in fresh water were relatively weaker, with diffusion of ions out of samples detected. Healing in water at pH 9 also gave greater strength than at pH7. It was suggested that higher electrolyte content and pH both promote dissolution of silica, which can then be redeposited at the weak joining points in the network to increase strength, although other theories were also discussed regarding the effect of electrolyte. Healing in additional CS also increased strength, presumably due to the added silica being able to dissolve and redeposit onto the existing gel network. A possible way to increase the strength of CS-grouted volumes

after installation, therefore, is to employ secondary injection of saline solution, such as $CaCl_2$, at alkaline pH, or even additional CS.

9.1.3 Addition of clay

Adding both kaolin and bentonite clays exponentially increased the viscosity and accelerated the gelation of CS grout, although bentonite had a far stronger effect due to its swelling behaviour. Significant quantities of kaolin could be added to the grout while maintaining viscosity suitable for permeation grouting. Replacing the silica content of the grout with kaolin had minimal effect on viscosity, and slowed gelation. NaCl concentration could be used to control the gelation of both CS/kaolin and CS/bentonite.

Adding kaolin was shown to increase the strength of CS/kaolin grout and grouted soil, although it had less effect than the silica concentration of the grout. CS/kaolin grout still increased in strength during curing and re-healed after damage according to power law relationships. Several mechanisms were suggested regarding kaolin's effect on the strength of CS grout.

Kaolin could be used to partially replace mass of silica in CS grout to reduce cost with a small decrease in strength. Bentonite's excellent properties, such as self-sealing and high sorption capacity, could be of great benefit in combination with CS grout.

9.1.4 Combination with polymers

Experiments were done to study the addition of polymers to CS grout, and investigate polymer hydrogels, aiming to form CS/polymer double-network nanocomposite gels with potential engineering application. In other fields, polymer hydrogels have been produced that are ultra-strong, flexible, and re-healable, which would be of great benefit in combination with CS grout. Three candidate polymers were identified via literature review, due to them being low cost, environmentally friendly and non-toxic, and having established gelation techniques: these were PEG, PAM, and PVA.

PEG could be dissolved in CS without interaction until the addition of NaCl, or reduction of pH. Two gel varieties were produced, depending on the amount of PEG added. At low PEG wt%, samples exhibited accelerated gelation, plastic deformation, and were apparently able to dry without cracking: these have potential as crack-resistant impermeable barriers. At higher PEG wt%, gels had greatly improved water retention, but at the cost of increased cracking. The interaction between PEG and CS arises from

adsorption of PEG onto CS particles, facilitated by suppression of CS's surface charge. At low PEG wt%, gelation is accelerated via bridging of the polymer, and transient interactions between PEG's ether groups and CS's surface silanols produce the plastic behaviour. At high PEG wt%, polymer chains coat particle surfaces, slowing gelation via a steric effect, and inhibiting bonding between particles, weakening structure.

PAM could be dissolved in CS with little effect, but its crosslinking agent PEI induced flocculation. PAM/PEI gels were produced using high molecular weight PAM (PAM-5m), which had high flexibility, but at the cost of high initial viscosity. Small quantities of CS could be added to these (up to 1 wt%), but no change in mechanical properties was noted. At higher silica wt%, gelation was slowed and eventually prevented, due to agglomeration of silica. PAM/PEI gels using lower PAM molecular weight (PAM-150k) were weaker and needed higher temperatures to gel, but had low initial viscosity, and could be mixed with high silica concentrations (~ 40 wt%). The increased temperature induced a reaction between PAM and CS (regardless of PEI content) to produce wax-like materials.

PVA could be dissolved in CS and would interact on addition of salt, or on lowering pH to 1. In the former case, a soft, plastically-deforming gel formed with potential for use as a crack-resistant grout. At pH 1, a condensed gel formed after phase separation, with potentially reduced hydraulic conductivity and increased strength, due to its greater density. PVA gels were created with excellent strength and flexibility through drying and freeze-thaw methods, due to PVA's ability to form self-crosslinks at high concentration. High quantities of CS could be added to freeze-thaw PVA gels, and improved their mechanical properties. These gels could be applied in the field via artificial ground freezing. Air-dry PVA gels could also be used as a spray coating for contaminated surfaces.

9.2 Future work

The research in this thesis could be continued and expanded upon in a variety of ways, as described in the following section:

- Shear and UCS tests could be conducted to better characterise the effect of groundwater pH on the strength of CS grout and grouted soil during curing and re-healing, testing across a fuller range of pH, as opposed to just pH 7 and 9, as was done here.

- A greater range of electrolytes could be used to investigate whether ionic strength is the determining factor in the effect of salts on the rate of strength increase during curing and re-healing, or if there are ion-specific effects at play, relating to, for example, the hydration behaviour of different cations. Monovalent salts with cations in the Hofmeister series (e.g., K^+ and Cs^+) could be studied, as well as common multivalent cations (e.g., Mg^{2+} and Al^{3+}), or anions (e.g., SO_4^{2-} and CO_3^{2-}).
- Additional structural analysis could be carried out to attempt to confirm the mechanisms proposed here for curing and re-healing, and to study the effect of different factors on these, as it was not possible to do so in this research using SEM. In pursuit of this aim, data was recorded for various CS grout samples using small angle x-ray and neutron scattering (SAXS and SANS), but there was not sufficient time to analyse the results and include them in the present thesis.
- Given the highly advantageous properties of bentonite, its combination with CS grout could be further investigated to characterise its effect on mechanical properties, contaminant sorption, hydraulic conductivity, and self-healing, with SEM imaging to investigate the microstructure of the grout.
- Further investigation could be carried out on some of the promising CS/polymer grout variants produced here, including additional mechanical and rheological testing, and microstructural analysis, for example using SEM. With further study, it may be possible to produce double-network silica-polymer nanocomposite gels, which combine the excellent properties of polymer gels with CS's own benefits. One potential way to achieve this could be to use lowered pH to gel the silica in CS/PVA mixtures, before employing freeze-thaw to gel the PVA in a two-stage process.

References

Abdelfatah, E. (2018). Modeling of Aggregation and Gelation of Nanoparticles Using Quadrature Method of Moments. *Petroleum & Petrochemical Journal*, *2*(2), 1-16.

Abhilash, P. P., Nayak, D. K., Sangoju, B., Kumar, R., & Kumar, V. (2021). Effect of nano-silica in concrete; a review. *Construction and Building Materials*, *278*, 122347.

Adibnia, V., & Hill, R. J. (2017). Viscoelasticity of near-critical silica-polyacrylamide hydrogel nanocomposites. *Polymer*, *112*, 457-465.

Agapoulaki, G. I., & Papadimitriou, A. G. (2018). Rheological Properties of Colloidal Silica Grout for Passive Stabilization Against Liquefaction. *Journal of Materials in Civil Engineering*, *30*(10), 04018251.

Aggarwal, P., Singh, R. P., & Aggarwal, Y. (2015). Use of nano-silica in cement based materials—A review. *Cogent Engineering*, *2*, 1078018.

Ahmad, S., Ahmad, S., & Sheikh, J. N. (2023). Silica centered aerogels as advanced functional material and their applications: A review. *Journal of Non-crystalline Solids*, *611*, 122322.

Ainomugisha, S., Matovu, M. J., & Manga, M. (2024). Influence mechanisms of silica nanoparticles' property enhancement in cementitious materials and their green synthesis: A critical review. *Case Studies in Construction Materials*, *20*, e03372.

Akbari, S., Mahmood, S. M., Tan, I. M., Ghaedi, H., & Ling, O. L. (2017). Assessment of Polyacrylamide Based Co-Polymers Enhanced by Functional Group Modifications with Regards to Salinity and Hardness. *Polymers*, *9*, 647.

Aksu, G., & Eskisar, T. (2023). The geomechanical properties of soils treated with nanosilica particles. *Journal of Rock Mechanics and Geotechnical Engineering*, *15*, 954-969.

Al-Moshin, A. M., Sherief, M. H., Alabdrabalnabi, M. I., & Muhammad, A. (2022). Colloidal NaSil Squeeze Operation to Successfully Isolate Water Zone in Horizontal Well. *The Aramco Journal of Technology*(Fall 2022), 2-13.

Al-Mulali, M. Z., Aljoumaily, Z. S., Ibrahim, T. H., Albayati, A. H., Oukaili, N. K., Al-Kheetan, M. J., & Ghaffar, S. H. (2026). Performance Analysis of Cement Mortar Modified with Nano-Silica and Nano-Alumina. *Buildings*, *16*, 929.

Albarran, N., Missana, T., García-Gutiérrez, M., Alonso, U., & Mingarro, M. (2011). Strontium migration in a crystalline medium: effects of the presence of bentonite colloids. *Journal of Containment Hydrology*, *122*, 76-85.

Alberdi, J., Barcala, J. M., Campos, R., Cuevas, A. M., & Fernandez, E. (2000). *FEBEX project: full-scale engineered barriers experiment for a deep geological repository for high level radioactive waste in crystalline host rock. Final report*.

Alghrairi, N., Aziz, F. N. A., Rashid, S. A., Bin Mohamed, M. Z., & Ibrahim, A. M. (2024). Impact of nano-silica on the mechanical properties of lightweight concrete. *IOP Conference Series: Earth and Environmental Science*, *1369*, 012033.

Ali, A., Al Ramadan, M., & Aljawad, M. S. (2024). Long-Term Investigation of Nano-Silica Gel for Water Shut-Off in Fractured Reservoirs. *Gels*, *10*, 651.

Ali, A., Al Ramadan, M., Aljawad, M. S., Elsayed, M., & Almohsin, A. (2024). Experimental Study of Nanosilica Gel as a Water Shut-Off Agent in Fractured Reservoirs. *Energy & Fuels*, *38*, 7167-7180.

Ali, A., Alabdrabalnabi, M., Al Ramadan, M., Aljawad, M. S., Almohsin, A., & Azad, M. (2024). A Review of Recent Developments in Nanomaterial Agents for Water Shutoff in Hydrocarbon Wells. *ACS Omega*, *9*(13), 14728-14746.

Ali, A. R. M., & Aziz, L. J. (2021). A Proposed Approach of Improving Soil Around a Single Lateral Loaded Pile Model by using Nano-Silica Sandy Soil Mixture Material. *IOP Conference Series: Materials Science and Engineering*, *1094*, 012014.

Allen, L. H., & Matijević, E. (1969). Stability of Colloidal Silica: 1. Effect of Simple Electrolytes. *Journal of Colloid and Interface Science*, *31*(3), 287-296.

Almoshin, A. M., Alabdrabalnabi, M. I., Sherief, M. H., & Almubarak, T. (2025). Selective Zonal Isolation in Horizontal Wells Using Colloidal Nanosilica. *ACS Omega*, *10*, 5489-5502.

Alonso, M. C., Calvo, J. L. G., Cuevas, J., Turrero, M. J., Fernández, R., Torres, E., & Ruiz, A. I. (2017). Interaction processes at the concrete-bentonite interface after 13 years of FEBEX-Plug operation. Part I: Concrete alteration. *Physics and Chemistry of the Earth*, *99*, 38-48.

Alsmaeil, A. W., Mohammed, S., Aldakkan, B. S., Chalmpes, N., Kouloumpis, A., Potsi, G., Galvin, A., Gadikota, G., Kanj, M. Y., & Giannelis, E. P. (2023). Fine-Tuning the Surface and Interfacial Chemistry of Silica Nanoparticles to Control Stability in High Ionic Strength Electrolytes and Modulate Assembly at Oil−Water Interfaces. *Chemistry of Materials*, *35*, 9150-9159.

AlTawaiha, H., Alhomaidat, F., & Eljufout, T. (2023). A Review of the Effect of Nano-Silica on the Mechanical and Durability Properties of Cementitious Composites. *Infrastructures*, *8*, 132.

Althoey, F., Zaid, O., Martínez-García, R., Alsharari, F., Ahmed, M., & M. Arbili, M. (2023). Impact of Nano-silica on the hydration, strength, durability, and microstructural properties of concrete: A state-of-the-art review. *Case Studies in Construction Materials*, *18*, e01997.

Alzoubi, M. A., Xu, M., Hassani, F. P., Poncet, S., & Sasmito, A. P. (2020). Artificial ground freezing: A review of thermal and hydraulic aspects. *Tunnelling and Underground Space Technology*, *104*, 103534.

Amir, Z., Saaid, I. M., Junaidi, M. U. M., & Bakar, W. Z. W. (2022). Weakened PAM/PEI Polymer Gel for OilfieldWater Control: Remedy with Silica Nanoparticles. *Gels*, *8*, 265.

Amir, Z., Said, I. M., & Jan, B. M. (2018). In situ organically cross-linked polymer gel for high-temperature reservoir conformance control: A review. *Polymers for Advanced Technologies*, *30*, 13-39.

Anindita, S. N., Conti, R., Zauchner, D., Paunović, N., Qiu, W., Buzhor, M. G., Krivitsky, A., Luo, Z., Müller, R., Grützmacher, H., Qin, X.-H., Leroux, J.-C., & Bao, Y. (2023). Tough PEG-only hydrogels with complex 3D structure enabled by digital light processing of "all-PEG" resins. *Aggregate*, *4*, e368.

Anyaezu, T., Musaab, M., & Salehi, S. (2023). Experimental investigation of PAM/PEI polymer mud for reducing lost circulation in high-temperature formations. *Geothermics*, *114*, 102786.

Apps, J. A., Persoff, P., Moridis, G., & Pruess, K. (1998). *Method for Formation of Subsurface Barriers Using Viscous Colloids* (USA Patent No. 5836390). U. S. P. Office.

Arcos, D., Grandia, F., & Domènech, C. (2006). *Geochemical evolution of the near field of a KBS-3 repository* (TR-06-16).

Arvidsson, A., Josefsson, P., Eriksson, P., Sandén, T., & Ojala, M. (2015). *System design of backfill - Project results* (TR-14-20).

Ashcroft, B., Woldmo, O., Neby, A., Berger, J., Nome, A. E., & Nomeland, T. (2025). Oslo's Fornebu Line metro project, part K2A – a grouting project with systematic

tunnelling? In F. Johansson, A. Ansell, D. Johansson, J. Funehag, & J. Norrman (Eds.), *Tunnelling into a Sustainable Future - Methods and Technologies* (1 ed.). CRC Press.

Audsley, A., & Aveston, J. (1962). 446. The polymerization of silicic acid [10.1039/JR9620002320]. *Journal of the Chemical Society (Resumed)*(0), 2320-2329.

Axelsson, M. (2006). Mechanical tests on a new non-cementitious grout, silica sol: A laboratory study of the material characteristics. *Tunnelling and Underground Space Technology*, *21*(5), 554-560.

Aziz, A. A., Nassar, H. F., Al-Shemy, M. T., & Mohamed, O. A. (2025). Boosting the mechanical performance and fire resistivity of white ordinary portland cement pastes via biogenic mesoporous silica nanoparticles. *Scientific Reports*, *15*, 2909.

Badley, R. D., Ford, W. T., McEnroe, F. J., & Assinks, R. A. (1990). Surface Modification of Colloidal Silica. *Langmuir*, *6*, 792-801.

Bahadur, A., Holter, K., & Pengelly, A. (2007, May). Cost-effective pre-injection with rapid hardening microcement and colloidal silica for water ingress reduction and stabilisation of adverse conditions in a headrace tunnel. World Tunnel Congress 2007 and 33rd ITA/AITES Annual General Assembly, Prague, Czech Republic.

Baird, J. C., & Walz, J. Y. (2006). The effects of added nanoparticles on aqueous kaolinite suspensions: I. Structural effects. *Journal of Colloid and Interface Science*, *297*, 161-169.

Baird, J. C., & Walz, J. Y. (2007). The effects of added nanoparticles on aqueous kaolinite suspensions: II. Rheological effects. *Journal of Colloid and Interface Science*, *306*, 411-420.

Bakaic, E., Smeets, N. M. B., & Hoare, T. (2015). Injectable hydrogels based on poly(ethylene glycol) and derivatives as functional biomaterials. *RSC Advances*, *5*, 35469.

Bakhshandeh, F., Noorzad, R., & Ta'Negonbadi, B. (2025). Experimental investigation of the properties of collapsible soil stabilized by colloidal silica. *Scientific Reports*, *15*(1).

Barbhuiya, G. H., Moiz, M. A., Hasan, S. D., & Zaheer, M. M. (2020). Effects of the nanosilica addition on cement concrete: A review. *Materials Today: Proceedings*, *32*, 560-566.

Basilio, E., Zougheib, S., Sahu, Q., Almohsin, A., Alabdrabalnabi, M., & Hoteit, H. (2025). Predicting gelation kinetics of colloidal silica for water shut-off treatments: A novel Arrhenius-based model. *Physics of Fluids*, *37*(4).

Batuk, D. N., Shiryaev, A. A., Kalmykov, S. N., Batuk, O. N., Romanchuk, A. Y., Shirshin, E. A., & Zubavichus, Y. V. (2011). Sorption and Speciation of Uranium on Silica Colloids. In S. N. Kalmykov & M. A. Denecke (Eds.), *Actinide Nanoparticle Research* (pp. 315-332). Springer.

Baxter, S., & Bryant, K. C. (1952). Silica Sols. Part III.* Accelerated Gelation, and Particle Size. *Journal of the Chemical Society*, 3024.

Bercea, M., Morariu, S., & Rusu, D. (2013). In situgelation of aqueous solutions of entangled poly(vinyl alcohol). *Soft Matter*, *9*(4), 1244-1253.

Bergaya, F., Theng, B. K. G., & Lagaly, G. (2006). *Handbook of Clay Science*. Elsevier.

Bergna, H. E., & Roberts, W. O. (2006). *Colloidal Silica: Fundamentals and Applications*. CRC Press.

Bernal-Chávez, S. A., Alcalá-Alcalá, S., Almarhoon, Z. M., Turgumbayeva, A., Gürer, E. S., Campos-Echeverria, M. D. L. D., Cortés, H., Romero-Montero, A., Prado-Audelo, M. L. D., Sharifi-Rad, J., & Leyva-Gómez, G. (2023). Novel ultra-stretchable and

self-healing crosslinked poly (ethylene oxide)-cationic guar gum hydrogel. *Journal of Biological Engineering*, *17*, 64.

Bird, P. G. (1941). *Colloidal Solutions of Inorganic Oxides* (USA Patent No. U. S. P. Office.

Birid, K., & Varak, S. (2024). Stabilisation of subsoil using colloidal silica beneath shallow foundation: a case study. *Proceedings of the Institution of Civil Engineers - Ground Improvement*, *178*(1), 49-61.

Bischoff, M., Biriukov, D., Předota, M., & Marchioro, A. (2021). Second Harmonic Scattering Reveals Ion-Specific Effects at the SiO_2 and TiO_2 Nanoparticle/Aqueous Interface. *The Journal of Physical Chemistry C*, *125*, 25261-25274.

Bish, D. L. (1998). *Smectite Dehydration and Stability: Applications to Radioactive Waste Isolation at Yucca Mountain, Nevada* (LA-21023-MS).

Blute, I., Pugh, R. J., van de Pas, J., & Callaghan, I. (2007). Silica nanoparticle sols 1. Surface chemical characterization and evaluation of the foam generation (foamability). *Journal of Colloid and Interface Science*, *313*(2), 645-655.

Bodvarsson, G. S., Boyle, W., Patterson, R., & Williams, D. (1999). Overview of scientific investigations at Yucca Mountain—the potential repository for high-level nuclear waste. *Journal of Containment Hydrology*, *38*, 3-24.

Boiero, A., Romero, E., Arroyo, M., & Spagnoli, G. (2026). Enhanced soil-pile friction using colloidal silica grouting in granular soils. *Geomechanics for Energy and the Environment*, *45*, 100780.

Bolt, G. H. (1957). Determination of the Charge Density of Silica Sols. *The Journal of Physical Chemistry*, *61*(9), 1166-1169.

Bots, P., Renshaw, J. C., Payne, T. E., Comarmond, M. J., Schellenger, A. E. P., Pedrotti, M., Calì, E., & Lunn, R. J. (2020). Geochemical evidence for the application of nanoparticulate colloidal silica gel for in situ containment of legacy nuclear wastes. *Environmental Science: Nano*, *7*(5), 1481-1495.

Brinker, C. J., & Scherer, G. W. (1990). *Sol-Gel Science: The Physics and Chemistry of Sol-Gel Processing*. Academic Press.

Buettner, N., Iyacu, G., & Akono, A.-T. (2024). Colloidal nanosilica promotes high-density calcium-silicate-hydrates in fine recycled concrete aggregate mortar. *Cement and Concrete Research*, *180*, 107498.

Butrón, C., Axelsson, M., & Gustafson, G. (2009). Silica sol for rock grouting: Laboratory testing of strength, fracture behaviour and hydraulic conductivity. *Tunnelling and Underground Space Technology*, *24*, 603-607.

Butrón, C., Gustafson, G., Fransson, Å., & Funehag, J. (2010). Drip sealing of tunnels in hard rock: A new concept for the design and evaluation of permeation grouting. *Tunnelling and Underground Space Technology*, *25*, 114-121.

Caliari, S. R., & Burdick, J. A. (2016). A practical guide to hydrogels for cell culture. *Nature Methods*, *13*(5), 405-414.

Cao, C., Cai, M., Zhao, L., & Li, G. (2024). Improving Water Stability of Soil Aggregates with Polyvinyl Alcohol as a Polymeric Binder. *Polymers*, *16*, 1758.

Cao, X., Zheng, L., Hou, D., & Hu, L. (2019). On the long-term migration of uranyl in bentonite barrier for high-level radioactive waste repositories: The effect of different host rocks. *Chemical Geology*, *525*, 46-57.

Carneiro, L. d. R. S., Houmard, M., Rocha, V. V., & Ludvig, P. (2022). The Effect of Nanosilica Incorporation on the Properties of Cement-Based Materials with and Without other Supplementary Admixtures – A Literature Review. *The Open Construction and Building Technology Journal*, *16*, e187483682207290.

Carroll, S. A., Maxwell, R. S., Bourcier, W., Martin, S., & Hulsey, S. (2002). Evaluation of silica-water surface chemistry using NMR spectroscopy. *Geochimica et Cosmochimica Acta*, *66*(6), 913-926.

Chai, J.-C., Miura, N., & Koga, H. (2005). Lateral Displacement of Ground Caused by Soil–Cement Column Installation. *Journal of Geotechnical and Geoenvironmental Engineering*, *131*(5), 623-632.

Chandler, H. D. (2019). A physical basis for non-Newtonian power-law viscosity. *Soft Materials*, *17*(2), 137-142.

Chang, S.-y., Liu, L., & Asher, S. A. (1994). Preparation and Properties of Tailored Morphology, Monodisperse Colloidal Silica-Cadmium Sulfide Nanocomposites. *Journal of the American Chemical Society*, *116*, 6739-6744.

Changizi, F., & Haddad, A. (2015). Strength properties of soft clay treated with mixture of nano-SiO_2 and recycled polyester fiber. *Journal of Rock Mechanics and Geotechnical Engineering*, *7*, 367-378.

Chen, L., Wang, J., Yu, L., Zhang, Q., Fu, M., Zhao, Z., & Zuo, J. (2018). Experimental Investigation on the Nanosilica-Reinforcing Polyacrylamide/Polyethylenimine Hydrogel for Water Shutoff Treatment. *Energy & Fuels*, *32*(6), 6650-6656.

Chen, Q., Chen, H., Zhu, L., & Zheng, J. (2015). Fundamentals of double network hydrogels. *Journal of Materials Chemistry B*, *3*(18), 3654-3676.

Cheng, M., Zeng, Y., Chen, L., & Yang, H. (2022). Long-term compressive strength and hydraulic property of nanosilica-improved sand in different soaking environments. *Materials Today Communications*, *33*, 104853.

Chirani, N., Gritsch, L., Motta, F. L., & Fare, S. (2015). History and applications of hydrogels. *Journal of biomedical sciences*, *4*(2).

Chiranjeevi, K., Abraham, M., Rath, B., & Praveenkumar, T. R. (2023). Enhancing the properties of geopolymer concrete using nano-silica and microstructure assessment: a sustainable approach. *Scientific Reports*, *13*, 17302.

Cho, W. J., Lee, J. O., & Chun, K. S. (1999). The temperature effects on hydraulic conductivity of compacted bentonite. *Applied Clay Science*, *14*, 47-58.

Choi, Y.-C. (2025). The Effect of Colloidal Nano-Silica on the Initial Hydration of High-Volume Fly Ash Cement. *Materials*, *18*, 2769.

Choobbasti, A. J., & Kutanaei, S. S. (2017). Microstructure characteristics of cement-stabilized sandy soil using nanosilica. *Journal of Rock Mechanics and Geotechnical Engineering*, *9*, 981-988.

Choobbasti, A. J., Vafaei, A., & Kutanaei, S. S. (2015). Mechanical Properties of Sandy Soil Improved with Cement and Nanosilica. *Open Engineering*, *5*, 111-116.

Chu, W.-B., Yang, J.-W., Liu, T.-J., Tiu, C., & Guo, J. (2007). The effects of pH, molecular weight and degree of hydrolysis of poly(vinyl alcohol) on slot die coating of PVA suspensions of TiO_2 and SiO_2. *Colloids and Surfaces A: Physicochemical and Engineering Aspects*, *302*, 1-10.

Ciardi, G., Bardotti, R., Vannucchi, G., & Madiai, C. (2020). Effects of high-diluted colloidal silica grouting on the behaviour of a liquefiable sand. *Geotechnical Research*, *7*(4), 193-208.

Clapsadle, L. J., & Syracuse, M. G. (1953). *Nongelling Aqueous Silica Sols Stabilized with Boron Compounds* (USA Patent No. 2630410). U. S. P. Office.

Conlee, C. T. (2010). *Dynamic properties of colloidal silica soils using centrifuge model tests and a full-scale field test* [Doctoral dissertation, Drexel University]. Philidelphia, PA.

Craig, R. F. (2004). *Craig's Soil Mechanics* (7 ed.). Spoon Press.

Cui, X., Wang, C., Huang, W., Zhang, S., Chen, H., Wu, B., Qin, D., & Zheng, X. (2023). Multiple Hydrogen Bonding-Assisted High-Strength Hydrogel of Silica/Polyacrylamide Nanocomposite Cross-Linked with Polyethylenimine. *ACS Omega*, *8*, 39401-39407.

Dadache, D., Rouabah, F., Bencid, A., & Barka, F. (2025). *Formation of PVA-SiO 2 hybrid fi lms by Sol-Gel method: Effect of processing parameters and SiO 2 content onthe structure and physico-chemical properties* [PREPRINT].

Deng, Z., Wang, H., Ma, P. X., & Guo, B. (2020). Self-healing conductive hydrogels: preparation, properties and applications. *Nanoscale*, *12*, 1224.

Depasse, J., & Watillon, A. (1969). The Stability of Amorphous Colloidal Silica. *Journal of Colloid and Interface Science*, *33*(3), 430-438.

Derjaguin, B., & Landau, L. (1941). Theory of the stability of strongly charged lyophobic sols and of the adhesion of strongly charged particles in solutions of electrolytes. *Acta Physicochimica URSS*, *14*(1), 633-662.

Di Giuseppe, E., Davaille, A., Mittelstaedt, E., & François, M. (2012). Rheological and mechanical properties of silica colloids: from Newtonian liquid to brittle behaviour. *Rheologica Acta*, *51*(5), 451-465.

Dietler, G., Aubert, C., Cannell, D. S., & Wiltzius, P. (1986). Gelation of Colloidal Silica. *Physical Review Letters*, *57*(24), 3117-3120.

Dixon, D., Sandén, T., Jonsson, E., & Hansen, J. (2011). *Backfilling of deposition tunnels: Use of bentonite pellets* (P-11-44).

Dohrmann, R., Kaufhold, S., & Lundqvist, B. (2013). Chapter 5.4 - The Role of Clays for Safe Storage of Nuclear Waste. In F. Bergaya & G. Lagaly (Eds.), *Developments in Clay Science* (Vol. 5, pp. 677-710). Elsevier.

Dollimore, D., & Heal, G. R. (1962). The Influence of pH on the Surface Characteristics of Silica Gel Soaked in Aqueous Solutions. *Journal of Applied Chemistry*, *12*, 445-450.

Döpke, M. F., Lützenkirchen, J., Moultos, O. A., Siboulet, B., Dufrêche, J.-F. o., Padding, J. T., & Hartkamp, R. (2019). Preferential Adsorption in Mixed Electrolytes Confined by Charged Amorphous Silica. *The Journal of Physical Chemistry C*, *123*, 16711-16720.

Durmusoglu, E., & Yavuz Corapcioglu, M. (2000). Experimental Study of Horizontal Barrier Formation by Colloidal Silica. *Journal of Environmental Engineering*, *126*(9), 833-841.

Duval, Y., Mielczarski, J. A., Pokrovsky, O. S., Mielczarski, E., & Ehrhardt, J. J. (2002). Evidence of the Existence of Three Types of Species at the Quartz−Aqueous Solution Interface at pH 0−10: XPS Surface Group Quantification and Surface Complexation Modeling. *The Journal of Physical Chemistry B*, *106*(11), 2937-2945.

Fan, L., Ge, X., Qian, Y., Wei, M., Zhang, Z., Yuan, W.-E., & Ouyang, Y. (2020). Advances in Synthesis and Applications of Self-Healing Hydrogels. *Frontiers in Bioengineering and Biotechnology*, *8*.

Fang, Y., Wang, J., Ma, H., Wang, L., Qian, X., & Qiao, P. (2021). Performance enhancement of silica fume blended mortars using bio-functionalized nano-silica. *Construction and Building Materials*, *312*, 125467.

Fernández, R., Torres, E., Ruiz, A. I., Cuevas, J., Alonso, M. C., Calvo, J. L. G., Rodríguez, E., & Turrero, M. J. (2017). Interaction processes at the concrete-bentonite interface after 13 years of FEBEX-Plug operation. Part II: Bentonite contact. *Physics and Chemistry of the Earth*, *99*, 49-63.

Finsterle, S., Moridis, G. J., Pruess, K., & Persoff, P. (1994). *Physical Barriers Formed From Gelling Liquids: 1. Numerical Design of Laboratory and Field Experiments* (LBL-35113).

Fraccica, A., Spagnoli, G., Romero, E., Arroyo, M., & Gómez, R. (2022). Permeation grouting of silt-sand mixtures. *Transportation Geotechnics*, *36*, 100800.

Fu, Q., Zhao, X., Zhang, Z., Xu, W., & Niu, D. (2022). Effects of nanosilica on microstructure and durability of cement-based materials. *Powder Technology*, *404*, 117447.

Funehag, J., & Fransson, Å. (2006). Sealing narrow fractures with a Newtonian fluid: Model prediction for grouting verified by field study. *Tunnelling and Underground Space Technology*, *21*, 492-498.

Funehag, J., & Gustafson, G. (2008a). Design of grouting with silica sol in hard rock - New methods for calculation of penetration length, Part I. *Tunnelling and Underground Space Technology*, *23*, 1-8.

Funehag, J., & Gustafson, G. (2008b). Design of grouting with silica sol in hard rock – New design criteria tested in the field, Part II. *Tunnelling and Underground Space Technology*, *23*, 9-17.

Gaharwar, A. K., Rivera, C., Wu, C.-J., Chan, B. K., & Schmidt, G. (2013). Photocrosslinked nanocomposite hydrogels from PEG and silica nanospheres: Structural, mechanical and cell adhesion characteristics. *Materials Science and Engineering C*, *33*, 1800-1807.

Gallagher, P. M. (2000). *Passive Site Remediation for Mitigation of Liquefaction Risk* [Doctoral dissertation, Virginia Polytechnic Institute and State University]. Blacksburg, VA.

Gallagher, P. M., Conlee, C. T., & Rollins, K. M. (2007). Full-Scale Field Testing of Colloidal Silica Grouting for Mitigation of Liquefaction Risk. *Journal of Geotechnical and Geoenvironmental Engineering*, *133*(2), 186-196.

Gallagher, P. M., & Finsterle, S. (2004). Physical and Numerical Model of Colloidal Silica Injection for Passive Site Stabilization. *Vadose Zone Journal*, *3*, 917-925.

Gallagher, P. M., & Lin, Y. (2009). Colloidal Silica Transport through Liquefiable Porous Media. *Journal of Geotechnical and Geoenvironmental Engineering*, *135*(11), 1702-1712.

Gallagher, P. M., & Mitchell, J. K. (2002). Influence of colloidal silica grout on liquefaction potential and cyclic undrained behavior of loose sand. *Soil Dynamics and Earthquake Engineering*, *22*, 1017–1026.

Gallagher, P. M., Spatari, S., & Cucura, J. (2013). Hybrid life cycle assessment comparison of colloidal silica and cement grouted soil barrier remediation technologies. *Journal of Hazardous Materials*, *250-251*, 421-430.

Gao, G., Xiao, Y., Wanga, Q., & Fu, J. (2016). Synergistic toughening of nanocomposite double network hydrogels by physical adsorption and chemical bonding of polymer chains to inorganic nanospheres and nanorods: a comparative study. *RSC Advances*, *6*, 37974.

Gao, Y.-Q., Cheng, H.-B., Li, G.-H., Li, H.-Y., Tan, H.-G., Zhang, J., & Zhu, D.-Y. (2026). Gelation and reservoir conformance control performance of in situ crosslinked polymer gels prepared with different crosslinkers. *Petroleum Science*.

Garcia Cordeiro Tessarolli, F., De Souza Gomes, A., & Regina Elias Mansur, C. (2018). Hydrogels Applied for Conformance-Improvement Treatment of Oil Reservoirs. In S. Haider & A. Haider (Eds.), *Hydrogels*. IntechOpen.

Gargallo, L., & Radić, D. (2009). *Physiochemical Behaviour and Supramolecular Organization of Polymers* (1 ed.). Springer.

Georgiannou, V., Pavlopoulou, E.-M., & Bikos, Z. (2017). Mechanical behaviour of sand stabilised with colloidal silica. *Geotechnical Research*, *4*(1), 1-11.

Ghadr, S., Assadi-Langroudi, A., Hung, C., O'Kelly, B. C., Bahadori, H., & Ghodsi, T. (2020). Stabilization of Sand with Colloidal Nano-Silica Hydrosols. *Applied Sciences*, *10*, 5192.

Ghaffari, Z., Rezvani, H., Khalilnezhad, A., Cortes, F. B., & Riazi, M. (2022). Experimental characterization of colloidal silica gel for water conformance control in oil reservoirs. *Scientific Reports*, *12*, 9628.

Ghriga, M. A., Grassl, B., Gareche, M., Khodja, M., Lebouachera, S. E. I., Andreu, N., & Drouiche, N. (2019). Review of recent advances in polyethylenimine crosslinked polymer gels used for conformance control applications. *Polymer Bulletin*, *76*(11), 6001-6029.

Ghriga, M. A., Lebouachera, S. E. I., Drouiche, N., & Grassl, B. (2021). Investigating the viscoelastic behavior of partially hydrolyzed polyacrylamide/polyethylenimine mixtures. *Journal of Polymer Research*, *28*, 275.

Gu, S., Shi, Y., Wang, L., Liu, W., & Song, Z. (2013). Modification of colloidal silica with sodium aluminate aluminate. *Applied Mechanics and Meterials*, *468*, 39-42.

Guggenheim, S. (1995). Definition of Clay and Clay Mineral: Joint Report of the AIPEA Nomenclature and CMS Nomenclature Committees. *Clays and Clay Minerals*, *43*(2), 255-256.

Guo, X.-J., Zhang, D., Xue, C.-H., Liu, B.-Y., Huang, M.-C., Wang, H.-D., Wang, X., Deng, F.-Q., Pu, Y.-P., & An, Q.-F. (2023). Scalable and Mechanically Durable Superhydrophobic Coating of SiO_2/Polydimethylsiloxane/Epoxy Nanocomposite. *ACS Applied Materials & Interfaces*, *15*, 4612-4622.

Hæreid, S., Anderson, J., Einarsrud, M. A., Hua, D. W., & Smith, D. M. (1995). Thermal and temporal aging of TMOS-based aerogel precursors in water. *Journal of Non-crystalline Solids*, *185*, 221-226.

Hakem, N., Al Mahamid, I., Apps, J., & Moridis, G. J. (1997). *Sorption of Cesium and Strontium on Savannah River Soils Impregnated with Colloidal Silica* International Containment Technology Conference, Petersburg, FL (United States).

Hamada, H., Shi, J., Yousif, S. T., Al Jawahery, M., Tayeh, B., & Jokhio, G. (2023). Use of nano-silica in cement-based materials – a comprehensive review. *Journal of Sustainable Cement-Based Materials*, *12*(10), 1286-1306.

Hamderi, M., & Gallagher, P. M. (2015). Pilot-scale modeling of colloidal silica delivery to liquefiable sands. *Soils and Foundations*, *55*(1), 143-153.

Han, L., Yan, L., Wang, K., Fang, L., Zhang, H., Tang, Y., Ding, Y., Weng, L.-T., Xu, J., Weng, J., Liu, Y., Ren, F., & Lu, X. (2017). Tough, self-healable and tissue-adhesive hydrogel with tunable multifunctionality. *NPG Asia Materials*, *9*(4), e372-e372.

Hatami, S., Hughes, T. J., Sun, H., Roshan, H., & Walsh, S. D. C. (2021). On the application of silica gel for mitigating CO2 leakage in CCS projects: Rheological properties and chemical stability. *Journal of Petroleum Science and Engineering*, *207*, 109155.

Haugsand, M. H., Neby, A., & Woldmo, O. (2025). Innovative data insights from high-resolution grout logs at Fornebubanen Metro Line. In F. Johansson, A. Ansell, D. Johansson, J. Funehag, & J. Norrman (Eds.), *Tunnelling into a Sustainable Future – Methods and Technologies* (1 ed.). CRC Press.

He, W., Wu, D., Li, J., Zhang, K., Xiang, Y., Long, L., Qin, S., Yu, J., & Zhang, Q. (2013). Surface Modification of Colloidal Silica Nanoparticles: Controlling the size and Grafting Process. *Bulletin of the Korean Chemical Society*, *34*(9), 2747.

Hemphill, G. B. (2013). *Practical Tunnel Construction*. John Wiley & Sons.

Hendrix, D., McKeon, J., & Wille, K. (2019). Behavior of Colloidal Nanosilica in an Ultrahigh Performance Concrete Environment Using Dynamic Light Scattering. *Materials*, *12*, 1976.

Hernqvist, L., Kvartsberg, S., Fransson, Å., & Gustafson, G. (2012). A Swedish Grouting Design Concept: Decision Method for Hard Rock Tunneling.

Hollmén, K., Funehag, J., Lyytinen, T., & Säippä, J. (2013). *Colloidal Silica - Grouting in Demonstration Tunnel 2 in Onkalo* (2012-84).

Holmboe, M., Wold, S., & Petterson, T. (2011). Effects of the injection grout Silica sol on bentonite. *Physics and Chemistry of the Earth, Parts A/B/C*, *36*(17-18), 1580-1589.

Holter, K.-G., & Hognestad, H.-O. (2012). Modern pre-injection in underground construction with rapid-setting microcements and colloidal silica – applications in conventional and TBM-tunnelling. *Geomechanics and Tunnelling*, *5*(1), 49-56.

Holter, K. G., Hyllseth, M., Strrømsvik, H., Bøyeie, K. M., & Minsaas, C. M. (2025). Dual stage pre-excavation grouting methodology with a completely dry tunnel as target. Experiences with an innovative approach during the construction of the Hestnes railroad tunnel, Norway. In F. Johansson, A. Ansell, D. Johansson, J. Funehag, & J. Norrman (Eds.), *Tunnelling into a Sustainable Future – Methods and Technologies* (1 ed.). CRC Press.

Hölttä, P., & Hakanen, M. (2008). *Silica Colloids and their Effect on Radionuclide Sorption – A Literature Review* (2008-29).

Hölttä, P., Hakanen, M., & Lahtinen, M. (2009). *Silica Colloids and their Effect on Radionuclide Sorption – Experimental Study* (2009-26).

Hou, C., & Kang, X. (2025). Development and Characterization of Engineering Superhydrophobic Silica Sol for Enhanced Subsurface Stability and Seepage Control. *Journal of Materials in Civil Engineering*, *37*(12), 04025475.

Huang, J., Al-Moshin, A., Bataweel, M., Karadkar, P., Li, W., & Shaikh, A. (2017, 6-9 March). *Systematic Approach to Develop a Colloidal Silica Based Gel System for Water Shut-Off* SPE Middle East Oil & Gas Show and Conference, Manama, Bahrain.

Huang, Y., & Wang, L. (2016). Laboratory investigation of liquefaction mitigation in silty sand using nanoparticles. *Engineering Geology*, *204*, 23-32.

Hulett, G. (1926). Solubility and Size of Particles. In J. Alexander (Ed.), *Colloid Chemistry* (pp. 637). Chemical Catalog Co.

Hunt, J. D., Ezzedine, S. M., Bourcier, W., & Roberts, S. (2013). *Kinetics of the Gelation of Colloidal Silica at Geothermal Cconditions, and Implications for Reservoir Modification and Management* Thirty-Eight Workship on Geothermal Reservoir Engineering, Stanford, CA.

Hunter, R. J. (1981). *Zeta Potential in Colloid Science: Principles and Applications*. Academic Press.

Iler, R. K. (1979). *The Chemistry of Silica: Solublity, Polymerization, Colloid and Surface Properties, and Biochemistry*. John Wiley & Sons.

Iswar, S., Malfait, W. J., Balog, S., Winnefeld, F., Lattuada, M., & Koebel, M. M. (2017). Effect of aging on silica aerogel properties. *Microporous and Mesoporous Materials*, *241*, 293-302.

Jia, H., Pu, W.-F., Zhao, J.-Z., & Jin, F.-Y. (2010). Research on the Gelation Performance of Low Toxic PEI Cross-Linking PHPAM Gel Systems as Water Shutoff Agents in Low Temperature Reservoirs. *Industrial and Engineering Chemcical Research*, *49*, 9618-9624.

Jia, Y., Chen, J., Liu, W., & Yin, D. (2019). Construction of highly stretchable silica/polyacrylamide nanocomposite hydrogels through hydrogen bond strategy. *Journal of Polymer Research*, *26*, 119.

Johnson, A.-C. J. H., Greenwood, P., Hagström, M., Abbas, Z., & Wall, S. (2008). Aggregation of Nanosized Colloidal Silica in the Presence of Various Alkali Cations Investigated by the Electrospray Technique. *Langmuir*, *24*, 12798-12806.

Johnsson, A.-C. J. H., Camerani, M. C., & Abbas, Z. (2011). Combined Electrospray-Scanning Mobility Particle Sizer (ES-SMPS) and Time-Resolved Synchrotron Radiation-Small-Angle X-ray Scattering (SR-SAXS) Investigation of Colloidal Silica Aggregation. Part II. Influence of Aggregation Initiator on Gel Stability. *The Journal of Physical Chemistry B*, *115*(31), 9547-9555.

Joudieh, Z., Cuisinier, O., Abdallah, A., & Masrouri, F. (2024). Artificial Ground Freezing - On the Soil Deformations during Freeze-Thaw Cycles. *Geotechnics*, *4*, 718-741.

Jurinak, J. J., & Summers, L. E. (1991a). Oilfield Applications of Colloidal Silica Gel. *SPE Production Engineering*, *6*(04), 406-412.

Jurinak, J. J., Summers, L. E., & Bennett, K. E. (1991b). Laboratory Testing of Colloidal Silica Gel for Oilfield Applications. *Society of Petroleum Engineers Journal*, Article 18505.

Kaide, A., Saeki, T., & Kikuchi, S. (2011). The Effect of Controlling the Aging Condition on the Gelling Property of Silica Sols. *Journal of the Society of Rheology, Japan*, *39*(5), 205-210.

Kakavand, A., & Dabiri, R. (2018). Experimental study of applying colloidal nano Silica in improving sand-silt mixtures. *International Journal of Nano Dimension*, *9*(4), 357-373.

Karami, A. (2009). Study on modification of colloidal silica surface with magnesium ions. *Journal of Colloid and Interface Science*, *331*, 379-383.

Karnland, O., Olsson, S., & Nilsson, U. (2006). *Mineralogy and sealing properties of various bentonites and smectite-rich clay materials* (TR-06-30).

Karol, R. H. (2003). *Chemical Grouting and Soil Stabilization* (3 ed.). Marcel Dekker.

Kashyap, V. S., Sancheti, G., Yadav, J. S., & Agrawal, U. (2023). Smart sustainable concrete: enhancing the strength and durability with nano silica. *Smart Construction and Sustainable Cities*, *1*, 20.

Katoueizadeh, E., Rasouli, M., & Zebarjad, S. M. (2021). The rheological behaviour of the non-Newtonian thixotropic colloidal silica gels from sodium silicate. *Materials Chemistry and Physics*, *272*, 124994.

Khan, K., Ahmad, W., Amin, M. N., & Nazar, S. (2022). Nano-Silica-Modified Concrete: A Bibliographic Analysis and Comprehensive Review of Material Properties. *Nanomaterials*, *12*, 1989.

Khedr, R. F., & Elhady, M. A. (2025). Development the Hydrophobic Property of Polyvinyl Alcohol/Silicon Dioxide/Titanium Dioxide Nanocomposites for Self-Cleaning and Soil Stabilization. *Molecules*, *30*, 1664.

Kim, S., Sung, J. H., Ahn, K. H., & Lee, S. J. (2009). Drying of the Silica/PVA Suspension: Effect of Suspension Microstructure. *Langmuir*, *25*(11), 6155-6161.

Kondiah, P. J., Choonara, Y. E., Kondiah, P. P. D., Marimuthu, T., Kumar, P., du Toit, L. C., & Pillay, V. (2016). A Review of Injectable Polymeric Hydrogel Systems for Application in Bone Tissue Engineering. *Molecules*, *21*, 1580.

Krishnan, J., Yadav, S. L., & Shukla, S. (2021). Experimental investigations of a pile in colloidal silica stabilized sand under vertical and lateral loads. *Arabian Journal of Geosciences*, *14*, 1314.

Kumar, G. P., & Rajasekhar, K. (2022). Effect of colloidal silica on compressive strength of concrete. *Materials Today: Proceedings*, *56*, 520-526.

Labaran, Y. H., Atmaca, N., Tan, M., Atmaca, K., Aram, S. A., & Kaky, A. T. (2024). Nano-enhanced concrete: unveiling the impact of nano-silica on strength, durability, and cost efficiency. *Discover Civil Engineering*, *1*, 116.

Lartiges, B. S., Bottero, J. Y., Derrendinger, L. S., Humbert, B., Tekely, P., & Suty, H. (1997). Flocculation of Colloidal Silica with Hydrolyzed Aluminum: An ^{27}Al Solid State NMR Investigation. *Langmuir*, *13*, 147-152.

Lee, G.-J., Yoon, S., & Cho, W.-J. (2024). Thermal Influence on Hydraulic Conductivity in Compacted Bentonite: Predictive Modeling Based on the Dry Density-Hydraulic Conductivity Relationship. *Journal of Nuclear Fuel Cycle and Waste Technology*, *22*(1), 17-25.

Lee, J. H. (2018). Injectable hydrogels delivering therapeutic agents for disease treatment and tissue. *Biomaterials Research*, *22*, 27.

Lei, S., Sun, J., Lv, K., Zhang, Q., & Yang, J. (2022). Types and Performances of Polymer Gels for Oil-Gas Drilling and Production: A Review. *Gels*, *8*, 386.

Leroy, P., Devau, N., Revil, A., & Bizi, M. (2013). Influence of surface conductivity on the apparent zeta potential of amorphous silica nanoparticles. *Journal of Colloid and Interface Science*, *410*, 81-93.

Levin, M., Sonn-Segev, A., & Roichman, Y. (2019). Structural changes in nanoparticle-hydrogel composites at very low filler concentrations. *The Journal of Chemical Physics*, *150*, 064908.

Li, J., & Mooney, D. J. (2016). Designing hydrogels for controlled drug delivery. *Nature Reviews Materials*, *1*(12), 16071.

Li, Q., Yu, X., Wang, L., Qu, S., Wu, W., Ji, R., Luo, Y., & Yang, H. (2022). Nano-silica hybrid polyacrylamide/polyethylenimine gel for enhanced oil recovery at harsh conditions. *Colloids and Surfaces A: Physicochemical and Engineering Aspects*, *633*, 127898.

Li, X., Sun, Q., Li, Q., Kawazoe, N., & Chen, G. (2018). Functional Hydrogels With Tunable Structures and Properties for Tissue Engineering Applications. *Frontiers in Chemistry*, *6*, Article 499.

Liang, Z., Li, W., Dong, B., Sun, Y., Tang, H., Zhao, L., & Wang, S. (2019). Double-function SiO_2-DMS coating with antireflection and superhydrophobic surface. *Chemical Physics Letters*, *716*, 211-214.

Lin, C.-C., & Anseth, K. S. (2009). PEG Hydrogels for the Controlled Release of Biomolecules in Regenerative Medicine. *Pharmaceutical Research*, *26*(3), 631-643.

Lin, C.-C., & Metters, A. T. (2006). Hydrogels in controlled release formulations: Network design and mathematical modeling. *Advanced Drug Delivery Reviews*, *58*, 1379-1408.

Liu, C., Xing, T., Wei, B., & Chen, G. (2018). Synergistic Effects and Mechanism of Modified Silica Sol Flame Retardant Systems on Silk Fabric. *Materials*, *11*, 1842.

Liu, M., Cheng, R., & Qian, R. (1995). Effect of Solution Concentration on the Gelation of Aqueous Polyvinyl Alcohol Solution. *Journal of Polymer Science, Part B: Polymer Physics*, *33*(12), 1731-1735.

Liu, Y., Dai, C., Wang, K., Zou, C., Gao, M., Fang, Y., Zhao, M., Wu, Y., & You, Q. (2017). Study on a Novel Cross-Linked Polymer Gel Strengthened with Silica Nanoparticles. *Energy & Fuels*, *31*, 9152-9161.

Lu, S., Bo, Q., Zhao, G., Shaikh, A., & Dai, C. (2023). Recent advances in enhanced polymer gels for profile control and water shutoff: A review. *Frontiers in Chemistry*, *11*, 1067094.

Lunn, R. J., Hamilton, A., Pedrotti, M., Bots, P., Wong, C., El Mountassir, G., Renshaw, J., Maddelena, C., Zhao, C., Stolkin, R., Fairweather, M., Tovey, L., Boxall, C., Hriljac, J. A., Hyatt, N. C., Kaltsoyannis, N., Lee, W. E., Read, D., & Scott, T. B. (2018, March 18-22). *The DISTINCTIVE University Consortium: Structural Integrity* WM2018 Conference, Phoenix, AZ, USA.

Luo, X., Akram, M. Y., Yuan, Y., Nie, J., & Zhu, X. (2019). Silicon dioxide/poly(vinyl alcohol) composite hydrogels with high mechanical properties and low swellability. *Journal of Applied Polymer Science*, *136*, 46895.

Ma, L., Wang, S., Long, Y., Zhu, C., Yang, H., Yang, T., Liu, X., Li, X., Bai, B., & Kang, W. (2017). Novel Environmentally Benign Hydrogel: Nano-Silica Hybrid Hydrolyzed Polyacrylamide/ Polyethyleneimine Gel System for Conformance Improvement in High Temperature High Salinity Reservoir. Abu Dhabi International Petroleum Exhibition & Conference,

Ma, M., Qi, Y., Chen, Q. a., & Zhang, Z. (2024). Robust Fluorescent Silica/Polyethylene Glycol Hydrogel Membrane for Tracking and Antifouling. *ACS Applied Polymer Materials*, *6*, 3534-3543.

MacLachlan, E., El Mountassir, G., & Lunn, R. J. (2013). Use of bacterial ureolysis for improved gelation of silica sol in rock grouting. *Géotechnique Letters*, *3*, 180-184.

Mahamoud, M. M., Kuwahara, Y., Ihara, H., & Takafuji, M. (2025). Impact of Silica Nanoparticles on Mechanical Properties and Self-Healing Performance of PVA Hydrogels. *Polymers*, *17*, 2883.

Mahanty, J., & Ninham, B. W. (1976). *Dispersion Forces*. Academic Press.

Manchester, K. R., North-Abbott, M. A., Zaluski, M. H., Trudnowski, J. M., & Bickford, J. L. (2001). Colloidal Silica Grout Selection and Characterization in Support of the Barrier Deployment at Brookhaven National Laboratory.

Mansourghanaei, M., Biklaryan, M., & Mardookhpour, A. (2024). Experimental study of the effects of adding silica nanoparticles on the durability of geopolymer concrete. *Australian Journal of Civil Engineering*, *22*(1), 81-93.

Mantha, S., Pillai, S., Khayambashi, P., Upadhyay, A., Zhang, Y., Tao, O., Pham, H. M., & Tran, S. D. (2019). Smart Hydrogels in Tissue Engineering and Regenerative Medicine. *Materials*, *12*(20), 3323.

Mao, X., Cheng, R., Zhang, H., Bae, J., Cheng, L., Zhang, L., Deng, L., Cui, W., Zhang, Y., Santos, H. A., & Sun, X. (2019). Self-Healing and Injectable Hydrogel for Matching Skin Flap Regeneration. *Advanced Science*, *6*, 1801555.

Marques, N. N., de Morais, S. C., da Câmara, P. C. F., de Souzab, E. A., & Balaban, R. C. (2023). Gelation Behavior of Polyacrylamide-Polyethyleneimine: Effects of Diethylenetriamine and Glycerol Addition. *Journal of the Brazilian Chemical Society*, *34*(10), 1373-1379.

Martin, J., Hosticka, B., Lattimer, C., & Norris, P. M. (2001). Mechanical and acoustical properties as a function of PEG concentration in macroporous silica gels. *Journal of Non-crystalline Solids*, *285*, 222-229.

Martinez, M. I. S., Carabali, V. S., Ramirez, A., Chaves-Guerrero, A., & Muñoz Navarro, S. (2025). Design of a Dual Molecular Weight Polymer Gel for Water-Shutoff Treatment in a Reservoir with Active Aquifer. *Polymers*, *17*, 1399.

Master Builders Solutions. (a). *MasterRoc MP 320: Technical Data Sheet*. Retrieved April 6, 2026 from https://master-builders-solutions.com/en-gb/products/masterroc/masterroc-mp-320/

Master Builders Solutions. (b). *MasterRoc MP 325 Data Sheet*. Retrieved April 6, 2026 from https://master-builders-solutions.com/en-us/products/masterroc/masterroc-mp-325/

Mayordomo, N., Degueldre, C., Alonso, U., & Missana, T. (2016). Size distribution of FEBEX bentonite colloids upon fast disaggregation in low-ionic strength water. *51*, 213-222.

Metin, C. O., Rankin, K. M., & Nguyen, Q. P. (2014). Phase behaviour and rheological characterization of silica nanoparticle gel. *Applied Nanoscience*, *4*, 93-101.

Miller, S. A., Horvath, A., & Monteiro, P. J. M. (2016). Readily implementable techniques can cut annual CO_2 emissions from the production of concrete by over 20%. *Environmental Research Letters*, *11*, 074029.

Millero, F. J., Feistel, R., Wright, D. G., & Mcdougall, T. J. (2008). The composition of Standard Seawater and the definition of the Reference-Composition Salinity Scale. *Deep Sea Research Part I: Oceanographic Research Papers*, *55*(1), 50-72.

Mirzababaei, M., Arulrajah, A., & Ouston, M. (2017). Polymers for stabilization of soft clay soils. *Procedia Engineering*, *189*, 25-32.

Missana, T., Alonso, Ú., García-Gutiérrez, M., & Mingarro, M. (2008). Role of bentonite colloids on europium and plutonium migration in a granite fracture. *Applied Geochemistry*, *23*, 1484-1497.

Mohamadabadi, S. D., Moayed, R. Z., & Nozari, M. A. (2019). Mechanical characteristics of sulfated clay stabilized with colloidal silica considering different number of freeze-thaw cycles. *159*, 86-93.

Mohamed, M. H., & Mohyaldinn, M. E. (2025). Polyacrylamide-Based Solutions: A Comprehensive Review on Nanomaterial Integration, Supramolecular Design, and Sustainable Approaches for Integrated Reservoir Management. *Polymers*, *17*, 2202.

Mollamahmutoglu, M., & Yilmaz, Y. (2010). Pre- and post-cyclic loading strength of silica-grouted sand. *Geotechnical Engineering*, *163*(GE6), 343-348.

Moore, E. P., Jr. (1973). *Stable Positively Charged Alumina Coated Silica Sols* (USA Patent No. 3745126). U. S. P. Office.

Moore, E. P., Jr., & Vurlicer, G. (1976). *Process for Preparing Stable Positively Charged Alumina Coated Silica Sols and Product Thereof* (USA Patent No. 3956171). U. S. P. Office.

Moradi-Araghi, A. (2000). A review of thermally stable gels for fluid diversion in petroleum production. *Journal of Petroleum Science and Engineering*, *26*(1-4), 1-10.

Morariu, S., Avadanei, M., & Nita, L. E. (2023). Effect of pH on the Poly(acrylic acid)/Poly(vinyl alcohol)/Lysozyme Complexes Formation. *Molecules*, *29*(1), 208.

Moridis, G. J., Apps, J., Persoff, P., Myer, L., Muller, S., Yen, P., & Pruess, K. (1996). *A Field Test of a Waste Containment Technology Using a New Generation of Injectable Barrier Liquids* (LBNL-38817).

Moridis, G. J., Finsterle, S., & Heiser, J. (1999). Evaluation of alternative designs for an injectable subsurface barrier at the Brookhaven National Laboratory Site, Long Island, New York. *Water Resources Research*, *35*(10), 2937-2953.

Moridis, G. J., James, A., & Oldenburg, C. (1997). Development of a design package for a viscous barrier at the Savannah River site. International Containment Technology Conference: February 9-12, 1997, St. Petersburg, Florida, USA: Conference Proceedings,

Moridis, G. J., Persoff, P., Apps, J. A., Myer, L., Pruess, K., & Yen, P. (1995). *A Field Test of Permeation Grouting in Heterogeneous Soils Using A New Generation of Barrier Liquids* Committed To Results: Barriers for Long-Term Isolation, Denver, CO.

Morrison, D., Pedrotti, M., Lunn, R., Draper, E., & Graham, J. (2022, March 6-10). *Modifying Colloidal Silica Grout for Nuclear Decommissioning Applications* WM2022 Conference, Phoenix, AZ, USA.

Morrison, D. W. T., Pedrotti, M., Lunn, R. J., & Draper, E. R. (2026). *An Experimental Investigation on the Effect of Grout Composition and Curing Conditions on the Strength of Colloidal Silica Grout* [Unpublished manuscript]. University of Strathclyde.

Moslemi, A. M., Khosravi, A., Izadinia, M., & Heydari, M. (2013). Application of Nano Silica in Concrete for Enhanced Resistance against Sulfate Attack. *Advanced Materials Research*, *829*, 874-878.

Mulholland, C., Ejohwomu, O. A., & Chan, P. W. (2019). Spatial-temporal dynamics of social value: Lessons learnt from two UK nuclear decommissioning case studies. *Journal of Cleaner Production*, *237*, 117677.

Navaie, F., Esmaeilnezhad, E., & Choi, H.-J. (2022). Effect of Rheological Properties of Polymer Solution on Polymer Flooding Characteristics. *Polymers*, *14*, 5555.

Nazir, M., Kawamoto, K., & Sakaki, T. (2021). Properties of Granulated Bentonite Mixtures for Radioactive Waste Disposal: A Review. *Internation Journal of GEOMATE*, *20*(81), 132-145.

Nezhad-Mokhtari, P., Ghorbani, M., Roshangar, L., & Rad, J. S. (2019). A review on the construction of hydrogel scaffolds by various chemically techniques for tissue engineering. *European Polymer Journal*, *117*, 64-76.

Nguyen, N. T., Milani, A. H., Jennings, J., Adlam, D. J., Freemont, A. J., Hoyland, J. A., & Saunders, B. R. (2019). Highly compressive and stretchable poly(ethylene glycol) based hydrogels synthesised using pH-responsive nanogels without free-radical chemistry. *Nanoscale*, *11*, 7921.

Nigam, M., & Verma, M. (2023). Effect of nano-silica on the fresh and mechanical properties of conventional concrete. *Forces in Mechanics*, *10*, 100165.

Noh, D.-H., Kim, S., Calaunan, J. M. F. V., Feng, Y., Eun, J., & Kim, Y.-R. (2025). Bentonite as an engineered barrier material for nuclear waste repository - Geotechnical perspectives, key properties, knowledge gaps, and opportunities. *Nuclear Engineering and Technology*, *57*, 103700.

Noll, M. R., Bartlett, C., & Dochat, T. M. (1992). In situ permeability reduction and chemical fixation using colloidal silica. 6th Annual Outdoor Action Conference on Aquifer Restoration, Las Vegas, NV.

Nonveiller, E. (1989). *Grouting Theory and Practice*. Elsevier.

North-Abbott, M. A., Manchester, K. R., Trudnowski, J. M., Moe, M. J., Bickford, J. L., & Zaluski, M. H. (2001, February 25 - March 1). *Colloidal Silica Barrier Deployment at Brookhaven National Laboratory* WM'01 Conference, Tucson, AZ, USA.

Northcroft, I. W. (2006). Innovative materials and methods for ground supprt, consolidation and water sealing for the mining industry. *Journal of the Southern African Institute of Mining and Metallurgy*, *106*, 835-844.

Odian, G. (2004). *Principles of Polymerization* (4 ed.). John Wiley & Sons, Inc.

Oguz, O., Candau, N., Bernhard, S. H. F., Soz, C. K., Heinz, O., Stochlet, G., Plummer, C. J. G., Yilgor, E., Yilgor, I., & Menceloglu, Y. Z. (2019). Effect of Surface Modification of Colloidal Silica Nanoparticles on the Rigid Amorphous Fraction and Mechanical Properties of Amorphous Polyurethane–Urea–Silica Nanocomposites. *Journal of Polymer Science, Part A: Polymer Chemistry*, *57*, 2543-2556.

Okazaki, K., & Kawaguchi, M. (2008). Influence of Monovalent Electrolytes on Rheological Properties of Gelled Colloidal Silica Suspensions. *Journal of Dispersion Science and Technology*, *29*, 77-82.

Pagano, A. G., El Mountassir, G., & Lunn, R. J. (2022a). Performance of colloidal silica grout at elevated temperatures and pressures for cement fracture sealing at depth. *Journal of Petroleum Science and Engineering*, *208*, 109782.

Pagano, A. G., El Mountassir, G., & Lunn, R. J. (2022b, March 6-10). *Reducing Hazard in Spent Fuel Removal Using Colloidal Silica Gel* WM2022 Conference, Phoenix, AZ, USA.

Pagano, A. G., El Mountassir, G., & Lunn, R. J. (2023). Colloidal silica as a grouting material for the temporary encapsulation of heat-generating radioactive waste during removal and transport operations: A proof of concept. *Frontiers in Energy Research*, *11*.

Paktiawal, A., & Alam, M. (2020). Nano-Silica and its Role on Performance of Cement Concrete-A Review of Experimental Investigation. *IOP Conference Series: Earth and Environmental Science*, *614*, 012085.

Pamuk, A., Gallagher, P. M., & Zimmie, T. F. (2007). Remediation of piled foundations against lateral spreading by passive site stabilization technique. *Soil Dynamics and Earthquake Engineering*, *27*, 864-874.

Pan, D., Zhang, N., Zhang, C., Qian, D., Han, C., & Yang, S. (2018). Long-term Mechanical Behaviour of Nano Silica Sol Grouting. *Nanomaterials*, *8*, 46.

Pantos, E., & West, J. B. (1994). Growth and Aging Phenomena in Silica Gels. *Journal of Sol-Gel Science and Technology*, *2*, 273-276.

Park, S.-J., & Seo, M.-K. (2011). Chapter 1 - Intermolecular Force. In S.-J. Park & M.-K. Seo (Eds.), *Interface Science and Composites* (Vol. 18, pp. 1-57). Elsevier.

Park, S., Son, Y., Kim, J.-g., Won, D.-J., & Choi, H. (2024). Thermal and mechanical impact of artificial ground-freezing on deep excavation stability in Nakdong River Deltaic deposits. *Engineering Geology*, *343*, 107796.

Payanda Konuk, O., Alsuhile, A. A. A. M., Yousefzadeh, H., Ulker, Z., Bozbag, S. E., García-González, C. A., Smirnova, I., & Erkey, C. (2023). The effect of synthesis conditions and process parameters on aerogel properties. *Frontiers in Chemistry*, *11*, 1294520.

Pedrotti, M., Lyons, J., El Mountassir, G., Kuras, O., & Lunn, R. J. (2026). *A transport model for the permeation of colloidal silica* [Unpublished manuscript].

Pedrotti, M., Wong, C., El Mountassir, G., & Lunn, R. J. (2017). An analytical model for the control of silica grout penetration in natural groundwater systems. *Tunnelling and Underground Space Technology*, *70*, 105-113.

Pedrotti, M., Wong, C., El Mountassir, G., Renshaw, J. C., & Lunn, R. J. (2020). Desiccation behaviour of colloidal silica grouted sand: A new material for the creation of near surface hydraulic barriers. *Engineering Geology*, *270*, 105579.

Peppas, N. A., Bures, P., Leobandung, W., & Ichikawa, H. (2000). Hydrogels in pharmaceutical formulations. *European Journal of Pharmaceutics and Biopharmaceutics*, *50*, 27-46.

Persoff, P., Apps, J., Moridis, G. J., & Whang, J. M. (1999). Effect of Dilution and Contaminants on Sand Grouted with Colloidal Silica. *Journal of Geotechnical and Geoenvironmental Engineering*, *125*(6), 461-469.

Persoff, P., Finsterle, S., Moridis, G. J., Apps, J., Pruess, K., & Muller, S. J. (1995). *Injectable Barriers for Waste Isolation* (LBL-36739).

Pinho De Aguiar, K. L. N., Frias De Oliveira, P., & Elias Mansur, C. R. (2020). A comprehensive review of in situ polymer hydrogels for conformance control of oil reservoirs. *Oil & Gas Science and Technology – Revue d'IFP Energies nouvelles*, *75*, 8.

Poncet-Legrand, C., Bordes, B., & Lafuma, F. (2001). Surface modification of colloidal silica particles. *Colloid and Polymer Science*, *279*, 114-121.

Potapov, V., Efimenko, Y., Fediuk, R., & Abhilash, P. P. (2026). Effects of nanosilica application in Portland cement concrete. *Engineering Structure and Civil Engineering*, *20*, 1074-1093.

Qin, Y., Liao, R., Luo, S., & Li, J. (2020). The Thermal Gelation Behavior and Performance Evaluation of High MolecularWeight Nonionic Polyacrylamide and Polyethyleneimine Mixtures for In-DepthWater Control in Mature Oilfields. *Materials*, *13*, 4142.

Quan, F.-y., Chen, L.-L., Xia, Y.-z., & Ji, Q. (2009). Structure and Properties of PVA/SiO2 Interpenetrating Polymer Network Materials Prepared by the Sol–Gel Method. *Polymers & Polymer Composites*, *17*(2), 97-100.

Raveendran, N., & Krishnan, V. (2025). Engineering performance and environmental assessment of sustainable concrete incorporating nano silica and metakaolin as cementitious materials. *Scientific Reports*, *15*, 1482.

Ren, Z., Niu, W., Zheng, Y.-y., Zaoui, A., Liu, J., & Wen, Z. (2025). Surface and structural improvements in PVA-modified expansive soils under cold conditions. *Materials Today Communications*, *48*, 113410.

Rose, S. v., Marcellan, A., Hourdet, D., Creton, C., & Narita, T. (2013). Dynamics of Hybrid Polyacrylamide Hydrogels Containing Silica Nanoparticles Studied by Dynamic Light Scattering. *Macromolecules*, *46*, 4567-4574.

Roshan, H., Lv, A., Aghighi, M. A., Sarmadivaleh, M., Siddiqui, M. A. Q., van As, D., & Ehsani, S. (2022). Stabilization of clay-rich interburdens using silica nanoparticles. *Journal of Petroleum Science and Engineering*, *211*, 110126.

Rubio, J., & Kitchener, J. A. (1976). The Mechanism of Adsorption of Poly(Ethylene Oxide) Flocculant on Silica *Journal of Colloid and Interface Science*, *57*(1), 132-141.

Saadatbakhsh, M., Asl, S. J., Kiani, M. J., & Nouri, N. M. (2020). Slip length measurement of pdms/hydrophobic silica superhydrophobic coating for drag reduction application. *Surface & Coatings Technology*, *404*, 126428.

Sabr, O. H., Hussein, A. A., & Obaid, M. N. (2021). Improving Mechanical and Morphological Characteristics Pva/Sio2 Nanocomposites for Food Packing Applications. *IOP Conference Series: Materials Science and Engineering*, *1094*, 012146.

Saleh, A. N., Attar, A. A., Algburi, S., & Ahmed, O. K. (2023). Comparative study of the effect of silica nanoparticles and polystyrene on the properties of concrete. *Results in Materials*, *18*, 100405.

Salomão, R., Martinatti, I. S., Fernandes, L., Sundblom, A., Greenwood, P., & Tiba, P. R. T. (2023). Novel silanized colloidal silica-MgO self-flowing dispersions with improved hydroxylation resistance. *Journal of the European Ceramic Society*, *43*, 5691-5705.

Sánchez-Moreno, M., García-Calvo, J. L., & Tavares-Pinto, E. (2022). Colloidal Nanosilica Treatments for Sealing Cracks in Mortar. *Materials*, *15*, 6338.

Schaller, C. (2025). *Polymer Chemistry*. LibreTexts. https://chem.libretexts.org/Bookshelves/Organic_Chemistry/Polymer_Chemistry_(Schaller)

Shahrajabian, F., & Behfarnia, K. (2018). The effects of nano particles on freeze and thaw resistance of alkali-activated slag concrete. *Construction and Building Materials*, *176*, 172-178.

Shamlooh, M., Hamza, A., Hussein, I. A., Nasser, M. S., Magzoub, M., & Salehi, S. (2019). Investigation of the Rheological Properties of Nanosilica-Reinforced Polyacrylamide/Polyethyleneimine Gels for Wellbore Strengthening at High Reservoir Temperatures. *Energy & Fuels*, *33*, 6829-6836.

Sharafutdinov, R. F., Kuznetsova, D. P., Morozov, V. S., & Stolyarov, Y. I. (2024). Sand stabilization with colloidal silica for protection from liquefaction caused by dynamic loads. In N. Guerra, M. M. Fernandes, C. Ferreira, A. G. Correia, A. Pinto, & P. S. Pinto (Eds.), *Geotechnical Engineering Challenges to Meet Current and Emerging Needs of Society* (1 ed.). CRC.

Sharkawi, A. M., Abd-Elaty, M. A., & Khalifa, O. H. (2018). Synergistic influence of micro-nano silica mixture on durability performance of cementious materials. *Construction and Building Materials*, *164*, 579-588.

Sharma, P., Krishnan, J., & Shukla, S. (2021, 2021//). Determination of Hydraulic Conductivity of Colloidal Silica Stabilized Sand to Be Used as an Impervious Liner. Proceedings of the Indian Geotechnical Conference 2019, Singapore.

Shen, P., Hankins, N., & Jefferis, S. (2017). Selection of Colloidal Silica Grouts with Respect to Gelling and Erosion Behaviour. *Geosciences*, *7*(1), 6.

Shi, F.-K., Zhong, M., Zhang, L.-Q., Liu, X.-Y., & Xie, X.-M. (2016). Robust and self-healable nanocomposite physical hydrogel facilitated by the synergy of ternary crosslinking points in a single network. *Journal of Materials Chemistry B*, *4*, 6221.

Shona Pek, Y., Wan, A. C. A., Shekaran, A., Zhuo, L., & Ying, J. Y. (2008). A thixotropic nanocomposite gel for three-dimensional cell culture. *Nature Nanotechnology*, *3*, 671-675.

Singh, L. P., Karade, S. R., Bhattacharyya, S. K., Yousuf, M. M., & Ahalawat, S. (2013). Beneficial role of nanosilica in cement based materials – A review. *Construction and Building Materials*, *47*, 1069-1077.

Singh, M. C., Singh, G., Bishnoi, C., Malik, A., & Al-Ansari, N. (2024). Impact of polyvinyl alcohol application and wheat straw mulching on soil loss and infiltration rate in semi-arid tropics. *Applied Water Science*, *14*, 223.

SKB. (2010a). *Buffer, backfill and closure process report for the safety assessment SR-Site* (TR-10-47).

SKB. (2010b). *Design and production of the KBS-3 repository* (TR-10-12).

SKB. (2010c). *Design, prouction and initial state of the buffer* (TR-10-15).

Smitha, S., Shajesh, P., Aravind, P. R., Rajesh Kumar, S., Krishna Pillai, P., & Warrier, K. G. K. (2006). Effect of aging time and concentration of aging solution on the porosity characteristics of subcritically dried silica aerogels. *Microporous and Mesoporous Materials*, *91*, 286-292.

Sobti, J., & Singh, S. K. (2017). Hydraulic conductivity and compressibility characteristics of bentonite enriched soils as a barrier material for landfills. *Innovative Infrastructure Solutions*, *2*, Article 12.

Sögaard, C., Funehag, J., & Abbas, Z. (2018). Silica sol as grouting material: a physio-chemical analysis. *Nano Convergence*, *5*(1).

Sögaard, C., Funehag, J., Gergorić, M., & Abbas, Z. (2018). The long term stability of silica nanoparticle gels in waters of different ionic compositions and pH values. *Colloids and Surfaces A*, *544*, 127-136.

Sögaard, C., Hagström, M., & Abbas, Z. (2023). Temperature and Particle-size Effects on the Formation of Silica Gels from Silica Sols. *Silicon*, *15*, 3441-3451.

Soleimani Dorcheh, A., & Abbasi, M. H. (2008). Silica aerogel; synthesis, properties and characterization. *Journal of Materials Processing Technology*, *199*, 10-26.

Sonnefeld, J., Löbbus, M., & Vogelsberger, W. (2001). Determination of electric double layer parameters for spherical silica particles under application of the triple layer model using surface charge density data and results of electrokinetic sonic amplitude measurements. *Colloids and Surfaces A: Physicochemical and Engineering Aspects*, *195*(1-3), 215-225.

Spagnoli, G., Collico, S., & Tintelnot, G. (2025). Advances in chemical grouting from a statistical perspective. In F. Johansson, A. Ansell, D. Johansson, J. Funehag, & J. Norrman (Eds.), *Tunnelling into a Sustainable Future - Methods and Technologies* (1 ed.). CRC Press.

Spagnoli, G., Fraccica, A., Arroyo, M., & Romero, E. (2024). *Sand and silt treatment with novel binders* IS-Porto 2023, Porto, Portugal.

Stoks, W., Berghmans, H., Moldenaers, P., & Mewis, J. (1988). Thermoreversible Gelation of Solutions of Poly(vinyl alcohol). *British Polymer Journal*, *20*, 361-369.

Sun, B., Wang, H., Liu, Y., Lv, W., Li, Y., Ma, S., Wang, X., & Cao, H. (2025). Shear-Induced Degradation and Rheological Behavior of Polymer-Flooding Waste Liquids: Experimental and Numerical Analysis. *Processes*, *13*, 2677.

Sverjensky, D. A. (2005). Prediction of surface charge on oxides in salt solutions: Revisions for 1:1 (M^+L^-) electrolytes. *Geochimica et Cosmochimica Acta*, *69*(2), 225-257.

Sydansk, R. D., & Argabright, P. A. (1988). *Conformance improvement in a subterranean hydrocarbon-bearing formation using a crosslinked polymer* US 4744419 United States Patent and Trademark Office, Box 9, Washington, DC 20232. NOV English).

Szymanek, K., Charmas, R., & Piasecki, W. (2021). Investigations of mechanism of Ca^{2+} adsorption on silica and alumina based on Ca-ISE monitoring, potentiometric titration, electrokinetic measurements and surface complexation modeling. *Adsorption*, *27*, 105-115.

Takeno, H., Aoki, Y., & Kimura, K. (2021). Effects of silica and clay nanoparticles on the mechanical properties of poly(vinyl alcohol) nanocomposite hydrogels. *Colloids and Surfaces A: Physicochemical and Engineering Aspects*, *630*, 127592.

Tan, X., Liang, C., Bai, S., Lan, P., Ren, Y., Zhao, J., & Rong, J. (2024). PVA/silica hybrid hydrogel with ultra-high strength and toughness. *Journal of Materials Science*, *59*, 6916-6928.

Tanaka, Y., Gong, J. P., & Osada, Y. (2005). Novel hydrogels with excellent mechanical performance. *Progress in Polymer Science*, *30*(1), 1-9.

Tavakoli, D., & Cizer, Ö. (2025). Effect of mesoporous silica nanoparticles on cement hydration and early-age performance. *Case Studies in Construction Materials*, *22*, e04909.

Teng, F., Sie, Y. C., & Kuo, C. (2025). Field experimental and numerical study on the formation and frost heave development of frozen soil under rapid freezing. *Case Studies in Construction Materials*, *22*, e04239.

Terui, T., Motohashi, T., Sasahara, S., & Inazumi, S. (2025). Development and application of geothermally derived silica grout for carbon-neutral soil stabilization. *Case Studies in Construction Materials*, *22*, e04297.

Tie, L., Yu, M., Li, X., Liu, W., Zhang, B., Chang, Z., & Zheng, Y. (2019). Research on polymer solution rheology in polymer flooding for Qikou reservoirs in a Bohai Bay oilfield. *Journal of Petroleum Exploration and Production Technology*, *9*, 703-715.

Todaro, C. (2021). Grouting of cohesionless soils by means of colloidal nanosilica. *Case Studies in Construction Materials*, *15*, e00577.

Tomar, A., Sharma, T., & Singh, S. (2020). Strength properties and durability of clay soil treated with mixture of nano silica and Polypropylene fiber. *Materials Today: Proceedings*, *26*, 3449-3457.

Travesset, A., & Vangaveti, S. (2009). Electrostatic correlations at the Stern layer: Physics or chemistry? *The Journal of Chemical Physics*, *131*(18), 185102.

Tripathi, A., & Mishra, A. (2024). Repairing of concrete structures using nano-silica concrete. *IOP Conference Series: Earth and Environmental Science*, *1326*, 012069.

Trompette, J.-L. (2017). Influence of Co-Ion Nature on the Gelation Kinetics of Colloidal Silica Suspensions. *The Journal of Physical Chemistry B*, *121*, 5654-5659.

Trompette, J. L., & Clifton, M. J. (2004). Influence of ionic specificity on the microstructure and the strength of gelled colloidal silica suspensions. *Journal of Colloid and Interface Science*, *276*(2), 475-482.

Trompette, J. L., & Meireles, M. (2003). Ion-specific effect on the gelation kinetics of concentrated colloidal silica suspensions. *Journal of Colloid and Interface Science*, *263*, 522-527.

Truex, M. J., Pierce, E. M., Nimmons, M. J., & Mattigod, S. V. (2011). *Evaluation of In Situ Grouting as a Potential Remediation Method for the Hanford Central Plateau Deep Vadose Zone* (PNNL-20051).

Tsai, M.-S., Huang, P. Y., Wu, W.-C., & Chen, C.-H. (2009). Effect of cerium modification on the formation of colloidal silica. *Materials Chemistry and Physics*, *114*, 247-251.

Tsai, M.-S., & Wu, W.-C. (2004). Aluminum modified colloidal silica via sodium silicate. *Materials Letters*, *58*, 1881-1884.

Tsuji, M., Funehag, J., Kobayashi, S., Sato, T., & Mikake, S. (2014, 14-16 October). *Comparison of grouting with silica sol in the Äspö Hard Rock Laboratory in Sweden and Mizunami Underground Research Laboratory in Japan* 8th Asian Rock Mechanics Symposium, Sapporo, Japan.

Tsuji, M., Kobayashi, S., Mikake, S., Sato, T., & Matsui, H. (2017). Post-Grouting Experiences for Reducing Groundwater Inflow at 500 m Depth of the Mizunami Underground Research Laboratory, Japan. *Procedia Engineering*, *191*, 543-550.

Tyler, R. H., Boyer, T. P., Minami, T., Zweng, M. M., & Reagan, J. R. (2017). Electrical conductivity of the global ocean. *Earth, Planets and Space*, *69*(1).

U.S. Army Corps of Engineers. (1995). *Chemical Grouting*. (EM 1110-1-3500). Washington, DC, USA

U.S. Army Corps of Engineers. (2017). *Grouting Technology*. (EM 1110-2-3506). Washinton, DC, USA

Van Der Linden, M., Conchúir, B. O., Spigone, E., Niranjan, A., Zaccone, A., & Cicuta, P. (2015). Microscopic Origin of the Hofmeister Effect in Gelation Kinetics of Colloidal Silica. *The Journal of Physical Chemistry Letters*, *6*(15), 2881-2887.

Venkateswara Rao, A., Pajonk, G. M., & Parvathy, N. N. (1994). Effect of solvents and catalysts on monolithicity and physical properties of silica aerogels. *Journal of Materials Science*, *29*, 1807-1817.

Verwey, E. J. W. (1947). Theory of the Stability of Lyophobic Colloids. *The Journal of Physical Chemistry*, *51*(3), 631-636.

Vigata, M., Meinert, C., Hutmacher, D. W., & Bock, N. (2020). Hydrogels as Drug Delivery Systems: A Review of Current Characterization and Evaluation Techniques. *Pharmaceutics*, *12*, 1188.

Villar, M. V., Gómez-Espina, R., & Lloret, A. (2010). Experimental investigation into temperature effect on hydro-mechanical behaviours of bentonite. *Journal of Rock Mechanics and Geotechnical Engineering*, *2*(1), 71-78.

Vinšová, H., Jedináková-Křížová, V., Kolaříková, I., Adamcová, J., Přikryl, R., & Zeman, J. (2008). The influence of temperature and hydration on the sorption properties of bentonite. *Journal of Environmental Radioactivity*, *99*, 415-425.

Volckaert, G., Bernier, F., Alonso, E., Gens, A., Samper, J., Villar, M., Martin-Martin, P. L., Cuevas, J., Campos, R., Thomas, H., Imbert, C., & Zingarelli, V. (1996). *Thermal-hydraulic-mechanical and geochemical behaviour of the clay barrier in readioactive waste repositories (model development and validation)* (EUR 16744). (Nuclear science and technology, Issue. E. Commission.

Wagner, A. M., & Yarmak, E. (2012). *Demonstration of an Artificial Frozen Barrier* [Technical report](Installation Technology Transfer Program, Issue. U. A. C. o. Engineers.

Wang, J., Lu, X., Ma, B., & Tan, H. (2022). Cement-Based Materials Modified by Colloidal Nano-Silica: Impermeability Characteristic and Microstructure. *Nanomaterials*, *12*, 3176.

Wang, K., Luo, M., Li, M., Gu, X., Li, X., Fan, Q., Pu, C., & Wang, L. (2024). Gelation and Plugging Performance of Low-Concentration Partially Hydrolyzed Polyacrylamide/Polyethyleneimine System at Moderate Temperature and in Fractured Low-Permeability Reservoir. *Polymers*, *16*, 1585.

Wang, Q., & Gao, Z. (2016). A constitutive model of nanocomposite hydrogels with nanoparticle crosslinkers. *Journal of the Mechanics and Physics of Solids*, *94*, 127-147.

Wang, Z., Cui, H., Liu, M., Grage, S. L., Hoffmann, M., Sedghamiz, E., Wenzel, W., & Levkin, P. A. (2022). Tough, Transparent, 3D-Printable, and Self-Healing Poly(ethylene glycol)-Gel (PEGgel). *Advanced Materials*, *34*, 2107791.

Warner, J. (2004). *Practical Handbook of Grouting: Soil, Rock, and Structures*. John Wiley & Sons.

Wijnen, P. W. J. G., Beelen, T. P. M., Rummens, C. P. J., Saeijs, J. C. P. L., & Van Santen, R. A. (1991). The Molecular Basis of Aging of Aqueous Silica Gel. *Journal of Colloid and Interface Science*, *145*(1), 17-32.

Wiśniewska, M., Bogatyrov, V., Ostolska, I., Szewczuk-Karpisz, K., Terpiłowski, K., & Nosal-Wiercińska. (2016). Impact of poly(vinyl alcohol) adsorption on the surface characteristics of mixed oxide $M_{nx}O_y$–SiO_2. *Adsorption*, *22*, 417-423.

Wong, C., Pedrotti, M., El Mountassir, G., & Lunn, R. J. (2018). A study on the mechanical interaction between soil and colloidal silica gel for ground improvement. *Engineering Geology*, *243*, 84-100.

Wong, C. S. K. (2021). *Colloidal Silica Grout for the Formation of Hydraulic Barriers: An Investigation of the Hydro-Mechanical and Gelling Behaviour* [Doctoral dissertation, University of Strathclyde]. Glasgow.

Wu, X., Fua, Q., Kumar, D., Ho, J. W. C., Kanhere, P., Zhou, H., & Chen, Z. (2016). Mechanically robust superhydrophobic and superoleophobic coatings derived by sol–gel method. *Materials and Design*, *89*, 1302-1309.

Xiang, Z., Zhang, N., Zhao, Y., Pan, D., Feng, X., & Xie, Z. (2022). Experiment on the silica sol imbibition of low-permeability rock mass: With silica sol particle sizes and rock permeability considered. *International Journal of Mining Science and Technology*, *32*, 1009-1019.

Xu, P., Wang, H., Tong, R., Du, Q., & Zhong, W. (2006). Preparation and morphology of SiO_2/PMMA nanohybrids by microemulsion polymerization. *Colloid and Polymer Science*, *284*(7), 755-762.

Yang, J., Han, C.-R., Duan, J.-F., Xu, F., & Sun, R.-C. (2013). Interaction of Silica Nanoparticle/Polymer Nanocomposite Cluster Network Structure: Revisiting the Reinforcement Mechanism. *The Journal of Physical Chemistry C*, *117*, 8223-8230.

Yang, R. W. (2013). *Contributions to micromechanical modelling of transport and freezing phenomena within unsaturated porous media* Université Paris-Est].

Yates, P. C. (1990). Kinetics of Gel Formation of Colloidal Silica Sols. Abstracts of Papers of the American Chemical Society,

Ye, L., Tang, Y., & Qiu, D. (2014). Enhance the mechanical performance of polyacrylamide hydrogel by aluminium-modified colloidal silica. *Colloids and Surfaces A: Physicochemical and Engineering Aspects*, *447*, 103-110.

Yossapol, N. (2002). *Remediation of chromium contaminated soils with colloidal silica* [PhD thesis, New Jersey Institute of Technology]. Newark, NJ, USA.

Yotsumoto, H., & Yoon, R.-H. (1993). Application of Extended DLVO Theory: II. Stability of Silica Suspensions. *Journal of Colloid and Interface Science*, *157*, 434-441.

Zelenev, A. S., Fu, J. M., & Keiser, B. A. (2007). Establishing the difference between colloidal borosilicate and boron-modified colloidal silica via chelation of boron with catechol and DL-tartaric acid. *Polyhedron*, *26*, 4941-4944.

Zhang, C., Liang, K., Zhou, D., Yang, H., Liu, X., Yin, X., Xu, W., Zhou, Y., & Xiao, P. (2018). High-Performance Photopolymerized Poly(vinyl alcohol)/Silica Nanocomposite Hydrogels with Enhanced Cell Adhesion. *ACS Applied Materials & Interfaces*, *10*, 27692-27700.

Zhang, H., Hassanali, A. A., Shin, Y. K., Knight, C., & Singer, S. J. (2011). The water–amorphous silica interface: Analysis of the Stern layer and surface conduction. *The Journal of Chemical Physics*, *134*(2), 024705.

Zhang, P., Sha, D., Li, Q., Zhao, S., & Ling, Y. (2021). Effect of Nano Silica Particles on Impact Resistance and Durability of Concrete Containing Coal Fly Ash. *Nanomaterials*, *11*, 1296.

Zhang, Y., & Ye, L. (2014). Structure and property of polyvinyl alcohol/precipitated silica composite hydrogels for microorganism immobilization. *Composites: Part B*, *56*, 749-755.

Zhang, Y. S., & Khademhosseini, A. (2017). Advances in engineering hydrogels. *Science*, *356*, 500.

Zhao, M., Liu, G., Zhang, C., Guo, W., & Luo, Q. (2019). State-of-the-Art of Colloidal Silica-Based Soil Liquefaction Mitigation: An Emerging Technique for Ground Improvement. *Applied Sciences*, *10*(1), 15.

Zhao, X., Li, Y., Li, B., Hu, T., Yang, Y., Li, L., & Zhang, J. (2019). Environmentally benign and durable superhydrophobic coatings based on SiO_2 nanoparticles and silanes. *Journal of Colloid and Interface Science*, *542*, 8-14.

Zheng, L., Liang, H., Tang, J., Zheng, Q., Chen, F., Wang, L., & Li, Q. (2025). Micrometer-scale poly(ethylene glycol) with enhanced mechanical performance. *Nature Communications*, *16*, 4391.

Zheng, L., Samper, J., Montenegro, L., & Fernánde, A. M. (2010). A coupled THMC model of a heating and hydration laboratory experiment in unsaturated compacted FEBEX bentonite. *Journal of Hydrology*, *386*, 80-94.

Zhu, J., & Marchant, R., E. (2011). Design properties of hydrogel tissue-engineering scaffolds. *Expert Reviews of Medical Devices*, *8*(5), 607-626.

Appendices

A.1 Chapter 3: Methodology

A.1.1 Identification of ideal compression rate

To identify the ideal rate at which to carry out UCS tests, three standard CS-grouted sand samples were produced and compressed at 5, 10, and 20 µm/min. The compression needed to be slow enough for water to drain gradually from samples, without the pore water pressure of the soil contributing to its compression response, but as fast as possible, for the sake of convenience. The 20 µm/min sample gave results clearly different from the other two rates, which were in agreement with each other. Therefore, the 20 µm/min rate was rejected, and the faster of the other two, 10 µm/min, was chosen to be the compression rate used for this investigation.

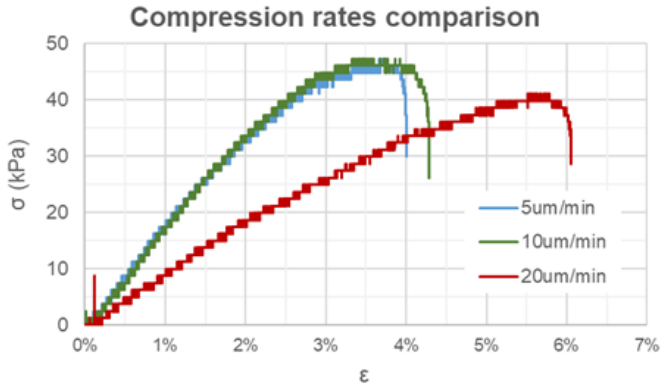

Figure A.1. Comparison of compression rates on CS-grouted sand samples.

A.2 Chapter 4: Effect of grout composition and curing conditions on the strength evolution of CS grout

A.2.1 Tables of samples

This subsection provides tables detailing CS grout and grouted sand samples tested using viscometer (Table A.1), shear vane (Table A.2), and UCS (Table A.3) in chapter 4, as additional information. Where duplicate samples were tested, the average values of the results are shown here.

Table A.1. CS grout samples for viscometer test (see 4.3.1).

Sample name	*Accelerator salt*	*Acc. salt conc. (M)*	*CS Silica wt%*	*Gel time (h)*
CS_{40}-$N_{1.3}$	NaCl	1.3	40%	8.14
CS_{40}-$N_{1.5}$		1.5		3.64
CS_{40}-$N_{1.7}$		1.7		1.69
CS_{40}-$N_{1.8}$		1.8		1.16
CS_{40}-$N_{1.9}$		1.9		0.871
CS_{40}-$N_{2.0}$		2.0		0.626
CS_{40}-$N_{2.5}$		2.5		0.106
CS_{35}-$N_{1.3}$	NaCl	1.3	35%	14.2
CS_{35}-$N_{1.5}$		1.5		6.95
CS_{35}-$N_{1.7}$		1.7		3.00
CS_{35}-$N_{1.8}$		1.8		2.26
CS_{35}-$N_{1.9}$		1.9		1.81
CS_{35}-$N_{2.0}$		2.0		1.46
CS_{30}-$N_{1.3}$	NaCl	1.3	30%	32.0
CS_{30}-$N_{1.5}$		1.5		15.0
CS_{30}-$N_{1.7}$		1.7		6.01
CS_{30}-$N_{1.8}$		1.8		5.31
CS_{30}-$N_{1.9}$		1.9		3.64
CS_{30}-$N_{2.0}$		2.0		3.45
CS_{30}-$N_{2.5}$		2.5		0.553
CS_{20}-$N_{1.5}$	NaCl	1.5	20%	40.2
CS_{20}-$N_{1.7}$		1.7		25.0
CS_{20}-$N_{1.9}$		1.9		12.5
CS_{20}-$N_{2.1}$		2.1		6.68
CS_{20}-$N_{2.3}$		2.3		3.82
CS_{20}-$N_{2.5}$		2.5		2.59
CS_{20}-$C_{0.1}$	$CaCl_2$	0.1	40%	n/a
CS_{20}-$C_{0.15}$		0.15		
CS_{20}-$C_{0.2}$		0.2		
CS_{20}-$C_{0.3}$		0.3		
CS_{20}-$C_{0.5}$		0.5		

Table A.2. CS grout samples for shear vane test (see 4.3.2). Samples marked with '*' were placed in curing water after 16 d curing.

Sample name	*Accelerator salt*	*Acc. NaCl conc. (M)*	*CS Silica wt%*	*Curing time (d)*	*Curing water*	τ_{max} *(kPa)*
CS_{40}-$N_{1.7}$-C_1				1		13.8
CS_{40}-$N_{1.7}$-C_3				3		18.6
CS_{40}-$N_{1.7}$-C_7	NaCl	1.7	40%	7	n/a	25.7
CS_{40}-$N_{1.7}$-C_{21}				21		35.1
CS_{40}-$N_{1.7}$-C_{57}				57		52.3
CS_{30}-$N_{2.22}$-C_1				1		5.27
CS_{30}-$N_{2.22}$-C_3				3		7.31
CS_{30}-$N_{2.22}$-C_7	NaCl	2.22	30%	7	n/a	10.0
CS_{30}-$N_{2.22}$-C_{21}				21		13.7
CS_{30}-$N_{2.22}$-C_{57}				57		19.6
CS_{20}-$N_{2.68}$-C_1				1		1.02
CS_{20}-$N_{2.68}$-C_3				3		1.76
CS_{20}-$N_{2.68}$-C_7	NaCl	2.68	20%	7	n/a	2.27
CS_{20}-$N_{2.68}$-C_{21}				21		3.52
CS_{20}-$N_{2.68}$-C_{57}				57		4.95
CS_{40}-$N_{2.5}$-$C_{0.25}$				0.25		12.9
CS_{40}-$N_{2.5}$-C_1				1		19.7
CS_{40}-$N_{2.5}$-C_3				3		28.1
CS_{40}-$N_{2.5}$-C_7				7		35.6
CS_{40}-$N_{2.5}$-C_{16}	NaCl	2.5	40%	16	n/a	48.5
CS_{40}-$N_{2.5}$-C_{21}				21		51.7
CS_{40}-$N_{2.5}$-C_{60}				60		77.7
CS_{40}-$N_{2.5}$-C_{64}				64		77.4
CS_{40}-$N_{2.5}$-C_{98}				98		91.5
CS_{40}-$N_{2.5}$-C_{64}-TW*	NaCl	2.5	40%	64	Tap water	60.1
CS_{40}-$N_{2.5}$-C_{64}-$CW_{1.0}$*				64	1M $CaCl_2$	104

Table A.3. CS-grouted sand samples for UCS test (see 4.3.3). Samples marked with '*' had their curing water regularly replaced.

Sample name	*Accelerator salt*	*Acc. NaCl conc. (M)*	*CS Silica wt%*	*Curing time (d)*	*Curing water*	σ_{max} *(kPa)*
CS_{40}-$N_{1.7}$-C_1-DW				1		21.1
CS_{40}-$N_{1.7}$-C_7-DW				7		42.3
CS_{40}-$N_{1.7}$-C_{21}-DW				21		53.5
CS_{40}-$N_{1.7}$-C_{56}-DW	NaCl	1.7	40%	56	DI water	64.7
CS_{40}-$N_{1.7}$-C_{112}-DW				112		85.8
CS_{30}-$N_{2.22}$-C_{231}-DW				231		128
CS_{30}-$N_{2.22}$-C_{448}-DW				448		201
CS_{40}-$N_{1.55}$-C_{28}-TW		1.55	40%			43.5
CS_{35}-$N_{1.73}$-C_{28}-TW	NaCl	1.73	35%	28	Tap water	24.9
CS_{30}-$N_{2.0}$-C_{28}-TW		2.0	30%			17.4
CS_{40}-$N_{1.92}$-C_7-DW				7		37.3
CS_{40}-$N_{1.92}$-C_{14}-DW		1.92		14		56.0
CS_{40}-$N_{1.92}$-C_{21}-DW				21		80.8
CS_{40}-$N_{1.92}$-C_{28}-DW				28		73.4
CS_{40}-$N_{1.7}$-C_7-DW				7		40.4
CS_{40}-$N_{1.7}$-C_{14}-DW	NaCl	1.7	40%	14	DI water	46.6
CS_{40}-$N_{1.7}$-C_{21}-DW				21		59.7
CS_{40}-$N_{1.58}$-C_7-DW				7		32.3
CS_{40}-$N_{1.58}$-C_{14}-DW		1.58		14		35.4
CS_{40}-$N_{1.58}$-C_{21}-DW				21		43.5
CS_{40}-$N_{1.58}$-C_{28}-DW				28		56.0
CS_{40}-$N_{1.7}$-C_{15}-TW*				15		49.1
CS_{40}-$N_{1.7}$-C_{22}-TW*				22	Tap water	68.4
CS_{40}-$N_{1.7}$-C_{29}-TW*				29		59.7
CS_{40}-$N_{1.7}$-C_{15}-$NW_{0.6}$*				15		80.8
CS_{40}-$N_{1.7}$-C_{22}-$NW_{0.6}$*				22	0.6M NaCl	77.1
CS_{40}-$N_{1.7}$-C_{29}-$NW_{0.6}$*				29		87.0
CS_{40}-$N_{1.7}$-C_{14}-$NW_{1.2}$				14		60.9
CS_{40}-$N_{1.7}$-C_{21}-$NW_{1.2}$	NaCl	1.7	40%	21	1.2M NaCl	72.7
CS_{40}-$N_{1.7}$-C_{28}-$NW_{1.2}$				28		88.3
CS_{40}-$N_{1.7}$-C_{114}-$NW_{1.2}$				114		119
CS_{40}-$N_{1.7}$-C_{14}-$CW_{0.6}$				14		70.9
CS_{40}-$N_{1.7}$-C_{21}-$CW_{0.6}$				21	0.6M $CaCl_2$	106
CS_{40}-$N_{1.7}$-C_{28}-$CW_{0.6}$				28		102
CS_{40}-$N_{1.7}$-C_{113}-$CW_{0.6}$				113		179

A.2.2 Derivation of equation 4.10

Provided here is additional information on the derivation of equation 4.10, if this is of interest. The left plot in Figure A.2 shows the natural log of the scale factors from the

exponential fits in Figure 4.1C, relating the gel time of CS grout to the accelerator NaCl concentration, for various silica wt%; and the right plot shows the rate constants from the same fits. Each of these have linear fits applied to them, with equations shown. After rearranging the ln(A) equation for A, the two fit equations were subbed into equation 4.1, in place of A and B, respectively, in order to obtain equation 4.10.

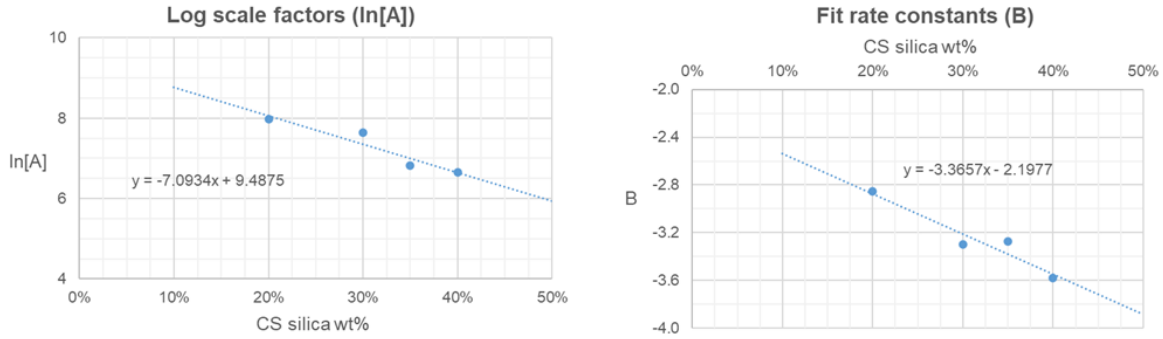

Figure A.2. *Left:* Plot of the natural log of the scale factors (A) from the exponential fit equations in Figure 4.1C (plus one additional), relating the gel time of CS grout to the accelerator NaCl concentration, for various silica wt%. *Right:* Plot of rate constats from the same exponential fits. The fits applied in both the left and right plots are linear, with equations shown.

A.3 Chapter 5: The re-healing ability of CS grout

A.3.1 Gelation of MP 325 CS grout

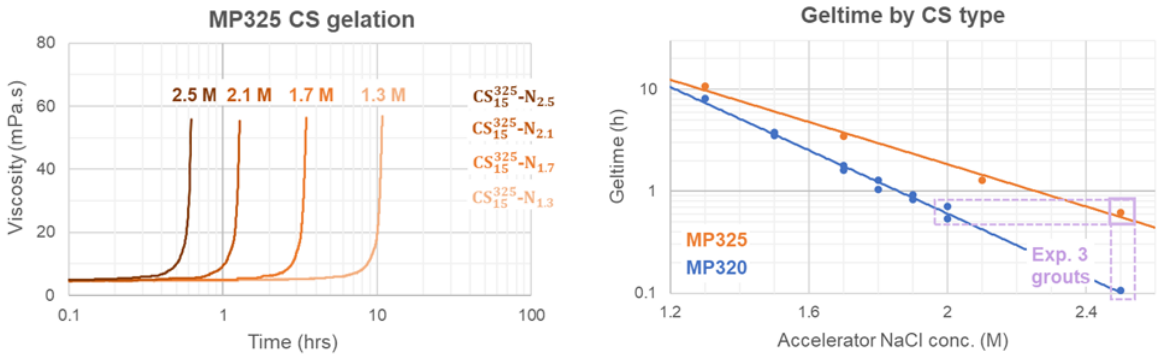

Figure A.3. *Left:* the change in viscosity during gelation of MP 325 CS grout samples with accelerators of different NaCl concentration. *Right:* A comparison of the gel times of MP 320 and MP 325 CS with accelerators of different NaCl concentration. Fit lines are exponential decays. The three grout mixes used in experiment 3 are identified with the purple dotted boxes: one MP 320 sample controls for gel time with respect to the MP 325 sample, and the other controls for accelerator NaCl concentration.

Gel time data for MP 325 CS grout with different accelerator NaCl concentrations was collected for experiment 3 in chapter 5, and is presented in Figure A.3. The left plot shows the increase in viscosity over time for the grouts, and the right plot shows their gel times compared with data previously obtained for MP 320 CS grout, in chapter 4. Similar to MP

320, decreasing NaCl concentration, c_{325}, gives increasing gel time, t_g, according to an exponential relationship,

$$t_g = 218e^{-2.39c_{325}}. \quad \text{(A.1)}$$

MP 325 gives longer gel times than MP 320 around the recommended accelerator concentration of 1.7 M, but the two fit lines intersect at ~ 1.2 M, with MP 320 giving longer gel times below this. The two fit equations may be combined to allow calculation of the NaCl concentration needed to give an MP 320 grout the same gel time as an MP 325 grout,

$$c_{320} = 0.354 + 0.667c_{325}. \quad \text{(A.2)}$$

The purple boxes in Figure A.3 highlight the three grout mixes used in experiment 3 in chapter 5, which control for both gel time and accelerator NaCl concentration.

A.3.2 Verifying change in sample and container size

In chapter 5, larger 280 mL jars were used for grouted sand shear vane samples. To validate that data from samples using these jars could still be compared to that of samples using the standard 55 mL jars, control samples were prepared, that were cured for different durations, using the larger jars, which were then tested. The results of this are shown in Figure A.4, along with equivalent data from tests using the standard jar size (previously presented in section 4.3.2), showing no significant difference. This therefore validates comparisons between samples using both jar types.

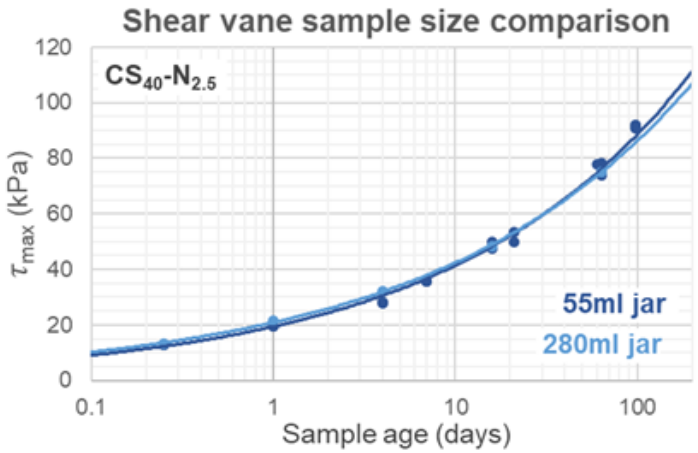

Figure A.4. Shear vane tests on CS_{40}-$N_{2.5}$ grout samples of different volumes (42 mL and 210 mL), prepared in 55 mL and 280 mL jars, showing equivalent results.

A.3.3 Tables of samples

This subsection provides tables outlining samples tested in chapter 5, investigating the effects of curing and healing times (Table A.4), double-breaking (Table A.5), grout properties (Table A.6), healing water (Table A.7), and presence of sand (Table A.8) on the re-healing of CS grout. Where duplicate samples were tested, average values are shown here.

Table A.4. Samples in experiment 1, investigating the effects of curing and healing times (see 5.3.1).

Set	*Grout*	*Test at break?*	*Cur. time (d)*	*Heal. Time (d)*	*Effect tested*
1	CS_{40}^{320}-$N_{2.5}$	Y	0.25	98	Curing time
			1	98	
			4	98	
			16	98	
			64	98	
			98	98	
2	CS_{40}^{320}-$N_{2.5}$	N	0.25	0.75	Healing time
			0.25	3.75	
			0.25	15.75	
			0.25	63.75	
			0.25	97.75	
			0.25	110.75	
			0.25	116.75	
3	CS_{40}^{320}-$N_{2.5}$	Y	0.25	16	Curing time
			1	16	
			4	16	
			16	16	
			64	16	
			98	16	
4	CS_{40}^{320}-$N_{2.5}$	N	16	0.17	Healing time
			16	1	
			16	4	
			16	16	
			16	64	
			16	98	

Table A.5. Experiment 2 sample, testing the effect of two breaking and re-healing cycles on CS grout re-healing.

Grout used	*Test at break?*	*Test at 2nd break?*	*Cur. time (d)*	*Heal. Time (d)*	*2nd heal. time (d)*
CS_{40}^{320}-$N_{2.5}$	Y	Y	7	7	7

Table A.6. Samples in experiment 3, investigating the effect of grout composition, including CS type and accelerator NaCl concentration on CS grout re-healing.

Set	*Grout*	*Test at break?*	*Cur. time (d)*	*Heal. Time (d)*	*Effect(s) tested*
1	CS_{15}^{325}-$N_{2.5}$	Y	0.25	-	CS type on shear strength
			1	-	
			4	-	
			16	-	
			48	-	
2	CS_{15}^{325}-$N_{2.5}$	N	16	0.25	CS type on re-healing
			16	1	
			16	4	
			16	16	
			16	48	
3	CS_{40}^{320}-$N_{2.0}$	Y	0.25	-	• Control for gel time • Accelerator NaCl conc. on CS shear strength
			1	-	
			4	-	
			16	-	
			48	-	
4	CS_{40}^{320}-$N_{2.0}$	N	16	0.25	• Control for gel time • Accelerator NaCl conc. on CS re-healing
			16	1	
			16	4	
			16	16	
			16	48	

Table A.7. Experiment 4 samples, testing the effect of healing water on CS grout re-healing.

Grout used	*Test at break?*	*Cur. time (d)*	*Heal. time (d)*	*Heal. Water*	*pH*
CS_{40}^{320}-$N_{2.5}$	N	14	14	Tap	7
				Tap	9
				0.5 M NaCl	9
				1 M NaCl	9
				2 M NaCl	9
				0.25 M $CaCl_2$	9
				0.5 M $CaCl_2$	9
				1 M $CaCl_2$	9
				MP 320 CS	9

Table A.8. Experiment 5 samples, testing re-healing in CS-grouted sand.

Set	*Grout used*	*Test at break?*	*In sand?*	*Cur. time (d)*	*Heal. Time (d)*
1	CS_{40}^{320}-$N_{2.5}$	Y	Y	0.25	7
			N	0.25	7
2	CS_{20}^{320}-$N_{2.68}$	Y	Y	3	7
			N	3	7
C	H_2O	Y	Y	-	-

A.4 Chapter 6: The addition of clays to CS grout

A.4.1 CS-grouted soil shear vane sample preparation method

This subsection describes the methods used to prepare CS-grouted sand and kaolin samples for shear vane test, as part of the investigation in chapter 6, but which were not included in the thesis proper. CS-grouted sand samples were prepared according to the method in 3.2.4, using standard CS_{40}-$N_{1.7}$ grout, and curing for 1 d. CS-grouted kaolin samples were prepared by first adding 100 g of kaolin powder to a 280 mL jar. 150 g of gelling CS_{40}-$N_{1.7}$ grout (118 mL) was then added to this, and the mixture was stirred by hand to ensure full saturation of the clay. After the sample had reached a gel strength of I according to the inversion test (3.3.2), which took ~ 10 min, a 25 mL film of water was added to the surface to limit evaporation. The jar was then sealed with its lid and parafilm, and the sample was cured at ambient temperature (~ 20°C) for 1 d. Information on the CS-grouted soil samples prepared in this study for shear vane test can be found in A.4.4, in Table A.12.

A.4.2 Re-healed CS-grouted grout soil shear vane sample preparation method

This subsection describes the methods used to prepare re-healed CS-grouted sand and kaolin samples for shear vane test. CS-grouted sand samples were prepared according to the method in section 3.2.6, by adapting from the CS-grouted sand shear vane samples in A.4.1. CS-grouted kaolin re-healing samples were prepared in the same manner, adapting from the CS-grouted kaolin samples, also in A.4.1. All the grouted soil samples were covered with water film for healing. The two CS-grouted sand samples were cured for 7 d and 18 d, and the CS-grouted kaolin sample for 7 d. Further information on the samples can be found in A.4.4, in Table A.12.

A.4.3 Validation of the use of the pre-mixing grouting method

Figure A.5 provides a comparison between a 'pre-mixing' grouting method, described in 6.3.2.6, and the standard 'penetration' method, described in 3.2.7, for creating grouted sand samples for UCS test. The figure shows that the two methods produce equivalent results, validating comparisons between data obtained from samples created using the two different techniques. The pre-mixing method, used in chapter 6, involves mixing the grout and sand first, before pouring the resulting slurry into the mould, rather than pouring grout onto and through the sand in the mould, penetrating through it. The penetration method data is that which was previously presented in section 4.3.3.1.

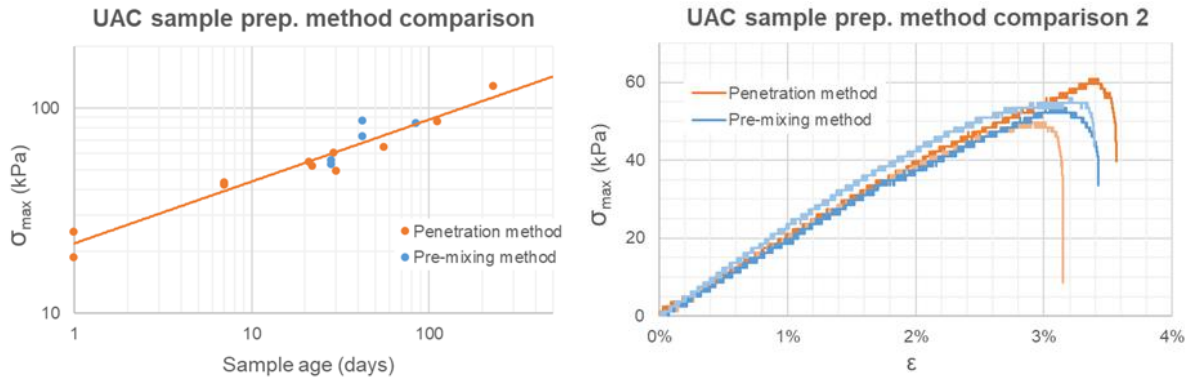

Figure A.5. Comparisons of the penetration and pre-mixing methods for preparing CS-grouted and CS/kaolin grouted sand samples for UCS tests. Left: GS_{40}-$N_{1.7}$-/-DW samples of various ages using the two methods. Right: GS_{40}-$N_{1.7}$-A_{28}-DW samples from both methods.

A.4.4 Tables of samples

This subsection provides tables outlining the compositions of samples tested as part of the investigation in chapter 6, studying the effect of adding clay on the viscosity (Table A.9), gelation (Table A.10), and strength and re-healing of CS/clay grouts (Table A.11) and grouted sand (Tables A.12 and A.13). In each case, sample compositions were calculated assuming no increase in volume occurred on the addition of clay to CS.

Table A.9. Table of samples from CS and CS/clay viscosity measurements, using viscometer (see 6.4.1.1).

Sample name	*Clay added* (wt%)	*Sample composition* (wt%)				*Viscosity* (mPa·s)
		Silica	*Kaolin*	*Bentonite*	*Water*	
CS_{40}	0%	40%	0%	0%	60%	10
CS_{40}/K_6	6%	38%	6%	0%	56%	13
CS_{40}/K_{16}	16%	34%	14%	0%	52%	20
CS_{40}/K_{33}	33%	30%	25%	0%	45%	65
CS_{40}/K_{65}	65%	24%	40%	0%	36%	1300
CS_{40}/B_1	1%	40%	0%	1%	59%	15
CS_{40}/B_2	2%	39%	0%	2%	59%	20
CS_{40}/B_3	3%	39%	0%	3%	58%	26
CS_{40}/B_5	5%	38%	0%	5%	57%	79

Table A.10. Table of samples from CS/kaolin and CS/bentonite grout gel time measurements, using viscometer (see 6.4.1.2 and 6.4.2.1).

Sample name	*Accelerator NaCl* (M)	*Sample composition* (wt%)					*Gel time* (h)
		Silica	*Kaolin*	*Bentonite*	*NaCl*	*Water*	
CS_{40}/K_6-$N_{1.7}$	1.7	32%	5.3%	0%	1.2%	61%	0.93
CS_{40}/K_{16}-$N_{1.7}$	1.7	30%	12%	0%	1.1%	57%	0.43
CS_{40}/K_{33}-$N_{1.7}$	1.7	27%	22%	0%	1.0%	50%	0.087
CS_{40}/K_{16}-$N_{1.7}$	1.7	30%	12%	0%	1.1%	57%	0.22
CS_{40}/K_{16}-$N_{1.5}$	1.5	30%	12%	0%	1.0%	57%	1.14
CS_{40}/K_{16}-$N_{1.3}$	1.3	30%	12%	0%	0.9%	57%	2.62
CS_{40}/B_5-$N_{1.5}$	1.5	33%	0%	4.3%	1.1%	62%	0.26
CS_{40}/B_5-$N_{1.3}$	1.3	33%	0%	4.3%	1.0%	62%	0.50
CS_{40}/B_5-$N_{1.1}$	1.1	33%	0%	4.3%	0.8%	62%	1.20
CS_{40}/B_5-$N_{0.9}$	0.9	33%	0%	4.3%	0.7%	62%	2.90
CS_{33}/K_{11}-$N_{1.3}$	1.3	26%	8.6%	0%	1.5%	64%	9.42
CS_{33}/K_{11}-$N_{1.5}$	1.5	26%	8.6%	0%	1.4%	64%	4.96
CS_{33}/K_{11}-$N_{1.7}$	1.7	26%	8.6%	0%	1.3%	64%	2.54
CS_{33}/K_{11}-$N_{1.8}$	1.8	26%	8.6%	0%	1.2%	64%	1.73
CS_{33}/K_{11}-$N_{1.9}$	1.9	26%	8.6%	0%	1.1%	64%	1.27
CS_{33}/K_{11}-$N_{2.0}$	2.0	26%	8.6%	0%	1.0%	64%	0.94
CS_{25}/K_{25}-$N_{1.3}$	1.3	17%	17%	0%	1.4%	64%	31.0
CS_{25}/K_{25}-$N_{1.5}$	1.5	17%	17%	0%	1.3%	64%	13.8
CS_{25}/K_{25}-$N_{1.7}$	1.7	17%	17%	0%	1.3%	64%	6.69
CS_{25}/K_{25}-$N_{1.8}$	1.8	17%	17%	0%	1.2%	64%	5.31
CS_{25}/K_{25}-$N_{1.9}$	1.9	17%	17%	0%	1.0%	64%	4.62
CS_{25}/K_{25}-$N_{2.0}$	2.0	17%	17%	0%	0.9%	64%	2.48

Table A.11. Table of samples from shear vane tests on CS/kaolin grout, including re-healed samples (see 6.4.1.3 and 6.4.2.2). A dash in a box indicates no test was performed.

Sample name	*Sample composition* (wt%)				*Cur. Time* (d)	*Test 1* τ_{max} (kPa)	*Heal. time* (d)	*Test 2* τ_{max} (kPa)
	Silica	*Kaolin*	*NaCl*	*Water*				
CS_{25}/K_{25}-$N_{2.3}$-$C_{0.25}$(-H_{16})	17%	17%	1.6%	64%	0.25	0.56	16	2.78
CS_{25}/K_{25}-$N_{2.3}$-$C_{0.25}$(-H_{16})	17%	17%	1.6%	64%	0.25	0.46	16	3.15
CS_{25}/K_{25}-$N_{2.3}$-C_{1}(-H_{16})	17%	17%	1.6%	64%	1	1.85	16	2.50
CS_{25}/K_{25}-$N_{2.3}$-C_{1}(-H_{16})	17%	17%	1.6%	64%	1	1.94	16	2.41
CS_{25}/K_{25}-$N_{2.3}$-C_{4}(-H_{16})	17%	17%	1.6%	64%	4	3.33	16	1.76
CS_{25}/K_{25}-$N_{2.3}$-C_{4}(-H_{16})	17%	17%	1.6%	64%	4	3.33	16	1.94
CS_{25}/K_{25}-$N_{2.3}$-C_{16}(-H_{16})	17%	17%	1.6%	64%	16	6.57	16	3.61
CS_{25}/K_{25}-$N_{2.3}$-C_{16}(-H_{16})	17%	17%	1.6%	64%	16	7.12	16	3.52
CS_{25}/K_{25}-$N_{2.3}$-C_{48}(-H_{16})	17%	17%	1.6%	64%	58	12.3	16	2.50
CS_{25}/K_{25}-$N_{2.3}$-C_{48}(-H_{16})	17%	17%	1.6%	64%	58	13.1	16	2.22
CS_{25}/K_{25}-$N_{2.3}$-C_{16}(-$H_{0.25}$)	17%	17%	1.6%	64%	16	-	0.25	1.39
CS_{25}/K_{25}-$N_{2.3}$-C_{16}(-$H_{0.25}$)	17%	17%	1.6%	64%	16	-	0.25	1.20
CS_{25}/K_{25}-$N_{2.3}$-C_{16}(-H_{1})	17%	17%	1.6%	64%	16	-	1	2.87
CS_{25}/K_{25}-$N_{2.3}$-C_{16}(-H_{1})	17%	17%	1.6%	64%	16	-	1	2.59
CS_{25}/K_{25}-$N_{2.3}$-C_{16}(-H_{4})	17%	17%	1.6%	64%	16	-	4	3.05
CS_{25}/K_{25}-$N_{2.3}$-C_{16}(-H_{4})	17%	17%	1.6%	64%	16	-	4	3.15
CS_{25}/K_{25}-$N_{2.3}$-C_{16}(-H_{58})	17%	17%	1.6%	64%	16	-	58	6.37
CS_{25}/K_{25}-$N_{2.3}$-C_{16}(-H_{58})	17%	17%	1.6%	64%	16	-	58	7.59

Table A.12. Table of samples from shear vane tests on CS-grouted sand, and CS-grouted kaolin (see 6.4.1.3). The test 1 τ_{max} measurements for the GS_{40}-$N_{1.7}$-C_1 samples exceeded the maximum measurement range of the shear vane.

Sample name	*Sample composition* (wt%)					*Cur. Time* (d)	*Test 1* τ_{max} (kPa)	*Heal. time* (d)	*Test 2* τ_{max} (kPa)
	Silica	*Kaolin*	*NaCl*	*Water*	*Sand*				
GS_{40}-$N_{1.7}$-C_1(-H_7)	10%	0%	0.4%	19%	70%	1	> lim	7	28.7
GS_{40}-$N_{1.7}$-C_1(-H_{18})	10%	0%	0.4%	19%	70%	1	> lim	18	45.3
GK_{40}-$N_{1.7}$-C_1(-H_7)	21%	40%	0.8%	39%	0%	1	32.6	7	19.0

Table A.13. Table of samples from UCS tests on CS grout and CS/kaolin grouts of different kaolin wt% (see 6.4.1.3).

Sample name	*Sample composition* (wt%)					*Cur. time* (d)	σ_{max} (kPa)
	Silica	*Kaolin*	*NaCl*	*Water*	*Sand*		
GS_{40}-$N_{1.7}$-C_{28}	8.6%	0%	0.33%	16%	75%	28	53.5
GS_{40}-$N_{1.7}$-C_{28}	8.6%	0%	0.33%	16%	75%	28	56.0
GS_{40}-$N_{1.7}$-C_{42}	8.6%	0%	0.33%	16%	75%	42	73.4
GS_{40}-$N_{1.7}$-C_{42}	8.6%	0%	0.33%	16%	75%	42	87.0
GS_{40}-$N_{1.7}$-C_{84}	8.6%	0%	0.33%	16%	75%	84	84.6
GS_{40}-$N_{1.7}$-C_{85}	8.6%	0%	0.33%	16%	75%	85	70.9
GS_{40}-$N_{1.7}$-C_{85}	8.6%	0%	0.33%	16%	75%	85	85.8
GS_{40}/K_{11}-$N_{1.7}$-C_{28}	7.9%	2.2%	0.30%	15%	75%	28	83.3
GS_{40}/K_{11}-$N_{1.7}$-C_{28}	7.9%	2.2%	0.30%	15%	75%	29	94.5
GS_{40}/K_{11}-$N_{1.7}$-C_{42}	7.9%	2.2%	0.30%	15%	75%	42	93.3
GS_{40}/K_{11}-$N_{1.7}$-C_{42}	7.9%	2.2%	0.30%	15%	75%	42	64.7
GS_{40}/K_{11}-$N_{1.7}$-C_{84}	7.9%	2.2%	0.30%	15%	75%	84	102
GS_{40}/K_{11}-$N_{1.7}$-C_{85}	7.9%	2.2%	0.30%	15%	75%	85	113
GS_{40}/K_{11}-$N_{1.7}$-C_{85}	7.9%	2.2%	0.30%	15%	75%	85	111
GS_{40}/K_{25}-$N_{1.7}$-C_{28}	7.7%	4.8%	0.30%	15%	73%	28	89.5
GS_{40}/K_{25}-$N_{1.7}$-C_{29}	7.7%	4.8%	0.30%	15%	73%	29	79.6
GS_{40}/K_{25}-$N_{1.7}$-C_{42}	7.7%	4.8%	0.30%	15%	73%	42	88.3
GS_{40}/K_{25}-$N_{1.7}$-C_{42}	7.7%	4.8%	0.30%	15%	73%	42	93.3
GS_{40}/K_{25}-$N_{1.7}$-C_{85}	7.7%	4.8%	0.30%	15%	73%	85	114
GS_{40}/K_{25}-$N_{1.7}$-C_{86}	7.7%	4.8%	0.30%	15%	73%	86	101

A.4.5 CS-grouted soil curing and re-healing

In this subsection, the results of shear vane tests on CS-grouted sand and kaolin during curing and re-healing are described. These were part of the investigation in chapter 6, but are not included in the main thesis as they were deemed to be too preliminary and limited in nature. Figure A.6A shows the shear stress response with increasing strain of a kaolin clay sample grouted with standard CS_{40}-$N_{1.7}$ grout, and cured for 1 d (GK_{40}-$N_{1.7}$-C_1). The response of the same sample after having been broken and re-healed for a further 7 d is also shown (GK_{40}-$N_{1.7}$-C_1-H_7). Figure A.6B shows the same for a sand sample grouted with CS_{40}-$N_{1.7}$ grout and cured for 1 d (GS_{40}-$N_{1.7}$-C_1), and again after breaking and healing for 7 d (GS_{40}-$N_{1.7}$-C_1-H_7), plus another sample healed for 18 d. Both CS-grouted sand and kaolin are therefore observed to re-heal after breaking, with longer healing time leading to increased strength recovery in the case of the sand (there was no data on this for grouted kaolin). The 1 d cured grouted sand sample exhibited far greater strength than the grouted kaolin: so much so that it exceeded the measurement limit of the shear vane before it could fail. However, the strength for sand and kaolin after breaking and re-healing was much more similar.

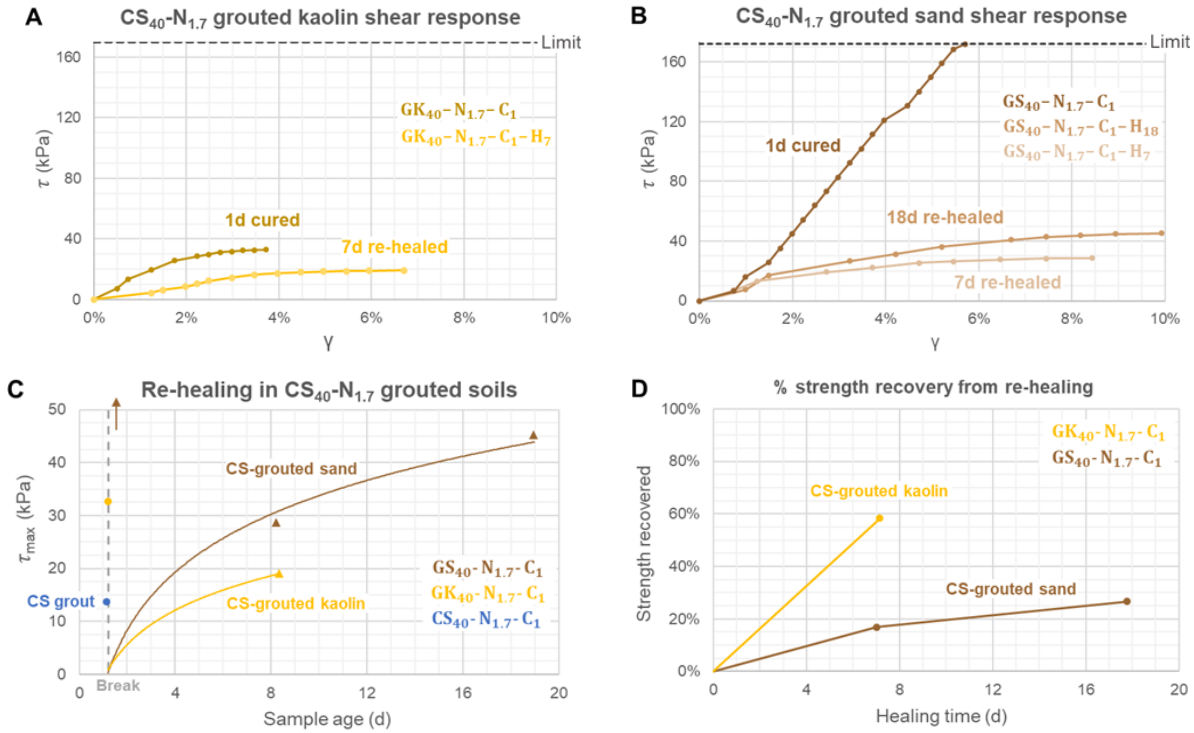

Figure A.6. *A:* Shear stress response of kaolin grouted with CS_{40}-$N_{1.7}$ to increasing shear strain, after curing for 1 d, and again, after breaking and re-healing for 7 d. *B:* The same for sand grouted with CS_{40}-$N_{1.7}$, after curing for 1 d, and breaking and re-healing for 7 d and 18 d. GS_{40}-$N_{1.7}$-C_1 exceeded the limit of the shear vane. *C:* The max. stress value of each sample, with that of CS_{40}-$N_{1.7}$-C_1 for comparison. The dotted line indicates the break at 1 d. The 'fit lines' are intended as a guide only. *D:* Percentage strength recovered for CS-grouted sand and kaolin samples, cured 1 d and re-healed. The measurement limit of the shear vane (170 kPa) was used as the original strength for GS_{40}-$N_{1.7}$-C_1.

Figure A.6C shows the maximum stress value recorded for each sample (excluding GS_{40}-$N_{1.7}$-C_1), with 1 d cured CS_{40}-$N_{1.7}$-C_1 data from section 4.3.2 also provided for comparison: however, there is currently no corresponding 7 d re-healed sample for CS_{40}-$N_{1.7}$ grout (i.e. CS_{40}-$N_{1.7}$-C_1-H_7). The dotted line in the plot indicates the break at 1 d, and the solid coloured lines are intended only as a visual guide showing the re-healing process. From the plot, the grouted kaolin is more than double the strength of the CS grout, and the grouted sand is at least 10× as strong. Plot D shows the strength recovered during re-healing as a percentage of the original strength prior to breaking. The shear vane measurement limit of 170 kPa was used as the original strength of GS_{40}-$N_{1.7}$-C_1. From this, it can be seen that the grouted kaolin recovered 3.4× as much strength as the CS-grouted sand.

From this data, the 1 d cured CS-grouted sand sample (GS_{40}-$N_{1.7}$-C_1) was far stronger than the CS-grouted kaolin (GK_{40}-$N_{1.7}$-C_1), to the extent that it exceeded the measurement limit of the shear vane. It was at least 5.2x stronger than CS-grouted kaolin, and 12% stronger

than CS grout. Although some difference in strength may be expected, the reason for this discrepancy may in large part be due to differences in sample composition resulting from their preparation methods. Table A.14 shows the compositions of the two samples, plus that of CS_{40}-$N_{1.7}$-C_1. From this, the GS_{40}-$N_{1.7}$-C_1 sample had 1.75× as much sand as the GK_{40}-$N_{1.7}$-C_1 had kaolin, and 0.5× as much silica. The reason for this is that, although both samples used about the same volume of soil, this corresponded to 300 g of sand and only 100 g of kaolin, due to differences in density. The samples used similar quantities of CS grout, but ~ 50 mL of this was removed from the sand sample, as it was simply sitting on top of the settled-out sand at the bottom of the jar. In contrast, the kaolin completely dispersed in the grout. To improve the experiment, greater care could have been taken to ensure that the samples had comparable compositions. The method could also have used a weaker grout, such as CS_{20}-$N_{2.7}$, to ensure that the grouted sand did not exceed the measurement limit.

Table A.14. Composition of CS_{40}-$N_{1.7}$ grouted sand and kaolin samples, plus the grout itself.

Sample	*Composition* (wt%)						*Description*
	Silica	*Kaolin*	*NaCl*	*Water*	*Sand*	*Solids*	
GS_{40}-$N_{1.7}$-C_1	10%	0%	0.4%	19%	70%	80%	CS-grouted sand
GK_{40}-$N_{1.7}$-C_1	21%	40%	0.8%	39%	0%	61%	CS-grouted kaolin
CS_{40}-$N_{1.7}$-C_1	34%	0%	1.3%	64%	0%	34%	CS grout

The strength of grouted sand and kaolin samples on re-healing was much more similar than for curing, being only 1.5× stronger after 7 d healing, and by considering strength recovery in terms of percentage of the original strength prior to breaking, the grouted kaolin recovered 3.4× more of its original strength than the grouted sand. It is not yet clear if the sand plays a comparatively minor role in the re-healing process, compared to the curing process, or if it is a question of gel strength, with sand amplifying the strength of stronger gels relative to weaker ones. More data could help to investigate this question.

A.5 Chapter 7: Combination of CS grout with polymers and hydrogels

A.5.1 Rheology and rheometers

Provided here is additional information on rheology and rheometers to provide more context for the research here, if needed. Rheology is the study of the flow and deformation of matter, being either fluid, solid, or some combination of both. Fluids continuously flow upon applied shear stress with the property of viscosity characterising their resistance to flowing. Viscosity arises as a result of molecular interactions and friction between

particles forced into contact during flow; it therefore depends on the nature and strength of intermolecular interactions, as well as the size, shape, and concentration of suspended particulates. Fluids can be described as being either Newtonian or non-Newtonian in nature, where for the latter, viscosity varies with strain rate, the relative flow velocity. Shear thinning, in which viscosity decreases with increasing shear rate, is therefore an example of non-Newtonian behaviour. Solids on the other hand have rigid structure and do not flow. They may instead deform, however, either elastically or plastically. Elastic materials resist a distorting force and return to their original dimensions upon relaxation, whereas plastic materials deform permanently.

Hydrogels, such as CS and polymer gels, are modelled as 'viscoelastic solids', as they exhibit behaviour associated with both fluids and elastic solids. The modulus (a quantity describing the resistance of a material to deformation) of such a material is comprised of both viscous and elastic components: the elastic component is termed the 'storage modulus', *G'*, and represents the energy stored in a material during deformation, through chemical bonds, whereas the viscous component is the 'loss modulus', *G"*, representing energy lost in the material on deformation, as heat. The 'complex modulus', comprising the two is

$$G* = G' + G". \tag{A.3}$$

Viscoelastic materials therefore both store and lose some energy during deformation.

A rheometer is used to study the rheology of materials. To measure the viscosity of a fluid it applies a known shear stress, τ, to the fluid at a shear rate, $\dot{\gamma}$. For the 'cone-and-plate' geometry configuration, the stress is given by

$$\tau = \frac{3T}{2\pi R^3}, \tag{A.4}$$

where T is the applied torque, and R is the radius of the cone, and the shear rate is

$$\dot{\gamma} = \frac{\omega}{\theta}, \tag{A.5}$$

where ω is the angular velocity of the cone's rotation, and θ is the cone angle. The viscosity is then

$$\eta = \frac{\tau}{\dot{\gamma}}. \tag{A.6}$$

To measure the storage and loss moduli of a viscoelastic solid, a sinusoidal shear strain of amplitude γ_0 is applied to the material, imparting a shear stress of amplitude τ_0. The torque response of the material to the applied deformation occurs with some angular phase lag, δ, depending on the nature of the material in that moment. The storage and loss moduli are then given by

$$G' = \frac{\tau_0}{\gamma_0}\cos\delta, \tag{A.7}$$

and

$$G'' = \frac{\tau_0}{\gamma_0}\sin\delta. \tag{A.8}$$

For an elastic solid, the response to deformation is instantaneous, meaning $\delta = 0°$, whereas for a true fluid, the response is fully out of phase, such that $\delta = 90°$. Viscoelastic solids exhibit elastic behaviour ($\delta \sim 0°$) up to a certain strain, at which point the internal structure of the material begins to break, resulting in a rise in phase angle: this is known as the 'yield point'. The 'flow point' of a material occurs when $\delta = 45°$, at which point it starts to behave more like a fluid than an elastic solid.

A.5.2 CS/PAM gel rheology

Figure A.7A shows the storage and loss moduli of CS grout with 1.5 wt% of PAM-5m added, alongside that of a standard CS grout, under increasing strain amplitude, and at angular frequency of 10 rad/s. Both gels were aged 1 d and used 1.7 M NaCl accelerator solution. These were tests performed as part of the investigation in chapter 7, but which were not included in the main thesis as they were deemed too preliminary. Figure A.7B, C, and D show the shear stress against strain, shear stress against phase angle, and the strain against phase angle for the same tests. No precise information is available on the gel time of the CS/PAM gel variant used here, but solid state test suggested it was similar to the control. From the plots, the CS/PAM gel has significantly higher G' than the standard CS gel. Its yield point is at a higher stress than the control, but a lower strain. Its flow point occurs at approximately the same strain as the control. As seen in 7.4.1.4, the control here also exhibits two distinct yield points in its G" curve which are not apparent for the CS/PAM gel.

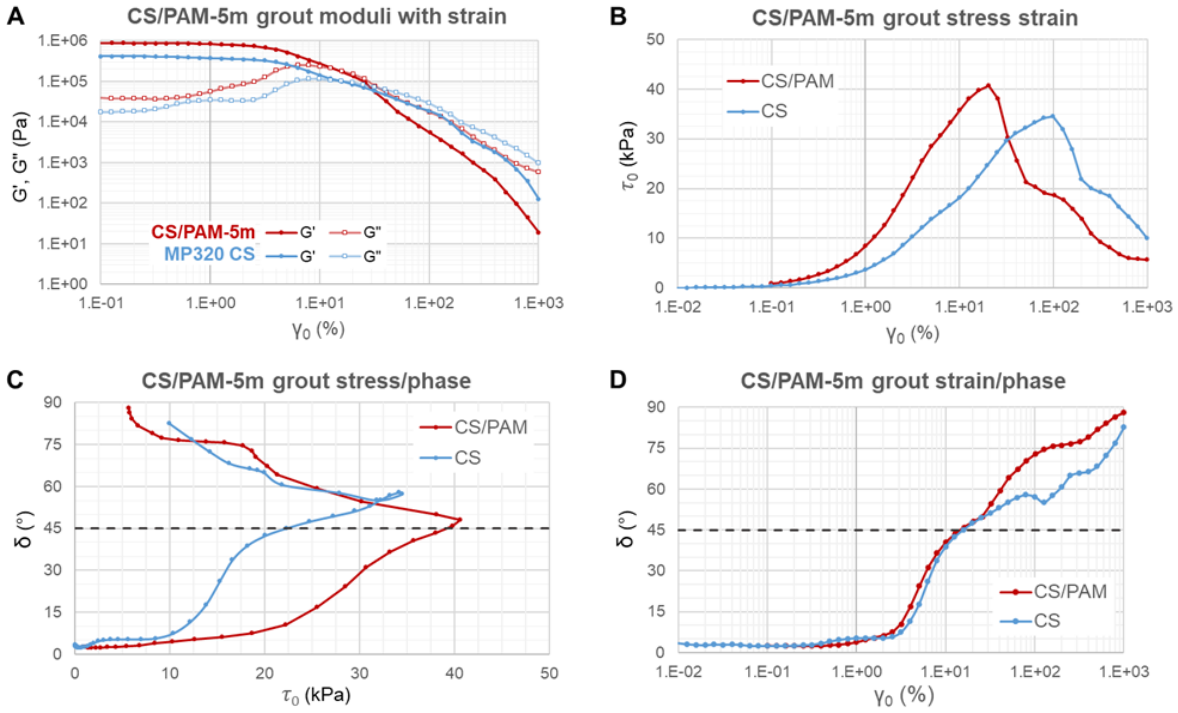

Figure A.7. *A:* Storage and loss moduli of CS grout with 1.5 wt% of PAM-5m added, and standard CS grout, under increasing strain amplitude, at angular frequency 10 rad/s; both gels were aged 1 d and used 1.7 M NaCl accelerator solution. The other plots show stress/strain (*B*), stress/phase angle (*C*), and strain/phase (*D*) angle from the same tests.

A.6 Other results

This section describes certain other experimental results from this PhD which did not fit into the scope of any of the chapters in this thesis, but which may still be of interest.

A.6.1 Effect of pH on CS grout gel time

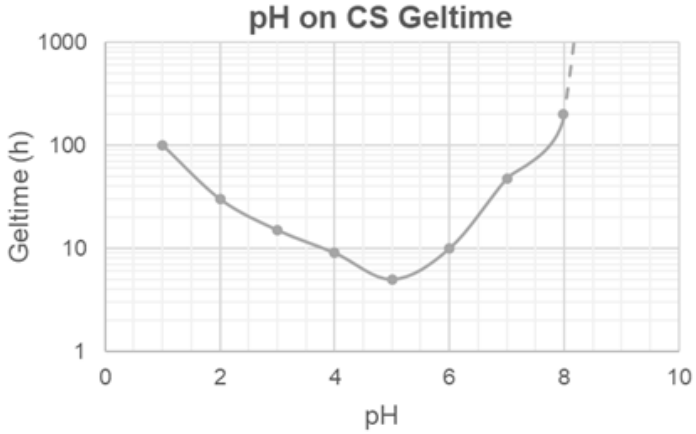

Figure A.8. Effect of pH on the gel time of MP320 CS grout, as measured by solid-state test. Line intended only as a guide.

Figure A.8 shows CS gel times over a pH range of 1-9, as measured by solid-state test. The data suggests that MP 320 CS has a solid-state gel time minimum at approximately pH 5,

which rises to apparent stability around pH 8-9.6 and around pH 1. This roughly agrees with previous experimental work which finds that CS in general should have a stability minimum in the range pH 6-7, and reach stability above pH 8 (Noll et al., 1992). The pH 1 sample was observed to gel after several months.

A.6.2 MP325 CS-grouted sand UCS

Figure A.9 shows a comparison of the compressive strength of MP 325 and MP 320 CS-grouted sand samples. 1.7 M NaCl accelerator was used for both sets of samples, meaning that gel time was not constant, as MP 325 gels faster than MP 320 (see A.3.1).

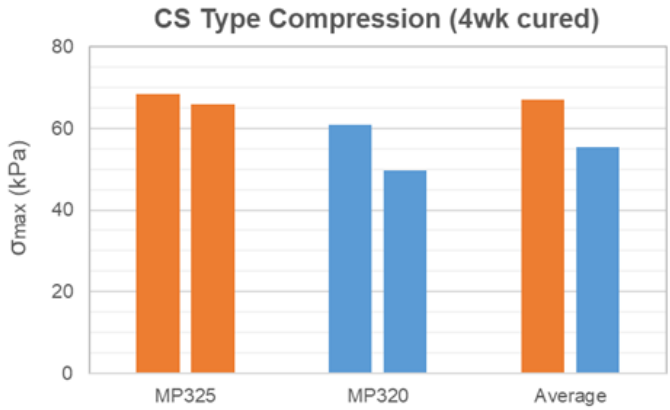

Figure A.9. Comparison of the compressive strength of MP 325 and MP 320 CS-grouted sand samples.